Charles University in Prague

First Faculty of Medicine

Programme: doctoral

Branch of study: Medical biophysics

FIRST FACULTY
OF MEDICINE
Charles University

Ing. Štěpán Kortus

Vápníková signalizace magnocelulárních neuronů supraoptického jádra potkanů

Ca^{2+} signalling in magnocellular neurones of the rat supraoptic nucleus

Dissertation Thesis

Supervisor: RNDr. Martin Zápotocký, Ph.D.

Consultant: Dr. Govindan Dayanithi, Ph.D.

Prague, 2019

Prohlášení

Prohlašuji, že jsem závěrečnou práci zpracoval samostatně a že jsem řádně uvedl a citoval všechny použité prameny a literaturu. Současně prohlašuji, že práce nebyla využita k získání jiného nebo stejného titulu. Souhlasím s trvalým uložením elektronické verze mé práce v databázi systému meziuniverzitního projektu Theses.cz za účelem soustavné kontroly podobnosti kvalifikačních prací.

V Praze dne _____.

Štěpán Kortus

_____

Identifikační záznam

KORTUS, Štěpán. *Vápníková signalizace magnocelulárních neuronů supraoptického jádra potkanů [Ca^{2+} signalling in magnocellular neurones of the rat supraoptic nucleus]*. Praha, 2019. 137 stran, 4 přílohy, Disertační práce (Ph.D.) Univerzita Karlova v Praze, 1. lékařská fakulta, Fyziologický ústav AV ČR. Vedoucí práce RNDr. Martin Zápotocký, Ph.D.

Acknowledgements

I would like to thank to my supervisor RNDr. Martin Zapotocky, Ph.D. and my supervising consultant Dr. Govindan Dayanithi for the continuous support of my scientific work since I have started my Ph.D. studies. The work presented in this thesis has been done in close collaboration with Department of Computational Neuroscience of Institute of Physiology and with Department of Molecular Neurophysiology of Institute of Experimental Medicine of Czech Academy of Sciences. I would like to thank to all my dear colleagues from the departments for fruitful discussion resulting in interesting results and publications. This work was supported by the grants 14-34077S and GACRP304/12/G069 from the Grant Agency of the Czech Republic and GAUK 22214 from the Grant Agency of Charles University in Prague. Last but not the least, I would like to thank my family and especially to my wife for supporting me spiritually throughout writing this thesis and my life in general.

Contents

Souhrn

Magnocelulární neurosekreční buňky hypotalamu vysílají své axony do neurohypofýzy, kde do krevního řečiště uvolňují hormony oxytocin a vazopresin. Oxytocin se uplatňuje zejména při porodu a je nezbytný pro stimulaci sekrece mléka během laktace. Základní fyziologickou funkcí vazopresinu je řízení re-absorpce vody v ledvinách, čímž se podílí na regulaci tělesné rovnováhy tekutin. K sekreci hormonů dochází zejména z terminálů neuronů v hypofýze, nicméně hormony jsou secernovány i z dendritů v supraoptickém jádru, kde difundují a ovlivňují okolní buňky skrze autokrinní efekt. Mechanismy řídící sekreci oxytocinu a vazopresinu byly intenzivně studovány během posledních dekád a předpokládá se, že zásadní, v porozumění fyziologie sekrece, je vztah mezi Ca^{2+} signalizací, sekrecí z dendritů a elektrickou aktivitou magnocelulárních neuronů.

V této práci kombinujeme matematickou analýzu s experimentálním měřením Ca^{2+} signálů izolovaných neuronů ze supraoptického jádra. K jejich identifikaci využíváme transgenní potkany exprimující vazopresin nebo oxytocin značený fluorescenčním proteinem. Studujeme změny Ca^{2+} homeostázy během těhotenství, laktace a dehydratace. Dále se zaměřujeme na spontánní a indukované Ca^{2+} signály a na to, jak autoregulační mechanismus vazopresinu může ovlivňovat sekreci hormonu.

Tato práce přináší detailní analýzu spontánních Ca^{2+} oscilací a depolarizací indukovaných Ca^{2+} odpovědí v izolovaných magnocelulárních neuronech. Ukazujeme, jak jsou tyto oscilace ovlivněny fyziologickým statusem organismu (dehydratace, laktace) a vystavením extracelulárním stimulům (osmotická změna, vazopresin). Zaměřujeme se dále na mechanismy nutné ke vzniku $[Ca^{2+}]_i$ oscilací a ukazujeme, že pro jejich existenci nejsou nutné akční potenciály, ale že jsou výsledkem vnitrobuněčné aktivity koordinující Ca^{2+} kanály a Na/Ca^{2+} výměník. Nad rámec toho prokazujeme, že vazopresin reguluje Ca^{2+} oscilace prostřednictvím autokrinní signalizace podobně, jako tomu bylo prokázánu u elektrické aktivity. U Ca^{2+} signálů vyvolaných depolarizací membrány detailně popisujeme, jak jsou odpovědi modulovány stavem naplnění vnitrobuněčných Ca^{2+} zásobníků. Celkově tato práce pokrývá mechanismy Ca^{2+} signalizace magnocelulárních buněk, které doposud nebyly dostatečně prostudovány, a jejichž znalost je zároveň nezbytná k plnému porozumění funkce oxytocinu a vazopresinu.

Abstract

The magnocellular neurosecretory cells (MNCs) of the hypothalamus project axons from the supraoptic nucleus to the posterior pituitary gland, where they secrete either oxytocin or vasopressin into the circulation. Oxytocin is important for delivery at birth and is essential for milk ejection during suckling. Vasopressin primarily promotes water reabsorption in the kidney to maintain body fluid balance.

The profile of oxytocin and vasopressin secretion is principally determined by the pattern of action potentials initiated at the cell bodies in the hypothalamus. MNCs principally secrete hormones from terminals in the pituitary, but the secretion also occurs from their dendrites in the supraoptic nucleus, where they diffuse and affect the neighbouring cells. Mechanisms controlling the oxytocin and vasopressin secretion from MNCs have been extensively studied over the last decades and it is assumed that the relationship between Ca^{2+} signalling, secretion from dendrites, and the firing patterns is essential in understanding the magnocellular neurosecretory system.

In this project, we combine mathematical analysis and experimental measurements of Ca^{2+} activity of MNCs of transgenic rats expressing an arginine vasopressin-enhanced green fluorescent protein (AVP-eGFP) or oxytocin-monomeric red fluorescent protein (OT-mRFP1). We report a detailed analysis of the spontaneous $[Ca^{2+}]_i$ oscillations and depolarization-induced $[Ca^{2+}]_i$ elevations in MNCs in isolated conditions. We show how these oscillations are affected by the physiological state of the animal (dehydration, lactation) and by exposure to extracellular stimuli (osmotic change, exposure to vasopressin). In terms of mechanisms underlying the oscillations, we show that they do not require action potentials but are rather mediated by intrinsic mechanisms driven by the action of Ca^{2+} channels and the membrane Na^+/Ca^{2+} exchanger. Furthermore, we prove that vasopressin has autoregulatory feedback on oscillating neurones similar to the autocrine signalling described for electrical activity. For depolarization-induced $[Ca^{2+}]_i$ elevation, we show, in detail, how the $[Ca^{2+}]_i$ responses are modulated by the filling state of the intracellular Ca^{2+} stores. Taken together, this study covers important Ca^{2+} signalling mechanisms in MNCs that have not yet been sufficiently described and are essential for understanding the physiology of oxytocin and vasopressin secretion.

Key words:

Vasopressin, Oxytocin, Hypothalamus, Calcium signalling, Magnocellular, Supraoptic nucleus, Calcium imaging, Fura-2.

Klíčová slova:

Vazopresin, oxytocin, hypotalamus, vápníková signalizace, magnocelulární, supraoptické jádro, vápníkové zobrazování, Fura-2.

1 Introduction

1.1 Physiological role of oxytocin and vasopressin in the organism

Vasopressin (AVP), the antidiuretic hormone, and oxytocin (OT) are neurohypophysial peptides synthesized by populations of magnocellular neurosecretory cells (MNCs) in the mammalian hypothalamus and are secreted into the systemic circulation from the posterior pituitary gland (Bourque and Oliet 1997). The peptides released into the bloodstream have effects on distant organs, such as the kidney, vascular smooth muscle, mammary gland and uterus but act also centrally in the hypothalamus (Armstrong, Wang et al. 2010). Oxytocin is primarily known for its role in milk ejection during lactation and as a humoral trigger for uterine contractions at birth (Brown, Bains et al. 2013). Vasopressin principally acts in the kidney to promote water reabsorption and on the vasculature to increase blood pressure via vasoconstriction (Armstrong and Johnson 2018). Together with other physiological mechanisms, vasopressin helps to maintain plasma osmolality at normal level near 300 mOsmol/kg. Even fluctuations of 3 mOsmol/kg away from the normal level lead to changes in salt and water retention in order to restore the normal osmolality (Prager-Khoutorsky and Bourque 2010). Under basal conditions, vasopressin concentration in the circulation is at approximately 1–3 pg/ml and causes reabsorption of approximately 30 l of water from the urine each day in humans, however, it can reach up to 100 pg/ml in response to extreme acute osmotic stimuli (Verbalis, Baldwin et al. 1986, Forsling, Montgomery et al. 1998, Brown, Bains et al. 2013). Apart from the well-known peripheral functions of AVP and OT, these neuropeptides also regulate differentiation and proliferation of stem cells (Tran, Yao et al. 2015, Forostyak, Forostyak et al. 2016) and have an important role in social behaviour (Viero, Shibuya et al. 2010).

1.2 Magnocellular neurosecretory system

1.2.1 Anatomy and localization

The magnocellular neurosecretory system is formed from vasopressinergic and oxytocinergic cells that are mainly located in two hypothalamic regions: the supraoptic (SON) and the paraventricular (PVN) nuclei (Armstrong 1995) (figure 1.1). This is where the majority of the cells is located; only a small subpopulation of magnocellular neurones can be found outside the nuclei (figure 1.2).

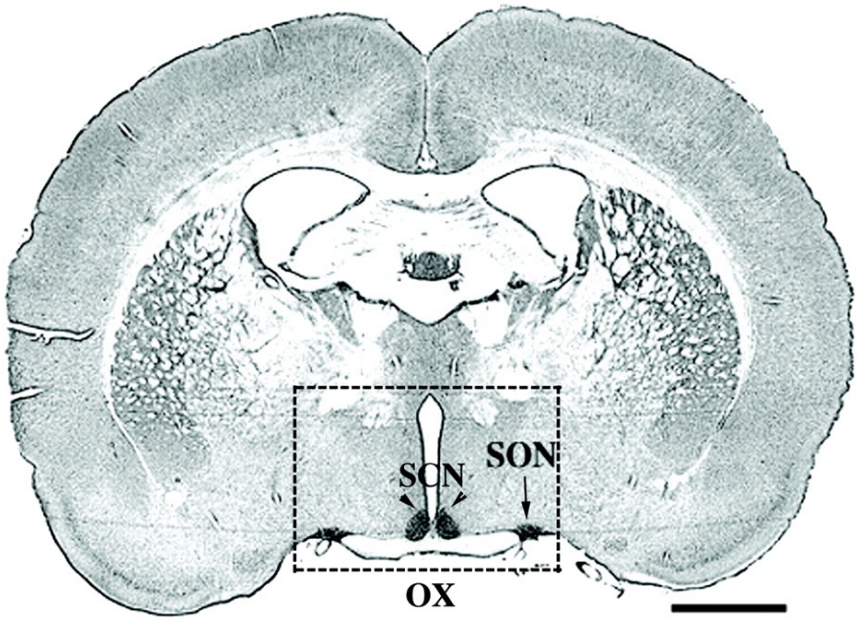

Figure 1.1: Illustration of a coronal section of the rat hypothalamus. Arrows indicate the MNCs in the SON and neurones in the suprachiasmatic nucleus (SCN) located above the optic chiasm (OX). Scale bar: 2 mm. The figure was copied from (Mutsuga, Shahar et al. 2004).

Altogether, the magnocellular nuclei may contain about 100 000 neurones in the human (Manaye, Lei et al. 2005) and approximately 10 000 in the rat (Rhodes, Morrell et al. 1981). The MNCs in the SON have typically one to three dendrites, and most of them course to the ventral glial lamina, from where they receive an afferent input (Stern and Armstrong 1998, Brown, Bains et al. 2013). A coronal section of MNCs in figure 1.2 shows immunologically identified AVP and OT cells in the SON and PVN. From the SON, the cells project their axons to the neurohypophysis, where the neuropeptides AVP

and OT are secreted in response to physiological stimulation (Hatton 1990). The MNCs in the PVN also contain cells that project to other brain regions, including central amygdala and other forebrain areas (Knobloch, Charlet et al. 2012, Brown, Bains et al. 2013). Both AVP and OT are synthesized in the SON and PVN cell bodies and are transported to the terminals by axonal transport. The terminals store vasopressin and oxytocin in dense-core vesicles prepared to be released directly into the blood system (Armstrong, Wang et al. 2010, Brown, Bains et al. 2013). Even though all the magnocellular cells are localized in the same nuclei, the production of the peptides is known to be specific for the magnocellular subtypes, and AVP and OT cells essentially synthesize either vasopressin or oxytocin (Armstrong 1995, Brown, Bains et al. 2013).

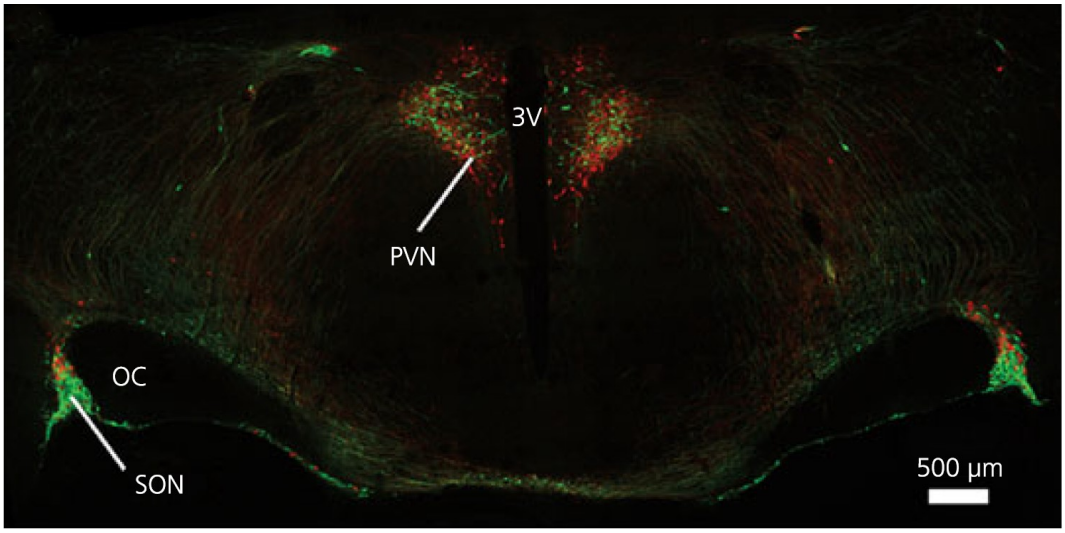

Figure 1.2: Detail of immunostained coronal section of the rat hypothalamus. Vasopressin cells are stained with fluorescent green, and oxytocin cells are stained with fluorescent red. The MNC cell bodies are principally located in the supraoptic nucleus (SON) and in the paraventricular nucleus (PVN). 3V stands for the third cerebral ventricle, OC for the optic chiasm. The figure was copied from (Brown, Bains et al. 2013).

1.2.2 Vasopressin and oxytocin secretion from MNCs

The schematic diagram in figure 1.3 illustrates the magnocellular neurosecretory system; the neuropeptides OT and AVP are transported by their axons from the SON to the neurohypophysis, where they are secreted directly into the blood from the axonal

terminals. The secretion of AVP and OT from the terminals occurs by exocytosis of dense-core vesicles in response to action potentials triggered in cell bodies in the SON or PVN and propagated down to the terminals in the posterior pituitary (Armstrong 2007). The MNC terminals themselves are not capable of sustaining intrinsic repetitive firing of action potentials, and so the secretion is principally determined by the action potentials initiated at the cell bodies in the SON or PVN (Cazalis, Dayanithi et al. 1985, Brown, Bains et al. 2013). The intensity of secretion largely depends not only on the frequency of action potential discharge but also on the firing pattern of neuronal activity, which can have irregular, phasic or tonic firing form (Cazalis, Dayanithi et al. 1985, MacGregor and Leng 2012) (see section 1.2.3 for details). Very importantly, the secretion occurs strictly via Ca^{2+}- regulated exocytosis (Komori, Tanaka et al. 2010) when a depolarization of axonal terminals causes the opening of voltage-gated Ca^{2+} channels (VGCCs), which in turn produces elevation of $[Ca^{2+}]_i$ and triggers the exocytotic process (Bourque, Kirkpatrick et al. 1998, Komori, Tanaka et al. 2010).

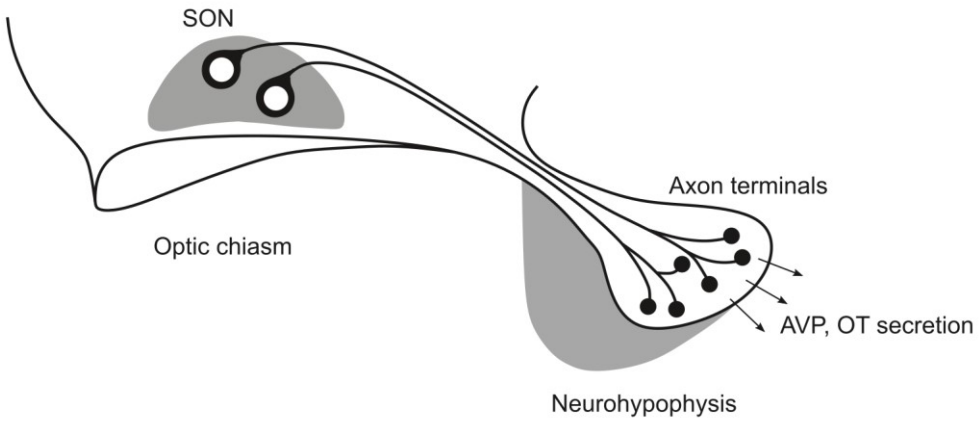

Figure 1.3: A schematic diagram of the magnocellular secretory system. The figure was adapted from (Fisher and Bourque 1996).

Secretion from the neurohypophysis into the blood circulation mediates the peripheral function of the peptides, however, the OT and AVP are also secreted within the SON from dendrites (Richard, Moos et al. 1997, Ludwig, Sabatier et al. 2002), where they function as autocrine or paracrine signals (Moos, Gouzenes et al. 1998, Ludwig, Sabatier et al. 2002). The somato-dendritic release of OT or AVP initiates signals that

are propagated via the activation of specific AVP and OT receptors expressed on the surface of the MNCs (Sabatier, Richard et al. 1998, Gouzenes, Sabatier et al. 1999, Sabatier, Shibuya et al. 2004). The activated AVP and OT receptors trigger an intracellular signalling pathway which causes an increase of cytosolic Ca^{2+} concentration (Dayanithi, Widmer et al. 1996). It is believed that in OT neurones, this increase in $[Ca^{2+}]_i$ results mainly from Ca^{2+} release from intracellular stores (Lambert, Dayanithi et al. 1994), whereas in AVP neurones, the $[Ca^{2+}]_i$ rise reflects both the Ca^{2+} influx through the voltage-gated Ca^{2+} channels and Ca^{2+} mobilization from the intracellular stores (Sabatier, Richard et al. 1997, Dayanithi, Sabatier et al. 2000). Participation of the somato-dendritic release as an autofeedback in the control of secretion as well as the determination of the intracellular signalling pathway is still a subject of discussion, and further investigation is needed (Dayanithi, Sabatier et al. 2000, MacGregor and Leng 2012).

1.2.3 Activity patterning

Both the AVP and OT neurone subtypes exhibit specific intrinsic electrical activities that are crucial for the efficient release of AVP and OT at the neurohypophysis (Cazalis, Dayanithi et al. 1985). The AVP subtype of MNCs exhibits a wide range of electrical activity patterns; in response to usual stimuli, such as an osmolality change, the AVP neurones display a silent, continuous or slow/irregular firing pattern, and particularly when facing specific physiological challenges, such as dehydration or haemorrhage, some of the neurones display a distinct “phasic” firing activity pattern (Armstrong 1995, Bourque, Kirkpatrick et al. 1998, Brown, Bains et al. 2013). The phasic pattern has been mainly associated with “high activity secretion state” (Cazalis, Dayanithi et al. 1985), however, it has been shown that AVP neurones commonly exhibit the whole range of activity patterns even under basal conditions (Armstrong 1995, MacGregor and Leng 2012). The activity patterns of AVP cells are illustrated in figure 1.5 (A–D). The phasic activity pattern, typical for AVP neurones (figure 1.5D), consists of bursts and interburst intervals each in the range of 20–40 seconds with essentially stochastic probability of burst termination or the next burst onset (Armstrong 1995). During the burst onset, neurones display clear frequency adaptation when, after achieving a maximum of about 25 spikes per second, the firing slows down to approximately 5–10 spikes per second (Brown 2004, Brown and Bourque 2006, Brown, Bains et al. 2013). Besides the phasic

activity, a continuous or tonic pattern of firing can be adapted by the AVP neurones (figure 1.5C). The mechanisms of switching between different patterns in AVP neurones are not yet completely understood (Armstrong 1995), however, it is hypothesized that the continuous pattern may be a transitional one between phasic and irregular patterns (Brown, Bains et al. 2013). This is supported by the fact that even the tonic spiking tends to be occasionally clustered to facilitate hormone release (Cazalis, Dayanithi et al. 1985). AVP neurones, in contrast to OT neurones, do not synchronize their firing pattern, and despite being exposed to the same physiological conditions, they display a wide range of activity patterns across the cell population (Scott, Bishop et al. 2009). Some of the cells fire no spontaneous spikes (silent), some fire spikes irregularly, some fire continuously, and some fire in a repetitive phasic pattern of bursts. Demands to AVP release are mediated via an afferent input on the level of individual neurones, while their response must still be coordinated to ensure the proper level of secretion. Thus, the secretion activity output of the population is characterized as the proportion of neurones that adapt the phasic pattern rather than as a "switch" of the whole population from a low-activity irregular firing pattern to the high-activity phasic firing pattern. This population-based regulatory mechanism has been shown to be more robust and efficient in terms of a sober distribution of a limited amount of the hormone during needful moments (MacGregor and Leng 2012). Taken together, as illustrated in figure 1.4, the release of AVP is a result of the integrated output of the whole population of AVP neurones, which in the end control the circulating concentration of vasopressin (MacGregor, Clayton et al. 2013).

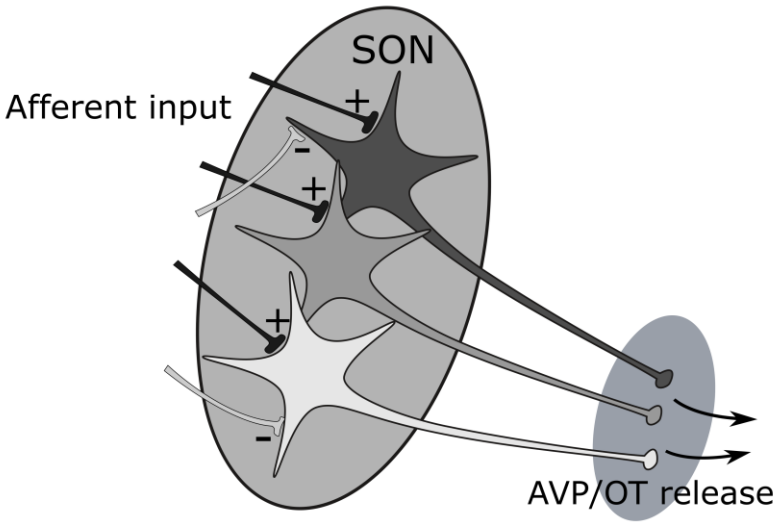

Figure 1.4: Afferent input of the magnocellular neurosecretory system. Osmosensitive cells in the brain generate electrical signals and relay them as afferent input to the SON. The MNCs in the SON respond by producing and secreting the vasopressin hormone. Importantly, the population of MNCs in the SON not only transmits the incoming signals to directly release the hormone, they must also coordinate their action over the population to prevent over- or under-response and depletion of limited amounts of vasopressin (Bourque and Oliet 1997).

Both OT and AVP neurones share similarities in their regulation mechanisms, but there are major differences between them. The firing rate of OT neurones under basal conditions is approximately 2–4 spikes/s, however, during parturition and suckling, the cells switch to high-frequency phasic firing that occurs every 5–10 min (Hatton and Wang 2008). In contrast to AVP neurones, the bursts in OT neurones are short, lasting only 1–2 s, but the action potential activity is more intense, often with firing rates of 50–100 spikes/s (figure 1.5E). A remarkable feature of the bursting pattern specific for OT neurones is that they are coordinated across the population of oxytocin MNCs located in two distinct bilateral nuclei (Belin, Moos et al. 1984, Belin and Moos 1986, Brown, Bains et al. 2013). The coordination among MNCs is required for the increased pulsatile release of oxytocin from the MNCs to control the rhythmic contractions of the uterus during parturition and contractions of the milk ducts for milk ejection (Lincoln and Wakerley 1975, Douglas, Scullion et al. 2001). Properties of the phasic firing pattern are described in detail in section 1.2.4.

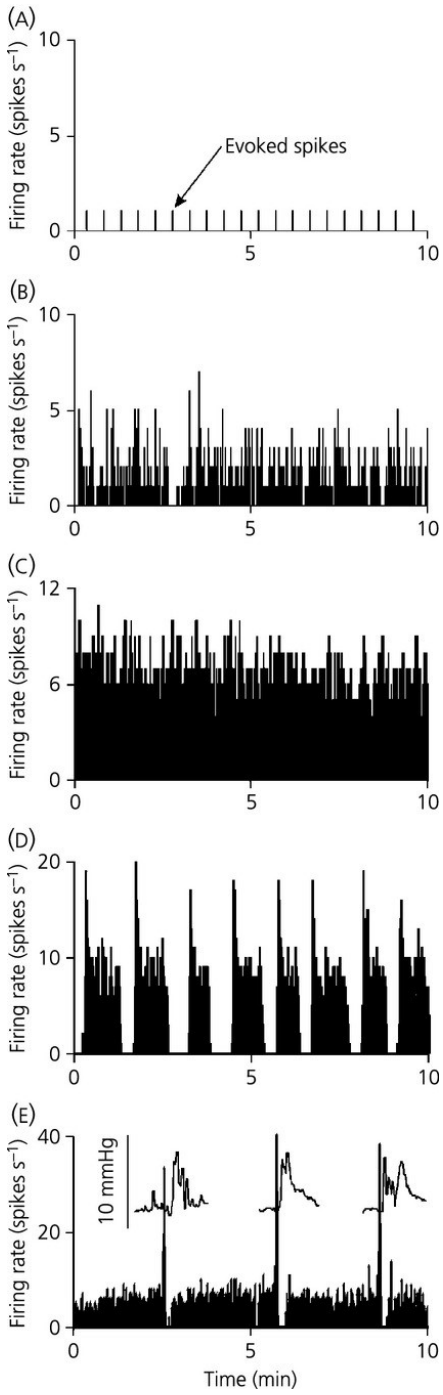

Figure 1.5: Firing patterns in magnocellular vasopressin (A–D) and oxytocin (E) cells in vivo. The spike rate records show individual examples of spontaneous activity (averaged in 1-s bins). Under basal conditions, AVP cells exhibit a range of activity patterns from silence (A), through irregular activity (B), to continuous activity (C) and phasic activity (D). In (A), action potentials were evoked in a silent MNC by electrical stimulation of the posterior pituitary gland every 30 s (evoked spikes). The recording in (E) is from an oxytocin MNC in an anesthetized rat being suckled during lactation and shows the typical high-frequency bursts evident in oxytocin MNCs during parturition and suckling. The insets in (E) show the intermammary pressure increase for milk ejection that follows each burst of activity in the oxytocin cells. The figure was copied from (Brown, Bains et al. 2013).

1.2.4 Phasic firing

Phasic firing has been studied extensively *in vivo* and *in vitro* in last decades (Bicknell, Brown et al. 1982, Andrew and Dudek 1984, Shibuya, Kabashima et al. 1998, Roper 2005). Although the overall activity of MNC population is a result of the integration of many cells that display silent, irregular, phasic or continuous firing under basal conditions, it is generally accepted that the distinct phasic activity is the most efficient firing pattern for secretion of AVP and OT from the posterior pituitary gland (Cazalis, Dayanithi et al. 1985). High-frequency action potentials are efficient at releasing the hormone because of an enhanced Ca^{2+} influx at the terminal. However, with continued activation and repetitive firing, fatigue turns up, strongly attenuating the amount of the released hormone. To avoid the fatigue, both cell types developed a phasic bursting pattern consisting of short periods of robust firing, interrupted with periods of relative quiescence. The phasic pattern maximizes hormone release, avoids release fatigue and allows recovery for the next batch of activity (Cazalis, Dayanithi et al. 1985, Roper, Callaway et al. 2004).

Oxytocin neurones display phasic activity in the form of short intense bursts of spikes during the birth and milk-ejection reflex (Viero, Shibuya et al. 2010). They fire typically at just a few spikes/s, and in response to the suckling stimulus, they suddenly discharge approximately 100 spikes in 2–3 s. The maximum discharge rate reaches up to 100 spikes/s within approximately 100 ms of the burst onset (Rossoni, Feng et al. 2008, Maicas Royo, Brown et al. 2016). As pregnancy and lactation are exceptional events, the OT neurones must undergo considerable changes in their morphological and physiological properties to produce such a dramatic change in their responsivity (Hatton 1990, Armstrong, Stern et al. 2002, Teruyama and Armstrong 2005). Studies using patch-clamp recording have demonstrated that the phasic pattern in both OT and AVP results from the activation and orchestration of several types of intrinsic afterpotential currents (Roper, Callaway et al. 2003). Changes in the intrinsic properties, specific to OT neurones during pregnancy, include an increase in the amplitude of the Ca^{2+}-dependent hyperpolarizing afterpotential (HAP) and a higher expression of the Ca^{2+}-dependent depolarizing afterpotential (DAP) (Armstrong, Stern et al. 2002, Teruyama and Armstrong 2005). The HAP itself is likely responsible for the “shape” of the milk-ejection burst and the manner in which it slows down after the peak of excitation (Roper, Callaway et al. 2003, Armstrong, Wang et al. 2010). These changes, which occur during late pregnancy, indicate

that OT neurones transform their intrinsic properties to be prepared for the increased activity demands during birth and lactation (Armstrong, Stern et al. 2002).

Contrary to the OT neurones, which display phasic activity only during pregnancy-related physiological conditions, AVP neurones are able to adapt the phasic pattern in acute response to hormone release demands (Verbalis, Baldwin et al. 1986). The pattern of phasic bursting in AVP cells is markedly different from the short bursts seen in the OT cells and is composed of bursts that last for tens of seconds to 1 min or more and that are separated by silences of a similar duration (Roper, Callaway et al. 2004). A typical record of phasic firing in AVP cells is shown in figure 1.5D. It has already been established that phasic activity results from an intrinsic mechanism supported by a continuous excitatory synaptic input. The combination of the intrinsic mechanism and the synaptic input has been shown to be essential for introducing and maintaining the phasic discharge in vasopressin MNCs *in vivo* (Brown, Bull et al. 2004, Armstrong, Wang et al. 2010). The intrinsic mechanism that generates the phasic activity in AVP neurones results from a complex set of afterpotentials (Roper, Callaway et al. 2003). Each afterpotential has a different amplitude and time course, which allows them to dominate the membrane potential at different times following each action potential. This is the key feature that enables the afterpotentials to summate over different timescales and to impact activity at different times over the course of bursts (Brown, Bains et al. 2013). Two different kinds of afterpotentials that follow each spike are involved in the burst: depolarizing afterpotential (DAP) and hyperpolarizing afterpotential (HAP). The HAP (figure 1.6A) follows each action potential and is induced by the activation of Ca^{2+}-dependent K^+ channels (Greffrath, Martin et al. 1998, Greffrath, Magerl et al. 2004). The DAPs are kinetically complex, slow (1–2 s) current afterpotentials (Roper, Callaway et al. 2003). The DAP is produced by spikes close in succession which in turn produce summation of the DAPs and generate a plateau potential that drives the burst duration (figure 1.6C). This feature of the time-dependent current summation is considered to be essential for producing phasic activity in AVP neurones (Andrew and Dudek 1983, Andrew and Dudek 1984, Armstrong, Wang et al. 2010). Importantly, in relation to Ca^{2+}, it has been shown that a special DAP subtype, the slow DAP (sDAP), also results from a voltage- and Ca^{2+}-dependent current (Li and Hatton 1997, Brown, Bains et al. 2013). Another long-lasting hyperpolarizing potential existing in the AVP cells is not activated by a single spike but requires a train of spikes to be fully developed. Such current (usually called after-hyperpolarizing potential, AHP) is responsible mainly for spike

frequency adaptation and for keeping cells silent during interburst periods (Roper, Callaway et al. 2004). A record of a typical AHP current developed after a train of spikes is shown in figure 1.6B. AHPs in AVP neurones are at least three: a large-amplitude fast after-hyperpolarization (fAHP) that lasts < 10 ms, a small-amplitude medium AHP (mAHP) that lasts several hundred ms and a very small-amplitude slow AHP (sAHP) that lasts several seconds (Kirkpatrick and Bourque 1996, Greffrath, Martin et al. 1998, Ghamari-Langroudi and Bourque 2004, Greffrath, Magerl et al. 2004, Brown, Bains et al. 2013).

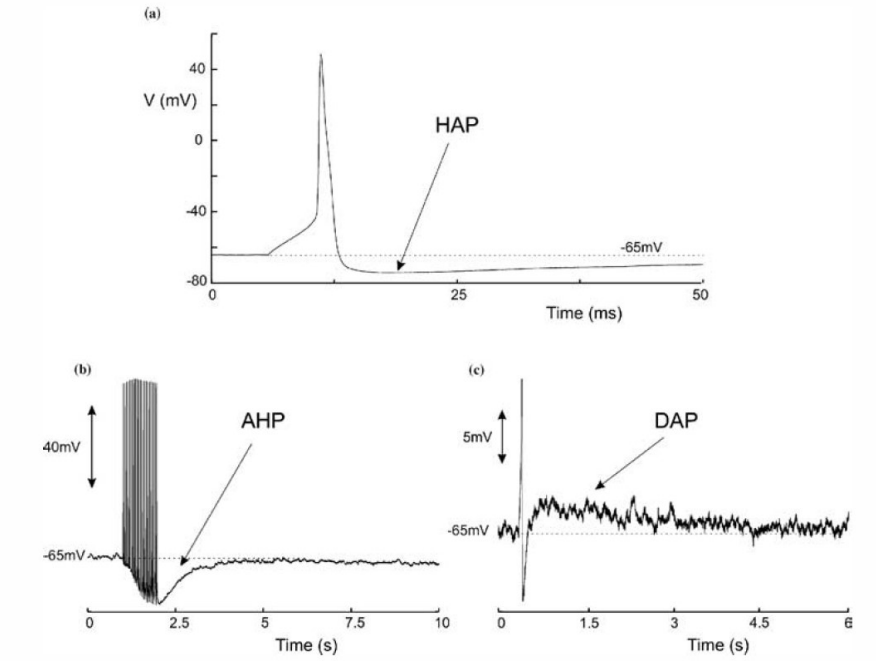

Figure 1.6: Spike afterpotentials in MNCs: (A) The hyperpolarizing afterpotential (HAP) follows each spike and lasts for 25–125 ms. (B) An after-hyperpolarizing potential (AHP) follows each spike train. It decays exponentially with τ ~ 500 ms and has a maximum amplitude of ~12.5 mV. (C) The depolarizing afterpotential (DAP) can last for several seconds and a single DAP can depolarize the cell by ~3 mV. The traces are taken from whole-cell (A, B) and sharp electrode (C) recordings in the slice and explant respectively. The figure was copied from (Roper, Callaway et al. 2003).

The medium-duration AHP (mAHP) (100–200 ms) is also Ca^{2+}-dependent and sensitive to apamin (Bourque and Brown 1987, Armstrong, Wang et al. 2010). The Ca^{2+}-dependency of the mAHP is specifically important in spike frequency adaptation in AVP neurones: summation of the mAHPs modulates the plateau potential and induces the

frequency adaptation over the first approximately 5–20 s of bursts (figure 1.5D). Blocking the mAHP with apamin suppresses spike frequency adaption at burst onset and also produces noticeable increases in interburst firing rates (Armstrong, Smith et al. 1994, Kirkpatrick and Bourque 1996, Armstrong, Wang et al. 2010). The Ca^{2+}-dependency and temporal overlapping of DAPs with HAPs and AHPs are together the crucial mechanisms needed to shape the phasic bursting in AVP cells (Roper, Callaway et al. 2003, Brown 2004, Armstrong, Wang et al. 2010).

In summary, the phasic activity pattern in MNCs has been intensively studied in the last two decades, and major underlying mechanisms have been proposed (Moos, Gouzenes et al. 1998, Roper, Callaway et al. 2003, Armstrong, Wang et al. 2010). Nevertheless, the mechanisms of burst termination and activity synchronization across the cell population have not yet been completely understood, although a role of somato-dendritic autocrine feedback has been proposed (Roper, Callaway et al. 2004, MacGregor and Leng 2012).

1.3 Calcium signalling

1.3.1 Intracellular Ca^{2+} signalling

Ca^{2+} is one of the most universal carriers of biological signals, controlling numerous cellular functions, including vesicular secretion, membrane excitability, muscle contraction, synaptic plasticity, gene transcription, programmed death, etc. (Berridge 1998). The most versatile aspect of Ca^{2+}, used for intracellular signalling, is a very wide time scale range, permitting to control multiple cellular processes. Cells can control exocytosis at synaptic endings within microseconds and muscle contraction in milliseconds, while at the other end of the scale, Ca^{2+} can operate over minutes to hours to control processes such as cell proliferation (Berridge 2012) or hormone secretion, as is the case in magnocellular neurones (Brethes, Dayanithi et al. 1987). Most cells need to maintain low resting concentration of Ca^{2+} in cytosol for a normal functioning of the Ca^{2+} signalling pathways. To achieve that, the cells are equipped with a kit of Ca^{2+} clearance mechanisms, which bring $[Ca^{2+}]_i$ to a resting level after elevation. These Ca^{2+} clearance mechanisms include Ca^{2+} pumps operating in both the plasmalemmal and the endoplasmic reticulum membrane, the plasmalemmal Na^+/Ca^{2+} exchanger and possibly the mitochondrial Ca^{2+} uptake (Berridge 2005, Komori, Tanaka et al. 2010). The main

mechanisms involved in maintaining the resting $[Ca^{2+}]_i$ level are illustrated in figure 1.1 Intracellular Ca^{2+} elevations are usually driven by Ca^{2+} influx from the extracellular space and Ca^{2+} release from intracellular stores that in turn generates Ca^{2+} intracellular signals (Bootman, Lipp et al. 2001).. The endoplasmic reticulum (ER), a prominent intracellular Ca^{2+} store, plays a major role in fast physiological signalling due to its ability to act as a rapid Ca^{2+} source. The concentration of Ca^{2+} stored in the ER ($[Ca^{2+}]_{ER}$) can easily achieve levels of 1000 times greater than those in the cytosol (Burdakov, Petersen et al. 2005).

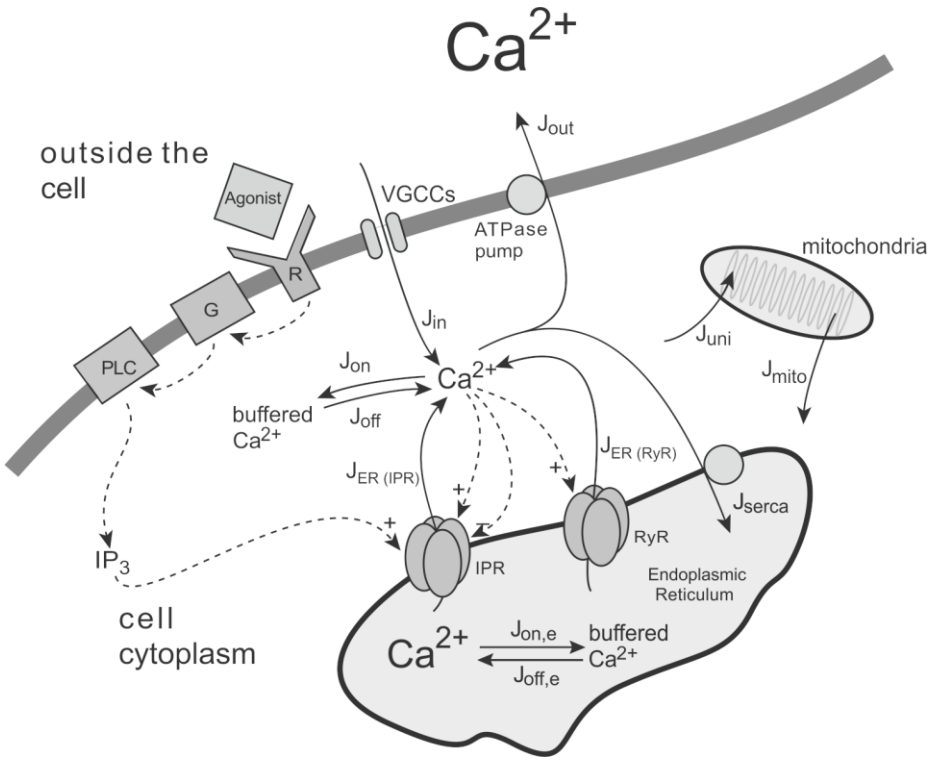

Figure 1.7: A diagram of major fluxes involved in the control of cytoplasmic Ca^{2+} concentration. Entry from the outside (J_{in}) is controlled by a variety of mechanism, mainly by VGCCs. Inside the cell, Ca^{2+} can be released from the endoplasmic reticulum (ER) through the IPR ($J_{er(IPR)}$) or RyR ($J_{er(RyR)}$), can be pumped from the cytoplasm into the ER (J_{serca}) or outside (J_{out}), can be taken up into (J_{uni}) or released from (J_{mito}) the mitochondria and can be bound to (J_{on}) or released from (J_{off}) Ca^{2+} buffers. The binding of an agonist to a cell membrane receptor (R) leads to the activation of a G-protein (G) and subsequent activation of phospholipase C (PLC). This activates an inositol trisphosphate ($InsP_3$) pathway. When $InsP_3$, which is free to diffuse through the cell cytoplasm, binds to an $InsP_3$ receptor (IPR) on the ER membrane, it causes the release of Ca^{2+} from the ER, and this

Ca^{2+} in turn modulates the open probability of the IPR and ryanodine receptors (RyR). The figure was adapted from (Keener and Sneyd 2009).

1.3.2 Voltage-gated Ca^{2+} channels

Voltage-gated Ca^{2+} channels (VGCCs) constitute the major Ca^{2+} entry pathway in excitable cells. VGCCs are heteromultimers composed of a pore-forming α1 subunit, β regulatory subunit and α2, γ and δ subunits (Catterall 2000). The channel structure contains S4 transmembrane segment of positively charged amino acids that are voltage-sensitive and are responsible for channel opening (Gueguinou, Chantome et al. 2014). Depending on electrophysiological and pharmacological criteria, the VGCCs have been classified into two major groups: high voltage-activated channels (HVA), which include L-, N-, P/Q- and R-type channels, and low voltage-activated channels (LVA), represented by T-type channels (Catterall 2011). VGCCs are further divided into three classes by their α1 subunits: Ca_v1, Ca_v2, Ca_v3.

The first class of VGCCs is L-type channels (Ca_v1) produce long-lasting Ca^{2+} currents and are generally considered to be HVA. They are pharmacologically identified by a strong sensitivity to the dihydropyridine class of drugs, which includes the nifedipine or nicardipine antagonists (Piedras-Rentería, Barrett et al. 2007). L-type Ca^{2+} channels are mainly responsible for calcium currents recorded in muscle and endocrine cells, where they initiate contraction and secretion, and require a strong depolarization for activation (Piedras-Rentería, Barrett et al. 2007).

The second class of VGCCs is Ca_v2 and includes P/Q-, N- and R-type Ca^{2+} channels. They are most prominent in neurones, and like the L-type Ca^{2+} channels, the Ca_v2 class belongs to HVA group. The N-type VGCCs are distinguished from the rest of the HVA channels by their intermediate voltage-dependency and faster inactivation when compared with the L-type (Catterall 2011). They are sensitive to the ω-conotoxin GVIA peptide (Tsien, Lipscombe et al. 1988). The P/Q-type channels are distinguished by their sensitivity to ω-agatoxin IVA with different affinities for the P- and Q-type respectively (Mintz, Adams et al. 1992, Catterall 2011). The last type of the Ca_v2 class, the R-type Ca^{2+} channel, is resistant to most specific organic and peptide channel blockers. In some cell types, they can be blocked by the SNX-482 peptide, a toxin isolated from tarantula venom (Newcomb, Szoke et al. 1998, Catterall 2011).

The third class of VGCCs is Ca_v3, represented by the LVA T-type channels. T-type channels activate at a very low voltage of about -70 mV, and their voltage-dependent inactivation is faster compared with other classes (Piedras-Rentería, Barrett et al. 2007). All the VGCCs classes and their specific antagonists are summarized in table 1.1.

Ca^{2+} current type	**α1 subunits**	**Specific blocker**	**Functions**
L	$Ca_v1.1$, $Ca_v1.2$, $Ca_v1.3$, $Ca_v1.4$	Dihydropyridine class (nifedipine, nicardipine)	Excitation-contraction coupling, endocrine secretion, cardiac pacemaking
N	$Ca_v2.1$	ω-conotoxin GVIA	Neurotransmitter release, dendritic Ca^{2+} transients
P/Q	$Ca_v2.2$	ω-agatoxin IVA	Neurotransmitter release, dendritic Ca^{2+} transients
R	$Ca_v2.3$	SNX-482	Neurotransmitter release, dendritic Ca^{2+} transients
T	$Ca_v3.1$, $Ca_v3.2$, $Ca_v3.3$	-No selective blocker for $Ca_v3.1$ and $Ca_v3.3$, -nickel and TTA-P2 with limited sensitivity for $Ca_v3.2$.	Pacemaking, repetitive firing

Table 1.1: Voltage-gated-Ca^{2+}-channel classification summary (Catterall 2011)

Multiple types of VGCCs are involved in the regulation of MNCs. Electrophysiological studies have found in the MNCs the expression of L-, N-, P/Q- and R-type Ca^{2+} currents, whereas the existence of the low voltage-activated T-type Ca^{2+} current is still unclear (Fisher and Bourque 1996, Foehring and Armstrong 1996, Dayanithi, Forostyak et al.

2012). In the nerve terminals of the neurohypophysis, the roles of L-, N- and P/Q-types in neuropeptide release have been identified (Wang, Dayanithi et al. 1997). The L- and N-type currents play equivalent roles in both vasopressin and oxytocin release from terminals, whereas the P/Q-type Ca^{2+} current is more prominent in the regulation of vasopressin (Wang, Dayanithi et al. 1999).

1.3.3 Calcium oscillations

Oscillations and waves of increased intracellular free calcium concentration ($[Ca^{2+}]_i$) are observed in a wide range of cell types, and although it is known that Ca^{2+} controls many cellular processes, the exact significance of Ca^{2+} oscillations is not completely understood (Thul, Bellamy et al. 2008). It is widely believed that the oscillations are frequency-encoded signals that allow a cell to use Ca^{2+} as a second messenger while avoiding the toxic effects of prolonged $[Ca^{2+}]_i$ elevation (Keener and Sneyd 2009, Parkash and Asotra 2012). However, there are still relatively few examples where the signal carried by a Ca^{2+} oscillation has been clearly decoded (Keener and Sneyd 2009). In the spatial domain, the spreading of a Ca^{2+} oscillation as a Ca^{2+} wave provides a mechanism by which the regulatory signal can be distributed throughout the cell. The extension of Ca^{2+} waves to adjacent cells by intercellular communication provides a mechanism by which multicellular systems can coordinate their function and responses to stimuli (Sneyd, Keizer et al. 1995). In general, two types of $[Ca^{2+}]_i$ oscillations can be recognized, depending on the main source of Ca^{2+}, which can come either from intracellular stores, such as the endoplasmic reticulum (ER), or from the extracellular space via plasmalemmal Ca^{2+} entry (Sneyd, Keizer et al. 1995). The ER-driven $[Ca^{2+}]_i$ oscillations result from the periodic release of Ca^{2+} usually mediated by the inositol 1,4,5-trisphosphate ($InsP_3$) receptor or the ryanodine receptor/Ca^{2+} release channel, whereas the extracellular Ca^{2+}-driven oscillations require Ca^{2+} entry through plasmalemmal channels or exchangers (Sneyd, Keizer et al. 1995). The overall processes that may contribute to internal Ca^{2+} signalling are shown schematically in figure 1.7. These include the influx of Ca^{2+} ions into the cell (J_{in}) through ion channels or by cotransporters and the transport of Ca^{2+} ions out of the cell (J_{out}) by Ca^{2+} pumps in the cell membrane. Other sources of cytosolic Ca^{2+} are internal Ca^{2+} stores, such as the endoplasmic reticulum (ER) and the mitochondria. The Ca^{2+} handling properties of the ER and of the other internal compartments vary in different regions of the cell, but details are

not known. Therefore, it is often necessary to simplify the Ca^{2+} handling properties of the internal stores, which is achieved by considering only a single ER-like compartment occupying a proportional part of the cell volume (Sneyd, Keizer et al. 1995). The filling of the ER with Ca^{2+} and the release of Ca^{2+} from the ER are in figure 1.7 represented by the J_{serca} and J_{er} fluxes. In addition to these fluxes, the buffering of free Ca^{2+} by cytoplasmic macromolecules, indicated in figure 1.7 as J_{on}/J_{off}, is another important component in the regulation of Ca^{2+} concentrations.

Several previous studies have periodically observed that some isolated AVP and OT neurones displayed spontaneous $[Ca^{2+}]_i$ oscillations under normal experimental conditions *in vitro* (Lambert, Dayanithi et al. 1994, Dayanithi, Widmer et al. 1996, Gouzenes, Sabatier et al. 1999, Dayanithi, Sabatier et al. 2000, Dayanithi, Forostyak et al. 2012). However, neither the identity nor the characteristics of these oscillatory neurones, nor the physiological properties of these $[Ca^{2+}]_i$ oscillations were clearly established. Studying the basic functional properties of spontaneous $[Ca^{2+}]_i$ oscillations and their physiological importance in MNCs is one of the major aims of this work.

1.4 Calcium imaging

Our understanding of the mechanisms of Ca^{2+} signalling and its ubiquitous role in cellular processes has rapidly grown in past decades. This growth has only been possible with the introduction of calcium imaging techniques and development of calcium-specific fluorescent dyes together with digital imaging microscopy (Knot, Laher et al. 2005). These recent techniques have allowed for the complex spatial and temporal dynamics of intracellular changes in $[Ca^{2+}]$ to be fully appreciated (Sneyd, Keizer et al. 1995). The most commonly used Ca^{2+} indicator is Fura-2, which belongs to the group of ratiometric indicators and was designed and described by Grynkiewicz (Grynkiewicz, Poenie et al. 1985). Other widely used Ca^{2+} indicators are Indo-1, Quin2, Calcium Green and many others, each specifically designed for particular applications (Grynkiewicz, Poenie et al. 1985, Lambert 2005). These indicators differ mainly by their affinity to Ca^{2+}, predetermining their use in a given range of measured Ca^{2+} concentrations. The Fura-2 dye, used in this work, is a dual excitation Ca^{2+} indicator with a broad excitation spectrum in a low Ca^{2+} concentration between 300 nm and 400 nm (figure 1.8). The excitation peak is

directly dependent on the Ca^{2+} concentration: in low Ca^{2+} concentration, the peak is approximately at 370 nm; but with higher Ca^{2+} concentration, the excitation peak rises in intensity and shifts more into short wavelengths of the UV spectrum. The emission of the dye has its peak approximately at 510 nm, far from the excitation wavelength range allowing an efficient separation by optical low pass filters. Consequently, when the dye is excited by UV light at 340 nm (f_{340}) and its emission is measured at 510 nm, Ca^{2+} binding will produce an increase in measured fluorescence intensity. Contrary Ca^{2+} binding will be observed as a decrease in fluorescent signal when the fluorescence is measured at 510 nm (the same value), but the dye is excited at 380 nm (f_{380}). Finally, when the dye is repetitively excited at 340 and 380 nm in quick succession, a ratio of the respective emission signals can be used to measure the cytoplasmic Ca^{2+} concentration (Grynkiewicz, Poenie et al. 1985, Lambert 2005). The ratiometric approach is generally independent of dye concentration (in the working range of the dye), which gives it an advantage over single-wavelength indicators (Lambert 2005).

Ca^{2+} indicators are usually charged molecules that cannot easily penetrate the cell membrane. Therefore, they can be either loaded into the cell directly by a sharp electrode (Grienberger and Konnerth 2012), or alternatively, they can be introduced into the cell in an esterified form of the indicator (Grynkiewicz, Poenie et al. 1985). An advantage is that the esterified form of the dye can easily diffuse into the cell, where intracellular esterases remove the ester group and leave the charged indicator trapped inside the cell (Lambert 2005). For more advanced Ca^{2+} imaging, it is also possible to introduce the indicator into intracellular compartments to monitor [Ca^{2+}] at subcellular localization. It can provide useful information about Ca^{2+} processes in specific organelles, such as the ER or mitochondria. Nevertheless, an information about cytoplasmatic concentration of the cell is lost, because introducing dyes into inner compartments usually requires permeabilization of the cell membrane. (Verkhratsky and Shmigol 1996, Lambert 2005).

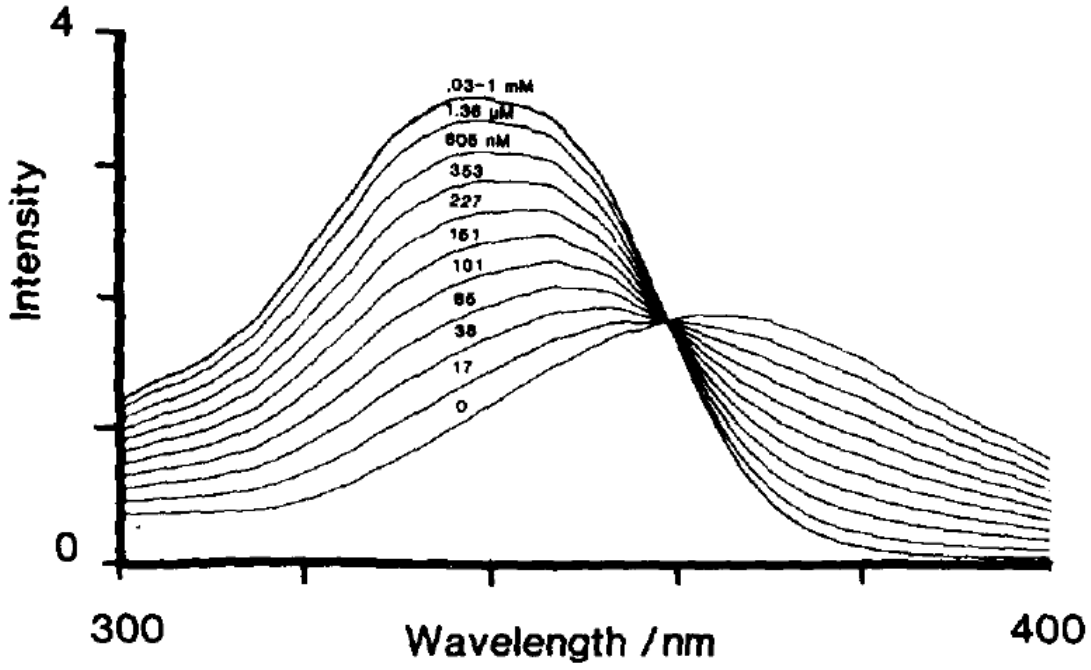

Figure 1.8: Excitation spectra of the Ca^{2+}-sensitive dye Fura-2 AM. The figure was copied from (Grynkiewicz, Poenie et al. 1985).

The signals of Ca^{2+}-sensitive fluorescent indicators must be processed with advanced imaging instrumentation. This includes technologically different approaches, like video imaging, high-speed confocal microscopy or two-photon microscopy. The exceptionally high signal intensity of the fluorescent probes in combination with these emerging technologies enables real-time fluorescence observations of biological processes at the single-cell level (Grienberger and Konnerth 2012). A major advance was achieved with the introduction of two-photon microscopy, which revolutionized the field of *in vivo* calcium imaging and is now used worldwide in many laboratories (Helmchen and Denk 2005).

A typical Ca^{2+} imaging setup used for imaging in the nervous system includes a light sensing device, light source, microscope, wavelength switching device and a digitizing device. The light sensing device is usually a photodetector, CCD or CMOS chip; the light source is usually a mercury or xenon lamp, or nowadays a laser or LED source (Grienberger and Konnerth 2012). The light sensing device is usually attached to the microscope and combined with an appropriate light source for the excitation of the calcium indicator dyes. Switching between two excitation wavelengths, as needed for ratiometric

dyes, can be performed rapidly by using a filter wheel, monochromatic light source or another convenient wavelength switching approach. The excitation and emission light are usually separated by a dichroic mirror that is located within the microscope (Yao 2005).

To make the measured fluorescence intensity more physiologically valid, the signal can be expressed as a concentration of Ca^{2+} in nM, provided that a calibration of the fluorescent indicator is performed. The calibration must be done specifically for the combination of used fluorescent dye, optic pathway, sample dishes, light source, temperature, etc. If any of the mentioned parts of the setup is changed, the calibration cannot be considered as valid anymore and needs to be performed again under the new conditions (Lambert 2005).

For the ratiometric dye Fura-2, the $[Ca^{2+}]_i$ in nM can be calculated from intensities obtained on indicator emission wavelengths f_{340} and f_{380} according to the Grynkiewicz equation (Grynkiewicz, Poenie et al. 1985):

$$[Ca^{2+}]_i = K_d \left(\frac{R - R_{min}}{R_{max} - R}\right) \beta,$$

where R is the measured ratio f_{340}/f_{380} and K_d is the dissociation constant for Fura-2, which is in usual experimental conditions (37°C, Ph = 7, 1 mM Mg^{2+} solution) equal to 224 nM (Kao 1994). R_{min}, R_{max} and β are the parameters that must be obtained by calibration. The parameter R_{min} is the limiting value of the ratio R when all of the indicator is in the Ca^{2+}-free form, and the R_{max} is the limiting value of the R when the indicator is saturated with Ca^{2+}. The factor β is a scaling parameter and represents a ratio of the measured fluorescence intensity when all of the indicator is Ca^{2+}-free to the intensity measured when all of the indicator is Ca^{2+}-bound; both measurements are taken at f_{340} as β = (f_{340} in 0 Ca^{2+}) / (f_{380} in saturating 39.8 μM Ca^{2+} buffer).

2 Aims of the thesis

2.1 Main goals

Secretion of AVP and OT from terminals is controlled by Ca^{2+}-dependent exocytosis driven by the arrival of action potentials initiated at the magnocellular cell bodies in the SON (Armstrong 1995). The direct control of the release from the terminals is well known, but less established is the central regulatory function in the SON (Armstrong, Wang et al. 2010, Dayanithi, Forostyak et al. 2012). In this study, we particularly focus on Ca^{2+} dynamics of MNCs, which may be the key element in the central regulation of hormone release. The motivation to study Ca^{2+} dynamics in detail lies in the distinct crosstalk between $[Ca^{2+}]_i$, electrical activity and dendritic release in the SON. The elevation of $[Ca^{2+}]_i$ in MNCs occurs as a response to extracellular input via a depolarization stimulus or in the form of spontaneous $[Ca^{2+}]_i$ oscillations. Although these spontaneous $[Ca^{2+}]_i$ oscillations have been observed in previous studies (Lambert, Dayanithi et al. 1994, Dayanithi, Widmer et al. 1996, Gouzenes, Sabatier et al. 1999, Dayanithi, Sabatier et al. 2000), the characteristics, the origin and the physiological properties of the oscillations needs to be established. In this work, we will explore the principal Ca^{2+} mechanisms of both spontaneous and induced origin, and we will investigate their role in the physiology of the central regulation of hormone release. Here we propose the main aims of the thesis, structured into three sections. This structure will be followed throughout the whole thesis.

2.1.1 Mechanisms of spontaneous $[Ca^{2+}]_i$ oscillations

In general, two types of $[Ca^{2+}]_i$ oscillations can be recognized, depending on the main source of Ca^{2+}: its release from intracellular stores, such as the endoplasmic reticulum (ER), or plasmalemmal Ca^{2+} entry (Sneyd, Keizer et al. 1995). The ER-driven $[Ca^{2+}]_i$ oscillations result from the periodic release of Ca^{2+} mediated by the inositol 1,4,5-trisphosphate ($InsP_3$) receptor or the ryanodine receptor/Ca^{2+} release channel (RyR), whereas the extracellular Ca^{2+}-driven oscillations require Ca^{2+} entry through the plasmatic membrane. In this part, we will determine the main source of Ca^{2+} and identify mechanisms that underlie the spontaneous Ca^{2+} dynamics and are necessary for exhibiting the oscillations in MNCs.

2.1.2 Mechanisms of induced $[Ca^{2+}]_i$ elevations

Influx of extracellular Ca^{2+} occurs typically in response to electrical activity which depolarizes the membrane, opens voltage-gated-calcium-channels (VGCCs) and provides the influx of extracellular Ca^{2+} (Armstrong 1995). By this principle, the $[Ca^{2+}]_i$ is elevated in phasically firing magnocellular neurones (Roper, Callaway et al. 2003, Roper, Callaway et al. 2004). The depolarization-induced Ca^{2+} influx is often accompanied by the release of Ca^{2+} from intracellular stores via Ca^{2+}-induced-Ca^{2+}-release (CICR) (Verkhratsky and Shmigol 1996). To fully understand the hormone release regulation, the role of intracellular Ca^{2+} stores in modulation of the membrane potential needs to be investigated. In this part, we want to study calcium dynamics induced by depolarization and evaluate the contribution of intracellular Ca^{2+} stores. We will use a combination of experimental and computational approaches to decompose measured intracellular high K^+-induced $[Ca^{2+}]_i$ elevations into separate Ca^{2+} fluxes and investigate how intracellular Ca^{2+} stores influence the depolarization-induced Ca^{2+} elevations.

2.1.3 Physiological role of $[Ca^{2+}]_i$ oscillations in MNCs

Spontaneous $[Ca^{2+}]_i$ oscillations have been shown to exist in both AVP and OT neurones, yet the physiological purpose of these $[Ca^{2+}]_i$ oscillations has not been characterized. The role of the oscillations in the central regulation of hormone release was not tested either. The main role of MNCs is the regulation of important processes, such as lactation, osmosensitivity, water balance, etc. In this part, we will develop approaches that will be used to study $[Ca^{2+}]_i$ oscillations in physiological states of dehydration or lactation and in conditions where we expose oscillating cells to extracellular confrontations mimicking physiological stimuli similar to osmotic change. Beside that, we want to search for possible differences between the cell subtypes (AVP and OT), and lastly, we will study the possible auto-regulatory mechanism of AVP receptors via dendritic release by exposing cells to their agonists and evaluating the effect of this action on the oscillations.

3 Methods

3.1 Animals

Adult male Wistar rats (wild type) and three different homozygous transgenic rats were used in this study: 1) transgenic rats expressing an arginine vasopressin-enhanced green fluorescent protein (AVP-eGFP) (Katoh, Fujihara et al. 2011), 2) transgenic male or female or lactating rats expressing an oxytocin-monomeric red fluorescent protein 1 (OT-mRFP1) (Katoh, Fujihara et al. 2011), 3) double transgenic (expressing both markers) to visualize AVP and OT neurones (Dayanithi, Forostyak et al. 2012). A homozygous line was identified among the offspring of two heterozygous parents by finding exclusively heterozygous progeny from the mating of transgenic offspring rat with a wild-type Wistar rat. The double transgenic AVP-eGFP/OT-mRFP line was generated by mating homozygous AVP-eGFP with OT-mRFP transgenic rats. All transgenic rats used in the study were screened by polymerase chain reaction analysis of genomic DNA extracted from rat ear or tail biopsies before breeding and use in the experiments. The PCR was performed using the oligonucleotide primers (AVP-eGFP: sense sequence, 5'-CAC CAT CTT CTT CAA GGA CGA C-3'; antisense sequence, 5'-ATG ATA TAG ACG TTG TGG CTG TTG T-3'; and OT-mRFP: sense sequence, 5'-GTG AAG CAC CCC GCC GAC AT-3'; antisense sequence, 5'- TGC ATT ACG GGG CCG TCG GA-3'). The animals (weighting 150 - 300 g; 4 - 8 weeks old) were bred and housed at 22˚C, 12:12 h light/dark cycle (lights on 07:00-19:00 h), with food and drinking water available ad libitum. In experiments with dehydration three groups of animals were prepared; in the control group, the rats were maintained under normal conditions (see above) with unlimited access to water, in two other groups, the animals were deprived of water for 3-day and 5-day, respectively, otherwise under normal laboratory conditions at 22˚C, 12:12 h light/dark cycle. In experiment with lactation all animals (transgenic OT-mRFP1 3 to 6-day-lactating rats; weighted about 500g; 12 - 16 weeks old) were bred and housed at 22˚C under normal laboratory conditions (12:12 h light/dark cycle, lights on 07:00 - 19:00h) with food and drinking water available *ad libitum*.

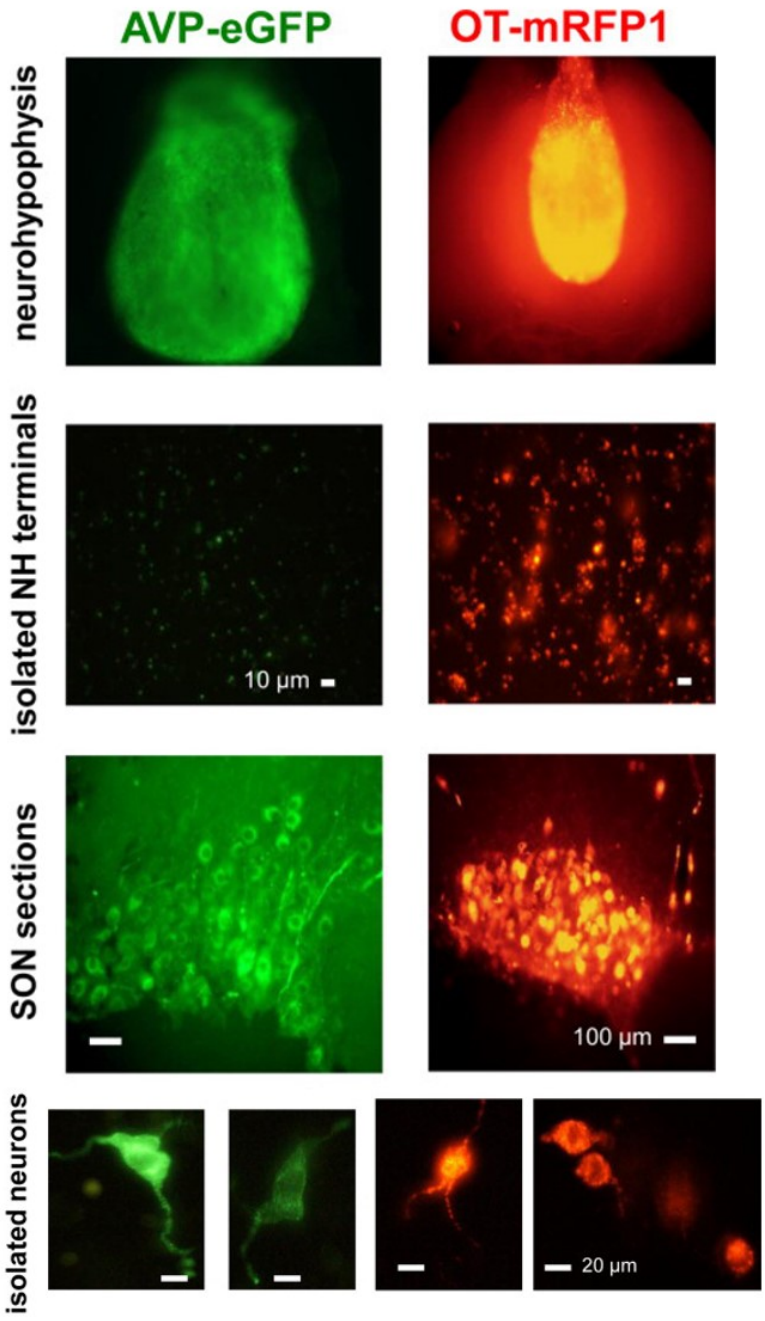

Figure 3.1: Visualization of fluorescent neurohypophysis (NH) and isolated magnocellular SON neurones from the transgenic rats for AVP-enhanced green fluorescent protein (eGFP) fusion transgene (AVP-eGFP), oxytocin-monomeric red fluorescent protein 1 (mRFP1) fusion transgene. The figure adapted from (Dayanithi, Forostyak et al. 2012).

3.1 Drugs and solutions

All experiments were done in HEPES-buffered normal Locke's solution (NL; in mM: 140 NaCl, 5 KCl, 2$CaCl_2$, 1 $MgCl_2$, 10 glucose, 10 HEPES, pH was adjusted to 7.25 with Tris; the osmolarity[1] was 298–300 mOsmol/l; temperature 37◦ C). In some experiments the $CaCl_2$ concentration in the NL was 200 nM or 500 nM. Unless otherwise indicated, all chemicals were purchased from Sigma–Aldrich (St. Louis, USA) or from Alomone labs (Jerusalem, Israel). Fura 2-AM, TTA-P2, nicardipine, KB-R7943, thapsigargin, CPA, CCCP, ryanodine and 4AP were dissolved in DMSO. The hypotonic solution was prepared by reducing the appropriate Na^+ concentration and in the hypertonic solution the osmolarity was increased by adding mannitol. In experiments where extracellular Ca^{2+} was removed, EGTA (100 nM) was added to NL with no added $CaCl_2$. To obtain Na^+ free solutions the NaCl was replaced with NMDG-Cl and osmolarity adjusted to 295–300 mOsmol/l. TTX and apamin were dissolved in acetic acid as suggested by the suppliers. Other drugs were dissolved in total ion-free distilled H_2O (EMD Millipore Corporation, Germany) and all stock solutions and buffers were prepared using this total-ion-free H_2O.

3.2 Isolation of magnocellular neurones

For each experiment, animals were sacrificed by decapitation after deep anaesthesia with 5% isoflurane for 5 min, the brain was rapidly removed, and SON was dissected. SON neurones were acutely dissociated by enzymatic and mechanical treatments. In brief, the blocks (1 mm × 0.5 mm× 0.5 mm) of SON tissues were dissected and enzymatically dissociated by incubation for 30 min in oxygenated HEPES-buffered normal Locke's solution (NL); with pH adjusted to 7.25; the osmolarity was 298–300 mOsmol/l; temperature 37°C) supplemented with 1 mg/ml deoxyribonuclease I, 0.5 mg/ml proteases X, and 0.5 mg/ml protease XIV. After incubation, tissues were washed with NL and triturated gently using a Gilson-Pipetman (1 ml) with a polypropylene white pipette-tip to isolate the SON cells. The cells were plated onto 22 mm glass Petri dishes (WillCo Wells-Amsterdam, The Netherlands). All experiments were performed in accordance with the

[1] For preparations of solutions, osmolarity was used as the measure of solute concentration as at concentrations near 300 mOsmol/l, the osmolarity and osmolality are very similar.

European Communities Council Directive of 24 November 1986 (86/609/EEC) regarding the use of animals in research and were approved by the Ethics Committee of the Institute of Experimental Medicine, Academy of Sciences of the Czech Republic, Prague, Czech Republic (project experiment license #CZ 205/2010 revised in 2013).

3.3 $[Ca^{2+}]_i$ measurements and drug applications.

The $[Ca^{2+}]_i$ measurements using a fluorescent probe Fura-2 AM were performed on isolated single neurones from WT or from transgenic (AVP-eGFP-positive and OT-mRFP-positive) rats. Neurones with minimal diameter size of 10 µm and persisted dendrites were randomly chosen for $[Ca^{2+}]_i$ measurements. Video imaging of $[Ca^{2+}]_i$ was performed using an inverted microscope Axio Observer D1 (Zeiss) equipped with a CCD camera and Lambda-DG4 fast rotating wheel illumination system (Sutter Instrument, Novato, USA) for double excitation at 340 nm and 380 nm. The fluorescence intensity of the Fura-2 emission was measured at 510 nm as a ratio of signals obtained after excitation at 340 and 380 nm. The microscope was also equipped with GFP and RFP filters for observing cells bearing fluorescent markers. To estimate the range of change in absolute $[Ca^{2+}]_i$ in nM concentration a calibration following the Grynkiewicz method (Grynkiewicz, Poenie et al. 1985) was performed. The calibration produced R_{min} = 0.2, R_{max} = 7.2, $f340_{max}/f380_{min}$ = 7.7, dissociation constant for Fura-2 at 37 ◦C Kd = 224 nM. An estimation of $[Ca^{2+}]_i$ was then calculated in MATLAB from the f340/f380 ratio using the Grynkiewicz equation (Grynkiewicz, Poenie et al. 1985). During the measurement cells were continuously perfused with NL solution at 37◦ C. Solutions were exchanged using a multiple capillary perfusion system, for details see (Komori, Tanaka et al. 2010, Kortus, Srinivasan et al. 2016, Kortus, Srinivasan et al. 2016). Briefly, the 200 µm inner diameter capillary tubing was placed close to the tested cell (<500 µm). Solutions were applied through a temperature controlled (set at 37◦C) device, applied through a computer controlled multichannel peristaltic pump (REGLO ICC, Ismatec) using tubing with 0.64 mm inner diameter. Each tubing was fed by a reservoir 20 cm above the bath and connected to a temperature control device (Model: TC-324B; Harvard-Paris, France). The solutions flow rate was set to 500 µl/min for inlet and about 5% slower for outlet. Additional out-let tubing was placed close to the edge of the dish for maintaining 2 mm solution (about 750 µl volume) level in the dish through-out the measurement period. This setup (illustrated in figure 3.2) ascertains

local perfusion with linear flow without any mechanical disturbance and minimal fluctuation of solution level.

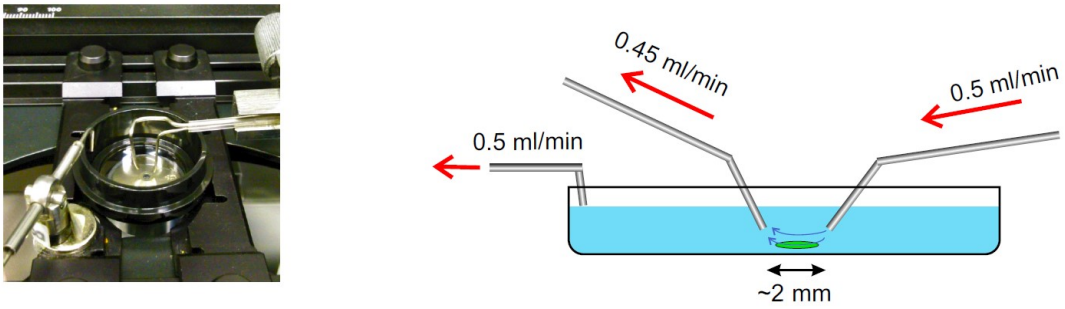

Figure 3.2: Drugs delivery by continuous perfusion ensuring local and fast exchange of solutions.

3.4 $[Ca^{2+}]_i$ oscillation analyses

3.4.1 Data pre-processing

Each $[Ca^{2+}]_i$ trace was first classified as oscillating or non-oscillating. Changes in $[Ca^{2+}]_i$ with an amplitude of at least 30 nM that occurred within 120 sec (or faster) were considered to be "Ca^{2+} events", and traces or parts of traces in which such events occurred repeatedly were considered to be $[Ca^{2+}]_i$ oscillations. The threshold of 30 nM was used as a value sufficient for excluding the interference of the noise inherent in the signal. Only $[Ca^{2+}]_i$ traces with sustained oscillations lasting for at least 10 minutes were included in further analysis. Traces with strong trend or obvious artefacts were removed from the data set. To reduce noise, all data were filtered by a 2^{nd}-order Butterworth low-pass filter with a cut-off frequency of 0.5 Hz (with filter coefficients estimated by the MATLAB function *butter* and filtration performed by *filtfilt*). MATLAB 2015a and its Statistics, Machine Learning, and Signal Processing toolboxes were employed in all numerical procedures.

3.4.2 Data analysis and statistical evaluation

Four basic parameters were computed for each individual trace or its analysed segment: the $[Ca^{2+}]_i$ baseline, the mean $[Ca^{2+}]_i$ level, the standard deviation of the trace, and the skewness of the $[Ca^{2+}]_i$ values. These parameters were computed separately for each trace segment

corresponding to a defined physiological condition (for example, application of AVP or change of extracellular osmolarity). Only trace segments longer than 300 sec were considered. An example of such evaluation is shown in figure 3.3. The $[Ca^{2+}]_i$ baseline c_B was estimated as the mean of the 20 smallest $[Ca^{2+}]_i$ values in each trace or trace segment. The mean $[Ca^{2+}]_i$ level was calculated as the average of all $[Ca^{2+}]_i$ values. I.e., $\bar{c} = \frac{1}{N}\sum_{k=1}^{N} c_k$, where N is the number of $[Ca^{2+}]_i$ samples in the trace segment and c_k are the sample values. The standard deviation SD_{Ca} was computed as the square root of the variance of $[Ca^{2+}]_i$ values within the trace segment. I.e., $SD_{Ca} = \sqrt{Var}$, where $Var = \frac{1}{N}\sum_{k=1}^{N}(c_k - \bar{c})^2$. The parameter SD_{Ca} quantifies the spread of the $[Ca^{2+}]_i$ values within the trace. The asymmetry of this spread is quantified by the distribution skewness γ, defined as

$$\gamma = \frac{\mu_3}{(SD_{Ca})^3} ,$$

where $\mu_3 = \frac{1}{N}\sum_{k=1}^{N}(c_k - \bar{c})^3$ is the third central moment of the distribution of $[Ca^{2+}]_i$ values. For a symmetric distribution (such as the normal distribution), $\gamma = 0$, while for an exponential distribution, $\gamma = 2$. Positive or negative values of γ indicate a distribution skewed to the right or to the left, respectively (figure 4.17). Differences between the trace segments were evaluated based on the four trace parameters defined above. For each parameter, the difference of its value before and after drug application was calculated for each cell trace (example in figure 3.3). This difference was then averaged over the cells in the given group, and the paired t-test was used to determine if the difference was statistically significant. The p-values reported in Results represent the significance level for rejecting the null hypothesis of zero difference. The MATLAB function *ttest* was used. In figures displaying data fitted by a linear approximation, least-squares fitting was performed using the MATLAB function *polyfit*. As a measure of goodness of the linear fit we use the coefficient of determination R^2 calculated as

$$R^2 = 1 - \frac{\sum_{k=1}^{N}(c_k - c_k')^2}{\sum_{k=1}^{N}(c_k - \bar{c})^2} ,$$

Where c_k denotes the measured $[Ca^{2+}]_i$ values and c_k' the values estimated by the linear approximation. In all $[Ca^{2+}]_i$ trace figures, the bars above the trace denote an application of

test substances. Unless otherwise indicated specifically, the data are presented as mean values ± SEM (n = the number of observations).

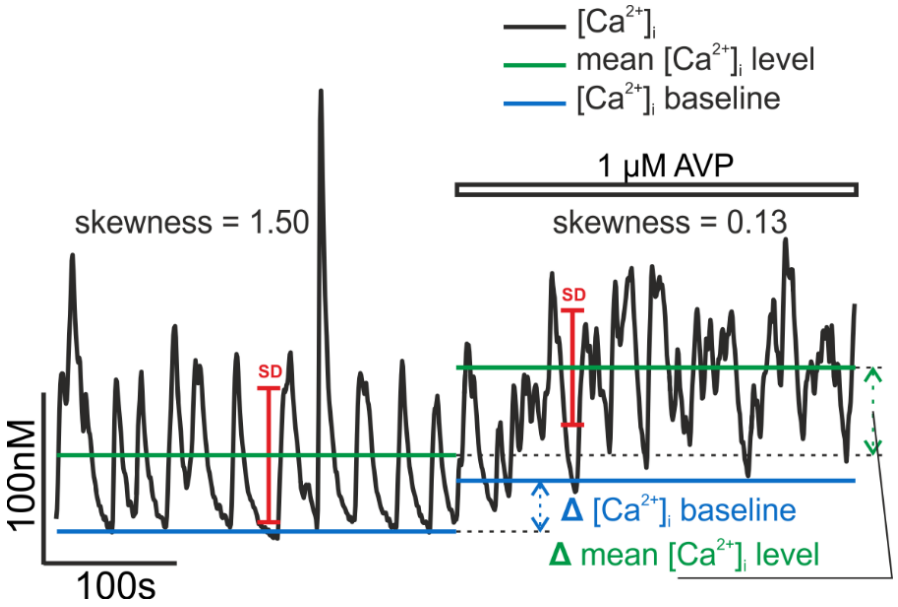

Figure 3.3: Example of evaluation of $[Ca^{2+}]_i$ oscillations. For both segments of the recording (300 s in NL buffer and 300 s with added 1 µM AVP), four basic parameters are evaluated: the $[Ca^{2+}]_i$ baseline, the mean $[Ca^{2+}]_i$ level, the standard deviation of the trace, and the skewness of the $[Ca^{2+}]_i$ distribution(for details, see methods, section 3.4.2). The difference in parameter values is shown graphically for the $[Ca^{2+}]_i$ baseline and the mean $[Ca^{2+}]_i$ level.

3.5 Analysis of depolarization-induced $[Ca^{2+}]_i$ responses

Ca^{2+} imaging permits to measure the intracellular Ca^{2+} concentration with a high temporal resolution, however, the measurements lack the information about individual fluxes, as they are integrated into the overall changes of Ca^{2+} concentration in cytosol. For our purpose, we designed an approach where the combination of several experimental protocols and mathematical post-processing permits us to evaluate the individual Ca^{2+} fluxes, even though only the overall $[Ca^{2+}]_i$ changes were actually measured during the experiment.

3.5.1 Pharmacological manipulation of CICR

To obtain experimental data suitable for the mathematical separation of the fluxes, we measure responses to the same depolarization stimulus in different situations, when one or more of the possible fluxes are pharmacologically eliminated. For the pharmacological manipulation of Ca^{2+} fluxes, we apply several approaches that are well-proven and applicable to MNCs (Sasaki, Dayanithi et al. 2005, Komori, Tanaka et al. 2010). As a depolarization stimulus, we use 50 mM K^+ NL buffer extracellularly applied for certain duration. The 50 mM K^+ concentration was chosen as a commonly used stimulus to mimic membrane depolarization and as a concentration that ensures the involvement of all the studied Ca^{2+} fluxes (Komori, Tanaka et al. 2010, Lemos, Ortiz-Miranda et al. 2012). In typical measurement, 50 mM K^+ induces $[Ca^{2+}]_i$ elevation from a resting baseline of ~100 nM to 600-800 nM $[Ca^{2+}]_i$ peak concentration. Coming back to the resting concentration usually takes about 5–10 min (Wang, Dayanithi et al. 1997, Komori, Tanaka et al. 2010).

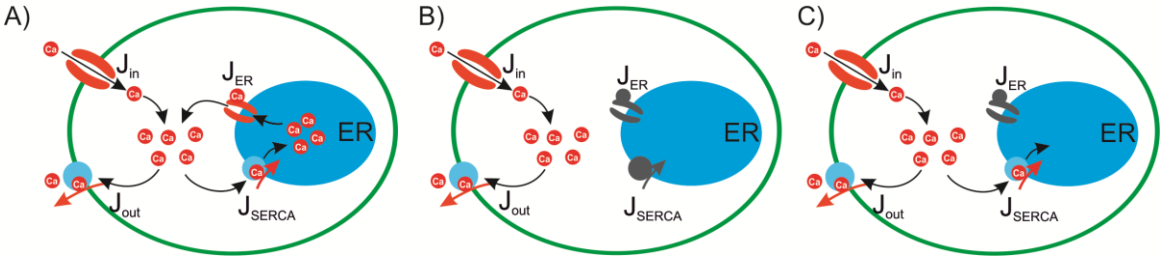

Figure 3.4: A schematic diagram of net Ca^{2+} fluxes across the plasmatic membrane (J_{in} and J_{out}) and across the intracellular membrane of the ER (J_{er} and J_{serca}) in three different situations. (A) Normal conditions: all the displayed Ca^{2+} fluxes are involved in the changes of $[Ca^{2+}]_i$. (B) Both fluxes across the membrane of the ER are suppressed: only the fluxes across the plasmatic membrane are involved. C) The Ca^{2+} flux from the ER to cytosol is eliminated by depletion of Ca^{2+} stored in the ER; no additional Ca^{2+} comes from the ER, while J_{serca} remains untouched and actively transports Ca^{2+} from cytosol and stores it in the ER.

The following three experimental protocols were designed with the aim to induce cells into the three different modes illustrated in figure 3.4 by a pharmacological suppression of one or more Ca^{2+} fluxes. The main principle of these experimental protocols

is exposing neurones to two K^+-induced depolarizations, the first being a control exposure and the second an exposure after the treatment supressing specific Ca^{2+} fluxes.

Protocol A) Normal conditions, all potential Ca^{2+} fluxes functioning

This protocol aims to record typical K^+-induced responses in normal conditions with all the Ca^{2+} fluxes functioning. The situation is schematically illustrated in figure 3.4A, and the drug applications are illustrated in a representative trace in figure 3.5A. First, a control 50 mM K^+ depolarization stimulus is applied for a duration of 60 seconds and is repeated again after 17 minutes with no additional treatments. The 17-minute break ensures enough time for the neurone to recover and reach the resting $[Ca^{2+}]_i$ level. Sufficient time between two depolarizations is also required for drug applications in other protocols. In-between the two exposures, the cell is bathed in NL buffer containing 3 mM GABA to prevent spontaneous Ca^{2+} oscillations that often occur in MNCs (Kortus, Srinivasan et al. 2016). In this case, all fluxes are functioning during both responses, and the representative trace (figure 3.5A) shows a typical K^+-induced biphasic elevation in $[Ca^{2+}]_i$ consisting of a rapid overshoot to a level of ~800 nM, followed by a slow decay to a plateau.

Protocol B) Inhibition of the ER Ca^{2+} fluxes

In this protocol, ER-targeting drugs are used as a tool to exclude the intracellular Ca^{2+} fluxes and record the K^+-induced response driven only by the extracellular Ca^{2+}. The situation is illustrated in figure 3.4B, and the drug application sequence is illustrated in a representative trace in figure 3.5B. First, the neurone is exposed to control 50 mM K^+ for 60 s, as in protocol A. After a sufficient break for the cell to recover and reach its baseline concentration, a combination of CPA (a potent reversible inhibitor of the ER SERCA pumps) and caffeine (ER Ca^{2+} mobilizer) is applied in the absence of the extracellular Ca^{2+} to effectively release Ca^{2+} stored in the ER. To clearly observe and confirm the effect of CPA and caffeine, the 0 Ca^{2+} buffer precedes the application of 10 mM caffeine and 10 uM CPA. In this sequence, the $[Ca^{2+}]_i$ elevation in 0 Ca^{2+} condition confirms that the caffeine and CPA has reached the ER, and the store is being depleted. After that, the solution is switched back to the normal 2 mM Ca^{2+} NL buffer, and suddenly (in about 10 s), the second 50 mM K^+ is being applied again for 60 seconds. This step prevents the influence of the rapid switching from 0 to 2 mM Ca^{2+} on the subsequent response to K^+. Note that while the caffeine was being added just for 5 minutes to induce the Ca^{2+} release from the ER and was removed before the second K^+ exposure, the CPA, as a partially reversible blocker, was

present for the rest of the experiment to prevent a re-accumulation of Ca^{2+} in the ER during the depolarization. Using only CPA without caffeine for the depletion of the ER was found to be inefficient and did not guarantee an effective depletion of the ER. The most efficient depletion of the ER was achieved with CPA combined with caffeine applied in 0 Ca^{2+} buffer, as described above.

Protocol C) Supressing the intracellular Ca^{2+} release

This protocol aims to supress the release of Ca^{2+} from the ER via the CICR mechanism during the depolarization stimulus. The ER is depleted before the response to K^+-induced depolarization is recorded, while the SERCA pump remains fully functioning. To achieve that, we use the same drug application sequence as in protocol B, but without using the SERCA blocker CPA. The situation is illustrated in figure 3.4C, and the drug application sequence is illustrated in a representative trace in figure 3.5C. In this protocol, we expect that the depleted ER will not serve as an additional source of Ca^{2+}, but on the contrary, the preserved function of the SERCA pump will remove part of the incoming extracellular Ca^{2+} and store it in the ER. This should cause a significant attenuation of the response, as it is presented in a representative trace in figure 3.5C, where the second response to K^+ reaches a much lower amplitude, compared with the first control response.

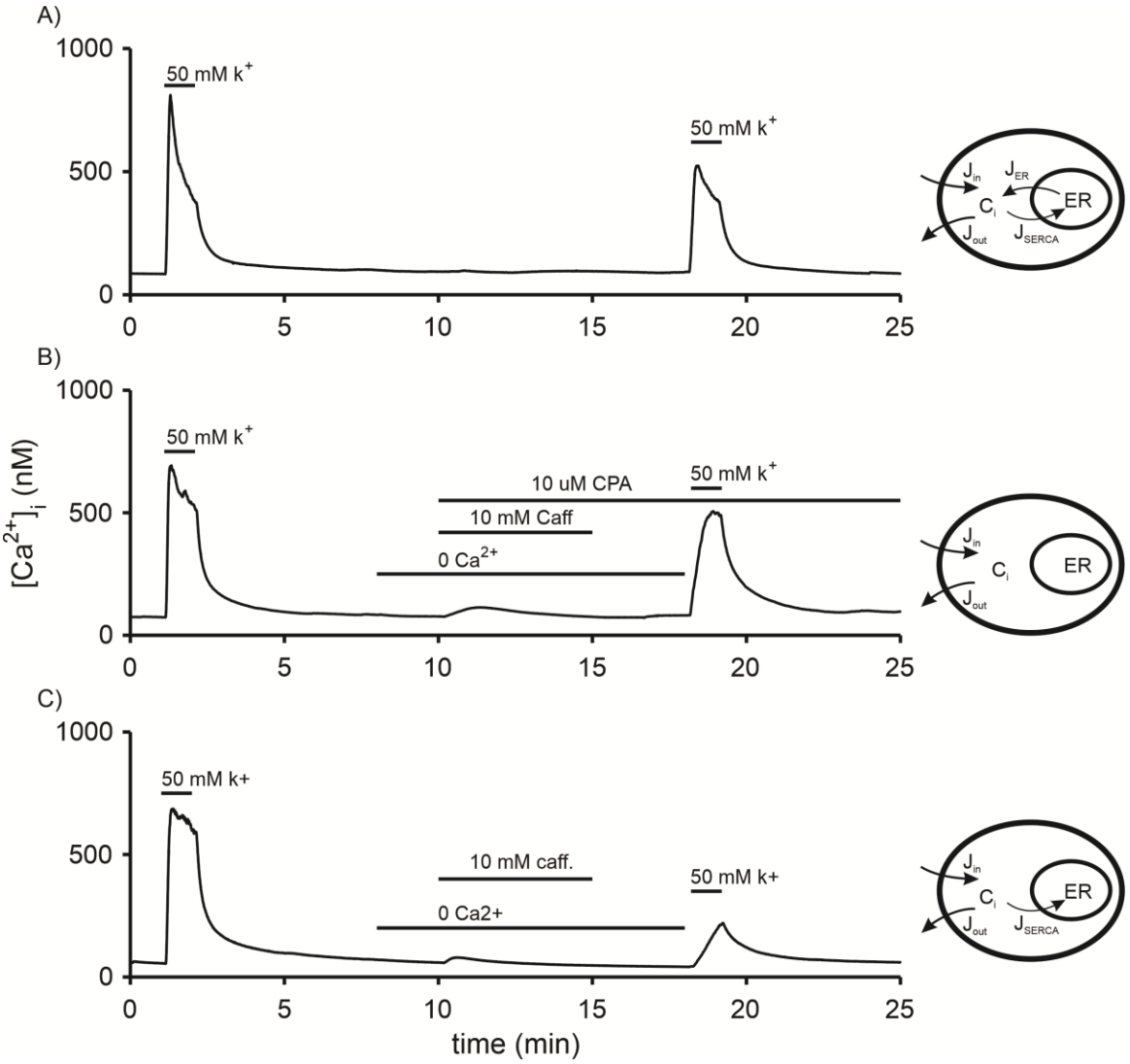

Figure 3.5: Representative $[Ca^{2+}]_i$ traces illustrating three experimental protocols used to pharmacologically manipulate Ca^{2+} fluxes involved in depolarization-induced responses. The bar labels indicate drug applications. In all the three protocols, cells are exposed to two 50 mM K^+ for 60 seconds with the following modifications: A) A trace representing control conditions: 50 mM K^+ is applied two times for 60 seconds with no other treatment in between. B) Before the second exposure to 50 mM K^+, the cell is first bathed in a low-Ca^{2+} solution for 10 minutes; 10 uM CPA and 10 mM caffeine are added into the low-Ca^{2+} solution for 5 minutes in order to deplete Ca^{2+} stores and block the SERCA pump. Just before the second 50 K^+ exposure (10s), the solution is switched back to the normal 2 mM Ca^{2+} NL buffer. Note that while caffeine was present only for 5 minutes, the CPA remained present till the end of the protocol to prevent Ca^{2+} re-uptake into the ER via the SERCA pump. C) The last protocol followed the same drug application sequence as the protocol in panel B with the only exception that no CPA was added before the second 50 K^+ exposure.

3.5.2 Mathematical estimation of Ca^{2+} fluxes

Depolarization-induced $[Ca^{2+}]_i$ response obtained from Ca^{2+} imaging represents overall changes in $[Ca^{2+}]_i$ resulting from multiple Ca^{2+} fluxes combined in the measured signal. To separate the overall changes into the individual fluxes, we introduce an estimation procedure consisting of several steps. We first assume that the cytoplasmic Ca^{2+} concentration (c_i)[2] during the depolarization-induced response is governed by four general fluxes: J_{in} – a depolarization-induced influx, J_{out} – a clearance outflux from cytosol to the extracellular space, J_{er} – CICR-driven release of Ca^{2+} from the ER and J_{serca} – a SERCA pump-driven uptake of Ca^{2+} from cytosol to the ER. This simplification into four major fluxes is often used for mathematical modelling of the Ca^{2+} dynamics in excitable cells (Sneyd, Tsaneva-Atanasova et al. 2004, Keener and Sneyd 2009). Equation 1 describes the rate of total Ca^{2+} transport by the respective fluxes:

$$dc_i/dt(t) = J_{in}(t) + J_{er}(t) - J_{serca}(t) - J_{out}(t). \qquad [eq.\ 1]$$

The cytosolic concentration c_i and its rate of change c_i/dt are the quantities directly known from the Ca^{2+} imaging, whereas the individual components are unknown. The fluxes from eq. 1 are schematically illustrated in figure 3.6 with the arrows indicating their preferred flow orientations.

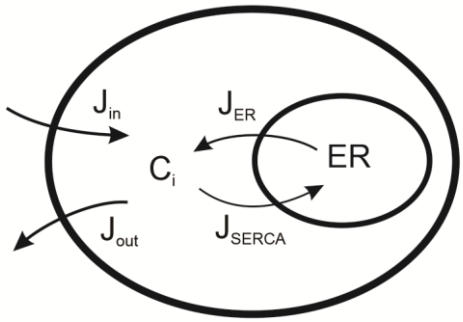

Figure 3.6: A schematic diagram of the four major Ca^{2+} fluxes responsible for dynamic changes of the intracellular Ca^{2+} concentration c_i

[2] In equations and analysis, the abbreviation c_i stands for the intracellular Ca^{2+} concentration ($[Ca^{2+}]_i$).

All the fluxes in eq. 1 are expressed as a function of time, however, it is widely accepted that the flux J_{out} responsible for the removal of Ca^{2+} from cytosol is strongly dependent on the intracellular Ca^{2+} concentration c_i (Sneyd, Tsaneva-Atanasova et al. 2004, Lee, Ho et al. 2009, MacGregor and Leng 2012). For further steps, we consider that the J_{out} is a sum of plasma membrane pumps and exchangers and is dependent only on the instantaneous calcium concentration (c_i) and so can be expressed as the function $J_{out}(c_i)$. Similarly as the J_{out}, the ER uptake flux J_{serca} is considered to be strongly modulated by both the cytoplasmic Ca^{2+} concentration and by the luminal Ca^{2+} concentration in the ER (Sneyd, Tsaneva-Atanasova et al. 2004, Keener and Sneyd 2009). However, the dependency is not described and confirmed in literature as well as for the J_{out}, and the lack of knowledge of the instantaneous Ca^{2+} concentration in the ER makes it difficult to incorporate the dependency into analyses. Therefore, for J_{serca}, we accept an estimation of the net exchange of Ca^{2+} between the ER and cytosol, which provides a valuable information about the inward/outward net flux in time domain.

The fluxes J_{er} and J_{serca} in eq. 1 are unknown, however, they can be omitted if the measured responses are obtained under the condition where these fluxes are inhibited and can be considered as equal to zero. An experimental protocol that supresses the ER Ca^{2+} fluxes J_{serca} and J_{er} was introduced in methods as protocol B (section 3.5.1). This protocol brings the cell into the condition where the ER is depleted and contains optimally no free Ca^{2+} ions to be released, and the SERCA pump is simultaneously pharmacologically inhibited by its specific blocker CPA. In such situation, we assume that the $[Ca^{2+}]_i$ changes during the depolarization-induced response are governed solely by the depolarization-induced influx J_{in} and by the opposite removal flux J_{out} (figure 3.4). Considering that the J_{out} depends only on the instantaneous calcium concentration (c_i), as described above, the eq. 1 is reduced into a simplified version:

$$dc_i/dt(t) = J_{in}(t) - J_{out}(c_i). \qquad \text{[eq. 2]}$$

Flux J_{in} in eq. 2 is generally unknown, however, it is directly controlled by exposure to K^+-induced depolarization. In resting conditions (no depolarization), J_{in} may have a non-zero value that is compensated by non-zero J_{out}, which in overall results in zero net Ca^{2+} flux and sets the resting Ca^{2+} concentration. For our purpose, we define the J_{in} and J_{out} values in resting conditions as zero baseline, and any changes from the baseline will be expressed as non-zero positive or negative values. During depolarization, the J_{in} switches

to a positive non-zero value and c_i rises. If no other processes are involved, the c_i rises until the J_{out} compensates the non-zero flux J_{in}, and a new equilibrium is settled. When the depolarization is removed, the flux J_{in} switches back to zero value, and the c_i starts to decline due to the suddenly dominating J_{out} flux. A hypothetical evolution of the c_i and the J_{in} and J_{out} fluxes during the depolarization are illustrated in figure 3.7. Note that the curves for J_{in} and J_{out} are negligibly shifted on the rate scale to distinguish the overlapping parts.

Most importantly, during the declining period (after ending the depolarization stimulus and before re-establishing the resting level of c_i), the J_{out} is the only remaining active flux out of the four general fluxes defined in eq. 1. It reduces eq. 1 into the simple form $dc_i/dt(t) = -J_{out}(c_i)$ and permits us to estimate the rates of Ca^{2+} clearance by fitting an exponential curve to the declining part of $c_i(t)$. By plotting the fitted curve as a rate against c_i, we establish the clearance function as the $[Ca^{2+}]_i$-dependent flux $J_{out}(c_i)$. For details about the estimation of the clearance function, see section 3.5.3.

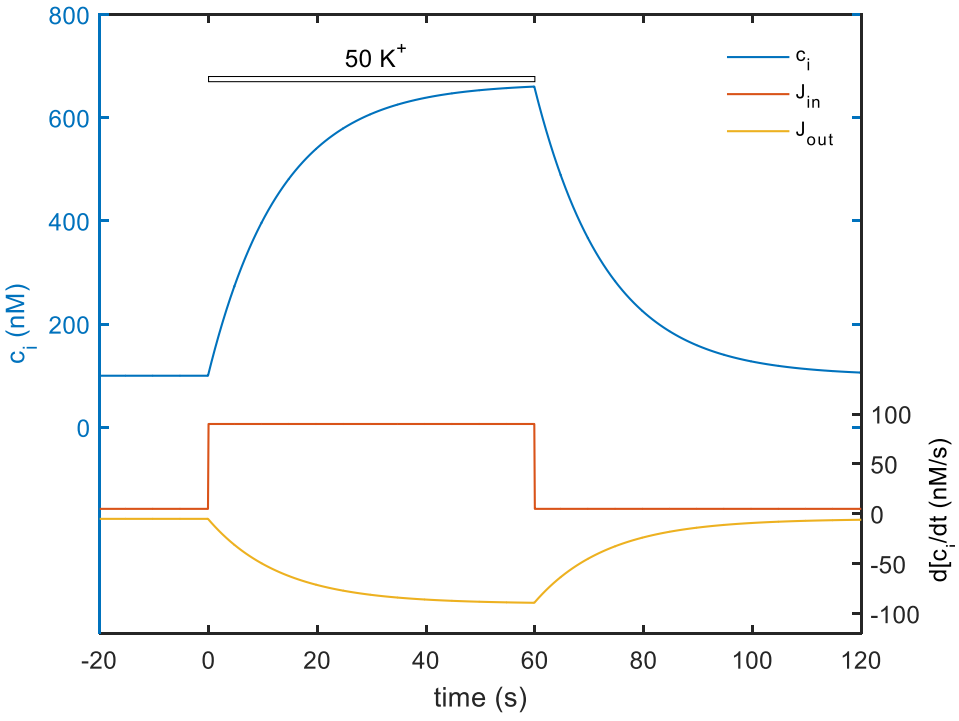

Figure 3.7: An illustrative example of a hypothetical evolution of Ca^{2+} fluxes during the depolarization-induced Ca^{2+} response in condition with supressed intracellular fluxes. The blue line represents an intracellular Ca^{2+} concentration (c_i) elevated by high K^+-induced depolarization. When intracellular fluxes are supressed, the elevation is driven by re-establishing of a new equilibrium between remaining fluxes J_{in} and J_{out}. The curves for J_{in}

(red) and J_{out} (yellow) are vertically shifted from zero baseline to distinguish overlapping parts.

Now, if the clearance function is known, the rate $J_{out}(c_i)$ in eq. 2 can be calculated for each time point of the measured $dc_i(t)/dt$ to obtain the clearance rate in time domain as $J_{out}(t)$. Using eq. 2, the calcium influx rate $J_{in}(t)$ during the depolarization-induced response can be calculated by subtracting the $J_{out}(t)$ from the measured rate $dc_i/dt(t)$.

The above-described estimation of the J_{out} and J_{in} fluxes is for a response obtained under conditions with a blocked ER, following the experimental protocol B (figure 3.5B). The response with the blocked ER, however, preceded a control response with no ER-targeting treatment (figure 3.5B). In this control response, the $dc_i/dt(t)$ is governed by all the four fluxes described in eq. 1. Based on the earlier consideration that the J_{out} is a function of c_i, the already estimated clearance function can be reused to calculate the $J_{out}(t)$ flux also for the control response. Similarly, we consider $J_{in}(t)$, which is in both conditions (control, blocked ER) induced by the same depolarization stimulus, to be identical in both cases. Using these assumptions, we can subtract the $J_{in}(t)$ and J_{out} fluxes (known from the response with the blocked ER) from the control response $dc_i/dt(t)$. This step reduces eq. 1 to a form describing the net Ca^{2+} exchange across the ER membrane $\Delta J_{er}(t)$:

$$dc_i/dt(t) = J_{er}(t) - J_{serca}(t) = \Delta J_{er}(t). \quad \text{[eq. 3]}$$

In other words, after subtracting the fluxes estimated from the response with the blocked ER, the remaining $[Ca^{2+}]_i$ changes must represent the net ER fluxes. This approach is, of course, suitable for cells where the ER Ca^{2+} exchange dominates over the other intracellular Ca^{2+} fluxes, which were omitted in eq. 1. Such fluxes could be a mitochondrial Ca^{2+} transport, high affinity intracellular Ca^{2+} buffers or other organelles. Establishing the net Ca^{2+} flux across the ER membrane does not give us a full description of the individual J_{er} and J_{serca} fluxes, but it provides us with valuable information at the moments when the flux into the ER overcomes the outcome and vice versa.

3.5.3 Estimation of a clearance function

The approach introduced in the previous section 3.5.2 requires a knowledge of the J_{out} flux as a function of $[Ca^{2+}]_i$. To acquire that, we estimate the rates of Ca^{2+} clearance by fitting a double-exponential curve to the decline of $[Ca^{2+}]_i$ of the K^+-induced response immediately

following the K^+ removal. The K^+-induced response must be elicited in a condition with inhibited intracellular fluxes of the endoplasmic reticulum. For that purpose, the experimental protocol B, introduced in section 3.5.1, was employed. The clearance function $J_{out}(c_i)$ is then obtained as a curve fitting the measured dc_i/dt vs. $[Ca^{2+}]i$. The fitting of the exponential decay was estimated by the MATLAB (edition 2015b) function *nlinfit* of the Curve fitting toolbox. Examples of the fitted decay and obtained clearance function are presented in figure 4.10 (section 4.2.4). Using double-exponential fitting is a commonly utilized approach in studies of Ca^{2+} clearance mechanisms (Fierro, DiPolo et al. 1998, Lee, Ho et al. 2009, Scullin and Partridge 2010). Our approach supposes that the fitted decay obtained in the ER-blocked condition represents the overall sum of plasmalemmal clearance mechanisms plasmatic-membrane-Ca^{2+}-ATPase (PMCA) and Na^+/Ca^{2+} exchanger (NCX).

4 Results

4.1 Mechanisms of $[Ca^{2+}]_i$ oscillations in magnocellular neurones

In this section, we analysed spontaneous $[Ca^{2+}]_i$ oscillations in isolated rat magnocellular neurones of the supraoptic nucleus using an extensive battery of specific pharmacological tools to propose the possible mechanisms driving these oscillations. The results presented in this section were published in (Kortus, Srinivasan et al. 2016) and are available in full form in appendix B.I.

4.1.1 Removal of external Ca^{2+} inhibits $[Ca^{2+}]_i$ oscillations

To probe the necessity if extracellular Ca^{2+}, we lowered its concentration during continuous measurement of $[Ca^{2+}]_i$ oscillations in isolated MNCs. Removal of extracellular Ca^{2+} led to an immediate cessation of spontaneous $[Ca^{2+}]$i oscillations in all tested neurones (n = 9; figure 4.1A). After extracellular Ca^{2+} removal the basal $[Ca^{2+}]_i$ of 133 ± 14 nM started to decline until it reached a low steady state level of 32 ± 6 nM in about 3 min. Inhibition of $[Ca^{2+}]_i$ oscillations by removal of external Ca^{2+} was reversible and the oscillations (as well as basal $[Ca^{2+}]_i$) were restored rapidly after switching perfusion back to the normal extracellular solution (figure 4.1A). The $[Ca^{2+}]_i$ oscillations still persisted when external Ca^{2+} was lowered from 2 mM to 500 nM (n = 6) or to 200 nM (n = 4), but no oscillations were observed at external Ca^{2+} concentration of 100 nM (n = 5).

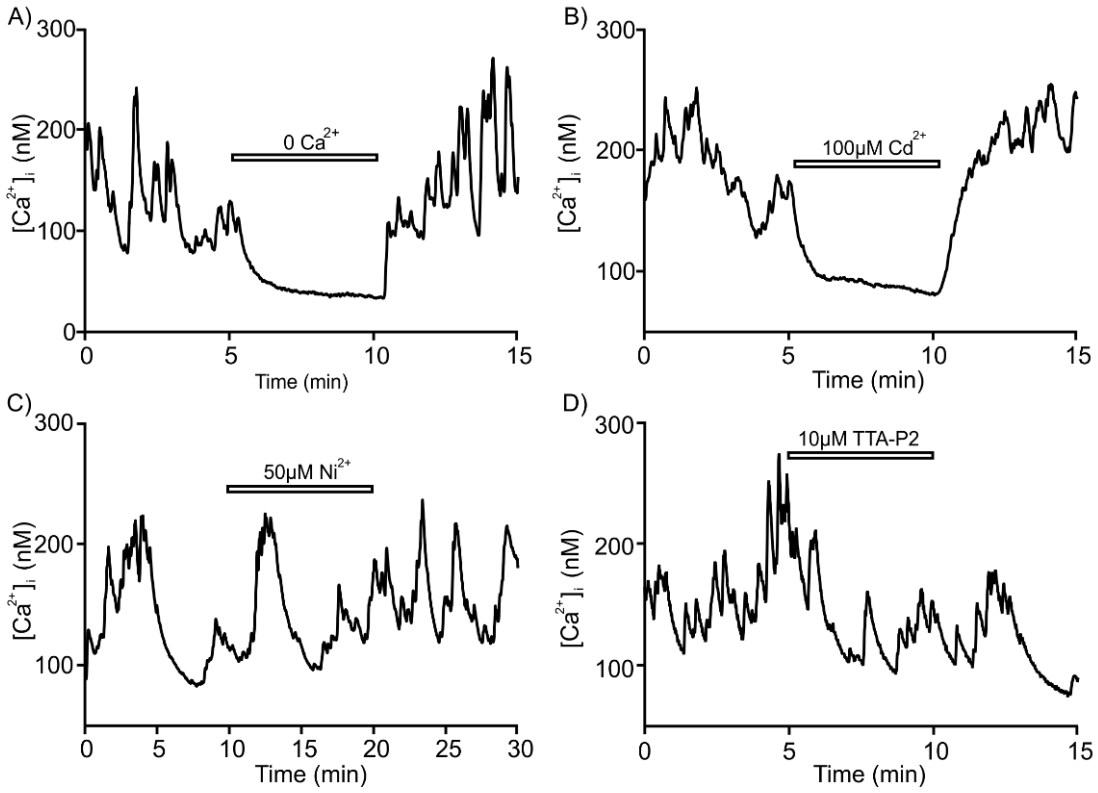

Figure 4.1: Effect of external Ca^{2+} removal and VGCC blockers on $[Ca^{2+}]_i$ oscillations. A: A typical $[Ca^{2+}]_i$ oscillations observed in a neurone before and after removal of external Ca^{2+}. B: Inhibition of spontaneous $[Ca^{2+}]_i$ oscillations by Cd^{2+}. C,D: Exposure of SON neurones to T-type VGCCs inhibitors Ni^{2+} and TTA-P2 failed to affect spontaneous $[Ca^{2+}]_i$ oscillations.

4.1.2 Voltage-dependent Ca^{2+} channels and $[Ca^{2+}]_i$ oscillations

A non-specific Ca^{2+} channel blocker Cd^{2+} at 50 µM or 100 µM led to a complete inhibition of $[Ca^{2+}]_i$ oscillations in all tested neurones (n = 17, figure 4.1B). In contrast, incubation with Ni^{2+} (50 µM, n = 10, figure 4.1C) or TTA-P2 (10 mM, n = 9, figure 4.1D), both being blockers of T-type VGCCs (Dreyfus, Tscherter et al. 2010), did not affect $[Ca^{2+}]_i$ oscillations. We further probed more specific antagonists of high-threshold VGCCs, the effects of which on spontaneous $[Ca^{2+}]_i$ oscillations are summarized in figure 4.2. Neither L-type channel blocker nicardipine (1 µM, n = 10, figure 4.2A), nor a specific blocker of the N-type channels ω-conotoxin GVIA (800 nM, n = 12, figure 4.2B), nor a specific blocker of the Q-type, ω-conotoxin MVIIC (100 nM, n = 6, 1µM, n = 2, figure 4.2C), nor

a specific blocker of the P/Q-type channels ω-agatoxin IVA (300 nM, n = 5, figure 4.2D) affected $[Ca^{2+}]_i$ oscillations.

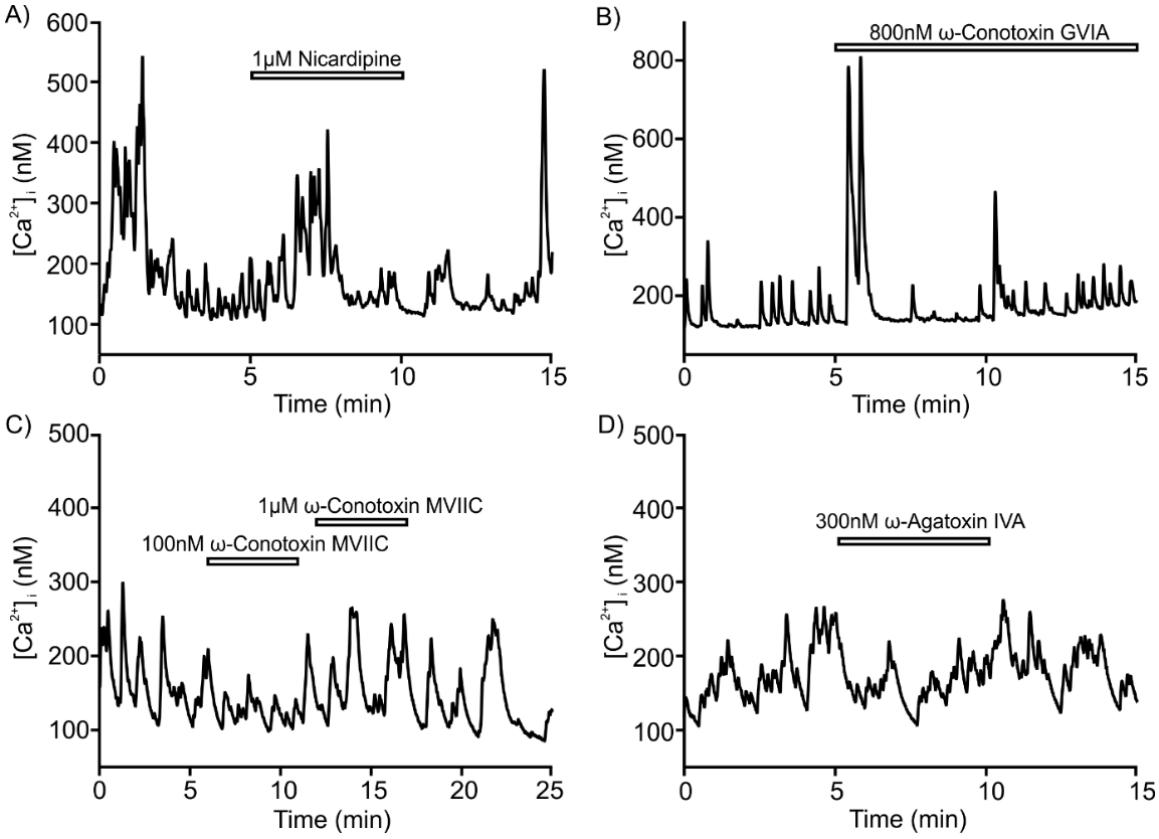

Figure 4.2: Effect of specific of HVGCC blockers on $[Ca^{2+}]_i$ oscillations. The representative traces showing the oscillations from individual neurones in the presence of different HVGCC blockers: nicardipine (1 μM) for L-type (A); ω-conotoxin GVIA (800 nM) for N-type (B); two different concentrations of ω-conotoxin MVIIC for P-type (C) and ω-agatoxin (300 nM) for P/Q-type (D). Note that none of the blockers affected the oscillations.

In contrast, a specific inhibitor of R-type VGCCs SNX-482 (Wang, Dayanithi et al. 1999, Bourinet, Stotz et al. 2001, Ortiz-Miranda, Dayanithi et al. 2005) affected $[Ca^{2+}]_i$ oscillations when applied at various concentrations. At 40 nM SNX-482 only partially inhibited $[Ca^{2+}]_i$ oscillations in 1 out of 6 neurones (data not shown). At 100 nM (figure 4.3A) of SNX-482 $[Ca^{2+}]_i$ oscillations were completely blocked in 9 out of 19 neurones, partially inhibited in 5 cells and had no effect in the remaining 5 neurones. In cells in which SNX-482 completely inhibited $[Ca^{2+}]_i$ oscillations, the basal $[Ca^{2+}]_i$ decreased from 153 ± 17 nM to 87 ± 6 nM (n = 9).

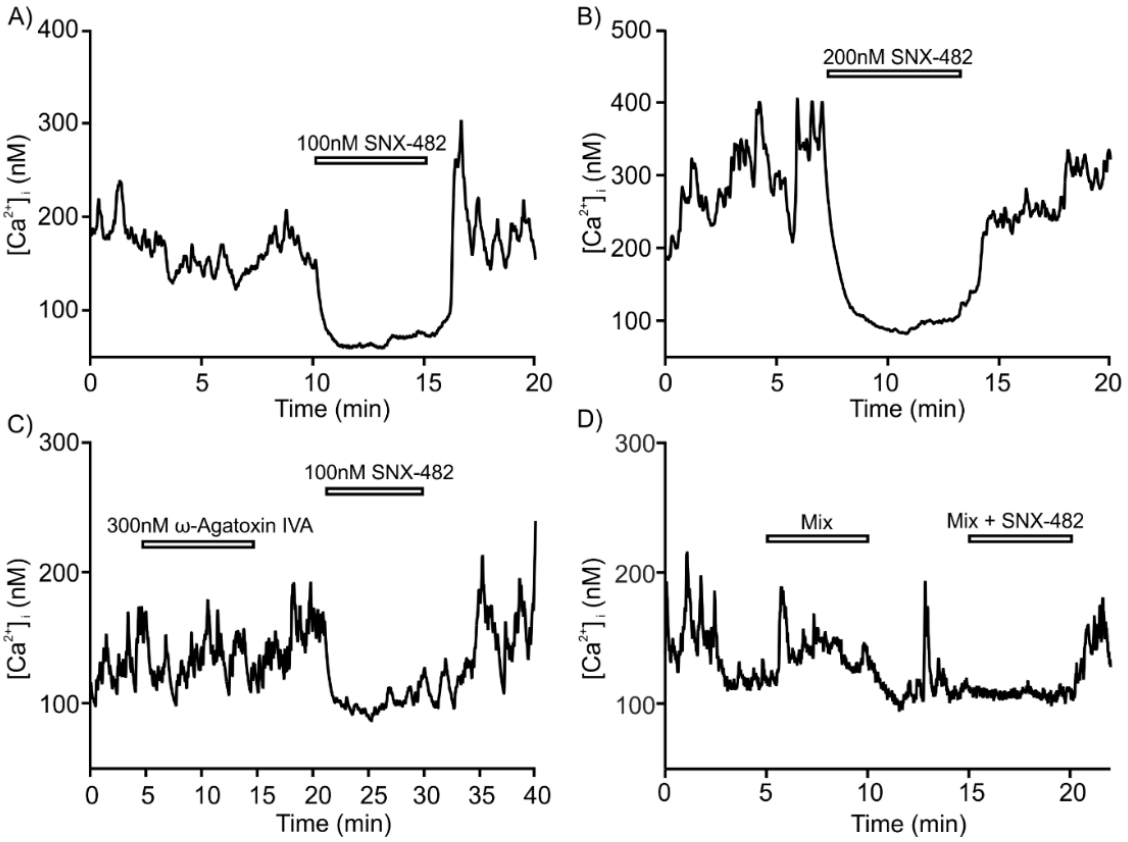

Figure 4.3: Effect of R-type VGCC blocker on $[Ca^{2+}]_i$ oscillations. Traces A and B show $[Ca^{2+}]_i$ oscillations from individual neurones recorded in the presence of 100 nM and 200 nM SNX-482, a specific blocker of R-type channels, respectively. The trace C shows the specific block of oscillations by SNX-482 in comparison with no effect of ω-agatoxin IVA. Trace D shows $[Ca^{2+}]_i$ oscillations from a neurone which was first exposed to the mixture of blockers of Ca^{2+} channels (L, N, P/Q-type) followed by the addition of SNX-482.

In neurones in which oscillations were only partially blocked the basal $[Ca^{2+}]_i$ also dropped from 143 ± 15 to 102 ± 12 nM (figure 4.3C). In the remaining 5 cells which were insensitive to the drug, the basal $[Ca^{2+}]_i$ did not change significantly. When applied at 200 nM (figure 4.3B), SNX-482 completely blocked $[Ca^{2+}]_i$ oscillations in 4 out of 6 neurones. To further corroborate the contribution of R-type VGCCs, the neurones were exposed to a mixture of specific blockers for L, N, P/Q and T-type channels (1μM nicardipine, 800 nM ω-agatoxin IVA, 300 nM ω-conotoxin GVIA and 50μM Ni^{2+}), which failed to inhibit $[Ca^{2+}]_i$ oscillations. The addition of 100 nM of SNX-482 to this cocktail however inhibited $[Ca^{2+}]_i$ oscillations in 3 out 3 neurones (figure 4.3D) and further indicated the contribution of R-type channels.

4.1.3 Role of Na^+ channels and Na^+ transport

To test whether the $[Ca^{2+}]_i$ oscillations are driven by electrical activity, we probed the oscillating cells with inhibitors of action potentials. Removal of extracellular Na^+ caused a complete, rapid and reversible block of $[Ca^{2+}]_i$ oscillations in 7 out of 11 neurones, significantly inhibited oscillations in 2 neurones and had no effect in the remaining 2 neurones (figure 4.4A). At the same time, treatment with the specific blocker of voltage-gated Na^+ channels TTX at concentrations between 750 nM to 5 μM (figure 4.4B) did not affect $[Ca^{2+}]_i$ oscillations in all tested cells (n = 26). On the contrary, treatment of oscillating neurones with KB-R7943, a selective inhibitor of the reverse mode of Na^+/Ca^{2+} exchanger, NCX (Kawano, Otsu et al. 2003, Brustovetsky, Brittain et al. 2011) caused a complete block of oscillations and lowered basal $[Ca^{2+}]_i$ to 95 ± 5 nM in 26 out of 33 neurones (figure 4.4C). In the remaining 7 neurones, the oscillations were inhibited only partially and the basal $[Ca^{2+}]_i$ also dropped to 102 ± 12 nM.

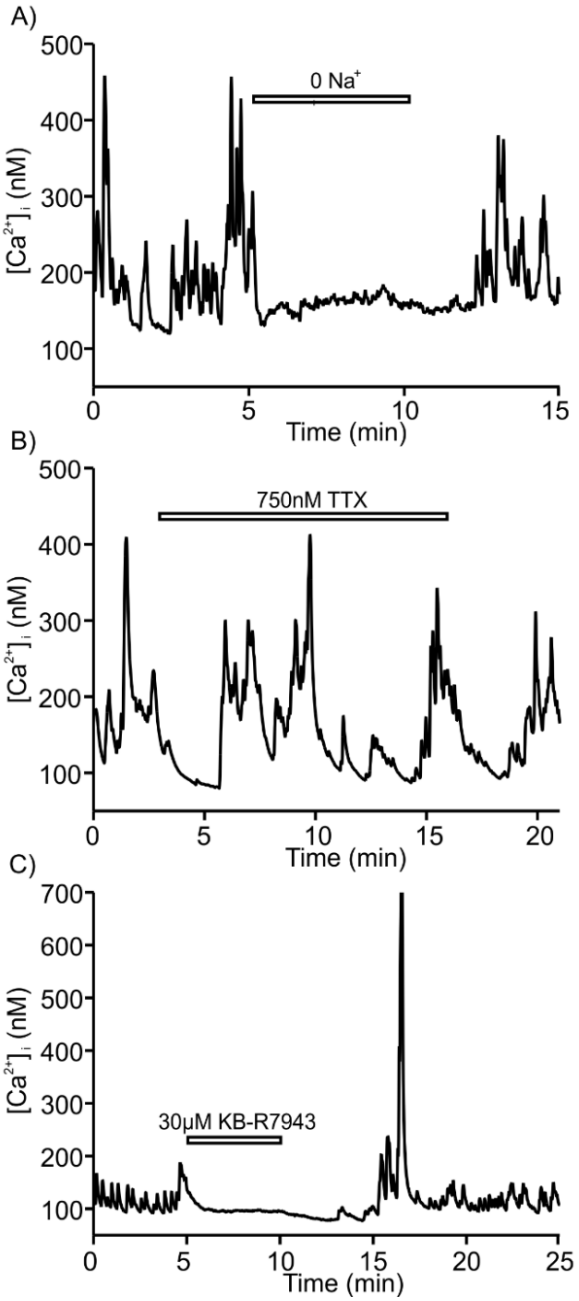

Figure 4.4: Role of extracellular Na^+, voltage-gated Na^+ channels and NCX. A: Removal of external Na^+ completely inhibited $[Ca^{2+}]_i$ oscillations; B: Inhibition of voltage-gated Na^+ channels with TTX did not affect spontaneous $[Ca^{2+}]_i$ oscillations. C: Exposure of magnocellular neurone to KB-R734, a specific inhibitor of NCX reverse mode) completely and reversibly inhibited spontaneous $[Ca^{2+}]_i$ oscillations.

4.1.4 Role of intracellular Ca^{2+} stores and Ca^{2+} clearance mechanisms

Ca^{2+} stored in Endoplasmic reticulum (ER) is known to serve as source of Ca^{2+} for oscillations in many cells (Ventura and Sneyd 2006, Keener and Sneyd 2009) and hence is a candidate also in MNCs. Treatment of SON neurones with TG (irreversible blocker of

ER SERCA pump) did not affect $[Ca^{2+}]_i$ oscillations in all tested neurones (n = 8), except of producing a short transient effect when oscillations were inhibited for 1-2 minutes after exposure to TG but fully recovered in the continuing presence of TG. This transient effect of TG was observed in 6 out of 8 neurones, example in figure 4.5A. Treatment of SON neurones (n = 4) with a reversible blocker of SERCA pumps cyclopiazonic acid (CPA, 10 μM) also had no visible effect on $[Ca^{2+}]_i$ oscillations in 3 out of 4 neurones; in 1 cell, similarly to TG, CPA produced transient inhibition (figure 4.5B). In addition, we tested the CPA effect in the absence of external Ca^{2+} by using 0 Ca^{2+} buffer and then exposing the neurones to 10 μM CPA; this resulted in a transient elevation of $[Ca^{2+}]_i$. When 0 Ca^{2+} buffer was switched back to the 2 mM Ca^{2+} NL, we observed an immediate transient increase in $[Ca^{2+}]_i$ and the oscillations were restored. Subsequent exposure to CPA failed to affect the ongoing oscillations. This protocol was tested with same result in 7 neurones (figure 4.5C). Ryanodine and caffeine, that mobilize Ca^{2+} from ER through activation of ryanodine receptors (RyRs) induced a transient elevation of $[Ca^{2+}]_i$ in non-oscillating SON neurones which lasted between 1 and 3 minutes (data not shown, for example see figure 3.5). However, application of ryanodine (10 μM, n = 6) or caffeine (10 mM, n = 4) to neurones exhibiting $[Ca^{2+}]_i$ oscillations did not affect the latter, except (similarly to TG and CPA), inducing a short (1 - 2 minute) transient inhibition that was observed in 2 out of 6 neurones treated with ryanodine and in 2 out of 4 neurones treated with caffeine. Subsequently, contribution of the PMCA was tested by applying 100 μM of Lanthanum (La^{3+}), which is known to effectively block plasmalemmal Ca^{2+} pump (Wanaverbecq, Marsh et al. 2003). Exposure to 100 μM of La^{3+} inhibited $[Ca^{2+}]_i$ oscillations in 8 out of 9 neurones (figure 4.5F). However, the neurones failed to recover the oscillations and did not survived for a long time after the treatment with La^{3+} indicating irreversible damage of the Ca^{2+} extrusion mechanisms.

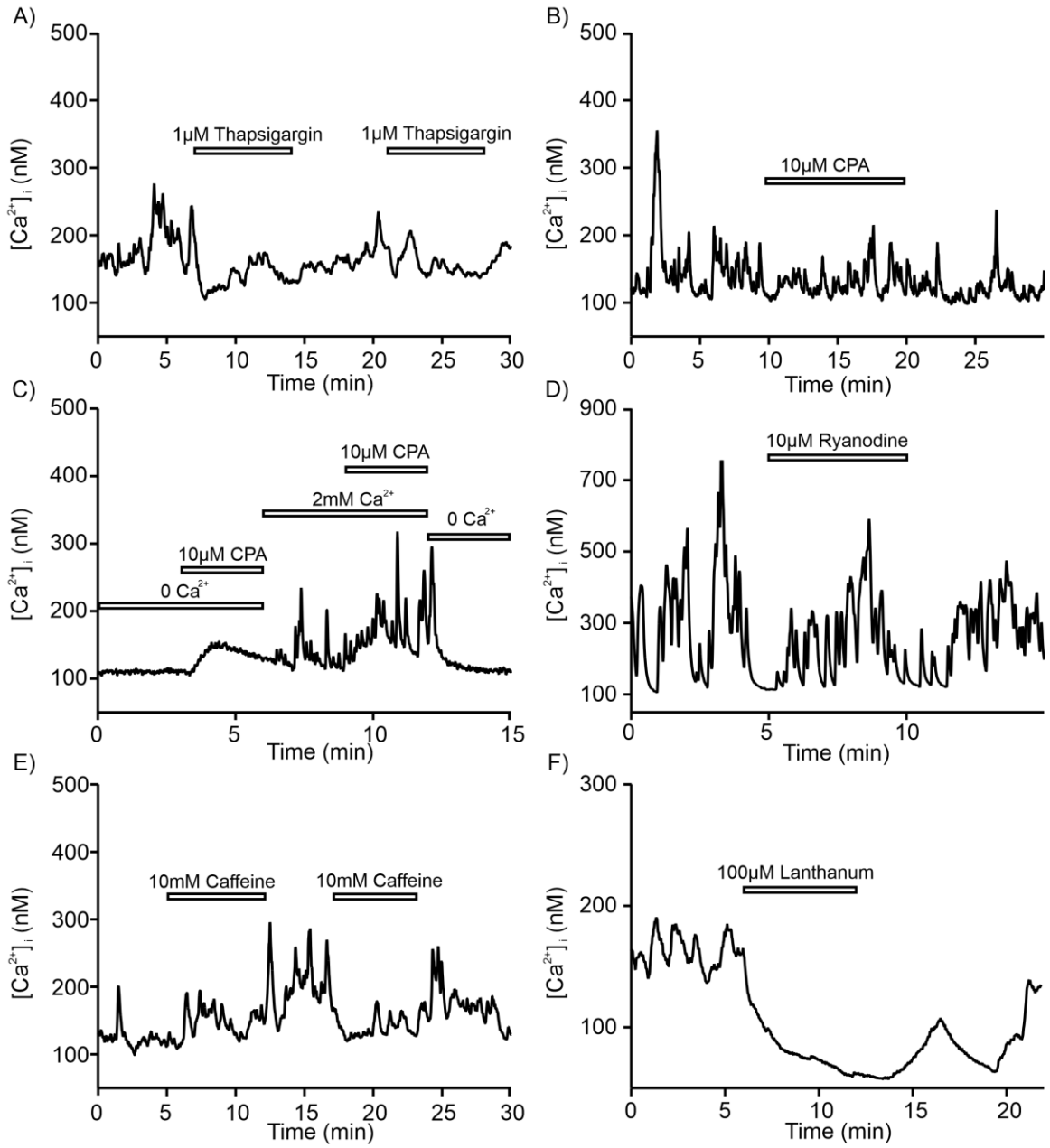

Figure 4.5: Effect of intracellular Ca^{2+} mobilizers and inhibitors of Ca^{2+}-clearance mechanisms. A, B: inhibition of endoplasmic reticulum Ca^{2+} SERCA pump by thapsigargin (A) and CPA (B) does not affect spontaneous $[Ca^{2+}]_i$ oscillations. C: shows the effect of CPA on $[Ca^{2+}]_i$ in the presence and absence of external Ca^{2+}. D, E: Mobilization of ER $Ca^{2+}$by 10 μM ryanodine (D) or 10 mM caffeine (E) does not influence spontaneous $[Ca^{2+}]_i$ oscillations. F: Exposure of magnocellular neurone to La^{3+}(a blocker of plasma membrane Ca^{2+}-ATPase) inhibits spontaneous Ca^{2+}oscillations.

4.1.5 Effect of GABA and blockers of K^+ currents on $[Ca^{2+}]_i$ oscillations

Effect of neurotransmitters was tested by exposure of magnocellular neurones to various concentrations of GABA (3 μM, n= 12; 20 μM, n = 4; and 50 μM, n = 4). All used concentrations completely inhibited $[Ca^{2+}]_i$ oscillations in all cells tested; this inhibition was fully reversible (examples: figure 4.6A, for 3 μM; figure 4.6B, with 10 μM gabazine). The inhibitory effect of GABA was completely blocked by $GABA_A$ antagonist gabazine (at 10 μM, n = 3). Similar (albeit slightly weaker) inhibition was induced by glycine (20 μM, in 4 cells blocked, in 1 partially blocked, in 3 no effect) and taurine (500 μM, in 6 cells blocked, in 1 partially blocked, in 2 no effect); figure 4.6 C and D respectively. Exposure of SON neurones to 10 - 50 mM of 4-AP (inhibitor of I_A K^+ channels) did not affect spontaneous $[Ca^{2+}]_i$ oscillations (n = 5, figure 4.6E); similarly impotent was the inhibitor of SK Ca^{2+}-dependent K^+ channels apamin (100 nM, n = 5, figure 4.6F).

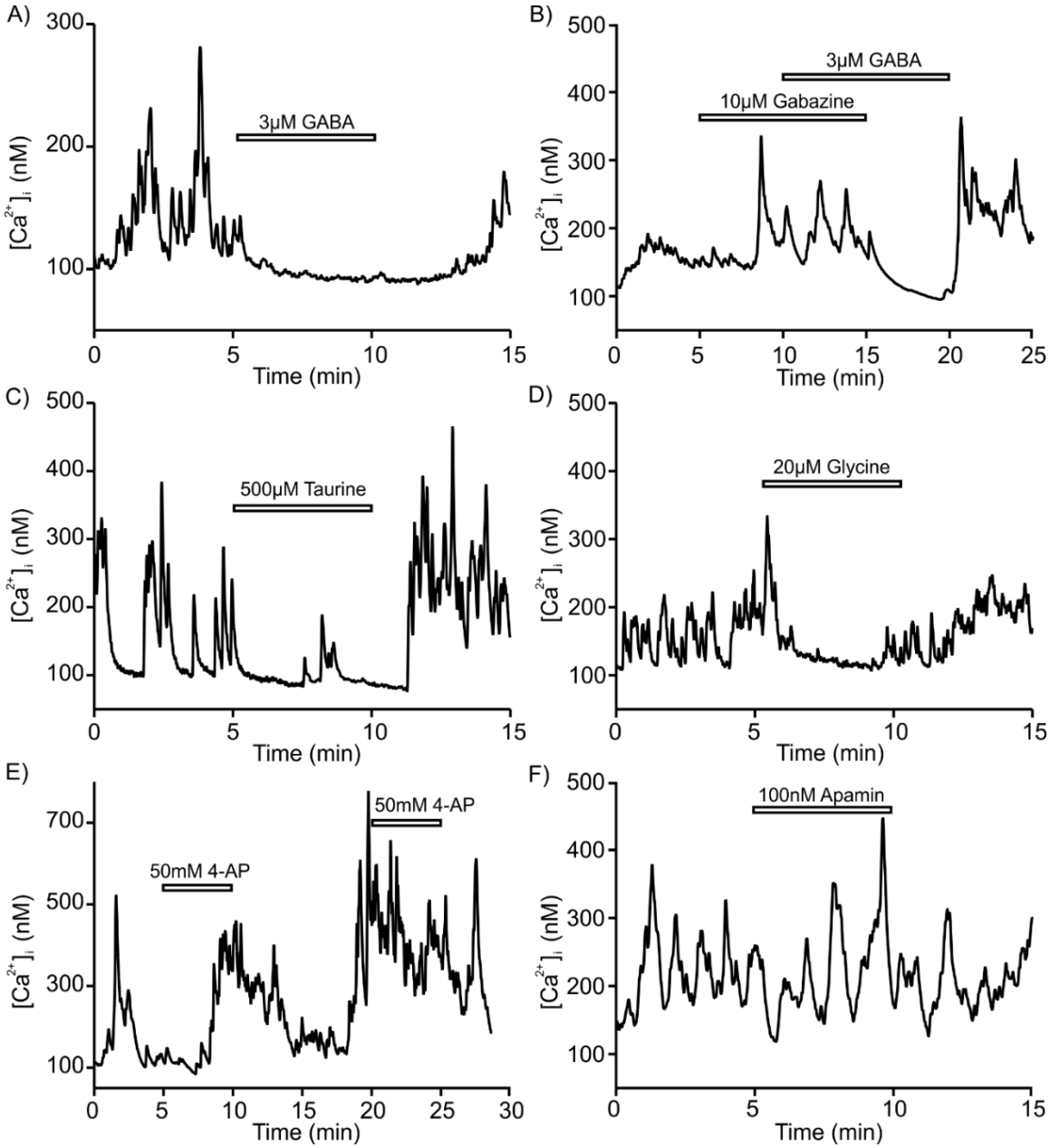

Figure 4.6: Effect of neurotransmitters and blockers of K^+ currents on $[Ca^{2+}]_i$ oscillations. A: Exposure to GABA at 3 μM reversibly inhibited spontaneous $[Ca^{2+}]_i$ oscillations. B: Gabazine completely inhibited effect of GABA. C, D: weaker but noticeable inhibitory effect of Taurine and Glycine. E, F: Exposure of magnocellular neurones to 4-AP, an inhibitor of A-type K^+ current (C) or to apamin, an inhibitor of Ca^{2+}-activated K^+-current, did not affect spontaneous Ca^{2+} oscillations.

4.2 Induced Ca^{2+} fluxes in magnocellular neurones

In this part of the work, we studied depolarization-induced $[Ca^{2+}]_i$ responses in isolated MNC neurones. We use a combination of experimental and computational approaches to decompose measured intracellular Ca^{2+} elevations into separate Ca^{2+} fluxes to investigate how intracellular Ca^{2+} stores influence depolarization-induced Ca^{2+} responses. This part of the work follows the results from the previous section 4.1 to cover the properties of both induced and spontaneous $[Ca^{2+}]_i$ dynamics in MNCs.

4.2.1 Depolarization-induced $[Ca^{2+}]_i$ responses

To probe the calcium dynamics in MNCs induced by a depolarization of the membrane, we exposed the isolated neurones to pulses of high extracellular K^+. While a short exposure typically triggered a rapid $[Ca^{2+}]_i$ elevation and slower exponential decay, a longer exposure uncovered a biphasic shape of the transients. To achieve a better separation of the rising and declining phases, we used prolonged exposures (>30 s) which highlight the time course of the two phases. figure 4.7A shows a typical recording of a train of $[Ca^{2+}]_i$ transients elicited by a repeated exposure to high K^+ (50 mM) in MNCs. The prolonged K^+ exposure induced a biphasic elevation in $[Ca^{2+}]_i$ consisting of a rapid overshoot to a level of ~1000 nM, followed by a slow decay to a plateau of ~500 nM. Typically, the cell recovers with repolarization after the K^+ is washed out, and the $[Ca^{2+}]_i$ quickly drops, following a fast exponential decay with a return to the basal concentration within several minutes. The overshoot is usually repeated with the next exposure to high K^+, but while the reached plateau retains its $[Ca^{2+}]_i$ level, the amplitude of the overshoot typically degrades with each repetition and eventually completely vanishes (figure 4.7A). However, with a sufficient break between two K^+ exposures, the neurone recovers, and the overshoot appears again. The ability to recover is captured in figure 4.7A: the amplitude of the last transient before the interruption of the K^+ train is only about 50% of the initial one. After a 5-minute break, the cell sufficiently recovered, and the amplitude of the consequent exposure reached about 80% of the initial one.

The transients from the trace in figure 4.7A are additionally displayed below in panel B: they are aligned with their declining edge and with their rising edge, respectively. It highlights that not only the amplitude but also the time course of the transient changes

with each repetition of the K^+-induced depolarization. figure 4.7B also uncovers that the declining phase after the K^+ washes out does not change visibly, contrary to the evolution of the overshoot and of the rate of Ca^{2+} elevation with an obvious trend of change. It indicates that a repeated exposure to a depolarization stimulus modulates the $[Ca^{2+}]_i$ elevation but does not affect the Ca^{2+} clearance ability of the neurone.

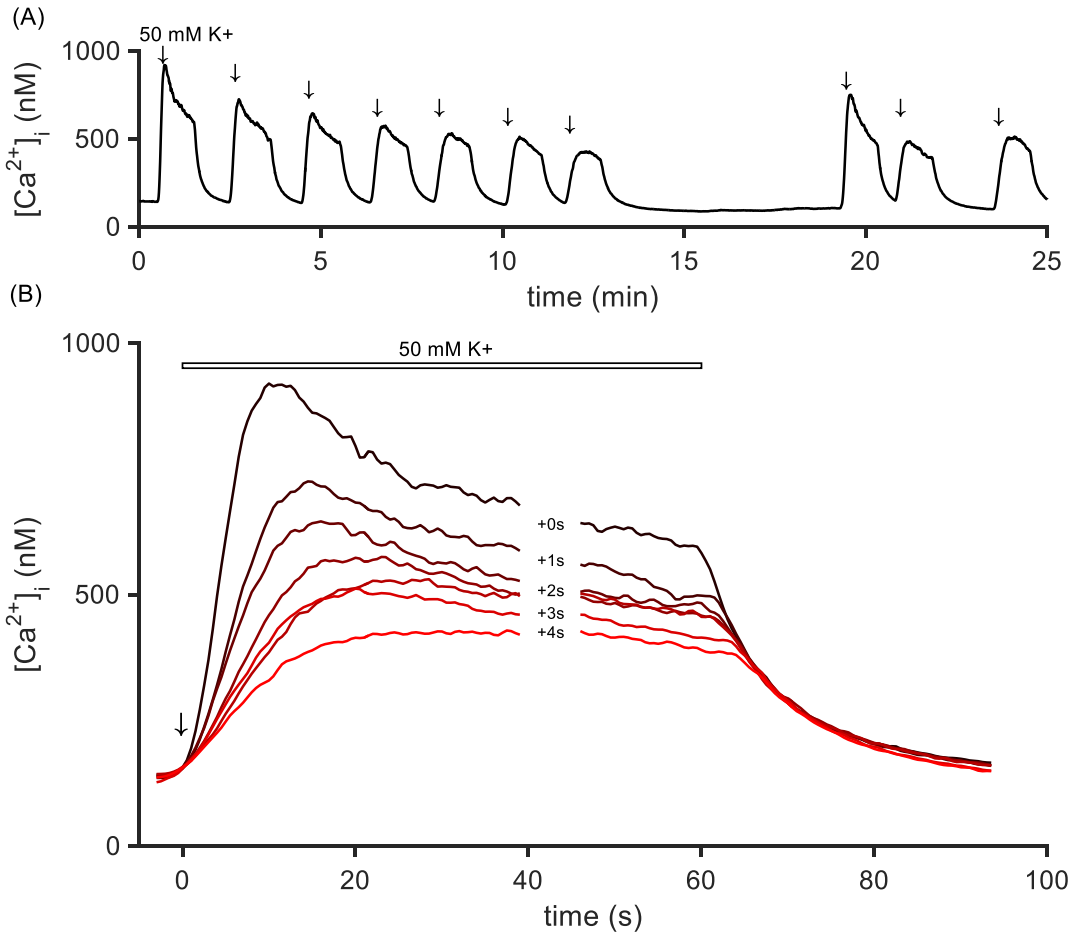

Figure 4.7: Repeated response to a high K^+-induced depolarization. A) A train of $[Ca^{2+}]_i$ transients in a single neurone elicited by a repeated exposure to 50 mM K^+ with a 60-s duration and 60-s break between the exposures. In 5 minutes after the last transient, more K^+ stimuli were applied to test the ability of the neurone to recover from multiple depolarizations. B) Transients from panel A are aligned with the rising and decay edges. The rising edges are aligned by their initiating point at t = 0. The decay edges are shifted to be aligned by the exponential decay phase with the shifts indicated in seconds.

Repeatability of the K^+ responses was further tested in an experiment with dose-dependent K^+ exposures (figure 4.8). The figure shows a representative $[Ca^{2+}]_i$ trace from a cell exposed to a series of different K^+ concentrations. The cell was first exposed to the highest 100 mM K^+ concentration followed by concentrations of 60, 40 and 25 mM K^+, after which the exposures were repeated in a reversed order from 25 mM to 100 mM. The plot shows that the second exposure to the same K^+ concentration results in a much smaller amplitude than the first response. Similar results were achieved with a protocol starting from the lowest concentration to the highest and subsequently from the highest to the lowest (data not shown). These results clearly show that depolarization-induced $[Ca^{2+}]_i$ responses in MNCs do not directly correspond to the strength of the depolarization (expressed as applied concentration of potassium). The strength of the response, characterized by its amplitude, has a strong dependency on the previous $[Ca^{2+}]_i$ activity of the neurone. To further investigate the role of the activity-dependent pattering of the $[Ca^{2+}]_i$ signals, in next sections, we focus on identifying the mechanisms underlying the appearance of the initial overshoot in MNCs.

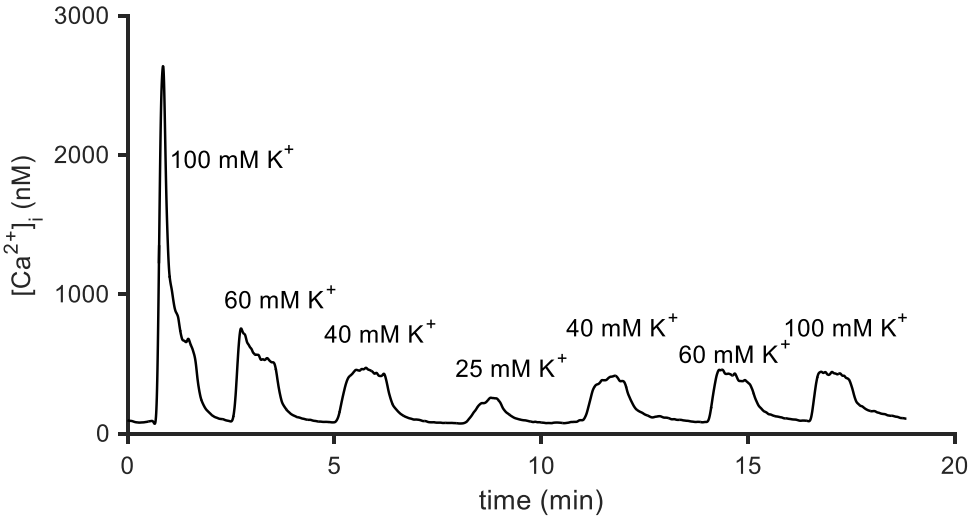

Figure 4.8: A typical repeated dose-dependent response to high K^+. The train of $[Ca^{2+}]_i$ transient was elicited by a K^+-induced depolarization. The K^+ concentration was increased from the basal 5 mM to the indicated concentrations during 60 second lasting exposures.

figure 4.7A and figure 4.8 show a typical record of a repeated exposure to K^+-induced depolarization. The $[Ca^{2+}]_i$ peak amplitude and the ability to recover between two exposures considerably varied cell to cell. In several observations, the cell did not recover

at all, and the initial peak was presented only in the first exposure. In other cases, the initial peak was recovered rapidly, and a very small degradation of the amplitude was observed. To overcome the variability in responses, further analyses were done with averaged responses calculated across a number of neurones.

4.2.2 Depletion of intracellular Ca^{2+} stores and blocking of the SERCA pump

To evaluate the contribution of intracellular Ca^{2+} stores to depolarization-induced $[Ca^{2+}]_i$ elevations, we measured responses to high K^+ in a situation where we pharmacologically eliminated intercellular Ca^{2+} fluxes and compared the results with responses under normal conditions. To efficiently achieve the elimination of intracellular fluxes, we used a combination of caffeine and CPA in 0 Ca^{2+} buffer according to the experimental protocols B and C introduced in the method section 3.5.1. Protocol B uses a combination of both caffeine and CPA to deplete the ER and to completely block the contribution of intracellular ER-driven fluxes to K^+-induced responses. Protocol C uses only caffeine to effectively deplete the ER and selectively inhibit the release of Ca^{2+} from the ER but at the same time leaves the ER clearance mechanism of the SERCA pump functioning. The exact drug applications with indicated durations of exposures and concentrations are illustrated in representative traces in figure 3.5 (panels B and C). Both protocols were repeated for n = 5 AVP and for n = 5 OT neurones, and averaged responses were calculated. The results for protocol B are shown in figure 4.9 for AVP neurones (panel A) and for OT neurones (panel B). Averaged control responses (red line) are compared with averaged responses after the caffeine/CPA treatment (black line). The control responses show a typical two-phase pattern consisting of a rapid rise component with an overshoot followed by a slow decay component reaching a steady concentration. After the K^+ is removed, the $[Ca^{2+}]_i$ follows a fast exponential decay reaching the basal level within minutes. Responses after the treatment with caffeine and CPA (black line) visibly changed their time course. The initial overshoot is completely absent, and the decay to the basal Ca^{2+} level after the K^+ removal is significantly slower. It indicates that the caffeine/CPA treatment attenuated the responses by an efficient depletion of the ER and slowed the overall clearance ability by the SERCA pump suppression.

The effect of treatment with caffeine/CPA elicited a similar effect in both AVP and OT neurones (panel A vs. panel B in figure 4.9). The rapid initial rise was supressed in both AVP and OT neurones, and the decay after the K^+ stimulus was slower for both cellular

subtypes. A possible difference between the OT and AVP neurones was observed in control responses, where the initial overshoot was more distinctive and more typical for the AVP neurones.

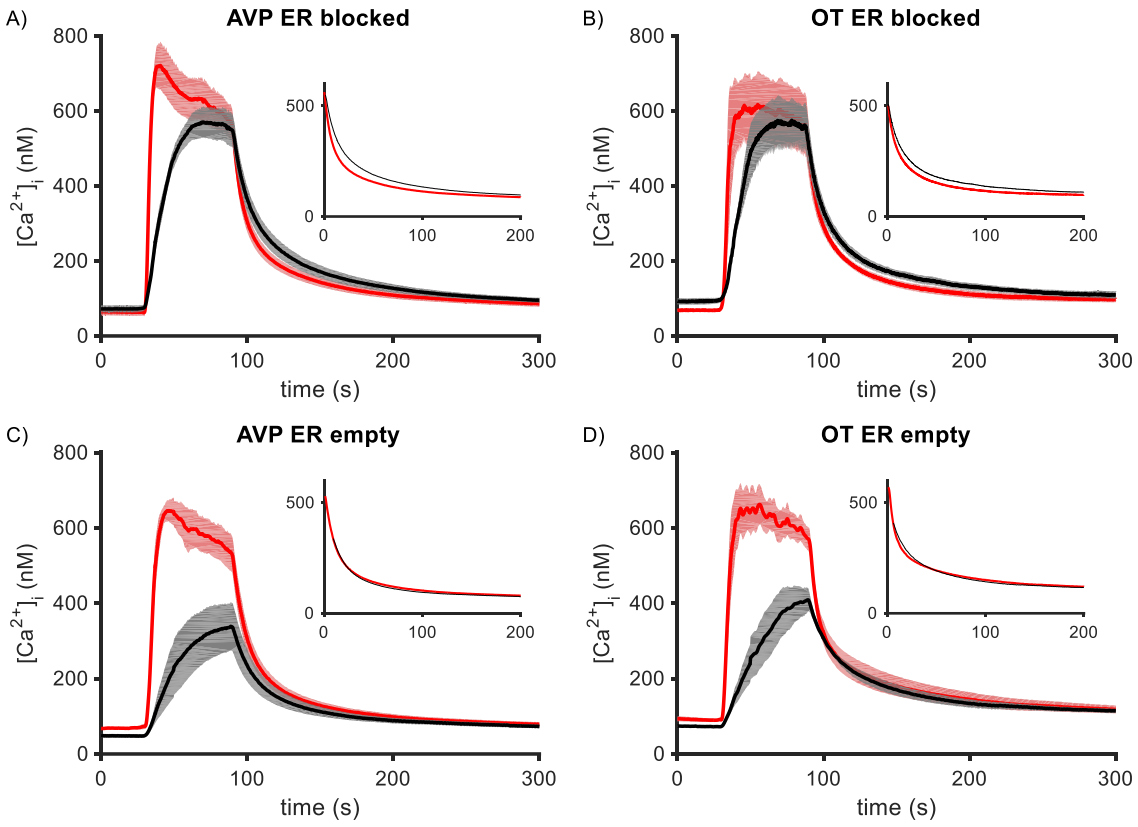

Figure 4.9: The effect of manipulation with caffeine-sensitive Ca^{2+} stores on K^+-induced responses. Responses elicited by 50 mM K^+ under control conditions (red line) are compared with responses obtained after treatment with CPA and/or caffeine (black line). The upper plots show responses in control conditions (red line) and after treatment with caffeine and CPA (ER blocked) from AVP neurones (panel A) and from OT neurones (panel B). The bottom panels compare control responses with responses after treatment with caffeine (ER empty) from AVP (panel C) and from OT (panel D) neurones. All the displayed $[Ca^{2+}]_i$ responses are averaged transients obtained from n = 5 different neurones; the grey shading around the lines indicates the standard error of the mean. The inner plots display the horizontally aligned declining phases.

The modified experiment according to protocol C (details in section 3.5.1 of methods) with the exclusion of CPA was repeated for n = 5 AVP and n = 5 OT neurones. The application of caffeine was aimed to cause a depletion of the ER, while the exclusion of CPA left the SERCA pump functioning. The averaged responses are plotted in figure 4.9C for AVP neurones and for OT neurones (figure 4.9D). The results clearly show a significant attenuation of the response to K^+ after the caffeine treatment (red line) compared with the control responses (black line) for both AVP and OT neurones. On the other hand, the decay phase to the resting level did not change visibly. The attenuation in panels C, D is even stronger compared with responses in panels A and B, where CPA was additionally used. It indicates that the ER was not only excluded from the response as an additional source of Ca^{2+}, but it functioned as a sink of Ca^{2+} that caused the stronger attenuation of the response by rapid re-accumulation of Ca^{2+} into ER.

4.2.3 Separation of the Ca^{2+} fluxes

Several different Ca^{2+} fluxes are involved in the depolarization-induced $[Ca^{2+}]_i$ elevation: here we categorize them as plasmatic membrane crossing fluxes and as intracellular Ca^{2+} fluxes. The plasmatic membrane crossing fluxes are represented by an influx of Ca^{2+} from the extracellular space into cytosol (J_{in}) and by a Ca^{2+} efflux with the opposite direction responsible for the removal of Ca^{2+} from cytosol back to the extracellular space (J_{out}). The intracellular fluxes incorporate the exchange of Ca^2 between intracellular Ca^{2+} stores, represented by ER, and cytosol. We further divide them into two fluxes by their primary direction: the uptake of Ca^{2+} into the ER (J_{serca}) and the release of Ca^{2+} from the ER to cytosol (J_{er}). The fluxes are illustrated in a schematic diagram in figure 1.7. Using a Ca^{2+} imaging technique, based on the fluorescent dye Fura-2, permits us to measure the instantaneous Ca^{2+} concentration in cytosol, which is the main pool of free Ca^{2+} shared by all the mentioned Ca^{2+} fluxes. To separate the individual Ca^{2+} fluxes and get an insight into the depolarization-induced Ca^{2+} dynamics, we use the estimation approach described in methods (see section 3.5.2).

4.2.4 Determination of the Ca^{2+} clearance function

To estimate the function that describes the clearance rate as a function of $[Ca^{2+}]_i$, we use responses recorded under the condition with blocked ER fluxes (figure 4.9A–B). The rising phase the response in this condition is optimally the result of the summed fluxes J_{in} and J_{out}

that coexist during the K^+ stimulus (the J_{er} and J_{serca} fluxes are pharmacologically excluded). As the J_{in} terminates with the end of the K^+ stimulus, the decay phase is quickly dominated by the outward flux and can be used as a good approximation for an estimation of the clearance flux J_{out}. To extrapolate the dependency of the clearance rate on $[Ca^{2+}]_i$, we fit the decay phase of the averaged responses with a double-exponential curve according to the approach introduced in methods, section 3.5.3. The fitted exponential curves (dashed red line) are plotted in figure 4.10A for AVP neurones and in figure 4.10B for OT neurones. Parameters of the obtained exponential fitting are inserted directly in the plot. The fitted decay is then expressed as the function of $[Ca^{2+}]_i$ and plotted as the clearance rate J_{out} against the $[Ca^{2+}]_i$ (figure 4.10C) separately for AVP neurones (black line) and for OT neurones (red line). The estimated clearance rate for AVP neurones (figure 4.10C, black line) is for clarity compared in figure 4.10D with the decay rate obtained under control conditions. A comparison of the estimated clearance rates between AVP and OT neurone subtypes in figure 4.10C does not show any difference in their Ca^{2+} clearance ability. It indicates that extrusion mechanisms work similarly in both subtypes, and possible differences in Ca^{2+} dynamics must be carried by other mechanisms. The estimated clearance functions $J_{out}([Ca^{2+}]_i)$ displayed in figure 4.10C are used in next sections for further analyses.

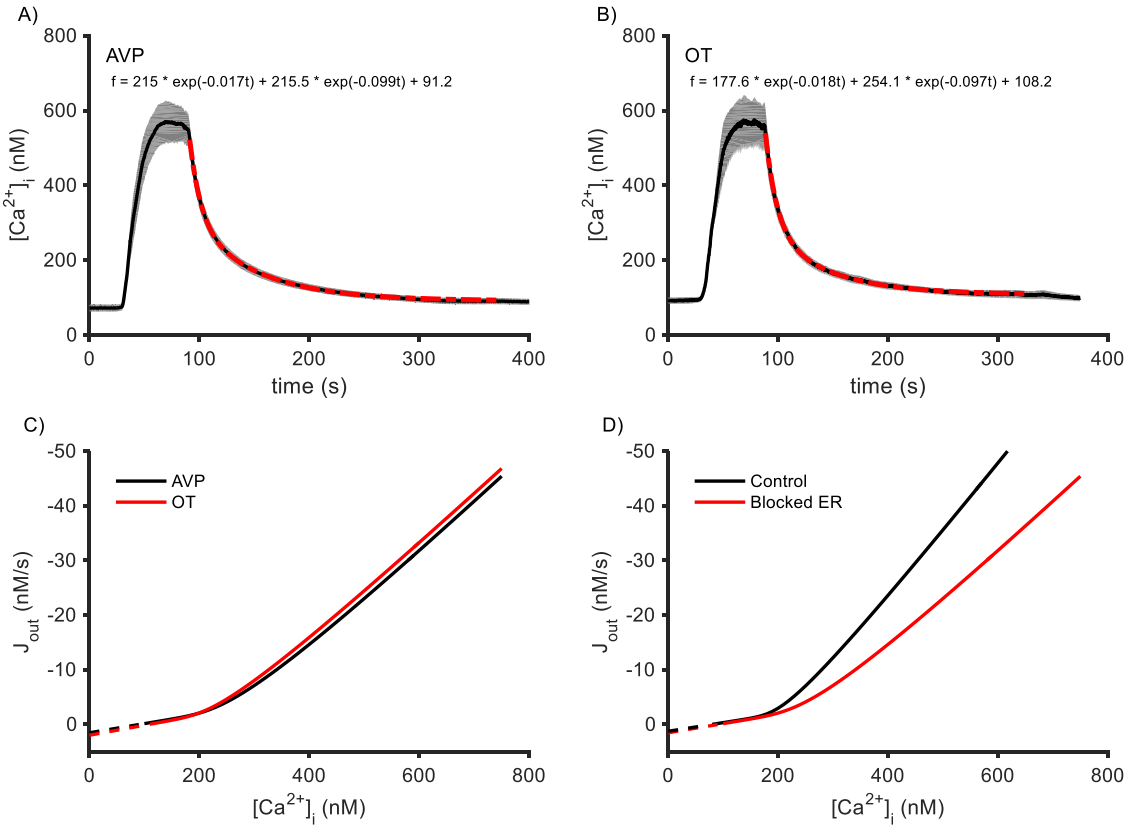

Figure 4.10: An estimation of the clearance function J_{out}. K^+-induced $[Ca^{2+}]_i$ responses were recorded under the condition with the blocked ER (depleted ER and inhibited SERCA pump). An averaged response from n = 5 neurones was calculated, and the decay phase of the responses was fitted with a double-exponential function. A) A fitted exponential decay of the averaged response from AVP neurones and panel B) from OT neurones. C) The fitted exponential decay rates are plotted against $[Ca^{2+}]_i$ for AVP (black line) and OT neurones (red line). D) An estimated clearance function of AVP neurones (blocked ER, red line) is compared with the decay rate obtained by fitting to the declining phase of responses recorded from same group of n = 5 neurones under control conditions.

4.2.5 Determination of the depolarization-induced Ca^{2+} influx

To separate the J_{in} flux from the K^+-induced responses, we use the approach introduced in the method section 3.5.2. The estimation procedure for AVP neurones is captured in figure 4.11. Panel A displays an averaged K^+-induced $[Ca^{2+}]_i$ (c_i) response from figure 4.10A, for which we have already determined the clearance function $J_{out}(c_i)$ in section 4.2.4. The known clearance function was used to calculate the clearance rate for each time point of

the response and plotted in panel B (red line) in time domain as $J_{out}(t)$. The black line in panel B shows the derivative dc_i/dt of the trace from panel A calculated with respect to time. To calculate the $J_{in}(t)$ flux, we simply subtracted the estimated $J_{out}(t)$ from the derivative $dc_i/dt(t)$ as

$$J_{in}(t) = dc_i/dt(t) - J_{out}(t) \qquad (3).$$

The estimated $J_{in}(t)$ flux is plotted in panel C (figure 4.11): the roughly rectangular shape of the $J_{in}(t)$ flux correlates with the exposure to K^+, indicated by a bar above the trace in panel A. In summary, a depolarization of 50 mM K^+ in AVP neurones elicited a flux at a rate of approximately 30 nM/s, which remained stable for the whole duration of the exposure. Similar results as for AVP neurones were achieved also for OT neurones (figure 4.12). The depolarization-induced influx $J_{in}(t)$ does not visibly change in time, and its fast rising and declining edges (compared with the relatively slow Ca^{2+} dynamics) indicate that the J_{in} flux is exclusively triggered by the depolarization in an "on/off" manner. The blocking of intracellular fluxes caused an attenuation of the responses, but it also led to a unification of the Ca^{2+} responses in AVP and OT neurones (figure 4.9A–B).

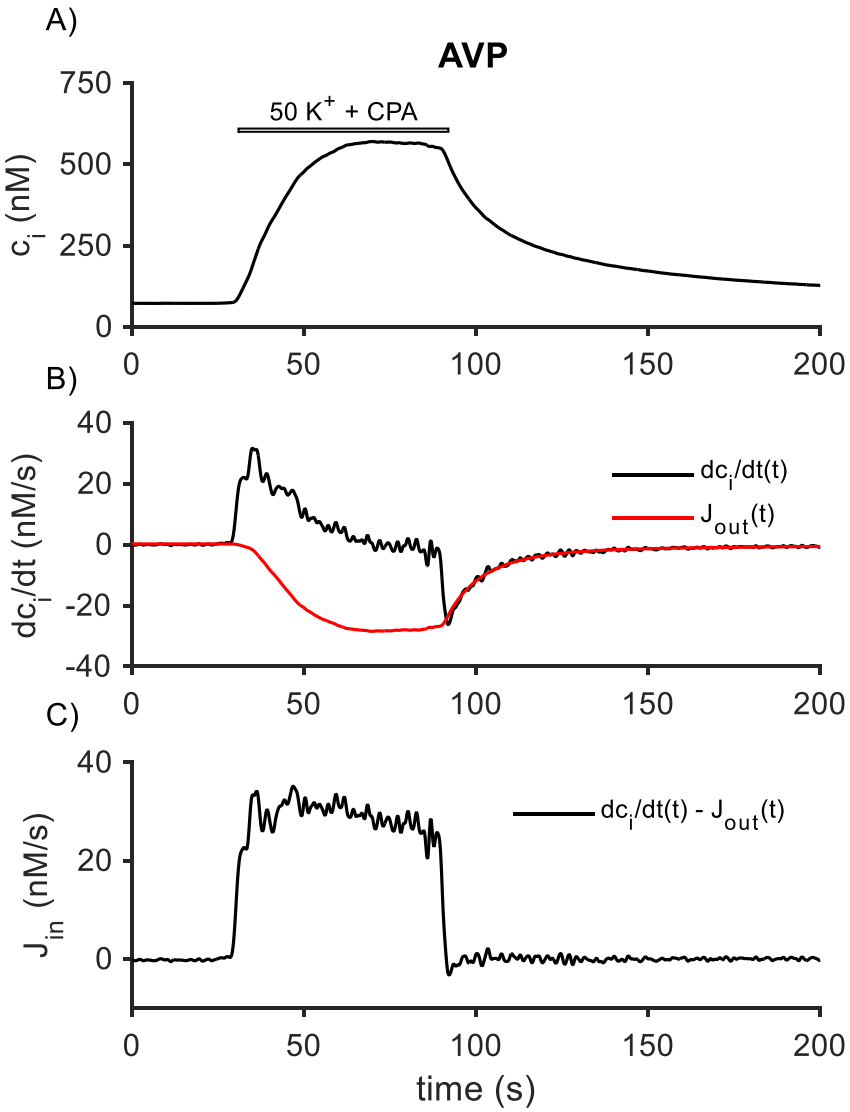

Figure 4.11: A determination of the depolarization-induced Ca^{2+} influx in AVP neurones. A) An averaged response from n = 5 AVP neurones measured after a pharmacological blocking of the intracellular Ca^{2+} fluxes. B) A derivative of the trace from panel A with respect to time. C) The red trace is the clearance rate $J_{out}(t)$ calculated for each time point of the trace in panel A. Finally, the black trace in panel C is the estimated J_{in} flux calculated by subtracting the $J_{out}(t)$ from the derivative dc_i/dt in panel B.

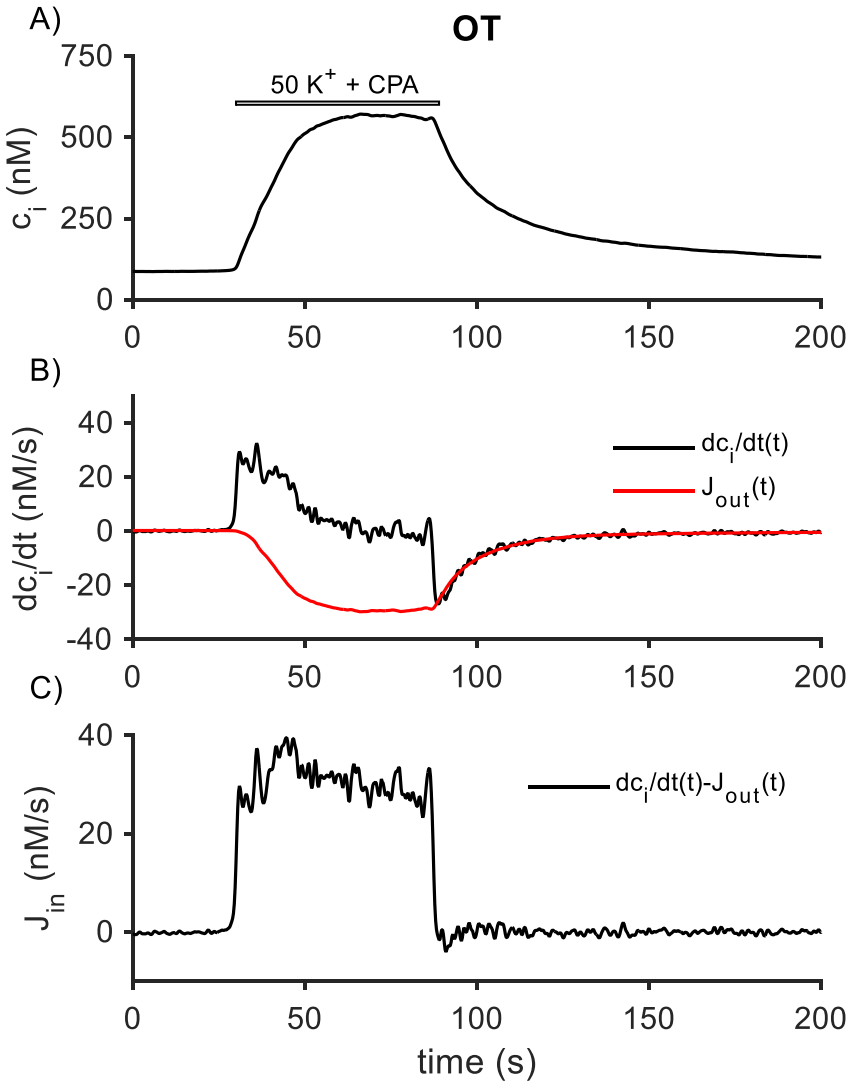

Figure 4.12: A determination of the depolarization-induced Ca^{2+} influx in OT neurones. A) An averaged response from n = 5 OT neurones measured after a pharmacological blocking of the intracellular Ca^{2+} fluxes. B) A derivative of the trace from panel A with respect to time. C) The red trace is the clearance rate $J_{out}(t)$ calculated for each time point of the trace in panel A. Finally, the black trace in panel C is the estimated J_{in} flux calculated by subtracting the $J_{out}(t)$ from the derivative dc_i/dt in panel B.

4.2.6 Determination of the net Ca^{2+} fluxes of the ER

In figure 4.11 and figure 4.12, we analysed K^+-induced $[Ca^{2+}]_i$ responses obtained under conditions with the blocked ER. These analyses resulted in the estimated flux $J_{in}(t)$. The same approach was applied in figure 4.13 on responses obtained in control conditions with the ER normally functioning. The trace in figure 4.13, panel A, is an averaged control response to 50 mM K^+, and panel B shows a derivative (black line) of this trace calculated with respect to time. The derivative has (compared with the derivative in figure 4.11B) a robust peak of maximum rate in the very beginning. This peak reflects the fast rising phase of $[Ca^{2+}]_i$ which was not presented in the ER-blocked response and confirms a prominent contribution of the intracellular stores in the shaping of the depolarization-induced responses.

The responses in figure 4.11A (ER blocked) and in figure 4.13A (control) were obtained in the same AVP neurones, and the clearance function $J_{out}(c_i)$ for them was already estimated in figure 4.10C (black line). Thus, here we use the known $J_{out}(c_i)$ to calculate the clearance rate $J_{out}(t)$ also for the control trace in figure 4.13A. The obtained flux $J_{out}(t)$ is plotted below in figure 4.13B (red line) together with the derivative $dc_i/dt(t)$.

In figure 4.11C, the known clearance rate $J_{out}(t)$ was used to calculate the Ca^{2+} flux $J_{in}(t)$ by subtraction of the $J_{out}(t)$ from the derivative $dc_i/dt(t)$ according to eq. 3 (section 3.5.2). The same calculation was performed for the control response, and the result in figure 4.13C reveals two components of the $[Ca^{2+}]_i$ elevation: a rapid component lasting only about 5 seconds, which is accompanied by a smaller but sustained component of about 30 mM/s that lasts for the whole duration of the transient. The smaller component finally drops with a visible flick below the zero value after the end of the depolarization stimulus. This is in contrast with the estimated J_{in} flux in figure 4.11C, which has a simple rectangular shape. The difference reflects the fact that while in figure 4.11C, the calculated result represents the single depolarization-induced flux $J_{in}(t)$ (ER fluxes are supressed), the result obtained in figure 4.13C comes out from a combination of the three remaining fluxes J_{in}, J_{er} and J_{serca}.

Panels A, B and C in figure 4.13 display analyses of the data from AVP neurones, and similar results were achieved also for OT neurones (figure 4.13D–F). As has been mentioned earlier in this work, both AVP and OT neurones behaved similarly in experiments on the depolarization-induced $[Ca^{2+}]_i$ responses. The only difference was

observed for the appearance of the initial overshoot, which was more typical for AVP neurones. Figure 4.13 supports this observation in panel B vs. panel E, where the maximum rate was slightly higher for AVP neurones. This hypothesis is generally in agreement with our earlier observations, yet it needs more evidence.

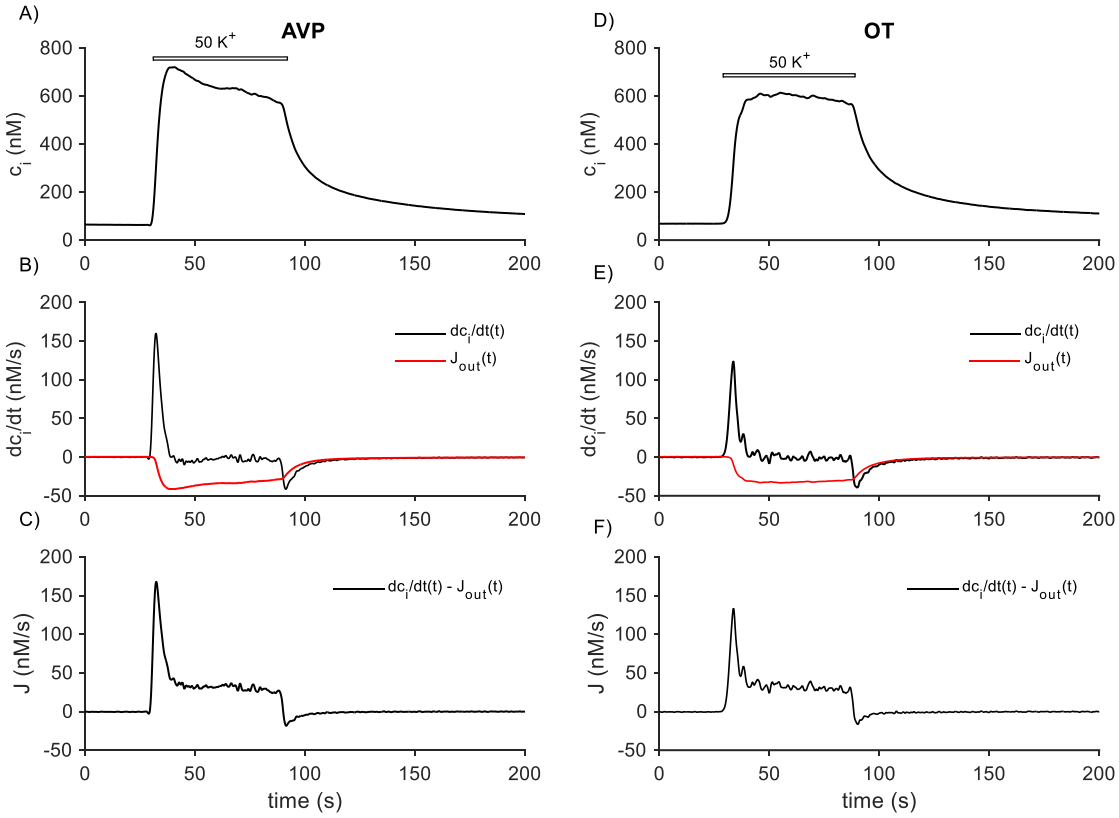

Figure 4.13: Analyses of control K^+-induced Ca^{2+} responses. A) An averaged response to 50 mM K^+ from n = 5 AVP neurones. B) A derivative of the trace from panel A with respect to time (black line) and the clearance rate $J_{out}(c_i)$ (red line) calculated for each time point of the trace in panel A. C) $J_{out}(t)$ subtracted from the derivative $dc_i/dt(t)$ from panel B; after the subtraction of the flux J_{out}, the plotted rate J represents a combination of the remaining fluxes J_{in}, J_{er} and J_{serca}. D), E) and F) are equivalent results obtained for OT neurones.

The results of the analyses from figure 4.11, figure 4.12 and figure 4.13 are summarized in figure 4.14. Panel A (AVP neurones) and panel D (OT neurones) show a comparison of the responses in control conditions (black line) and in conditions with the blocked ER (red line). Panels B and E show the results of the analyses for both cases; the blue area represents the component $J_{in}(t)$ from figure 4.11C, and the green area represents the combination of $J_{in}(t)$, $J_{er}(t)$ and $J_{serca}(t)$ from figure 4.13C. The overlay of the green and blue areas clearly illustrates that the rapid component is presented only in the response with the functioning ER (green area), while the slow component is shared by both traces. To enhance the difference between the two results, we subtracted the blue area from the green one. This operation reduces the trace represented by the blue area into a combination of the two intracellular fluxes J_{er} and J_{serca}. Because these fluxes have an opposite direction, the final flux represents the net flux across the ER membrane $\Delta J_{er}(t)$:

$$\Delta J_{er}(t) = J_{er}(t) - J_{serca}(t). \qquad \text{[eq. 4]}$$

By this action, one by one, we subtracted the $J_{in}(t)$ and $J_{out}(t)$ fluxes from the control response and thus eliminated the plasmatic membrane crossing fluxes. The result of the subtraction is plotted in panel C for AVP neurones and in panel F for OT neurones. We see a rapid peak followed by a zero net flux, and finally the trace ends with a small negative flux indicating the domination of the Ca^{2+} flux into the ER over the release of Ca^{2+} from the ER to cytosol.

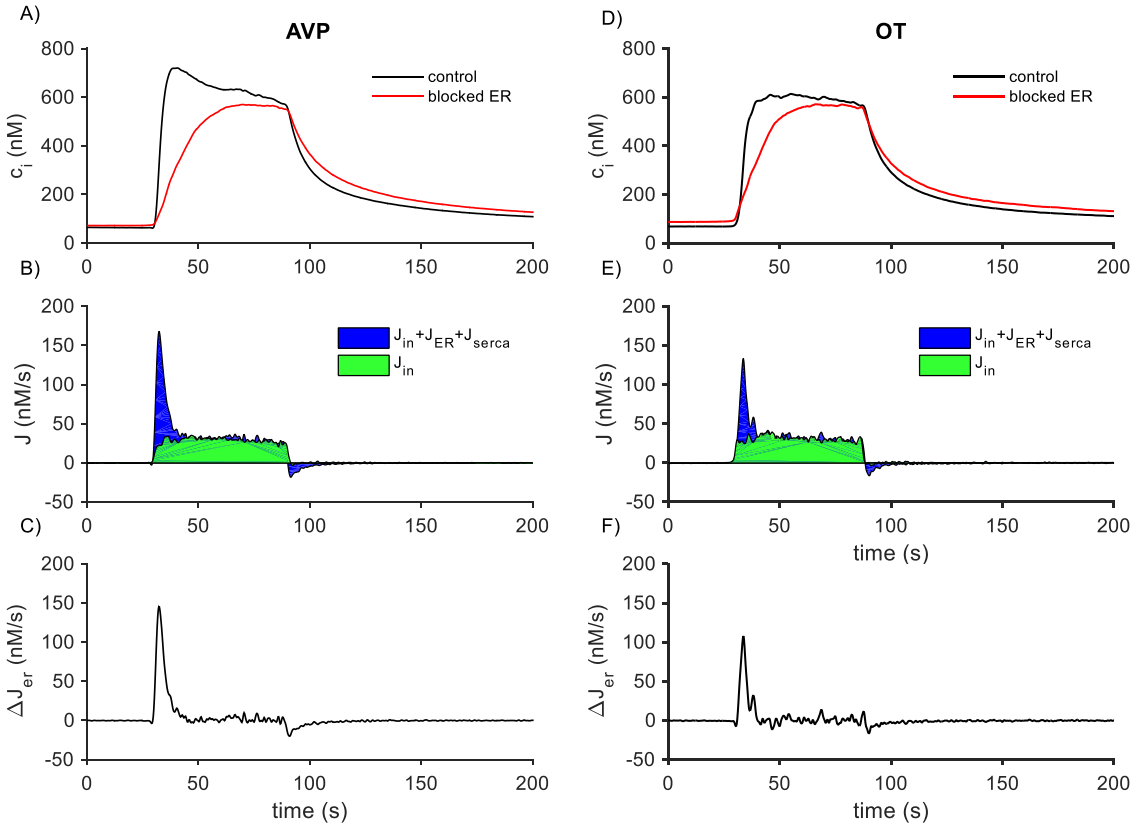

Figure 4.14: A determination of the net intracellular Ca^{2+} fluxes during the K^+-induced Ca^{2+} response. A): A 50K^+-induced $[Ca^{2+}]_i$ response from AVP neurones in control (black line) conditions and in conditions with the blocked ER (red line). Both traces are averaged responses from n = 5 AVP neurones. D), E) and F) are equivalent results obtained for OT neurones.

4.2.7 Depletion of Ca^{2+} stores strongly attenuates induced $[Ca^{2+}]_i$ responses

In figure 4.9, we analysed $[Ca^{2+}]_i$ responses measured in neurones where we artificially depleted the ER Ca^{2+} stores using caffeine pre-treatment prior to an exposure to 50 mM K^+. To emphasize how a filling state of the ER modulates the Ca^{2+} dynamics, we plotted results from all three situations (control, ER blocked, ER empty) together in figure 4.15. The response obtained after depletion of ER (blue line) is shown together with the responses obtained in control conditions (black line) and in conditions with completely blocked ER fluxes (red line). Note that contrary to all previous results, where we compared only responses measured in the same neurones, in figure 4.15, we compare data obtained from different groups of neurones. Nevertheless, all traces are averaged responses from n = 5

neurones, and even though the data are not feasible to make precise analyses, we can get an illustrative view of the range of Ca^{2+} dynamics modulation by the filling state of the ER. The difference in all the three responses is most prominent for the rate of the rising $[Ca^{2+}]_i$ towards the maximum amplitude. While in the case of the control response, the maximum rate reaches about 180 nM/s, in the case of the response with the depleted ER, the maximum rate reaches only about 12 nM/s. If we consider that the estimated rate of J_{in} for 50 mM K^+ stimuli was about 30 nM/s (figure 4.11C and figure 4.12C), we can easily calculate that the depleted ER removes Ca^{2+} during depolarization by a rate of about -18 nM/s and causes an attenuation of the overall $[Ca^{2+}]_i$ rise to the indicated 12 nM/s. This declares a very wide range of depolarization-induced Ca^{2+} dynamics in MNCs.

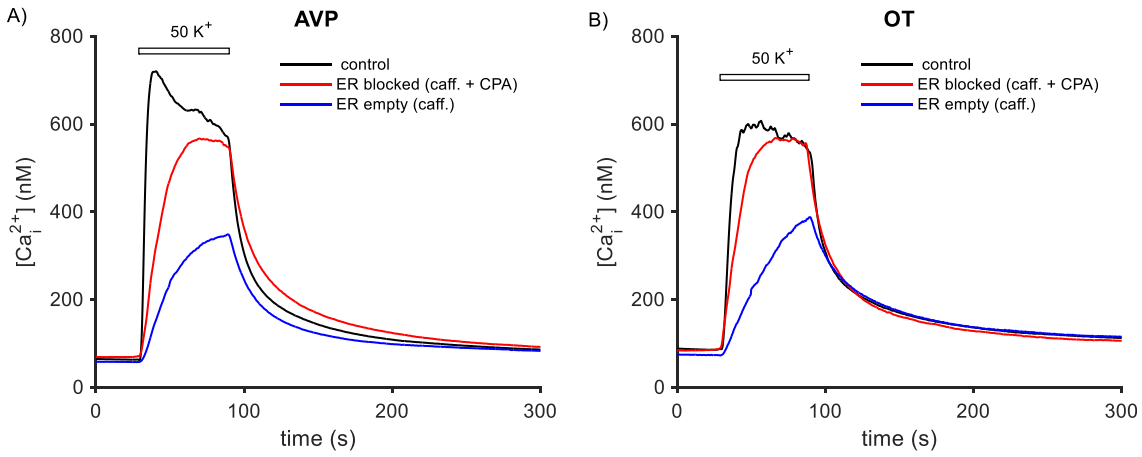

Figure 4.15: A comparison of control K^+-induced $[Ca^{2+}]_i$ responses with responses obtained after a pharmacological manipulation with the ER. Responses obtained in control conditions (black line), in conditions with depleted and blocked ER by a combination of caffeine and CPA (red line) and in conditions with the ER depleted just by caffeine (blue line). A): Traces averaged from n = 5 AVP neurones. B): Traces averaged from n = 5 OT neurones.

These results, however, were obtained after an artificial manipulation with the intracellular Ca^{2+} stores with the aim to force the ER depletion and thus may not be the perfect representative example in terms of the natural ability of the MNCs to regulate their responses. For further evaluation, we recorded responses where no pharmacological treatment was used, and the amplitude adaptation was only a result of a repeated exposure

to depolarization. An example of such measurement is in figure 4.7. In this case, we recorded responses with a range of maximum rate from 50 nM/s (for the last response of the train) to 500 nM/s (for the initial one). All the responses in the train were elicited by the same strength of depolarization (50 mM K^+), and no ER-targeting drugs were used. This clearly shows that the ability of adaptation rises from the intrinsic properties of the individual MNCs and thus represents an extensive range of response modulation.

4.3 Physiology of spontaneous $[Ca^{2+}]_i$ oscillations

In this section, we studied spontaneous $[Ca^{2+}]_i$ oscillations of the SON AVP and OT neurones in an isolated condition. We have analysed how these oscillations are affected by the physiological state of the animal (dehydration, lactation) and by an exposure to extracellular stimuli (osmotic change, activation of autocrine signals by an extracellular application of AVP). We studied $[Ca^{2+}]_i$ dynamics in unidentified SON neurones from wild type adult male and virgin Wistar rats and in identified neurones from transgenic rats expressing i) an arginine vasopressin (AVP)-enhanced green fluorescent protein (AVP-eGFP) (Ueta, Fujihara et al. 2005), ii) an oxytocin-monomeric red fluorescent protein 1 (OT-mRFP1) and iii) double transgenic rats bearing both AVP-eGFP and OT-mRFP1 to visualize both AVP and OT neurones in the same animal (Ueta, Dayanithi et al. 2011, Dayanithi, Forostyak et al. 2012). The results presented in this section have been published separately as (Kortus, Srinivasan et al. 2016) and are available in full form in appendix B.II.

4.3.1 General features of the $[Ca^{2+}]_i$ oscillations in SON neurones

We observed spontaneous $[Ca^{2+}]_i$ oscillations in 79 out of 112 unidentified neurones (71%). Among identified neurones, 12 out of 15 AVP cells (80%) and 9 out of 15 OT cells (60%) exhibited oscillations. figure 4.16 shows a typical example of $[Ca^{2+}]_i$ oscillation in an identified OT-mRFP1 neurone (panel A) and in AVP-eGFP neurone (panel B).

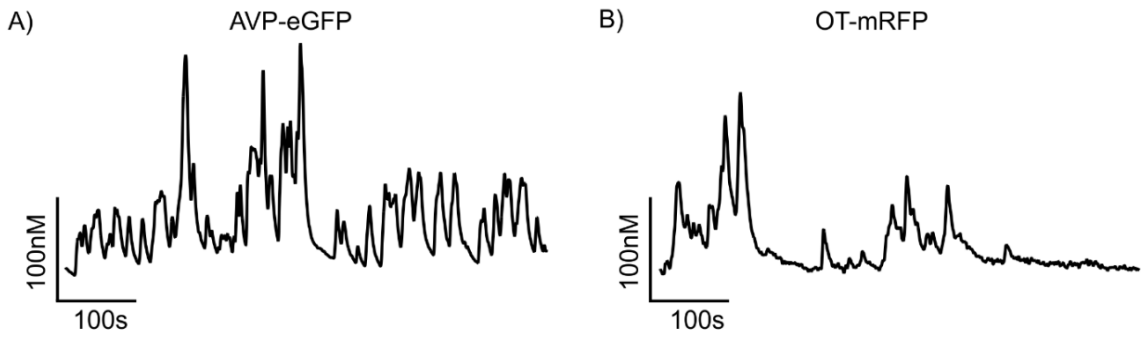

Figure 4.16: Representative traces of spontaneous $[Ca^{2+}]_i$ oscillations recorded under normal condition in identified OT neurone (A) and AVP neurone (B).

For each spontaneous oscillation trace, we computed the four basic parameters defined in section 3.4 of methods. We then evaluated if these parameter values differed among the three cell groups (unidentified, AVP and OT). No statistically significant difference was found (assessed by unpaired t-test). This primarily reflects the large variability among the oscillation traces within each cell group.

The pattern of $[Ca^{2+}]_i$ oscillations was highly heterogeneous and can be qualitatively classified into the following three types. The type I pattern is characterized by Ca^{2+} events of regular amplitude and frequency (figure 4.17A); type II consists of irregular events that frequently overlap and form bursts (figure 4.17B); type III contains of oscillations of high frequency, during which $[Ca^{2+}]_i$ remains continually elevated above the baseline level (figure 4.17C). We visually examined the $[Ca^{2+}]_i$ traces recorded in 79 unidentified neurones and classified them, based on the qualitative criteria stated above. Type I activity was observed in 29 cells, type II in 34, and type III in 16 cells.

As we observed that the pattern of oscillation often changed when an external stimulus was presented (see following subsections), we sought a simple quantitative classifier that would allow us to systematically express such pattern changes. The frequency or amplitude of the oscillation peaks could not be used for this purpose, as these parameters become ill-defined for irregular oscillations (figure 4.17C). We found, however, that the skewness of the distribution of $[Ca^{2+}]_i$ values permits distinguishing the basic oscillation patterns. As shown in figure 4.17D-F, the distribution of the $[Ca^{2+}]_i$ values within the trace has a highly asymmetrical shape in case of the oscillation pattern of Type I (as in figure 4.17A), moderately asymmetrical for the Type II pattern (as in figure 4.17B), and symmetrical for the Type III pattern (as in figure 4.17C). The strong asymmetry of the distribution in type I arises from the shape of the stereotypical oscillation peaks: a fast rise in $[Ca^{2+}]_i$ followed by a slower, exponential decay. Correspondingly, the distribution of $[Ca^{2+}]_i$ values is approximately exponential, with skewness value $\gamma = 1.83$ in the example in figure 4.17D. In type II, the irregular parts of the oscillation result in a nonexponential tail in the distribution and a lower skewness ($\gamma = 0.93$, figure 4.17E). Finally in type III, the fast deviations up and down from the mean $[Ca^{2+}]_i$ level result in an approximately symmetrical distribution with nearly zero skewness ($\gamma = 0.23$ in figure 4.17F). figure 4.17G shows the range of skewness values in the neurones of each type, where the type was determined by visual examination of the trace as discussed above. As these ranges have low overlap, the skewness can be used as a quantitative classifier, replacing the qualitative

visual inspection. In the following, we consider traces with skewness above 1.52 as Type I, between 1.52 and 0.43 as Type II, and below 0.43 as Type III.

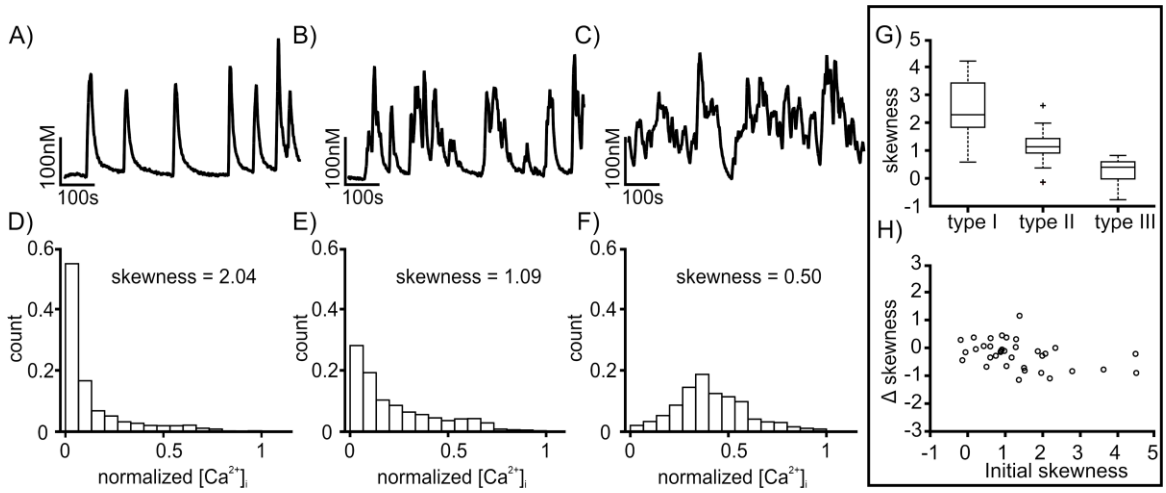

Figure 4.17: A-C show representative traces from AVP-eGFP neurones in normal condition, and correspond to oscillations of type I, II, and III, respectively (see main text). D-F show the corresponding histograms of $[Ca^{2+}]_i$ values recorded in the traces located above the histograms. (G) Range of skewness values (showed as standard box plot) in oscillation traces of the indicated type. (H) Control plot showing the difference of skewness in 2nd half and 1st half of $[Ca^{2+}]_i$ trace recorded in normal conditions (compare with figure 4.18C, D and figure 4.20C).

4.3.2 Effect of osmolarity on spontaneous $[Ca^{2+}]_i$ oscillations

To evaluate the effect of osmolarity, $[Ca^{2+}]_i$ dynamics in oscillating neurones was monitored for 300 sec in NL with a standard osmolarity of 295-300 mOsmol/l. Then the perfusion solution was switched to either hypo-osmotic (275 mOsmol/l) or hyper-osmotic (325 mOsmol/l) solution and $[Ca^{2+}]_i$ dynamics was monitored for another 300 sec. Representative examples of oscillating neurones subjected to hyper- (A) or to hypo- (B) osmotic stimuli are shown in figure 4.18.

For each neurone, we calculated the four basic trace parameters (for details see section 3.4), and evaluated if the change in these parameters in normal vs. hypo- or hyper osmolarity condition was statistically significant (using the paired t-test as described in section 3.4.2). The results are summarized in figure 4.19. For neurones exposed to hypo-osmotic solution (n = 20) we recorded a significant decrease in mean $[Ca^{2+}]_i$ level (22.8 ±

5.0 nM, p-value 0.01) and in the spread SD_{Ca} of $[Ca^{2+}]_i$ within the trace segment (28.3 ± 8.0 nM, p-value 0.02). The other two evaluated parameters, the $[Ca^{2+}]_i$ baseline and the skewness of the $[Ca^{2+}]_i$ distribution, did not change significantly (p = 0.82 and 0.08). For neurones exposed to hyper-osmotic solution (n = 48), the increase of mean $[Ca^{2+}]_i$ level was 11.8 ± 5.1 nM and the increase of SD_{Ca} was 7.0 ± 3.7 nM. Similarly, the hypo-osmotic case, these changes were statistically significant (with p-value 0.02), while the changes in baseline and skewness were not (p = 0.1 and 0.9).

Even though the change in skewness was not significant when averaged over all neurones in the group, we did observe significant trends when the initial state of the neurone (i.e., the state in the normal osmotic condition) was taken into account. The skewness of the $[Ca^{2+}]_i$ distribution tends to increase in neurones that had low initial value of skewness, and to decrease in neurones that had high initial skewness (figure 4.18). This observation is valid for both hyper- (figure 4.18C) and hypo- (figure 4.18D) osmotic stimuli. To summarize, exposure to an osmotic stimulus tends to make $[Ca^{2+}]_i$ activity more regular, bringing the oscillation into a type II pattern (intermediate range of skewness values, marked in yellow in figure 4.18C, D).

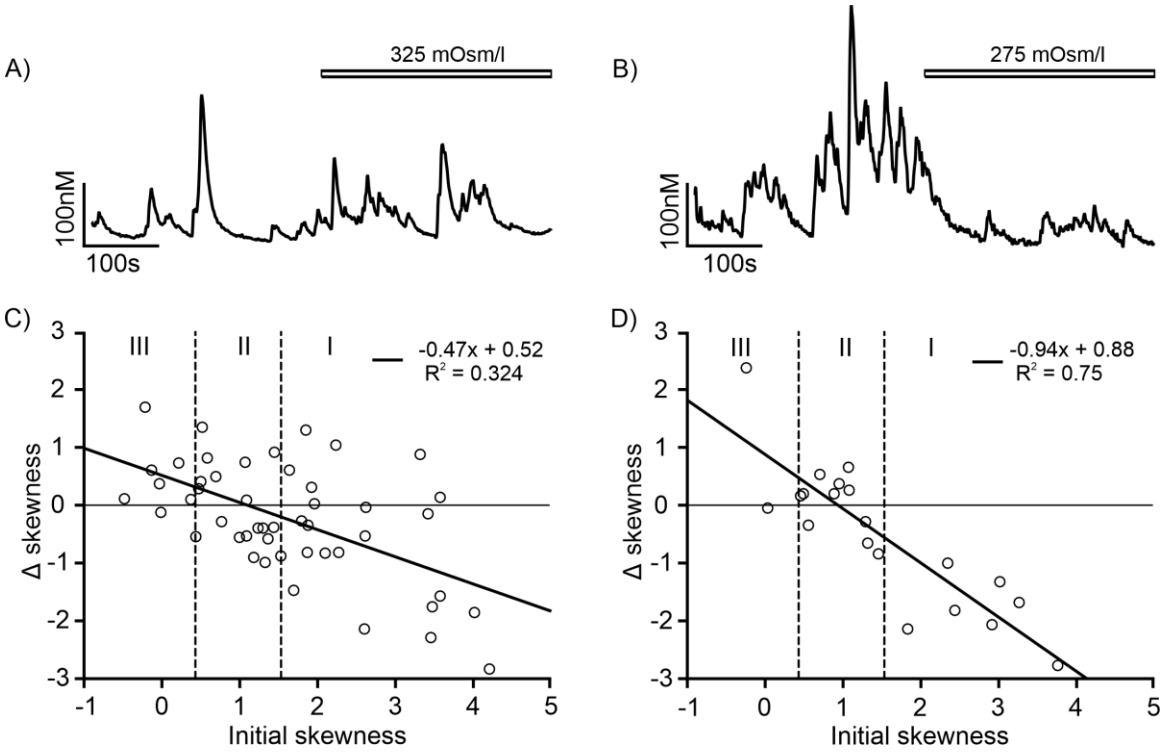

Figure 4.18: Effect of osmotic change on $[Ca^{2+}]_i$ oscillations. (A, B): The $[Ca^{2+}]_i$ trace from neurones subjected to A: hypertonic solution (325 mOsmol/l; bar), B: hypotonic

solution (275 mOsmol/l; bar). (C, D) Change in skewness resulting from exposure to tonic solution, plotted as function of initial skewness (before exposure). C: hypertonic, D: hypotonic solution.

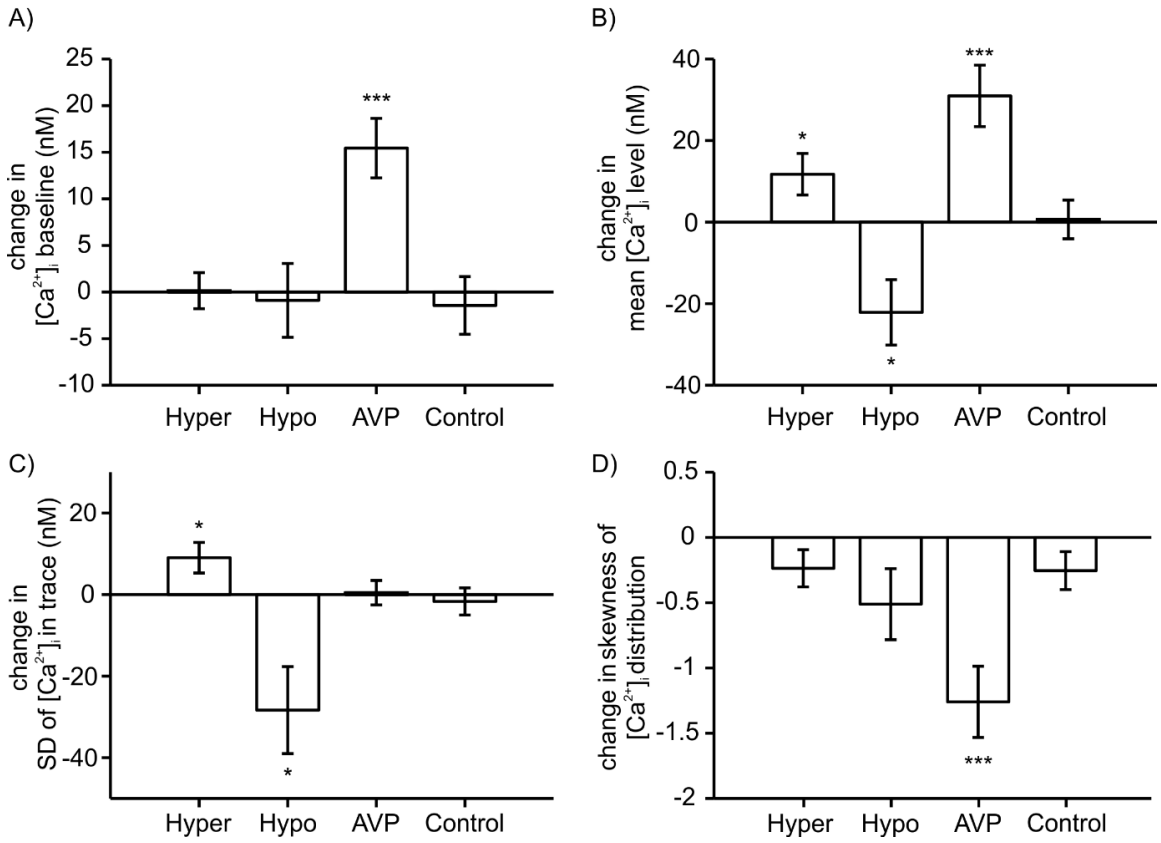

*Figure 4.19: Modulatory effect of AVP and osmolarity on $[Ca^{2+}]_i$ oscillations. The four panels show, for each evaluated $[Ca^{2+}]_i$ trace parameter, the change in its value following the application of the specified stimulus (hyper-osmolar, hypo-osmolar, AVP). The respective numbers of measured neurones are: hyper-osmolar, n = 48; hypo-osmolar, n = 20; AVP, n = 31. Panel A) shows the change in $[Ca^{2+}]_i$ baseline, B) in mean $[Ca^{2+}]_i$ level, C) in spread (SD) of $[Ca^{2+}]_i$ within the trace, and D) in skewness of the $[Ca^{2+}]_i$ distribution. The bars show the mean value of the parameter change and the respective standard error of the mean. Statistical significance is indicated as: * for p-value < 0.05; ** for p < 0.01, and *** for p< 0.001 (paired t-test). In the column marked "Control", the panels show the differences between the first and second half of a $[Ca^{2+}]_i$ trace, with the entire trace recorded in normal condition (no stimulus); n = 38. None of these differences were statistically significant.*

4.3.3 Effect of AVP on $[Ca^{2+}]_i$ oscillations

We tested the response of 28 oscillating neurones to 1 μM AVP. In each neurone, we compared the oscillations before and after application AVP; the results are summarized in figure 4.19. In majority of neurones the AVP had an obvious enhancing effect on the oscillation (for an example, see figure 4.20A). While SD_{Ca} of $[Ca^{2+}]_i$ for the trace did not change (figure 4.19C), AVP caused a highly significant increase ($p = 0.0003$) of the mean $[Ca^{2+}]_i$ level with average change of 31.0 ± 7.5 nM and a highly significant increase ($p = 0.0002$) of $[Ca^{2+}]_i$ baseline with an average change of 13.4 ± 3.2 nM. In addition, AVP elicited very significant ($p = 0.001$) negative change in the skewness of the $[Ca^{2+}]_i$ distribution giving a strong average decrease of 1.26 ± 0.27. When the initial skewness was in the intermediate range (type II oscillation), it was only weakly affected by AVP, while in neurones with high initial skewness (type III), AVP typically prompted a switch to type II oscillatory behaviour (figure 4.20C). Beside the effect on oscillating neurones, in some cases ($n = 5$) AVP triggered oscillations in silent neurone (example in figure 4.20B) and in one case, the AVP attenuated the oscillations (figure not shown). These results mainly indicate a strong enhancing effect of the AVP on $[Ca^{2+}]_i$ oscillations in magnocellular neurones. These AVP effects on oscillations were mimicked by the specific AVP-V_{1a} receptor agonist (Gouzenes, Sabatier et al. 1999).

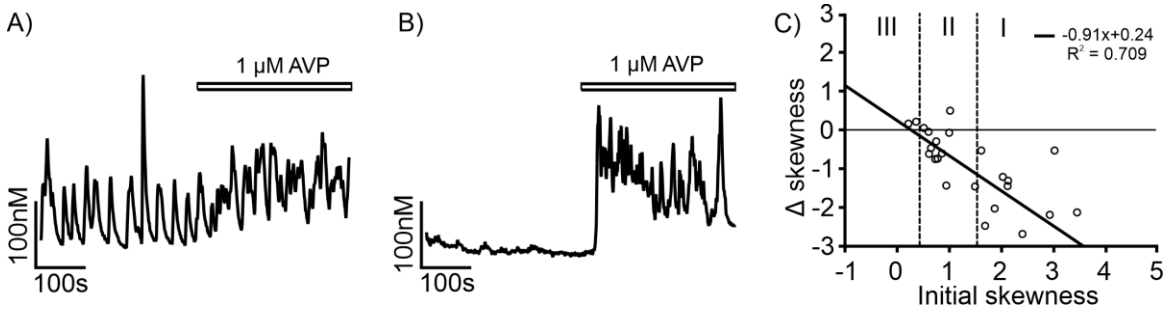

Figure 4.20: Trace A represents spontaneous Ca^{2+} oscillations observed in SON neurone. The same neurone was subjected to 1 μM AVP (shown in bar). Trace B is an example of a silent and non-oscillating neurone to which 1μM AVP was applied and triggered oscillation. C: Change of the skewness introduced by application of AVP plotted as a function of initial skewness. Indexed areas correspond to oscillatory types (left - type III, middle - type II, right - type I) introduced in figure 4.17. Majority of neurones display decrease in skewness corresponding to higher activity.

4.3.4 $[Ca^{2+}]_i$ oscillations in neurones from dehydrated or lactating rats

Three groups of animals were prepared. In the control group, the rats were maintained under normal conditions (see Methods in section 3.1) with unlimited access to water. In two other groups, the animals were deprived of water for 3- day and 5- day, respectively. In neurones obtained from 3-day dehydrated rats 18 of 20 cells were spontaneously oscillating. In neurones isolated from 5-day dehydrated rats 9 of 10 neurones were continuously oscillating. The percentages of the spontaneously oscillating neurones form both 3-day and 5-day dehydration animals were 90%, as compared with 71% in the control group of unidentified neurones (section 4.3.1). The pattern of oscillations obtained from dehydrated rats was not different from oscillations in normal conditions and none of the four trace parameters exhibited statistically significant differences among these groups (unpaired t-test).

We also measured the $[Ca^{2+}]_i$ oscillations in identified OT-mRFP1 neurones from 3 to 5-day-lactating rats (figure 4.21). The number of oscillating neurones isolated from lactating animals was 18 of 23 recorded cells.

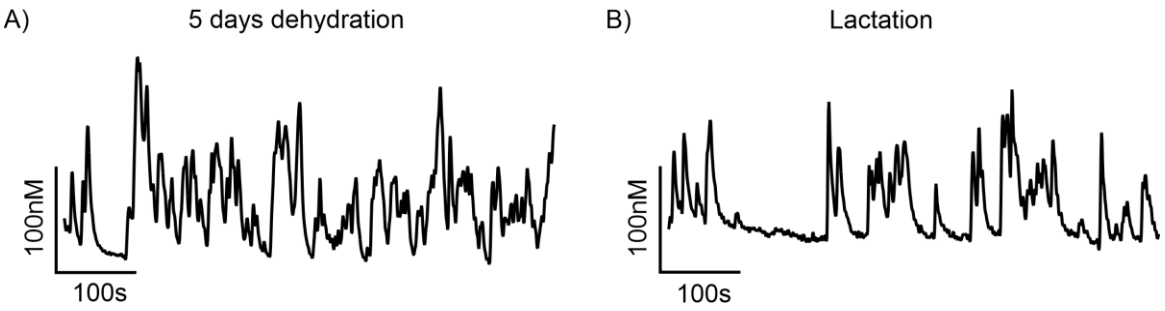

Figure 4.21: Traces of spontaneous $[Ca^{2+}]_i$ oscillations recorded in neurone obtained from 5 days dehydrated rat (A) and from 6-day lactating rat (B).

5 Discussion and conclusions

The following section is intended to interpret the results introduced earlier in this work and discuss them on the background of recent studies of the magnocellular neurosecretory system in literature. The structure of the discussion will follow the outline of the introduction and the results section of this work. First, we will discuss the results concerning mechanisms underlying the spontaneous Ca^{2+} oscillations from section 4.1 and mechanisms underlying the induced $[Ca^{2+}]_i$ responses from section 4.2. In a separate section, we will also discuss the properties of the spontaneous Ca^{2+} oscillations with a focus on the possible physiological consequences on the regulation of OT and AVP secretion. Finally, we will summarize the most important results and propose hypothetical conclusions of this work.

5.1 Mechanisms of spontaneous $[Ca^{2+}]_i$ oscillations

In the result section 4.1, we performed an extensive screening of the contribution of the plasmalemmal Ca^{2+} and Na^+ ion channels, the Na^+/Ca^{2+} exchanger (NCX), the intracellular Ca^{2+} release channels (IPRs and RyRs), the Ca^{2+} storage organelles and the plasma membrane Ca^{2+} pump to the spontaneous $[Ca^{2+}]_i$ oscillations. In excitatory cells, an influx of extracellular Ca^{2+} occurs typically in response to an electrical activity which depolarizes the membrane, opens the VGCCs and provides an influx of the extracellular Ca^{2+} (Berridge 2005). A similar situation occurs in the magnocellular neurones, where action potentials directly activate the Ca^{2+} entry (Roper, Callaway et al. 2003). However, in terms of spontaneous $[Ca^{2+}]_i$ activity, our experiments show that the inhibition of electrical activity with tetrodotoxin (TTX) did not affect the spontaneous $[Ca^{2+}]_i$ oscillations, indicating that the electrical activity and the spontaneous $[Ca^{2+}]_i$ oscillations are separate. Such dissociation of electrical activity and spontaneous $[Ca^{2+}]_i$ oscillations suggests an existence of a specific pacemaker behind the oscillations.

Besides the lack of effect of a direct suppression of action potentials with TTX, the spontaneous $[Ca^{2+}]_i$ oscillations in SON neurones were effectively inhibited by the removal of extracellular Na^+ (figure 4.4B). The very same inhibition was achieved by KB-R7943 (figure 4.4C), a specific inhibitor of the reverse mode of the Na^+/Ca^{2+} exchanger (NCX).

The theoretical reversal potential of the exchanger in SON neurones (at a resting level of $[Ca^{2+}]_i$ = 130 nM, $[Na^+]_i$ = 10 mM, $[Na^+]_o$ = 140 mM) is about -45 to -50 mV. Thus, considering the resting membrane potential of MNCs of about -65 mV (Armstrong 1995), a moderate depolarization is capable to reverse the NCX operation and possibly cause the inhibition of the oscillations, as we have observed (figure 4.4). In the reverse mode, the NCX provides Ca^{2+} entry, which logically contributes to the observed Ca^{2+} oscillations. The involvement of the extracellular Ca^{2+} via the NCX is in contrast to numerous examples of spontaneous $[Ca^{2+}]_i$ dynamics originating from the Ca^{2+} release from the endoplasmic reticulum (Kawano, Otsu et al. 2003, Sneyd, Tsaneva-Atanasova et al. 2004, Verkhratsky 2005). In SON neurones, the involvement of the endoplasmic reticulum (ER) does not seem to be the case. Beside the temporal distortion of the oscillations in few neurones, targeting the ER using TG, CPA, ryanodine or caffeine failed to affect the $[Ca^{2+}]_i$ oscillations (figure 4.5). Caffeine has a double action of the ER activating the RyRs and effectively inhibiting the $InsP_3$ receptors (Wakui, Osipchuk et al. 1990, Bezprozvanny, Bezprozvannaya et al. 1994); TG and CPA effectively inhibit the function of the ER SERCA pump. Nevertheless, the role of the ER is questionable; we have proved that the repetitive release of Ca^{2+} from the ER is not required for the oscillations; however, we have also showed that the ER plays a critical role in repeated depolarization induced $[Ca^{2+}]_i$ responses (results in section 4.2.7). Based on the temporal distortion of the oscillations by the ER-targeting drugs, it is possible that the ER plays a modulatory function in contribution to the $[Ca^{2+}]_i$ oscillations.

The absence of inhibitory effect of ER-targeting drugs on the spontaneous $[Ca^{2+}]_i$ oscillations argues against the role of the ER Ca^{2+} release as the main source of Ca^{2+}. At the same time, the removal of the extracellular Ca^{2+} effectively blocked the spontaneous $[Ca^{2+}]_i$ dynamics and strongly indicates the importance of extracellular Ca^{2+} for the oscillations. The NCX, however, is not the only mechanism for Ca^{2+} delivery associated with the spontaneous $[Ca^{2+}]_i$ activity of SON neurones. Our screening of the VGCCs indicates that the $[Ca^{2+}]_i$ oscillations appear to be specifically associated with the R-type VGCCs. Treatment with a selective blocker of R-type channels, SNX-482, reversibly inhibited the $[Ca^{2+}]_i$ oscillations in a concentration-dependent manner (figure 4.3). A pharmacological screening of an inhibition of the other VGCCs (T, L, N and P/Q types) showed no visible effect on the oscillations. Similarly, an inhibition of the intercellular second messenger cascades and plasmalemmal K^+ channels did not affect the spontaneous $[Ca^{2+}]_i$ activity either.

According to our results, we propose the three mechanisms of the R-type, the NCX and the PMCA as the mechanism directly involved in forming and maintaining the $[Ca^{2+}]_i$ oscillations. This is supported by the fact that only a specific inhibition of these mechanisms inhibited the oscillations. The role of the NCX and the R-type Ca^{2+} channels is also supported (albeit indirectly) by the inhibitory action of GABA, which completely blocked the spontaneous $[Ca^{2+}]_i$ dynamics (figure 4.6A). This action was mediated through GABA A receptors (as revealed by gabazine sensitivity) and most likely resulted from cell hyperpolarization (figure 4.6B). The latter, arguably, prevented the reversal of the NCX and the activation of the R-type Ca^{2+} channels. Involvement of other mechanisms, not covered in this study, is possible, as no theoretical model of $[Ca^{2+}]_i$ oscillations based exclusively on these three mechanisms is known at present.

5.2 Depolarization-induced $[Ca^{2+}]_i$ elevations

Responses to K^+ depolarization have often been used as a tool for studying the cellular Ca^{2+} mechanisms in MNCs that require depolarization for their activation (Brethes, Dayanithi et al. 1987, Oliet and Bourque 1992, Sabatier, Richard et al. 1997, Ludwig, Sabatier et al. 2002). The elevation of $[Ca^{2+}]_i$ with high K^+ was described as strictly dose-dependent in MNCs (Sabatier, Richard et al. 1997, Dayanithi, Forostyak et al. 2012). In section 4.2, we studied the properties of depolarization-induced $[Ca^{2+}]_i$ responses in isolated MNCs. A single prolonged 60-s exposure to 50 mM K^+ evoked typical biphasic responses consisting of a rapid elevation, which formed an initial peak (overshoot), followed by a slow decrease until reaching a steady-state level. Finally, after the end of the depolarization stimulus, the $[Ca^{2+}]_i$ quickly declined towards the basal level. The slow decay during the depolarization stimulus has been discussed earlier in (Komori, Tanaka et al. 2010), where it was attributed to the K^+ channel desensitization. A random appearance of the initial overshoot was also mentioned and hypothesized to be specific for a subpopulation of MNCs, preferentially the AVP neurones. However, here we repeatedly observed the initial peak in both MNC subtypes, and the responses were not strictly dose dependent. In experiments with repeated exposures, the cells displayed a progressive degradation of the response amplitude, even though they were elicited by the same K^+ stimulus (figure 4.7). The expectation of dose-dependent responses was further tested by an exposure to a train of different K^+

concentrations (figure 4.8), clearly showing that MNC neurones do not keep their K^+ dose-dependency when challenged by repetitive depolarizations.

Here we hypothesize that the response to high K^+-induced depolarization in MNCs consists of two major components: a depolarization-dependent Ca^{2+} influx and a component of the intracellular Ca^{2+} release from the ER via the CICR mechanism which accompanies the influx and forms the initial peak. The appearance of the initial peak is then determined by the filling state of the ER, which gradually decreases during repeated responses and supresses or completely abolishes the appearance of the peak.

Experimental support for these conclusions:

1) The K^+-induced $[Ca^{2+}]_i$ responses are not strictly dose-dependent. MNCs do not preserve the dose-dependency after repeated K^+ exposures (figure 4.8).
2) The amplitude of $[Ca^{2+}]_i$ elevations evoked by K^+ depolarization degrades with repetitions but is effectively re-established after a sufficient break between two depolarization stimuli (figure 3.5A). It indicates a gradual depletion of the Ca^{2+} accumulated in the intracellular stores and its subsequent re-accumulation (figure 4.7).
3) The initial high $[Ca^{2+}]_i$ peak is completely attenuated when the ER Ca^{2+} stores are depleted with caffeine and the SERCA uptake is blocked with CPA (figure 4.9A–B).
4) The response is even more attenuated when the Ca^{2+} stores are depleted by caffeine, while the SERCA pump is left untouched. It indicates that part of the incoming Ca^{2+} is immediately stored to the emptied ER by the SERCA pump, causing the strong attenuation (figure 4.9C–D).
5) The separation of the individual Ca^{2+} fluxes in figure 4.14 revealed two major Ca^{2+} income components: the low-rate steady J_{in} flux and the high-rate rapidly decaying J_{er} flux.
6) The high-rate component J_{er} quickly decays, lasting only several seconds, and is completely abolished after treatment with caffeine and CPA. It provides strong evidence that the flux is driven by the release of Ca^{2+} from the ER.
7) The low-rate component J_{in} is not affected by caffeine/CPA treatment, is exclusively associated with the presence of the depolarization stimulus and is stable during the whole duration of stimulus, showing no signs of channel desensitization.

These are reasonable grounds to assign the low-rate component to the depolarization-induced Ca^{2+} entry (J_{in}) and the high-rate component to the rapid Ca^{2+} release from the ER (J_{er}). The combination of the two fluxes provides a better explanation of the slow decay during the stimulus than the K^+ channel desensitization. The response starts with two fluxes and quickly reaches the maximum amplitude, then the rapid flux fatigues, and the $[Ca^{2+}]_i$ starts to decay to reach a new steady level. The depolarization-dependent J_{in} flux persists for the whole duration of the depolarization stimulus, and if we take into consideration the relatively slow dynamics of $[Ca^{2+}]_i$ responses, we conclude that the J_{in} flux is triggered by the depolarization in an "on/off" manner.

In terms of differences between OT and AVP neurones, as mentioned above, we have observed and recorded responses in identified OT and AVP neurones multiple times, and the initial overshoot was presented in both subtypes. The AVP and OT neurones also showed very similar behaviour under treatment by the ER-targeting drugs. The only possible difference was found in the maximum amplitude of the overshoot, which was, in our data, usually greater in AVP neurones. In the AVP neurones, the overshoot reached up to double of the $[Ca^{2+}]_i$ level in the steady phase of the response. We have never recorded an overshoot of such intensity in an OT neurone. The results also show that the CICR mechanism in MNC neurones does not require the presence of caffeine, unlike some other cell types (Albrecht, Colegrove et al. 2001), and is triggered directly by a rapid rise of $[Ca^{2+}]_i$ induced by the depolarization.

The presented data clearly describe a very wide range of $[Ca^{2+}]_i$ responses. The rate of response to the 50 mM K^+ depolarization stimulus varied from 20 nM/s to 500 nM/s depending on the filling state of the ER. During the phasic activity in AVP neurones, the $[Ca^{2+}]_i$ is elevated at a level of about 400–500 nM (Roper, Callaway et al. 2004). In the full ER condition, the cell can reach this level within 1 s, whereas when the store is depleted, the time rises to tens of seconds.

As a possible consequence, these results strongly indicate that the $[Ca^{2+}]_i$ responses of MNCs are highly dependent on the inner conditions of the cell, which in turn depend on its previous actions. The history of previous Ca^{2+} activity controls the initial overshoot pattern of the biphasic $[Ca^{2+}]_i$ response and enables to act as a memory. The ER helps to achieve a higher concentration of $[Ca^{2+}]_i$, but it is able to remove Ca^{2+} when depleted after an intense period of activity. The ER can accelerate the rise of $[Ca^{2+}]_i$ by a rate of >200 nM/s when fully charged, and on the contrary, the depleted ER is able to temporarily

remove Ca^{2+} with a rate of about -20 nM/s. Such rate is very close to the estimated rate of the J_{in} flux for 50 mM K^+ (30 nM/s). By this mechanism, the MNCs can significantly delay the $[Ca^{2+}]_i$ elevation and perhaps enable a protection against large sustained increases in $[Ca^{2+}]_i$. This not only plays an important role in the shaping of $[Ca^{2+}]_i$ signals, but the memory effect of the ER may also have a function in the regulation of AVP and OT release. The elevated $[Ca^{2+}]_i$ causes hyperpolarization and works against the firing consecutive action potentials. Based on a previous study, the shift from silent/sporadic firing to bursting is not smooth but is rather a hard switch from one mode to another (MacGregor and Leng 2012). The filled ER can work as a barrier that prevents the cell from randomly switching from silent/sporadic firing to the bursting mode. When only a few spikes are fired, the cell responds by a rapid elevation of $[Ca^{2+}]_i$ and quickly suppresses the initiation of the burst. To effectively trigger the burst, the cell would require an intensive and prolonged afferent stimulation, which causes a depletion of the ER, attenuates the $[Ca^{2+}]_i$ response, and, in turn, lets the cell switch to the bursting mode.

The importance of intracellular Ca^{2+} stores has been previously shown for both OT and AVP neurones (Ludwig, Sabatier et al. 2002, Ludwig, Bull et al. 2005); the irreversible blocker of the SERCA completely disturbed the regulation of the hormone and resulted in overdone responses to K^+ by the secretion of an extensively larger amount of the hormone. These and our present results point out the important role of the intracellular Ca^{2+} stores, yet the exact role in the regulation of MNCs needs to be explained.

5.3 Physiological properties of $[Ca^{2+}]_i$ oscillations

Until now, we have discussed the properties of cellular mechanisms that are responsible for forming induced or spontaneous Ca^{2+} signals. In this part, we focus on the general characterization and physiological purpose of the spontaneous $[Ca^{2+}]_i$ oscillations in MNCs. In results from section 0, we have reported a detailed analysis of the spontaneous $[Ca^{2+}]_i$ oscillations observed on MNCs under a variety of physiological or pathophysiological conditions. We have tested how $[Ca^{2+}]_i$ oscillations are affected during dehydration or lactation and how they are modulated by an exposure to extracellular stimuli mimicking osmotic change or autocrine stimulation by AVP.

Spontaneous $[Ca^{2+}]_i$ oscillations exhibited a wide range of patterns, ranging from regular oscillations with stereotypical $[Ca^{2+}]_i$ peaks to irregular fast oscillations (figure 4.17 in section 4.3.1). The heterogeneous character of the oscillations did not permit a consistent characterization by frequency and amplitude. Instead, we relied on a combination of four quantitative parameters: the $[Ca^{2+}]_i$ baseline, the mean $[Ca^{2+}]_i$ elevation, the spread (standard deviation) of $[Ca^{2+}]_i$ values and the skewness of the $[Ca^{2+}]_i$ distribution (details in section 3.4 of the methods).

In our experiments, the majority of AVP neurones (>70%) and some OT neurones (>50%) were oscillatory, in the OT neurones of lactating female rats, the number of oscillating neurones rose (up to 80–90%) and equalled the number of the AVP oscillating neurones. This may indicate that the OT neurones undergo changes that activate Ca^{2+} mechanisms behind the oscillations. However, further experiments are necessary to identify whether spontaneous $[Ca^{2+}]_i$ oscillations of OT neurones play a regulatory role during lactation. The effects of dehydration on AVP and OT neuronal activity, as well as on the release of AVP and OT at the level of the soma and the neurohypophysis, have been widely discussed (Knight, Ji et al. 2010, Trudel and Bourque 2012). We have found that almost all MNCs preserved their ability to display $[Ca^{2+}]_i$ oscillations during 3–5 days of dehydration and that the proportion of oscillating neurones reached 90%. This observation is consistent with the need to have more AVP released both at the soma and at nerve terminals; and therefore, to increase the plasma AVP level to fulfil the physiological demands.

The osmosensitivity of isolated MNCs and their behaviour under osmotic change are already known; notably, the electrical activity of AVP neurones acutely isolated from the rat supraoptic nucleus is increased by hypertonicity and inhibited by hypotonicity in the absence of neighbouring glial cells and without any synaptic connectivity (Oliet and Bourque 1992, Trudel and Bourque 2012). Hypertonic stimuli excite the cells by increasing the activity of non-selective cation channels, thus causing membrane depolarization, whereas hypo-osmotic solutions inhibit AVP neurones through a hyperpolarization caused by a reduction in the basal activity of the non-selective cation channels. In terms of Ca^{2+} signalling, we report that a majority of MNCs were sensitive to osmotic changes, suggesting that both AVP and OT neurones employ Ca^{2+} signals for osmoregulation. We have found that both hypo- and hyper-osmolarity changed the mean $[Ca^{2+}]_i$, the elevation as well as the amplitude of the oscillations expressed as variations around this mean (i.e., the SD of $[Ca^{2+}]_i$ in the traces changed).

Another aspect of our study was in examining the various effects of AVP on the spontaneous $[Ca^{2+}]_i$ oscillations. In previous studies, using *in vivo* electrophysiology, the somato-dendritic release of AVP has been shown to modulate the electrical activity of magnocellular neurones (Moos, Rossi et al. 1997, Moos, Gouzenes et al. 1998). Here we have demonstrated that $[Ca^{2+}]_i$ oscillations observed in AVP neurones similarly display several patterns, and AVP modulated these oscillations in an excitatory manner: in silent neurones, AVP triggered the oscillations; in oscillating neurones, AVP intensified these oscillations (figure 4.20).

The excitatory effect of AVP was, however, different from a similar effect introduced by acute hyper-osmotic stimuli. Both AVP and osmotic stimuli modulated the mean $[Ca^{2+}]_i$ level of the oscillations: AVP and hyper-osmotic stimuli elevated the mean $[Ca^{2+}]_i$, hypo-osmolarity decreased it (figure 4.19B). For osmolarity, the change in mean $[Ca^{2+}]_i$ was caused by a change in the amplitude of the oscillatory peaks represented by the standard deviation of the trace (figure 4.19C). In the case of AVP, the amplitude was not changed, and the elevation of the $[Ca^{2+}]_i$ mean level was caused by an overall elevation of the baseline of the oscillatory pattern (figure 4.19A). Besides the effect on the baseline of the oscillations, AVP also significantly modified the pattern of the oscillations, captured by the skewness parameter of the $[Ca^{2+}]_i$ traces (figure 4.19D). This indicates that the modulatory effect of somatic exposure to AVP or osmotic change involves different mechanisms and provides independent pathways in the regulation of the spontaneous $[Ca^{2+}]_i$ activity of the MNCs.

5.4 Conclusions

Among all the discussed results, we would like to point out the most important conclusions of this thesis. We show that magnocellular AVP and OT neurones exhibit distinct spontaneous $[Ca^{2+}]_i$ oscillations in an isolated state under various experimental conditions. These oscillations rise from an intrinsic mechanism that does not require action potentials or external pacing. The properties of the oscillations are shown to mimic their intrinsic electrical behaviour under physiological conditions such as osmotic change, dehydration and lactation. We demonstrate the ability of magnocellular neurones to sense osmolarity through the modulatory effect of acute osmotic change on the oscillation pattern. The

understanding of the autoregulatory mechanisms of AVP neurones, regulated by a peptide they synthesize on their own, is reinforced by the presented data. The effects of AVP and osmotic change on the $[Ca^{2+}]_i$ oscillation pattern are summarized in the table in figure 5.1A.

In terms of mechanisms underlying the spontaneous $[Ca^{2+}]_i$ oscillations, we demonstrate that the oscillations in the MNCs are driven by the extracellular Ca^{2+} and require plasmalemmal R-type Ca^{2+} channels and the Na^+/Ca^{2+} exchanger oscillation between forward and reverse modes and the plasmalemmal Ca^{2+} pump. Figure 5.1B schematically illustrates these Ca^{2+} transport mechanisms.

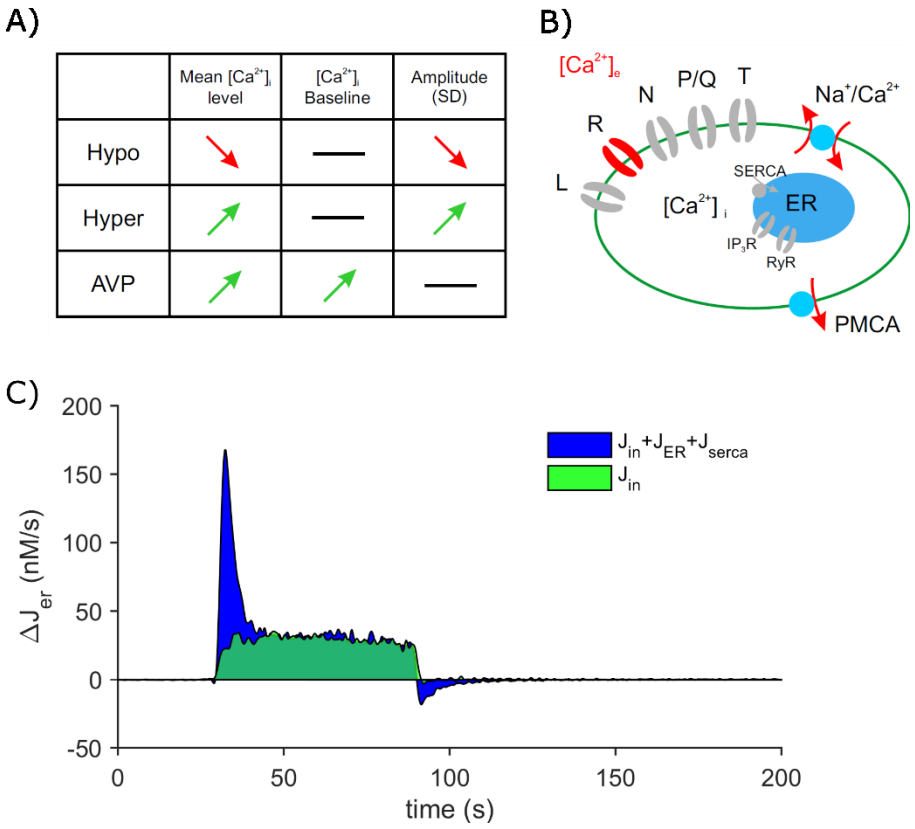

Figure 5.1: An illustration of the thesis conclusions. A) The effect of osmolarity change (hypo, hyper) and exposure to AVP on the pattern of $[Ca^{2+}]_i$ oscillations. The arrows indicate a significant change of the measured parameter from its control value. In general, the upward arrows stand for an excitatory effect, whereas the downward arrows stand for an inhibitory effect, and the horizontal bar indicates no change. For details, see the result in section 0. B) Mechanisms underlying spontaneous $[Ca^{2+}]_i$ oscillations. This schematic diagram shows the Ca^{2+} transport mechanisms with highlights (red) of those that were identified as essential for the $[Ca^{2+}]_i$ oscillations in the MNCs. C) Separated components that shape depolarization-induced $[Ca^{2+}]_i$ responses in MNCs; the blue area represents a

sustained depolarization-induced Ca^{2+} influx, the green area is the rapid net release of Ca^{2+} from the ER.

For induced activity, we show that $[Ca^{2+}]_i$ elevations evoked by depolarization are strongly modulated by caffeine-sensitive stores of the ER. The ER have the ability to either amplify or attenuate the depolarization-induced $[Ca^{2+}]_i$ elevation, depending on the filling state of the stores. Filled stores can amplify the response by a rapid release of Ca^{2+} and form the initial high peak of the $[Ca^{2+}]_i$ elevation. The overall rate of $[Ca^{2+}]_i$ elevation is then given by a summation of two components: depolarization-evoked Ca^{2+} entry producing a sustained Ca^{2+} income over the whole duration of the depolarization stimulus and the Ca^{2+} release which lasts only several seconds and whose amplitude depends on the filling state of the stores. The two components are graphically illustrated in figure 5.1C. By this mechanism, the ER can act as a memory that modulates the activity of the cell based on its previous actions. In exceptional situations, the attenuation of the response happens when the stores are empty and actively absorb some of the incoming Ca^{2+}. The empty stores then do not work as a source of Ca^{2+} but rather as a sink. Taken together, this work provides an extensive study of Ca^{2+} dynamics of the rat magnocellular neurones and stands as a motivation for further *in vivo* studies combining Ca^{2+} and electrical dynamics with mathematical analyses, that will become even more important in understanding of such complicated regulatory systems.

List of used abbreviations

AHP	After-Hyperpolarizing Potential
AVP	Arginine-vasopressin
Caff.	Caffeine
CICR	Ca^{2+}-Induced-Ca^{2+}-Release
CPA	Cyclopiazonic Acid
DAP	Depolarizing Afterpotential
eGFP	Enhanced Green Fluorescent Protein
ER	Endoplasmic Reticulum
HAP	Hyperpolarizing Afterpotential
HVGCCs	High-Voltage-Gated Ca^{2+} Channels
$InsP_3$	1,4,5-trisphosphate
IPR	$InsP_3$ receptor
LVGCCs	Low-Voltage-Gated Ca^{2+} Channels
MNCs	Magnocellular Neurosecretory Cells
mRFP	Monomeric Red Fluorescent Protein
OT	Oxytocin
PMCA	Plasma Membrane Ca^{2+}-ATPase
PVN	Paraventricular Nucleus
RyR	Ryanodine Receptor
SERCA	Sarco/Endoplasmic Reticulum Ca^{2+} ATPase
SON	Supraoptic Nucleus
TG	Thapsigargin
VGCCs	Voltage-Gated Ca^{2+} Channels
WT	Wild Type (rat)

Literature

[1] Albrecht, M. A., S. L. Colegrove, J. Hongpaisan, N. B. Pivovarova, S. B. Andrews and D. D. Friel (2001). "Multiple modes of calcium-induced calcium release in sympathetic neurons I: attenuation of endoplasmic reticulum Ca2+ accumulation at low [Ca2+](i) during weak depolarization." J Gen Physiol **118**(1): 83-100.

[2] Andrew, R. D. and F. E. Dudek (1983). "Burst Discharge in Mammalian Neuroendocrine Cells Involves an Intrinsic Regenerative Mechanism." Science **221**(4615): 1050-1052.

[3] Andrew, R. D. and F. E. Dudek (1984). "Analysis of Intracellularly Recorded Phasic Bursting by Mammalian Neuroendocrine Cells." J Neurophysiol **51**(3): 552-566.

[4] Armstrong, L. E. and E. C. Johnson (2018). "Water Intake, Water Balance, and the Elusive Daily Water Requirement." Nutrients **10**(12).

[5] Armstrong, W. E. (1995). "Morphological and electrophysiological classification of hypothalamic supraoptic neurons." Progress in Neurobiology **47**(4-5): 291-339.

[6] Armstrong, W. E. (2007). "The neurophysiology of neurosecretory cells." Journal of Physiology-London **585**(3): 645-647.

[7] Armstrong, W. E., B. N. Smith and M. Tian (1994). "Electrophysiological characteristics of immunochemically identified rat oxytocin and vasopressin neurones in vitro." J Physiol **475**(1): 115-128.

[8] Armstrong, W. E., J. E. Stern and R. Teruyama (2002). "Plasticity in the electrophysiological properties of oxytocin neurons." Microscopy Research and Technique **56**(2): 73-80.

[9] Armstrong, W. E., L. Wang, C. Li and R. Teruyama (2010). "Performance, Properties and Plasticity of Identified Oxytocin and Vasopressin Neurones In Vitro." Journal of Neuroendocrinology **22**(5): 330-342.

[10] Belin, V. and F. Moos (1986). "Paired recordings from supraoptic and paraventricular oxytocin cells in suckled rats: recruitment and synchronization." J Physiol **377**: 369-390.

[11] Belin, V., F. Moos and P. Richard (1984). "Synchronization of oxytocin cells in the hypothalamic paraventricular and supraoptic nuclei in suckled rats: direct proof with paired extracellular recordings." Exp Brain Res **57**(1): 201-203.

[12] Berridge, M. J. (1998). "Neuronal calcium signaling." Neuron **21**(1): 13-26.

[13] Berridge, M. J. (2005). "Neuronal calcium signaling." Journal of Neurochemistry **94**: 7-7.

[14] Berridge, M. J. (2012). "Calcium signalling remodelling and disease." Biochemical Society Transactions **40**: 297-309.

[15] Bezprozvanny, I., S. Bezprozvannaya and B. E. Ehrlich (1994). "Caffeine-induced inhibition of inositol(1,4,5)-trisphosphate-gated calcium channels from cerebellum." Molecular Biology of the Cell **5**(1): 97-103.

[16] Bicknell, R. J., D. Brown, C. D. Ingram and G. Leng (1982). "Rapid Fatigue of Vasopressin Secretion from the Isolated Rat Neurohypophysis during Sustained Electrical-Stimulation." Journal of Physiology-London **327**(Jun): P38-P39.

[17] Bootman, M. D., P. Lipp and M. J. Berridge (2001). "The organisation and functions of local Ca2+ signals." Journal of Cell Science **114**(12): 2213-2222.

[18] Bourinet, E., S. C. Stotz, R. L. Spaetgens, G. Dayanithi, J. Lemos, J. Nargeot and G. W. Zamponi (2001). "Interaction of SNX482 with domains III and IV inhibits activation gating of alpha(1E) (Ca(V)2.3) calcium channels." Biophys J **81**(1): 79-88.

[19] Bourque, C. W. and D. A. Brown (1987). "Apamin and d-tubocurarine block the afterhyperpolarization of rat supraoptic neurosecretory neurons." Neurosci Lett **82**(2): 185-190.

[20] Bourque, C. W., K. Kirkpatrick and C. R. Jarvis (1998). "Extrinsic modulation of spike afterpotentials in rat hypothalamoneurohypophysial neurons." Cellular and Molecular Neurobiology **18**(1): 3-12.

[21] Bourque, C. W. and S. H. R. Oliet (1997). "Osmoreceptors in the central nervous system." Annual Review of Physiology **59**: 601-619.

[22] Brethes, D., G. Dayanithi, L. Letellier and J. J. Nordmann (1987). "Depolarization-induced Ca2+ increase in isolated neurosecretory nerve terminals measured with fura-2." Proc Natl Acad Sci U S A **84**(5): 1439-1443.

[23] Brown, C. H. (2004). "Rhythmogenesis in vasopressin cells." J Neuroendocrinol **16**(9): 727-739.

[24] Brown, C. H., J. S. Bains, M. Ludwig and J. E. Stern (2013). "Physiological Regulation of Magnocellular Neurosecretory Cell Activity: Integration of Intrinsic, Local and Afferent Mechanisms." Journal of Neuroendocrinology **25**(8): 678-710.

[25] Brown, C. H. and C. W. Bourque (2006). "Mechanisms of rhythmogenesis: insights from hypothalamic vasopressin neurons." Trends Neurosci **29**(2): 108-115.

[26] Brown, C. H., P. M. Bull and C. W. Bourque (2004). "Phasic bursts in rat magnocellular neurosecretory cells are not intrinsically regenerative in vivo." Eur J Neurosci **19**(11): 2977-2983.

[27] Brustovetsky, T., M. K. Brittain, P. L. Sheets, T. R. Cummins, V. Pinelis and N. Brustovetsky (2011). "KB-R7943, an inhibitor of the reverse Na+/Ca2+exchanger, blocks N-methyl-D-aspartate receptor and inhibits mitochondrial complex I." British Journal of Pharmacology **162**(1): 255-270.

[28] Burdakov, D., O. H. Petersen and A. Verkhratsky (2005). "Intraluminal calcium as a primary regulator of endoplasmic reticulum function." Cell Calcium **38**(3-4): 303-310.

[29] Catterall, W. A. (2000). "Structure and regulation of voltage-gated Ca2+ channels." Annual Review of Cell and Developmental Biology **16**: 521-555.

[30] Catterall, W. A. (2011). "Voltage-Gated Calcium Channels." Cold Spring Harbor Perspectives in Biology **3**(8).

[31] Cazalis, M., G. Dayanithi and J. J. Nordmann (1985). "The role of patterned burst and interburst interval on the excitation-coupling mechanism in the isolated rat neural lobe." J Physiol **369**: 45-60.

[32] Dayanithi, G., O. Forostyak, Y. Ueta, A. Verkhratsky and E. C. Toescu (2012). "Segregation of calcium signalling mechanisms in magnocellular neurones and terminals." Cell Calcium **51**(3-4): 293-299.

[33] Dayanithi, G., N. Sabatier and H. Widmer (2000). "Intracellular calcium signalling in magnocellular neurones of the rat supraoptic nucleus: understanding the autoregulatory mechanisms." Exp Physiol **85 Spec No**: 75S-84S.

[34] Dayanithi, G., H. Widmer and P. Richard (1996). "Vasopressin-induced intracellular Ca2+ increase in isolated rat supraoptic cells." J Physiol **490 (Pt 3)**: 713-727.

[35] Douglas, A., S. Scullion, I. Antonijevic, D. Brown, J. Russell and G. Leng (2001). "Uterine contractile activity stimulates supraoptic neurons in term pregnant rats via a noradrenergic pathway." Endocrinology **142**(2): 633-644.

[36] Dreyfus, F. M., A. Tscherter, A. C. Errington, J. J. Renger, H. S. Shin, V. N. Uebele, V. Crunelli, R. C. Lambert and N. Leresche (2010). "Selective T-type calcium channel block in thalamic neurons reveals channel redundancy and physiological impact of I(T)window." J Neurosci **30**(1): 99-109.

[37] Fierro, L., R. DiPolo and I. Llano (1998). "Intracellular calcium clearance in Purkinje cell somata from rat cerebellar slices." J Physiol **510 (Pt 2)**: 499-512.

[38] Fisher, T. E. and C. W. Bourque (1996). "Calcium-channel subtypes in the somata and axon terminals of magnocellular neurosecretory cells." Trends Neurosci **19**(10): 440-444.

[39] Foehring, R. C. and W. E. Armstrong (1996). "Pharmacological dissection of high-voltage-activated Ca2+ current types in acutely dissociated rat supraoptic magnocellular neurons." J Neurophysiol **76**(2): 977-983.

[40] Forostyak, O., S. Forostyak, S. Kortus, E. Sykova, A. Verkhratsky and G. Dayanithi (2016). "Physiology of Ca2+ signalling in stem cells of different origins and differentiation stages." Cell Calcium **59**(2-3): 57-66.

[41] Forsling, M. L., H. Montgomery, D. Halpin, R. J. Windle and D. F. Treacher (1998). "Daily patterns of secretion of neurohypophysial hormones in man: Effect of age." Experimental Physiology **83**(3): 409-418.

[42] Ghamari-Langroudi, M. and C. W. Bourque (2004). "Muscarinic receptor modulation of slow afterhyperpolarization and phasic firing in rat supraoptic nucleus neurons." J Neurosci **24**(35): 7718-7726.

[43] Gouzenes, L., N. Sabatier, P. Richard, F. C. Moos and G. Dayanithi (1999). "V1a- and V2-type vasopressin receptors mediate vasopressin-induced Ca2+ responses in isolated rat supraoptic neurones." J Physiol **517 (Pt 3)**: 771-779.

[44] Greffrath, W., W. Magerl, U. Disque-Kaiser, E. Martin, S. Reuss and G. Boehmer (2004). "Contribution of Ca2+-activated K+ channels to hyperpolarizing after-potentials and discharge pattern in rat supraoptic neurones." J Neuroendocrinol **16**(7): 577-588.

[45] Greffrath, W., E. Martin, S. Reuss and G. Boehmer (1998). "Components of after-hyperpolarization in magnocellular neurones of the rat supraoptic nucleus in vitro." J Physiol **513 (Pt 2)**: 493-506.

[46] Grienberger, C. and A. Konnerth (2012). "Imaging Calcium in Neurons." Neuron **73**(5): 862-885.

[47] Grynkiewicz, G., M. Poenie and R. Y. Tsien (1985). "A new generation of Ca2+ indicators with greatly improved fluorescence properties." J Biol Chem **260**(6): 3440-3450.

[48] Grynkiewicz, G., M. Poenie and R. Y. Tsien (1985). "A New Generation of Ca-2+ Indicators with Greatly Improved Fluorescence Properties." Journal of Biological Chemistry **260**(6): 3440-3450.

[49] Gueguinou, M., A. Chantome, G. Fromont, P. Bougnoux, C. Vandier and M. Potier-Cartereau (2014). "KCa and Ca2+ channels: The complex thought." Biochimica Et Biophysica Acta-Molecular Cell Research **1843**(10): 2322-2333.

[50] Hatton, G. I. (1990). "Emerging concepts of structure-function dynamics in adult brain: the hypothalamo-neurohypophysial system." Progress in Neurobiology **34**(6): 437-504.

[51] Hatton, G. I. and Y. F. Wang (2008). "Neural mechanisms underlying the milk ejection burst and reflex." Prog Brain Res **170**: 155-166.

[52] Helmchen, F. and W. Denk (2005). "Deep tissue two-photon microscopy." Nature Methods **2**(12): 932-940.

[53] Kao, J. P. (1994). Practical aspects of measuring [Ca2+] with fluorescent indicators. Methods in Cell Biology. **40:** 113-152.

[54] Katoh, A., H. Fujihara, T. Ohbuchi, T. Onaka, T. Hashimoto, M. Kawata, H. Suzuki and Y. Ueta (2011). "Highly Visible Expression of an Oxytocin-Monomeric Red Fluorescent Protein 1 Fusion Gene in the Hypothalamus and Posterior Pituitary of Transgenic Rats." Endocrinology **152**(7): 2768-2774.

[55] Kawano, S., K. Otsu, S. Shoji, K. Yamagata and M. Hiraoka (2003). "Ca2+ oscillations regulated by Na+-Ca2+ exchanger and plasma membrane Ca2+ pump induce fluctuations of membrane currents and potentials in human mesenchymal stem cells." Cell Calcium **34**(2): 145-156.

[56] Keener, J. and J. Sneyd (2009). Mathematical Physiology I: Cellular Physiology. New York, Springer.

[57] Kirkpatrick, K. and C. W. Bourque (1996). "Activity dependence and functional role of the apamin-sensitive K+ current in rat supraoptic neurones in vitro." J Physiol **494 (Pt 2)**: 389-398.

[58] Knight, W. D., L. L. Ji, J. T. Little and J. T. Cunningham (2010). "Dehydration followed by sham rehydration contributes to reduced neuronal activation in

vasopressinergic supraoptic neurons after water deprivation." Am J Physiol Regul Integr Comp Physiol **299**(5): R1232-1240.

[59] Knobloch, H. S., A. Charlet, L. C. Hoffmann, M. Eliava, S. Khrulev, A. H. Cetin, P. Osten, M. K. Schwarz, P. H. Seeburg, R. Stoop and V. Grinevich (2012). "Evoked axonal oxytocin release in the central amygdala attenuates fear response." Neuron **73**(3): 553-566.

[60] Knot, H. J., I. Laher, E. A. Sobie, S. Guatimosim, L. Gomez-Viquez, H. Hartmann, L. S. Song, W. J. Lederer, W. F. Graier, R. Malli, M. Frieden and O. H. Petersen (2005). "Twenty years of calcium imaging: cell physiology to dye for." Mol Interv **5**(2): 112-127.

[61] Komori, Y., M. Tanaka, M. Kuba, M. Ishii, M. Abe, N. Kitamura, A. Verkhratsky, I. Shibuya and G. Dayanithi (2010). "Ca(2+) homeostasis, Ca(2+) signalling and somatodendritic vasopressin release in adult rat supraoptic nucleus neurones." Cell Calcium **48**(6): 324-332.

[62] Kortus, S., C. Srinivasan, O. Forostyak, Y. Ueta, E. Sykova, A. Chvatal, M. Zapotocky, A. Verkhratsky and G. Dayanithi (2016). "Physiology of spontaneous [Ca(2+)]i oscillations in the isolated vasopressin and oxytocin neurones of the rat supraoptic nucleus." Cell Calcium **59**(6): 280-288.

[63] Kortus, S., C. Srinivasan, O. Forostyak, M. Zapotocky, Y. Ueta, E. Sykova, A. Chvatal, A. Verkhratsky and G. Dayanithi (2016). "Sodium-calcium exchanger and R-type Ca(2+) channels mediate spontaneous [Ca(2+)]i oscillations in magnocellular neurones of the rat supraoptic nucleus." Cell Calcium **59**(6): 289-298.

[64] Lambert, D. G. (2005). Calcium Signaling Protocols. Totowa, New Jersey, Humana Press.

[65] Lambert, R. C., G. Dayanithi, F. C. Moos and P. Richard (1994). "A rise in the intracellular Ca2+ concentration of isolated rat supraoptic cells in response to oxytocin." J Physiol **478 (Pt 2)**: 275-287.

[66] Lee, S. H., W. K. Ho and S. H. Lee (2009). "Characterization of somatic Ca2+ clearance mechanisms in young and mature hippocampal granule cells." Cell Calcium **45**(5): 465-473.

[67] Lemos, J. R., S. I. Ortiz-Miranda, A. E. Cuadra, C. Velazquez-Marrero, E. E. Custer, T. Dad and G. Dayanithi (2012). "Modulation/physiology of calcium channel sub-types in neurosecretory terminals." Cell Calcium **51**(3-4): 284-292.

[68] Li, Z. H. and G. I. Hatton (1997). "Ca2+ release from internal stores: Role in generating depolarizing after-potentials in rat supraoptic neurones." Journal of Physiology-London **498**(2): 339-350.

[69] Lincoln, D. W. and J. B. Wakerley (1975). "Factors governing the periodic activation of supraoptic and paraventricular neurosecretory cells during suckling in the rat." J Physiol **250**(2): 443-461.

[70] Ludwig, M., P. M. Bull, V. A. Tobin, N. Sabatier, R. Landgraf, G. Dayanithi and G. Leng (2005). "Regulation of activity-dependent dendritic vasopressin release from rat supraoptic neurones." J Physiol **564**(Pt 2): 515-522.

[71] Ludwig, M., N. Sabatier, P. M. Bull, R. Landgraf, G. Dayanithi and G. Leng (2002). "Intracellular calcium stores regulate activity-dependent neuropeptide release from dendrites." Nature **418**(6893): 85-89.

[72] MacGregor, D. J., T. F. Clayton and G. Leng (2013). "Information coding in vasopressin neurons-The role of asynchronous bistable burst firing." Biosystems **112**(2): 85-93.

[73] MacGregor, D. J. and G. Leng (2012). "Phasic Firing in Vasopressin Cells: Understanding Its Functional Significance through Computational Models." Plos Computational Biology **8**(10).

[74] Maicas Royo, J., C. H. Brown, G. Leng and D. J. MacGregor (2016). "Oxytocin Neurones: Intrinsic Mechanisms Governing the Regularity of Spiking Activity." J Neuroendocrinol **28**(4).

[75] Manaye, K. F., D. L. Lei, Y. Tizabi, M. I. Davila-Garcia, P. R. Mouton and P. H. Kelly (2005). "Selective neuron loss in the paraventricular nucleus of hypothalamus in patients suffering from major depression and bipolar disorder." Journal of Neuropathology and Experimental Neurology **64**(3): 224-229.

[76] Mintz, I. M., M. E. Adams and B. P. Bean (1992). "P-Type Calcium Channels in Rat Central and Peripheral Neurons." Neuron **9**(1): 85-95.

[77] Moos, F., L. Gouzenes, D. Brown, G. Dayanithi, N. Sabatier, L. Boissin, A. Rabie and P. Richard (1998). "New aspects of firing pattern autocontrol in oxytocin and vasopressin neurones." Adv Exp Med Biol **449**: 153-162.

[78] Moos, F. C., K. Rossi and P. Richard (1997). "Activation of N-methyl-D-aspartate receptors regulates basal electrical activity of oxytocin and vasopressin neurons in lactating rats." Neuroscience **77**(4): 993-1002.

[79] Mutsuga, N., T. Shahar, J. G. Verbalis, M. J. Brownstein, C. C. Xiang, R. F. Bonner and H. Gainer (2004). "Selective gene expression in magnocellular neurons in rat supraoptic nucleus." Journal of Neuroscience **24**(32): 7174-7185.

[80] Newcomb, R., B. Szoke, A. Palma, G. Wang, X. H. Chen, W. Hopkins, R. Cong, J. Miller, L. Urge, K. Tarczy-Hornoch, J. A. Loo, D. J. Dooley, L. Nadasdi, R. W. Tsien, J. Lemos and G. Miljanich (1998). "Selective peptide antagonist of the class E calcium channel from the venom of the tarantula Hysterocrates gigas." Biochemistry **37**(44): 15353-15362.

[81] Oliet, S. H. and C. W. Bourque (1992). "Properties of supraoptic magnocellular neurones isolated from the adult rat." J Physiol **455**: 291-306.

[82] Ortiz-Miranda, S., G. Dayanithi, E. Custer, S. N. Treistman and J. R. Lemos (2005). "Micro-opioid receptor preferentially inhibits oxytocin release from neurohypophysial terminals by blocking R-type Ca2+ channels." J Neuroendocrinol **17**(9): 583-590.

[83] Parkash, J. and K. Asotra (2012). "Calcium oscillations and waves in cells." Adv Exp Med Biol **740**: 521-529.

[84] Piedras-Rentería, E. S., C. F. Barrett, Yu-QingCao and R. W. Tsien (2007). Voltage-gated calcium channels, calcium signaling, and channelopathies.

Calcium: A Matter of Life or Death. J. Krebs and M. Michalak. Amsterdam, Elsevier. **41:** 127-166.

[85] Prager-Khoutorsky, M. and C. W. Bourque (2010). "Osmosensation in vasopressin neurons: changing actin density to optimize function." Trends Neurosci **33**(2): 76-83.

[86] Rhodes, C. H., J. I. Morrell and D. W. Pfaff (1981). "Immunohistochemical Analysis of Magnocellular Elements in Rat Hypothalamus - Distribution and Numbers of Cells Containing Neurophysin, Oxytocin, and Vasopressin." Journal of Comparative Neurology **198**(1): 45-64.

[87] Richard, P., F. Moos, G. Dayanithi, L. Gouzenes and N. Sabatier (1997). "Rhythmic activities of hypothalamic magnocellular neurons: autocontrol mechanisms." Biol Cell **89**(9): 555-560.

[88] Roper, P. (2005). "Frequency-dependent depletion of secretory vesicle pools modulates bursting in vasopressin neurones of the rat supraoptic nucleus." Neurocomputing **65**: 485-491.

[89] Roper, P., J. Callaway and W. Armstrong (2004). "Burst initiation and termination in phasic vasopressin cells of the rat supraoptic nucleus: A combined mathematical, electrical, and calcium fluorescence study." Journal of Neuroscience **24**(20): 4818-4831.

[90] Roper, P., J. Callaway, T. Shevchenko, R. Teruyama and W. Armstrong (2003). "AHP's, HAP's and DAP's: how potassium currents regulate the excitability of rat supraoptic neurones." Journal of Computational Neuroscience **15**(3): 367-389.

[91] Rossoni, E., J. Feng, B. Tirozzi, D. Brown, G. Leng and F. Moos (2008). "Emergent synchronous bursting of oxytocin neuronal network." PLoS Comput Biol **4**(7): e1000123.

[92] Sabatier, N., P. Richard and G. Dayanithi (1997). "L-, N- and T- but neither P- nor Q-type Ca2+ channels control vasopressin-induced Ca2+ influx in magnocellular vasopressin neurones isolated from the rat supraoptic nucleus." J Physiol **503 (Pt 2)**: 253-268.

[93] Sabatier, N., P. Richard and G. Dayanithi (1998). "Activation of multiple intracellular transduction signals by vasopressin in vasopressin-sensitive neurones of the rat supraoptic nucleus." J Physiol **513 (Pt 3)**: 699-710.

[94] Sabatier, N., I. Shibuya and G. Dayanithi (2004). "Intracellular calcium increase and somatodendritic vasopressin release by vasopressin receptor agonists in the rat supraoptic nucleus: involvement of multiple intracellular transduction signals." J Neuroendocrinol **16**(3): 221-236.

[95] Sasaki, N., G. Dayanithi and I. Shibuya (2005). "Ca2+ clearance mechanisms in neurohypophysial terminals of the rat." Cell Calcium **37**(1): 45-56.

[96] Scott, V., V. R. Bishop, G. Leng and C. H. Brown (2009). "Dehydration-induced modulation of kappa-opioid inhibition of vasopressin neurone activity." Journal of Physiology-London **587**(23): 5679-5689.

[97] Scullin, C. S. and L. D. Partridge (2010). "Contributions of SERCA pump and ryanodine-sensitive stores to presynaptic residual Ca2+." Cell Calcium **47**(4): 326-338.

[98] Shibuya, I., N. Kabashima, K. Tanaka, V. S. Setiadji, J. Noguchi, N. Harayama, Y. Ueta and H. Yamashita (1998). "Patch-clamp analysis of the mechanism of PACAP-induced excitation in rat supraoptic neurones." Journal of Neuroendocrinology **10**(10): 759-768.

[99] Sneyd, J., J. Keizer and M. J. Sanderson (1995). "Mechanisms of calcium oscillations and waves: a quantitative analysis." FASEB J **9**(14): 1463-1472.

[100] Sneyd, J., K. Tsaneva-Atanasova, D. I. Yule, J. L. Thompson and T. J. Shuttleworth (2004). "Control of calcium oscillations by membrane fluxes." Proc Natl Acad Sci U S A **101**(5): 1392-1396.

[101] Stern, J. E. and W. E. Armstrong (1998). "Reorganization of the dendritic trees of oxytocin and vasopressin neurons of the rat supraoptic nucleus during lactation." J Neurosci **18**(3): 841-853.

[102] Teruyama, R. and W. E. Armstrong (2005). "Enhancement of calcium-dependent afterpotentials in oxytocin neurons of the rat supraoptic nucleus during lactation." J Physiol **566**(Pt 2): 505-518.

[103] Thul, R., T. C. Bellamy, H. L. Roderick, M. D. Bootman and S. Coombes (2008). "Calcium oscillations." Adv Exp Med Biol **641**: 1-27.

[104] Tran, T. D., S. Yao, W. H. Hsu, J. M. Gimble, B. A. Bunnell and H. Cheng (2015). "Arginine vasopressin inhibits adipogenesis in human adipose-derived stem cells." Mol Cell Endocrinol **406**: 1-9.

[105] Trudel, E. and C. W. Bourque (2012). "Circadian modulation of osmoregulated firing in rat supraoptic nucleus neurones." J Neuroendocrinol **24**(4): 577-586.

[106] Tsien, R. W., D. Lipscombe, D. V. Madison, K. R. Bley and A. P. Fox (1988). "Multiple Types of Neuronal Calcium Channels and Their Selective Modulation." Trends Neurosci **11**(10): 431-438.

[107] Ueta, Y., G. Dayanithi and H. Fujihara (2011). "Hypothalamic vasopressin response to stress and various physiological stimuli: visualization in transgenic animal models." Horm Behav **59**(2): 221-226.

[108] Ueta, Y., H. Fujihara, R. Serino, G. Dayanithi, H. Ozawa, K. Matsuda, M. Kawata, J. Yamada, S. Ueno, A. Fukuda and D. Murphy (2005). "Transgenic expression of enhanced green fluorescent protein enables direct visualization for physiological studies of vasopressin neurons and isolated nerve terminals of the rat." Endocrinology **146**(1): 406-413.

[109] Ventura, A. C. and J. Sneyd (2006). "Calcium oscillations and waves generated by multiple release mechanisms in pancreatic acinar cells." Bull Math Biol **68**(8): 2205-2231.

[110] Verbalis, J. G., E. F. Baldwin and A. G. Robinson (1986). "Osmotic Regulation of Plasma Vasopressin and Oxytocin after Sustained Hyponatremia." American Journal of Physiology **250**(3): R444-R451.

[111] Verkhratsky, A. (2005). "Physiology and pathophysiology of the calcium store in the endoplasmic reticulum of neurons." Physiol Rev **85**(1): 201-279.

[112] Verkhratsky, A. and A. Shmigol (1996). "Calcium-induced calcium release in neurones." Cell Calcium **19**(1): 1-14.

[113] Viero, C., I. Shibuya, N. Kitamura, A. Verkhratsky, H. Fujihara, A. Katoh, Y. Ueta, H. H. Zingg, A. Chvatal, E. Sykova and G. Dayanithi (2010). "REVIEW: Oxytocin: Crossing the bridge between basic science and pharmacotherapy." CNS Neurosci Ther **16**(5): e138-156.

[114] Wakui, M., Y. V. Osipchuk and O. H. Petersen (1990). "Receptor-activated cytoplasmic Ca2+ spiking mediated by inositol trisphosphate is due to Ca2(+)-induced Ca2+ release." Cell **63**(5): 1025-1032.

[115] Wanaverbecq, N., S. J. Marsh, M. Al-Qatari and D. A. Brown (2003). "The plasma membrane calcium-ATPase as a major mechanism for intracellular calcium regulation in neurones from the rat superior cervical ganglion." Journal of Physiology-London **550**(1): 83-101.

[116] Wang, G., G. Dayanithi, S. Kim, D. Hom, L. Nadasdi, R. Kristipati, J. Ramachandran, E. L. Stuenkel, J. J. Nordmann, R. Newcomb and J. R. Lemos (1997). "Role of Q-type Ca2+ channels in vasopressin secretion from neurohypophysial terminals of the rat." J Physiol **502 (Pt 2)**: 351-363.

[117] Wang, G., G. Dayanithi, R. Newcomb and J. R. Lemos (1999). "An R-type Ca(2+) current in neurohypophysial terminals preferentially regulates oxytocin secretion." J Neurosci **19**(21): 9235-9241.

[118] Yao, N. W., Z. L. (2005). Handbook of microscopy for nanotechnology. Atlanta, GA, USA, KLUWER ACADEMIC PUBLISHERS.

List of publications

1. Kortus, S., C. Srinivasan, O. Forostyak, M. Zapotocky, Y. Ueta, E. Sykova, A. Chvatal, A. Verkhratsky and G. Dayanithi (2016). "Sodium-calcium exchanger and R-type Ca(2+) channels mediate spontaneous [Ca(2+)]i oscillations in magnocellular neurones of the rat supraoptic nucleus." Cell Calcium 59(6): 289-298.

2. Kortus, S., C. Srinivasan, O. Forostyak, Y. Ueta, E. Sykova, A. Chvatal, M. Zapotocky, A. Verkhratsky and G. Dayanithi (2016). "Physiology of spontaneous $[Ca^{2+}]_i$ oscillations in the isolated vasopressin and oxytocin neurones of the rat supraoptic nucleus." Cell Calcium 59(6): 280-288.

3. Forostyak, O., S. Forostyak, S. Kortus, E. Sykova, A. Verkhratsky and G. Dayanithi (2016). "Physiology of Ca2+ signalling in stem cells of different origins and differentiation stages." Cell Calcium 59(2-3): 57-66.

Appendix A - Copyright permission statements

A.I Copyright permission statements

This work contains reused copyright material in form of reprinted figures. All the figures listed below were used in agreement with a copyright policy of their original source. I all cases, I have obtained a permission of publisher that allows to reproduce their content, free of charge, for non-commercial use, including dissertation thesis. The reused content is also attributed to the original source with a proper citation.

Figure 1.1: Illustration of a coronal section of the rat hypothalamus.

Copied from: (Mutsuga, Shahar et al. 2004).

Permission: not required for non-commercial use, including dissertation thesis.

Figure 1.2: Detail of immunostained coronal section of the rat hypothalamus.

Copied from: (Brown, Bains et al. 2013).

Permission: Obtained licence for non-commercial use (licence number: 4636550896609).

Figure 1.5: Firing patterns in magnocellular vasopressin (A–D) and oxytocin (E) *cells in vivo*.

Copied from: (Brown, Bains et al. 2013).

Permission: Obtained licence for non-commercial use (licence number: 4636550896609).

Figure 1.6: Spike afterpotentials in MNCs

Copied from: (Roper, Callaway et al. 2003).

Permission: Obtained licence for non-commercial use (licence number: 4636551089950).

Figure 1.7: A diagram of major fluxes involved in the control of cytoplasmic Ca^{2+} concentration.

Adapted from: (Keener and Sneyd 2009)

Permission: Obtained licence for non-commercial use (licence number: 4636550539439).

Figure 1.8: Excitation spectra of the Ca^{2+}-sensitive dye Fura-2 AM.

Copied from: (Grynkiewicz, Poenie et al. 1985)

Permission: not required for non-commercial use, including dissertation thesis.

Figure 3.1: Visualization of fluorescent neurohypophysis (NH) and isolated SON neurones from the transgenic rats for AVP-enhanced green fluorescent protein (eGFP) fusion transgene (AVP-eGFP), oxytocin-monomeric red fluorescent protein 1 (mRFP1) fusion transgene.

Adapted from: (Dayanithi, Forostyak et al. 2012).

Permission: Obtained licence for non-commercial use (licence number: 4638180884992).

Appendix B - Publications

B.I Sodium-calcium exchanger and R-type Ca^{2+} channels mediate spontaneous $[Ca^{2+}]_i$ oscillations in magnocellular neurones of the rat supraoptic nucleus

Kortus, S., C. Srinivasan, O. Forostyak, M. Zapotocky, Y. Ueta, E. Sykova, A. Chvatal, A. Verkhratsky and G. Dayanithi (2016). "Sodium-calcium exchanger and R-type Ca(2+) channels mediate spontaneous [Ca(2+)]i oscillations in magnocellular neurones of the rat supraoptic nucleus." Cell Calcium 59(6): 289-298.

Cell Calcium 59 (2016) 289–298

Contents lists available at ScienceDirect

Cell Calcium

journal homepage: www.elsevier.com/locate/ceca

Sodium-calcium exchanger and R-type Ca^{2+} channels mediate spontaneous $[Ca^{2+}]_i$ oscillations in magnocellular neurones of the rat supraoptic nucleus

Stepan Kortus[a,b,c], Chinnapaiyan Srinivasan[a], Oksana Forostyak[a,d], Martin Zapotocky[b,c], Yoichi Ueta[e], Eva Sykova[d,f], Alexandr Chvatal[d,g], Alexei Verkhratsky[h,i,j,k,**], Govindan Dayanithi[a,l,m,*]

[a] Department of Molecular Neurophysiology, Institute of Experimental Medicine, Czech Academy of Sciences, Videnska 1083, 14220 Prague, Czech Republic
[b] Institute of Physiology, Czech Academy of Sciences, Videnska 1083, 14220 Prague, Czech Republic
[c] Institute of Biophysics and Informatics, First Medical Faculty, Charles University in Prague, Salmovska 1, 12000 Prague, Czech Republic
[d] Department of Neuroscience, Charles University, Second Medical Faculty, V Uvalu 84, 15006 Prague, Czech Republic
[e] Department of Physiology, School of Medicine, University of Occupational and Environmental Health, Kitakyushu 807-8555, Japan
[f] Department of Neuroscience, Institute of Experimental Medicine, Czech Academy of Sciences, Videnska 1083, 14220 Prague, Czech Republic
[g] Department of Cellular Neurophysiology, Institute of Experimental Medicine, Czech Academy of Sciences, Videnska 1083, 14220 Prague, Czech Republic
[h] University of Manchester, School of Biological Sciences, D.4417 Michael Smith Building, Oxford Road, M13 9PT Manchester, United Kingdom
[i] Achucarro Center for Neuroscience, IKERBASQUE, Basque Foundation for Science, 48011 Bilbao, Spain
[j] Department of Neurosciences, University of the Basque Country UPV/EHU and CIBERNED, Leioa, Spain
[k] University of Nizhny Novgorod, Nizhny Novgorod 603022, Russia
[l] Institut National de la Santé et de la Recherche Médicale, Unité de recherche U1198, Université Montpellier, 34095 Montpellier, France
[m] Ecole Practique des Hautes Etudes, Sorbonne, 75014 Paris, France

ARTICLE INFO

Article history:
Received 1 March 2016
Received in revised form 30 March 2016
Accepted 30 March 2016
Available online 31 March 2016

Keywords:
Ca^{2+} signalling
Voltage-gated Ca^{2+} channels
Ca^{2+} homeostasis
Ca^{2+} imaging
Ca^{2+} oscillations
Ca^{2+} clearance
Transgenic rats
Vasopressin
Oxytocin

ABSTRACT

Isolated supraoptic neurones generate spontaneous $[Ca^{2+}]_i$ oscillations in isolated conditions. Here we report in depth analysis of the contribution of plasmalemmal ion channels (Ca^{2+}, Na^+), Na^+/Ca^{2+} exchanger (NCX), intracellular Ca^{2+} release channels ($InsP_3$Rs and RyRs), Ca^{2+} storage organelles, plasma membrane Ca^{2+} pump and intracellular signal transduction cascades into spontaneous Ca^{2+} activity. While removal of extracellular Ca^{2+} or incubation with non-specific voltage-gated Ca^{2+} channel (VGCC) blocker Cd^{2+} suppressed the oscillations, neither Ni^{2+} nor TTA-P2, the T-type VGCC blockers, had an effect. Inhibitors of VGCC nicardipine, ω-conotoxin GVIA, ω-conotoxin MVIIC, ω-agatoxin IVA (for L-, N-, P and P/Q-type channels, respectively) did not affect $[Ca^{2+}]_i$ oscillations. In contrast, a specific R-type VGCC blocker SNX-482 attenuated $[Ca^{2+}]_i$ oscillations. Incubation with TTX had no effect, whereas removal of the extracellular Na^+ or application of an inhibitor of the reverse operation mode of Na^+/Ca^{2+} exchanger KB-R7943 blocked the oscillations. The mitochondrial uncoupler CCCP irreversibly blocked spontaneous $[Ca^{2+}]_i$ activity. Exposure of neurones to Ca^{2+} mobilisers (thapsigargin, cyclopiazonic acid, caffeine and ryanodine); 4-aminopyridine (A-type K^+ current blocker); phospholipase C and adenylyl cyclase pathways blockers U-73122, Rp-cAMP, SQ-22536 and H-89 had no effect. Oscillations were blocked by GABA, but not by glutamate, apamin or dynorphin. In conclusion, spontaneous oscillations in magnocellular neurones

Abbreviations: AVP, arginine vasopressin; OT, oxytocin; SON, supraoptic nucleus; $[Ca^{2+}]_i$, intracellular Ca^{2+} concentration; SERCA, sarcoendoplasmic reticulum Ca^{2+}-ATPase; VGCC, voltage-gated Ca^{2+} channels; EGTA, ethylene glycol (bis-aminoethyl ether)-*N,N,N′,N′*-tetra acetic acid; TTX, tetrodotoxin; PMCA, plasmatic-Ca^{2+}-ATPase; CCCP, carbonyl cyanide 3-chlorophenylhydrazone; 4-AP, 4-aminopirydine; PACAP, pituitary adenylate cyclase activating polypeptide; NCX, Na^+/Ca^{2+} exchanger; GABA, gamma-aminobutyric acid; AHP, after hyperpolarisation; DAP, depolarizing after potential; $InsP_3$, 1,4,5-trisphosphate; DMSO, dimethyl sulfoxide; eGFP, enhanced green fluorescent protein; mRFP, monomeric red fluorescent protein; NMDG-Cl, *N*-methyl-d-glutamine; CPA, cyclopiazonic acid; ER, endoplasmic reticulum.

* Corresponding author at: Department of Molecular Neurophysiology, Institute of Experimental Medicine, Czech Academy of Sciences, Videnska 1083, CZ-142 20 Prague 4, Czech Republic.
** Corresponding author at: University of Manchester, School of Biological Sciences, D.4417 Michael Smith Building, Oxford Road, M13 9PT Manchester, United Kingdom.
E-mail addresses: Alexej.Verkhratsky@manchester.ac.uk (A. Verkhratsky), gdaya@univ-montp2.fr, gdaya@biomed.cas.cz (G. Dayanithi).

http://dx.doi.org/10.1016/j.ceca.2016.03.010
0143-4160/

Hypothalamus
Supraoptic nucleus
Na^+/Ca^{2+} exchanger
Mitochondria
Plasma membrane calcium pump
Sarcoendoplasmic reticulum
Ca^{2+}-ATPase
GABA
Glutamate
1,4,5-Trisphosphate
Tetrodotoxin
Ca^{2+} channel toxins

are mediated by a concerted action of R-type Ca^{2+} channels and the NCX fluctuating between forward and reverse modes.

1. Introduction

Neurosecretory oxytocin (OT) and arginine-vasopressin (AVP) magnocellular neurones in the rat supraoptic nucleus (SON) project their axons to neurohypophysis where they secrete AVP and OT into the bloodstream in response to physiological stimulation: this secretion is also modulated by central mechanisms within the SON [1]. Circulating AVP regulates water reabsorption in kidney and instigates vasoconstriction to increase blood pressure. OT is released as a part of the milk-ejection reflex and during parturition when it induces uterine contraction to facilitate labour [2,3]. Apart from their peripheral actions, both OT and AVP are also secreted within the SON from dendrites [4,5]; they stimulate OT and AVP receptors expressed in magnocellular neurones activating the intracellular signalling pathway that causes the increase of cytosolic Ca^{2+} concentration ($[Ca^{2+}]_i$) [6]. In OT neurones, this increase in $[Ca^{2+}]_i$ resulted from Ca^{2+} release from intracellular stores [7], whereas in AVP neurones, the $[Ca^{2+}]_i$ rise reflects both the Ca^{2+} influx through voltage-gated Ca^{2+} channels (VGCCs) and Ca^{2+} mobilisation from intracellular stores [1,8]. These responses are mediated via the activation of specific AVP and OT receptors [9,10] and multiple intracellular transduction signals [11].

The release of OT and AVP from terminals in neurohypophysis and from dendrites in the hypothalamus occurs strictly by Ca^{2+}-regulated exocytosis [12]. In terminals the $[Ca^{2+}]_i$ elevation is triggered by action potential arriving from the SON neurones. In the SON, any agent that increases $[Ca^{2+}]_i$ (by intracellular Ca^{2+} release or plasmalemmal Ca^{2+} entry) evokes the release of hormone from dendrites without increasing the electrical activity of the cell body, and without inducing secretion from the nerve terminals [4,13]. Both AVP and OT neurones exhibit specific intrinsic electrical activities. AVP neurones exhibit 'phasic' firing activity with intervals, whereas OT neurones fire high frequency synchronized bursts of action potentials without intervals; these bursts are associated with suckling-induced milk ejection [2]. These characteristic electrical patterns are crucial for the efficient release of AVP and OT at the neurohypophysis [14]. Both cell types exhibit Ca^{2+}-dependent after-hyperpolarisations (AHPs), including an apamin-sensitive, medium duration AHP and a slower, apamin-insensitive AHP (sAHP) [2]. AVP neuronal excitability is also influenced by slow (sDAP) and fast (fDAP) depolarising after potentials that underlie phasic bursting activity [15].

Freshly isolated SON neurones exhibited spontaneous $[Ca^{2+}]_i$ oscillations [7,16]. Experiments on transgenic animals showed that these $[Ca^{2+}]_i$ oscillations exist in both AVP and OT neurones [1,17] yet mechanisms underlying these oscillations remain unknown; similarly unknown is the effect of $[Ca^{2+}]_i$ oscillations on the release of AVP and OT [17]. Spontaneous $[Ca^{2+}]_i$ oscillations, similar to those exhibited in freshly isolated SON neurones may be the key element in the regulation of hormone release. In general, two types of $[Ca^{2+}]_i$ oscillations can be recognised, depending on the main source of Ca^{2+}, i.e., release from intracellular stores such as endoplasmic reticulum (ER) or plasmalemmal Ca^{2+} entry [18]. The ER-driven $[Ca^{2+}]_i$ oscillations result from the periodical release of Ca^{2+} mediated by the inositol 1,4,5-trisphosphate ($InsP_3$) receptor or the ryanodine receptor/Ca^{2+} release channel, whereas the extracellular Ca^{2+} driven oscillations require Ca^{2+} entry through plasmalemmal channels or exchangers. Cellular Ca^{2+} and electrical properties of the SON neurones are closely and mutually associated although they can operate independently. In this study, we analysed spontaneous $[Ca^{2+}]_i$ oscillations using a battery of specific pharmacological tools and propose the possible mechanism driving these oscillations.

2. Materials and methods

2.1. Animals and experimental procedures

Adult male Wistar rats (wild type) and homozygous transgenic male rats carrying a fluorescent reporter for AVP (AVP-eGFP), or OT (OT-mRFP), or double transgenic rats simultaneously expressing reporters for both AVP-eGFP and OT-mRFP, were used as described in detail in earlier work [17,19,20]. All animals (weighting 150–300 g; 4–8 weeks old) were bred and housed at 22–23° C, 12:12 h light/dark cycle (lights on 07:00–19:00 h), with food and drinking water available *ad libitum*. The animals were sacrificed by decapitation after anaesthesia with 5% isoflurane for 5 min, the brain was rapidly removed and the SON was dissected. All experiments were performed in accordance with the European Communities Council Directive of 24 November 1986 (86/609/EEC) and were approved by the Ethics Committee of the Institute of Experimental Medicine, AS CR, Prague, Czech Republic (license #CZ 205/2010-Revised in 2013).

2.2. Isolation of supraoptic neurones

SON neurones were acutely dissociated by enzymatic and mechanical treatments of the tissues as described previously [6,7] with modifications [12,21]. In brief, the blocks (1 mm × 0.5 mm × 0.5 mm) of SON tissues were dissected and enzymatically dissociated by incubation for 30 min in oxygenated HEPES-buffered normal Locke's solution (NL; in mM: 140 NaCl, 5 KCl, $2CaCl_2$, 1 $MgCl_2$, 10 glucose, 10HEPES, pH was adjusted to 7.25 with tris; the osmolarity was 298–300mosm l^{-1}; temperature 37° C) supplemented with 1 mg/ml deoxyribonuclease I, 0.5 mg/ml proteases X, and 0.5 mg/ml protease XIV. After incubation, tissues were washed with NL and triturated gently using a Gilson-Pipetman (1 ml) with a polypropylene white pipette-tip to isolate the SON cells. The cells were plated onto 22 mm glass Petri dishes (WillCo Wells-Amsterdam, The Netherlands). Unless otherwise indicated, all chemicals were purchased from Sigma–Aldrich (St. Louis, USA) or from Alomone labs (Jerusalem, Israel). Fura-

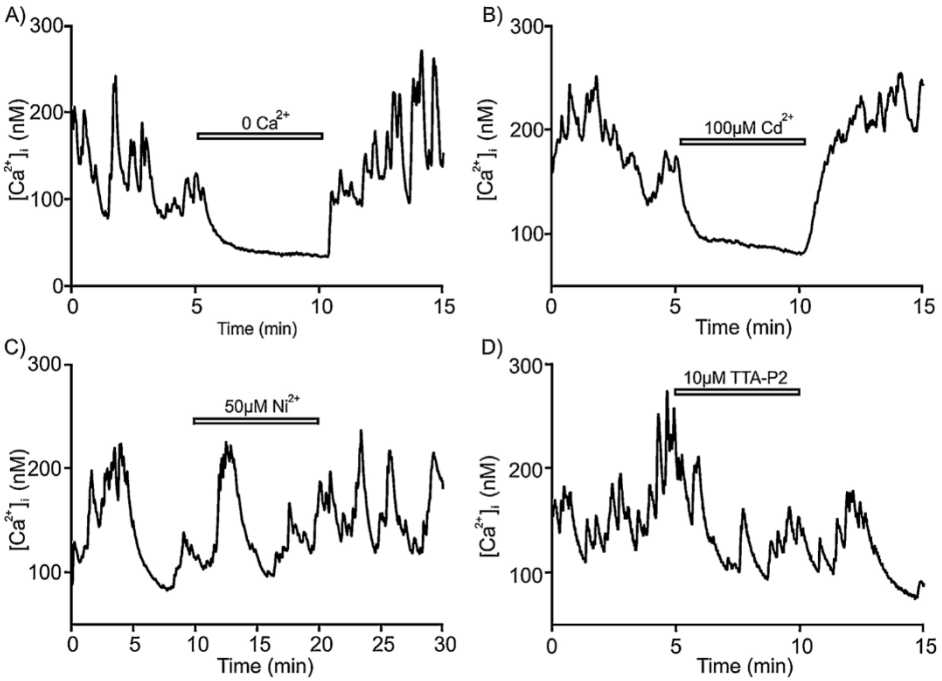

Fig. 1. Effect of external Ca^{2+} removal and VGCC blockers on $[Ca^{2+}]_i$ oscillations.
A: A typical $[Ca^{2+}]_i$ oscillation observed in a neurone before and after removal of external Ca^{2+}. B: Inhibition of spontaneous $[Ca^{2+}]_i$ oscillations in the presence of Cd^{2+}. C,D: Exposure of SON neurones to T-type VGCCs inhibitors Ni^{2+} and TTA-P2 fail to affect spontaneous $[Ca^{2+}]_i$ oscillations.

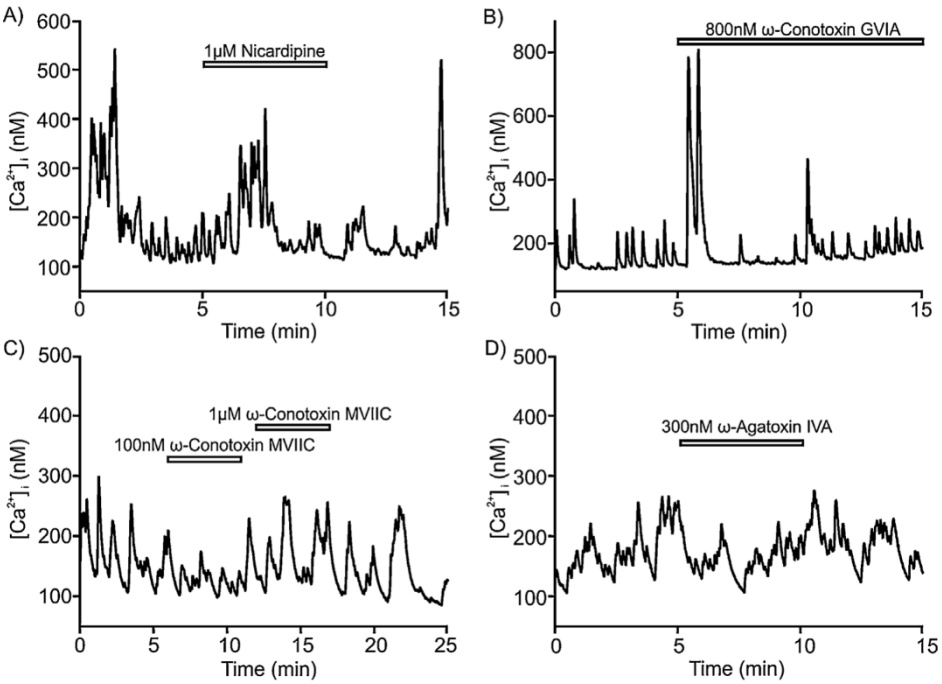

Fig. 2. Effect of specific HVGCC blockers on $[Ca^{2+}]_i$ oscillations.
The representative traces showing the oscillations from individual neurones in the presence of different HVGCC blockers: nicardipine (1 μM) for L-type (A); ω-conotoxin GVIA (800 nM) for N-type (B); two different concentrations of ω-conotoxin MVIIC for P-type (C) and ω-agatoxin (300 nM) for P/Q-type (D). Note that none of the blockers affected the oscillations.

2-AM, TTA-P2, nicardipine, KB-R7943, thapsigargin, CPA, CCCP, ryanodine and 4AP were dissolved in DMSO. TTX and apamin were dissolved in acetic acid as suggested by the suppliers. Other drugs were dissolved in total ion-free distilled H_2O (EMD Millipore Corporation, Germany) and all stock solutions and buffers were prepared using this total-ion-free H_2O.

2.3. $[Ca^{2+}]_i$ measurements and drug applications

The $[Ca^{2+}]_i$ measurements using a fluorescent probe Fura-2 AM were performed on isolated single neurones from WT [7,21,22] or from transgenic (AVP-eGFP-positive and OT-mRFP-positive) rats as described previously [17,19,21,23]. Video imaging of $[Ca^{2+}]_i$ was

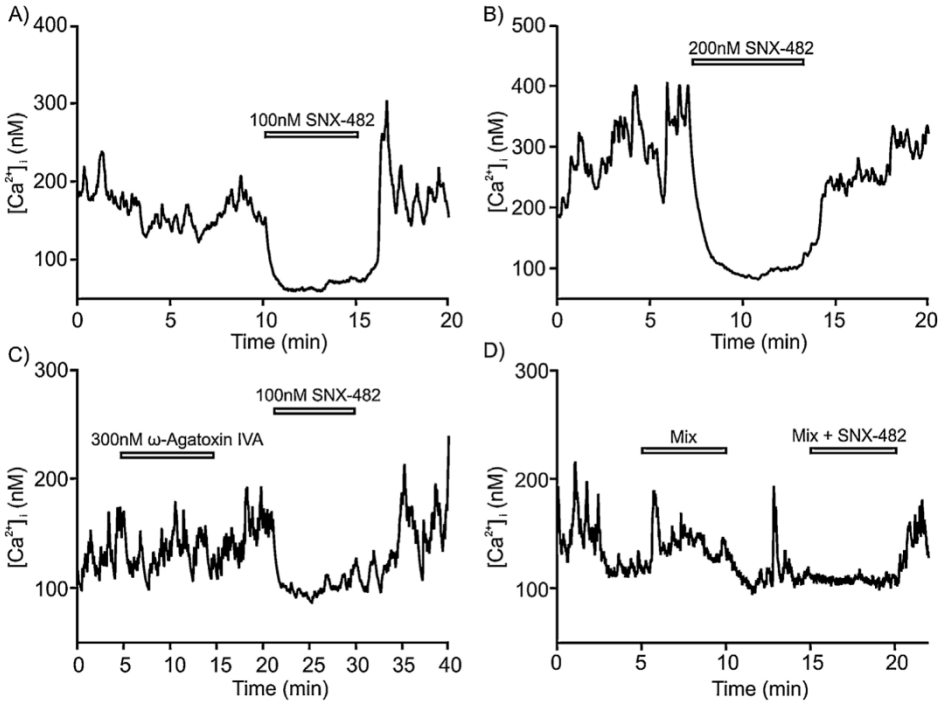

Fig. 3. Effect of R-type VGCC blocker on $[Ca^{2+}]_i$ oscillations.
Traces A and B show $[Ca^{2+}]_i$ oscillations from individual neurones recorded in the presence of 100 nM and 200 nM SNX-482, a specific blocker of R-type channels, respectively. The trace C shows the specific block of oscillations by SNX-482 in comparison to no effect of ω-agatoxin IVA. Trace D shows $[Ca^{2+}]_i$ oscillations from a neurone that was first exposed to the mixture of blockers of Ca^{2+} channels (L-, N-, P/Q-type) followed by the addition of SNX-482.

performed using an inverted microscope AxioObserver D1 (Zeiss) equipped with a CCD camera and Lambda-DG4 fast rotating wheel illumination system (Sutter Instrument, Novato, USA) for double excitation at 340 and 380 nM. The fluorescence intensity of the Fura-2 emission was measured at 510 nM as a ratio of signals obtained after excitation at 340 and 380 nM. The microscope was also equipped with GFP and RFP filters for observing cells bearing fluorescent markers. To estimate the range of change in absolute $[Ca^{2+}]_i$ in nM a calibration following the Grynkiewicz method [24] was performed on a few neurones. The calibration produced $R_{min} = 0.2$, $R_{max} = 7.2$, $f340_{max}/f380_{min} = 7.7$, dissociation constant for Fura-2 at 37 °C $K_d = 224$ nM. An estimation of $[Ca^{2+}]_i$ was then determined from the f_{340}/f_{380} ratio using the Grynkiewicz equation [24].

Cells were continuously perfused with NL solution at 37° C. In some experiments the $CaCl_2$ concentration in the NL was 200 nM or 500 nM. In experiments where extracellular Ca^{2+} was removed, EGTA (100 nM) was added to NL with no added $CaCl_2$. To obtain Na^+ free solutions the NaCl was replaced with NMDG-Cl and osmolarity adjusted to 295–300 mOsmol/l. Solutions were exchanged using a multiple capillary perfusion system, as described previously [25,26], with appropriate modifications [12,21,27] using a computer controlled multichannel peristaltic pump (REGLO ICC, Ismatec, Germany). Neurones with minimal diameter size of 10 μm and persisted dendrites were randomly chosen for $[Ca^{2+}]_i$ measurements.

2.4. Data analysis

Data are presented as mean values ± SEM (n = the number of tested neurones). All experiments were performed in at least two independent sessions.

3. Results

3.1. Removal of external Ca^{2+} inhibits $[Ca^{2+}]_i$ oscillations

Removal of extracellular Ca^{2+} led to an immediate cessation of spontaneous $[Ca^{2+}]_i$ oscillations in all tested neurones (n = 9; Fig. 1A). After extracellular Ca^{2+} removal the basal $[Ca^{2+}]_i$ of 133 ± 14 nM started to decline until it reached a low steady state level of 32 ± 6 nM in about 3 min. Inhibition of $[Ca^{2+}]_i$ oscillations by removal of external Ca^{2+} was reversible and the oscillations (as well as basal $[Ca^{2+}]_i$) were restored rapidly after switching perfusion back to the normal extracellular solution (Fig. 1A). The $[Ca^{2+}]_i$ oscillations still persisted when external Ca^{2+} was lowered from 2 mM to 500 nM (n = 6) or to 200 nM (n = 4), but no oscillations were observed at external Ca^{2+} concentration of 100 nM (n = 5).

3.2. Voltage dependent Ca^{2+} channels and $[Ca^{2+}]_i$ oscillations

A non-specific Ca^{2+} channel blocker Cd^{2+} at 50 μM or 100 μM led to a complete inhibition of $[Ca^{2+}]_i$ oscillations in all tested neurones (n = 17, Fig. 1 B). In contrast, incubation with Ni^{2+} (50 μM, n = 10, Fig. 1C) or TTA-P2 (10 mM, n = 9, Fig. 1D), both being blockers of T-type VGCCs [28], did not affect $[Ca^{2+}]_i$ oscillations. We further probed more specific antagonists of high-threshold VGCCs, the effects of which on spontaneous $[Ca^{2+}]_i$ oscillations are summarised in Fig. 2. Neither L-type channel blocker nicardipine (1 μM, n = 10, Fig. 2A), nor a specific blocker of the N-type channels ω-conotoxin GVIA (800 nM, n = 12, Fig. 2B), nor a specific blocker of the Q-type, ω-conotoxin MVIIC (100 nM, n = 6, 1 μM, n = 2, Fig. 2C), nor a specific blocker of the P/Q-type channels ω-agatoxin IVA (300 nM, n = 5, Fig. 2D) blocked the $[Ca^{2+}]_i$ oscillations. In contrast, a specific inhibitor of R-type VGCCs SNX-482 [29–31] affected $[Ca^{2+}]_i$ oscillations when applied at various concentrations. At 40 nM SNX-482 only partially inhibited $[Ca^{2+}]_i$ oscillations in 1 out of 6 neurones

(data not shown). At 100 nM of SNX-482 $[Ca^{2+}]_i$ oscillations were completely blocked in 9 out of 19 neurones, partially inhibited in 5 cells and had no effect in the remaining 5 neurones. In cells in which SNX-482 completely inhibited $[Ca^{2+}]_i$ oscillations, the basal $[Ca^{2+}]_i$ decreased from 153 ± 17 nM to 87 ± 6 nM (n = 9; Fig. 3A). In neurones in which oscillations were only partially blocked the basal $[Ca^{2+}]_i$ also dropped from 143 ± 15 to 102 ± 12 nM (see Fig. 3C). In the remaining 5 cells which were insensitive to the drug, the basal $[Ca^{2+}]_i$ did not change significantly. When applied at 200 nM SNX-482 $[Ca^{2+}]_i$ oscillations were completely blocked in 4 out of 6 neurones (Fig. 3B). To further corroborate the contribution of R-type VGCCs, the neurones were exposed to a mixture of specific blockers for L-, N-, P/Q- and T-type channels (1 μM nicardipine, 800 nM ω-agatoxin IVA, 300 nM ω-conotoxin GVIA and 50 μM Ni^{2+}), which failed to inhibit $[Ca^{2+}]_i$ oscillations. The addition of 100 nM of SNX-482 to this cocktail, however inhibited $[Ca^{2+}]_i$ oscillations (n = 3, Fig. 3D) again indicating the role of R-type channels.

3.3. Role of Na^+ channels and Na^+ transport

Removal of extracellular Na^+ caused a complete, rapid and reversible block of $[Ca^{2+}]_i$ oscillations in 7 neurones and significantly inhibited oscillations in 2 cells (Fig. 4A). At the same time, treatment with the specific blocker of voltage-gated Na^+ channels TTX at concentrations between 750 nM to 5 μM (Fig. 4B) did not affect $[Ca^{2+}]_i$ oscillations in all tested cells (n = 26). On the contrary, treatment of oscillating neurones with KB-R7943, a selective inhibitor of the reverse mode of Na^+/Ca^{2+} exchanger, NCX [32,33] caused a complete block of oscillations and lowered basal $[Ca^{2+}]_i$ to 95 ± 5 nM in 26 out of 33 neurones (Fig. 4C). In the remaining 7 neurones, the oscillations were inhibited only partially and the basal $[Ca^{2+}]_i$ also dropped to 102 ± 12 nM.

3.4. Role of intracellular Ca^{2+} stores and Ca^{2+} clearance mechanisms

The treatment of SON neurones with TG (irreversible blocker of SERCA) did not affect $[Ca^{2+}]_i$ oscillations in all tested neurones (n = 8), except for producing a short transient effect when oscillations were inhibited for 1–2 min after exposure to TG but fully recovered in the continuing presence of TG. This transient effect of TG was observed in 6 out of 8 neurones (Fig. 5A). The treatment of SON neurones (n = 4) with a reversible blocker of SERCA pumps CPA (10 μM) also had no visible effect on $[Ca^{2+}]_i$ oscillations in 3 out of 4 neurones; in 1 cell, similarly to TG, CPA produced transient inhibition (Fig. 5B). In addition, we tested the CPA effect in the absence of external Ca^{2+} by using $0Ca^{2+}$ buffer and then exposing the neurones to 10 μM CPA. This resulted in a transient elevation of $[Ca^{2+}]_i$. When $0Ca^{2+}$ buffer was switched back to the 2 mM Ca^{2+} NL, we observed an immediate transient increase in $[Ca^{2+}]_i$ and the oscillations were restored. Subsequent exposure to CPA failed to affect the ongoing oscillations. This protocol was tested with the same result in 7 neurones (Fig. 5C).

Ryanodine and caffeine are known to mobilize Ca^{2+} from ER in SON neurones [12] through activation of RyRs; in addition caffeine is a potent inhibitor of $InsP_3$ receptors [34,35]. Both drugs induced a transient elevation of $[Ca^{2+}]_i$ in non-oscillating SON neurones which lasted between 1–3 min (data not shown). However, application of ryanodine (10 μM, n = 6) or caffeine (10 mM, n = 4) to neurones exhibiting $[Ca^{2+}]_i$ oscillations did not affect the latter, except (similar to TG and CPA), inducing a short (1–2 min) transient inhibition that was observed in 2 out of 6 neurones treated with ryanodine and in 2 out of 4 neurones treated with caffeine (Fig. 5D, E). Subsequently, contribution of the PMCA was tested by applying 100 μM of Lanthanum (La^{3+}), which is known to effectively block plasmalemmal Ca^{2+} pump [12,17,36]. Exposure to 100 μM of La^{3+}

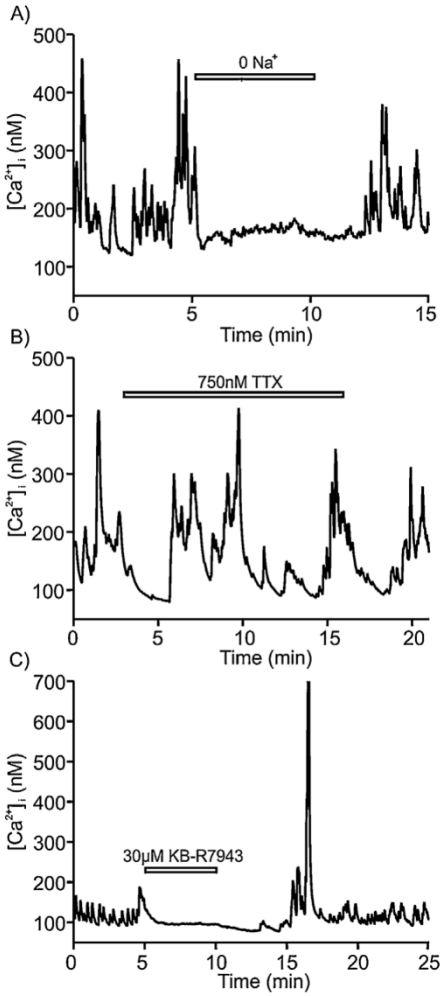

Fig. 4. Role of extracellular Na^+, voltage-gated Na^+ channels and NCX.
A: Removal of external Na^+ completely inhibits $[Ca^{2+}]_i$ oscillations;
B: Inhibition of voltage-gated Na^+ channels with TTX does not affect spontaneous $[Ca^{2+}]_i$ oscillations.
C: Exposure of magnocellular neurone to KB-R734, a specific inhibitor of NCX reverse mode, completely inhibits spontaneous $[Ca^{2+}]_i$ oscillations.

inhibited $[Ca^{2+}]_i$ oscillations in 8 out of 9 neurones (Fig. 5F) with rather poor recovery.

To test the role of mitochondria in spontaneous oscillations, treatment of the oscillating SONs with CCCP, an H^+ ionophore and uncoupler of oxidative phosphorylation in mitochondria, caused a complete and irreversible block of $[Ca^{2+}]_i$ oscillations in 6 out of 7 neurones (Fig. 5G).

3.5. Effect of neurotransmitters and blockers of K^+ currents on $[Ca^{2+}]_i$ oscillations

Exposure of magnocellular neurones to various concentrations of GABA (3 μM, n = 12; 20 μM, n = 4; and 50 μM, n = 4) completely inhibited $[Ca^{2+}]_i$ oscillations in all cells tested; this inhibition was fully reversible (examples: Fig. 6A, for 3 μM). The inhibitory effect of GABA was completely blocked by $GABA_A$ antagonist gabazine (at 10 μM, n = 8; Fig. 6B). Similar (albeit slightly weaker) inhibition was observed using taurine (500 μM, in 6 cells blocked, in 1 partially blocked, in 2 no effect; Fig. 6C) and using glycine (20 μM, in 4 cells blocked, in 1 partially blocked, in 3 no effect; Fig. 6D).

Other neurotransmitters such as glutamate or NMDA were shown to have an excitatory effect on SON neurones [37,38]. In our

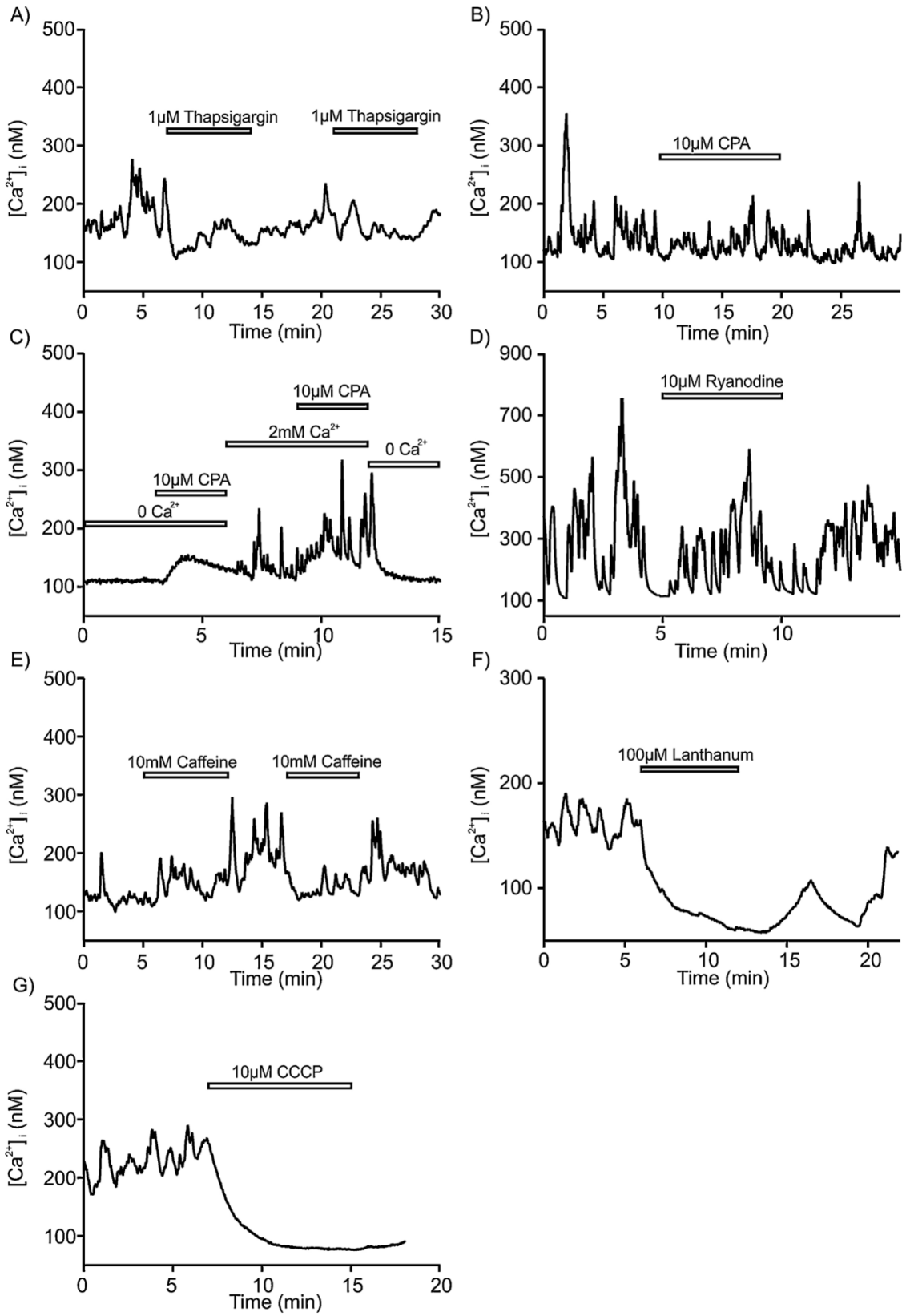

Fig. 5. Effect of intracellular Ca^{2+} mobilisers and inhibitors of Ca^{2+} clearance mechanisms.
A, B: Inhibition of endoplasmic reticulum Ca^{2+} pumps (of SERCA type) by thapsigargin (A) and CPA (B) does not affect spontaneous $[Ca^{2+}]_i$ oscillations.
C: Shows the effect of CPA on $[Ca^{2+}]_i$ in the presence and absence of external Ca^{2+}. The CPA-induced $[Ca^{2+}]_i$ rebound after readmission of extracellular Ca^{2+} reflects store-operated Ca^{2+} entry (SOCE) activation.
D, E: Mobilisation of ER Ca^{2+} by 10 μM ryanodine (D) or 10 mM caffeine (E) does not influence spontaneous $[Ca^{2+}]_i$ oscillations.
F: Exposure of magnocellular neurone to La^{3+} (a blocker of plasma membrane Ca^{2+}-ATPase) inhibits spontaneous Ca^{2+} oscillations.
G: Mitochondrial uncoupler CCCP completely and irreversibly inhibits spontaneous $[Ca^{2+}]_i$ oscillations.

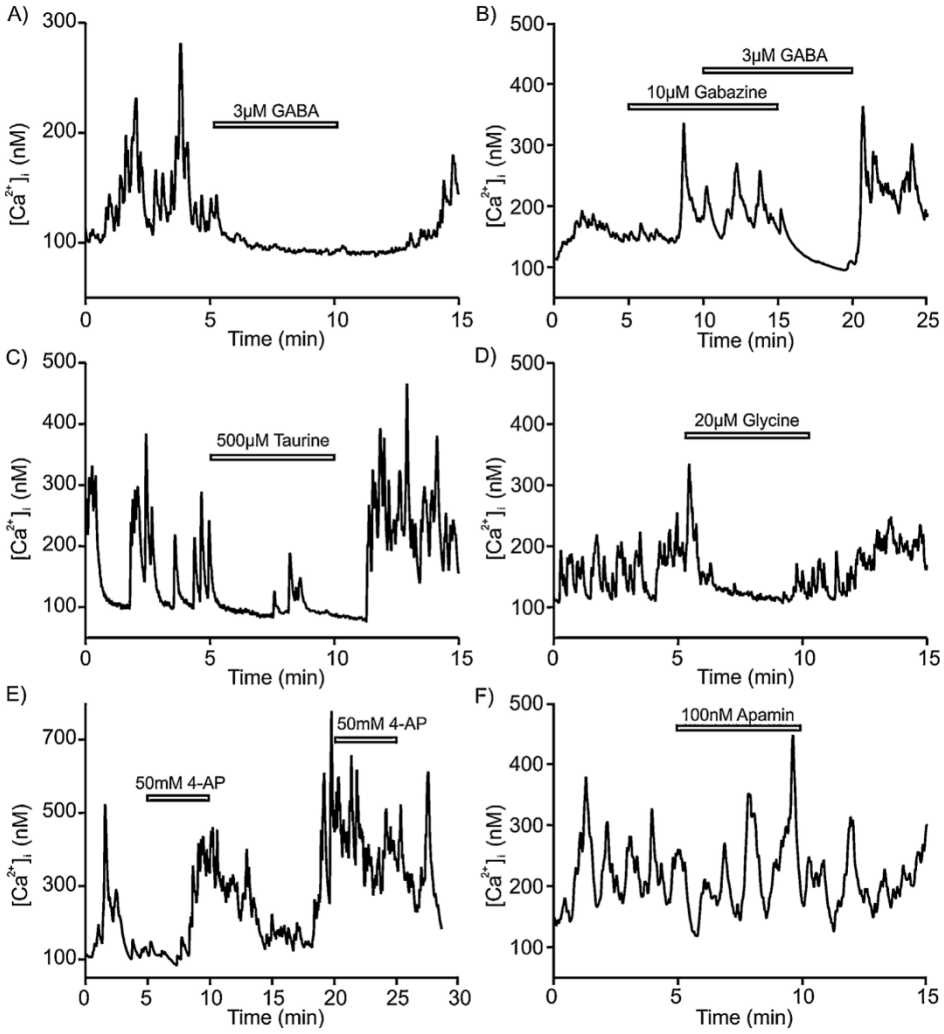

Fig. 6. Effect of neurotransmitters and blockers of K^+ currents on $[Ca^{2+}]_i$ oscillations.
A: Trace showing the blocking effect of GABA (3 μM) on spontaneous $[Ca^{2+}]_i$ oscillations.
B: Trace showing the reversibility of GABA effect by its antagonist, gabazine.
C, D: Traces showing the blocking effect of taurine and glycine on spontaneous $[Ca^{2+}]_i$ oscillations.
Exposure of magnocellular neurones to 4-AP (E), an inhibitor of A-type K^+ current or to apamin (F), an inhibitor of Ca^{2+}-activated K^+-current, did not affect spontaneous Ca^{2+} oscillations.

hands, neither glutamate (in concentrations up to 100 μM; n = 4) nor NMDA (100 μM; n = 5) influenced spontaneous $[Ca^{2+}]_i$ oscillations (data not shown). Exposure of SON neurones to 10–50 mM of 4-AP (inhibitor of I_A K^+ channels) did not affect spontaneous $[Ca^{2+}]_i$ oscillations (n = 5); the inhibitor of SK Ca^{2+}-dependent K^+ channels apamin (100 nM, n = 5, Fig. 6E, F) was also similarly impotent.

3.6. Second messengers and spontaneous $[Ca^{2+}]_i$ oscillations

We used specific blockers of PLC (5 μM U-73211; Fig. 7A): a competitive antagonist of cAMP dependent PKA (50 μM Rp-cAMP; Fig. 7B), an AC inhibitor (10 μM SQ-22536; Fig. 7C) and an inhibitor of PKA (10 μM H-89; Fig. 7D). While none of these inhibitors affected the oscillations in all tested cells (n = 5–8 neurones for each drug), H-89 partially blocked the oscillations only in a few neurones (3 out of 8). Finally, dynorphin, known to modulate the bursting properties of AVP neurones [39] did not affect spontaneous $[Ca^{2+}]_i$ oscillations (at 100 nM; n = 10, Fig. 7E).

4. Discussion

4.1. Spontaneous oscillations are not linked to electrical activity

Action potentials fired by SON neurones activate Ca^{2+} entry [15], in our experiments, however, inhibition of electrical excitability with TTX did not affect $[Ca^{2+}]_i$ oscillations, indicating that action potentials are not involved in the spontaneous $[Ca^{2+}]_i$ oscillations. Of note, the pituitary adenylyl cyclase-activating peptide-induced $[Ca^{2+}]_i$ oscillations in SON neurones were sensitive to TTX [16], which probably reflects their peculiar nature. Complete dissociation of action potentials and spontaneous $[Ca^{2+}]_i$ dynamics reflects the operation of a specific pacemaker.

4.2. Spontaneous oscillations are Na^+ dependent and result from transmembrane Ca^{2+} entry

Removal of extracellular Na^+ effectively inhibited spontaneous $[Ca^{2+}]_i$ oscillations in SON neurones. The very same inhibition was achieved by KB-R7943, a specific inhibitor of the reverse mode of NCX. The reversal potential of the exchanger in SON neurones (at

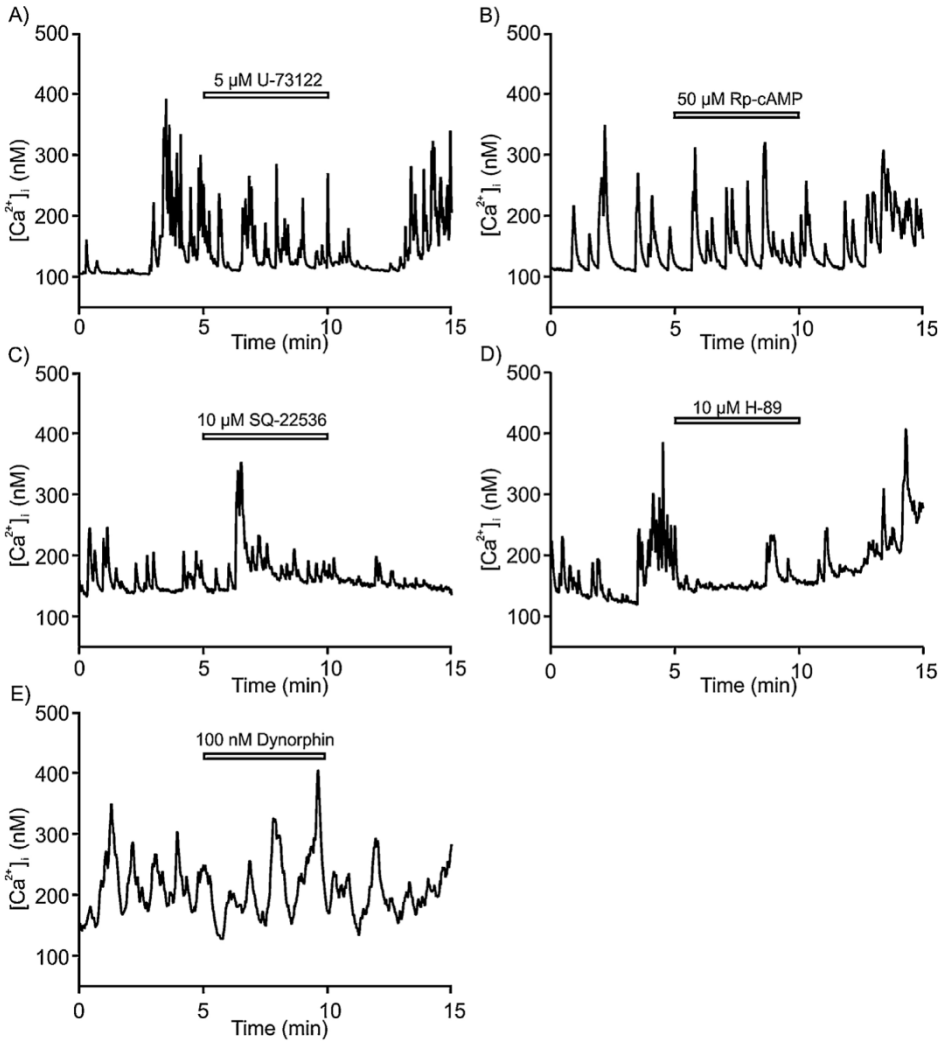

Fig. 7. The effect of blockers of phospholipase C and adenylyl cyclase intracellular transduction pathways on oscillations.
A-D: Inhibition of signalling cascades by PLC blocker (U-73122; A), competitive blocker of cAMP-dependent PKA (Rp-cAMP; B), an AC blocker (SQ-22536; C) and PKA blocker (H-89; D) does not affect spontaneous $[Ca^{2+}]_i$ oscillations. E: Trace showing the absence of effect of dynorphin on spontaneous $[Ca^{2+}]_i$ oscillations.

$[Ca^{2+}]_i$ = 130 nM, $[Na^+]_i$ = 10 mM, $[Na^+]_o$ = 140 mM) is about −45 to −50 mV, and thus a moderate depolarisation will reverse the NCX operation. In the reverse mode NCX provides for Ca^{2+} entry, which logically, underlies observed Ca^{2+} oscillations. This is in contrast to numerous examples of spontaneous $[Ca^{2+}]_i$ dynamics originating from Ca^{2+} release from the ER [32,40,41]. In SON neurones this seems not to be the case. Targeting the ER using TG, CPA, ryanodine or caffeine failed to affect $[Ca^{2+}]_i$ oscillations. Caffeine has a double action on the ER activating RyRs and effectively inhibiting $InsP_3$ receptors [34,35]; absence of any effect on spontaneous $[Ca^{2+}]_i$ oscillations argued against the role of ER Ca^{2+} release. At the same time removal of extracellular Ca^{2+} effectively blocked spontaneous $[Ca^{2+}]_i$ dynamics. It's of interest to note that the dependence of oscillations on extracellular Ca^{2+} has been observed in OT-sensitive SON neurones [7] and in AVP-sensitive neurones [6]. The NCX, however, is not the only mechanism for Ca^{2+} delivery associated with spontaneous $[Ca^{2+}]_i$ activity of SON neurones. Of interest, in nerve terminal preparations, the release of AVP was unexpectedly modulated by extracellular Na^+: removal of Na^+ inhibited secretion, whereas increases of extracellular Na^+ (in Na^+-depleted media) increased AVP secretion suggesting that the Na^+/Ca^{2+} exchanger has a particular functional role in the regulation of secretion—both somatic as well as at the level of the releasing nerve terminals in the neurohypophysis [42]. The $[Ca^{2+}]_i$ oscillations appear to be specifically associated with R-type VGCCs: treatment with a selective blocker of these channels, SNX-482, inhibited $[Ca^{2+}]_i$ oscillations in a concentration-dependent manner. The pharmacological inhibition of other VGCCs (T-, L-, N- and P/Q-types) was without effect. Similarly, inhibition of intercellular second messenger cascades and plasmalemmal K^+ channels did not affect spontaneous $[Ca^{2+}]_i$ activity. The role for NCX and R-type Ca^{2+} channels are also supported (albeit indirectly) by the inhibitory action of GABA that completely blocked spontaneous $[Ca^{2+}]_i$ dynamics. This action was mediated through $GABA_A$ receptors (as revealed by gabazine sensitivity) and most likely resulted from cell hyperpolarisation. The latter, arguably, prevented reversal of the NCX and activation of R-type Ca^{2+} channels.

4.3. *The need for ATP-dependent Ca^{2+} extrusion*

Efficient Ca^{2+} clearance from the cytosol is another necessary component for maintaining spontaneous $[Ca^{2+}]_i$ oscillations. Inhibition of PMCA by La^{3+} effectively suppressed spontaneous Ca^{2+} dynamics; the same effect was achieved by mitochondrial uncoupling. Thus we may conclude that energy dependent Ca^{2+} extrusion

joins NCX and R-type VGCCs in creating a pacemaker mechanism driving Ca^{2+} oscillatory activity.

5. Conclusions

Taken together, these results unveil, for the first time, the idiosyncrasies of Ca^{2+} signalling in AVP and OT neurones and demonstrate that the spontaneous $[Ca^{2+}]_i$ oscillations in the SON neurones are driven by plasmalemmal R-type Ca^{2+} channels and the Na^+/Ca^{2+} exchanger oscillation between forward and reverse modes; maintenance of oscillations also requires the activity of the plasmalemmal Ca^{2+} pump.

Conflict of interest

The authors state that they have no conflict of interest pertaining to this manuscript.

Authors' contribution

SK, CS, GD: performed experiments.

YU, OF: prepared and maintained the heterozygous and homozygous transgenic rats for both AVP and OT and developed double transgenic rats for AVP and OT; performed genotyping, manuscript writing.

SK, MZ, AV, GD: prepared the concept of the project, manuscript writing, data and statistical analysis.

AC, ES, GD: project management and logistics, manuscript writing.

Acknowledgements

This work was supported by the grants 14-34077S and GACR P304/12/G069 from the Grant Agency of the Czech Republic and GAUK 22214 from the Grant Agency of Charles University in Prague, and by institutional support RVO#67985823. CS and GD were supported in part by the FP7 Initial Training Network Edu-GLIA program (PITN-GA-2009-237956). This publication is partly a result of the "Advanced Bioimaging of Living Tissues" project, registration number #CZ.2.16/3.1.00/21527, which was financed from the budget of the European Regional Development Fund and public budgets of the Czech Republic through the Operational Programme Prague-Competitiveness. AV was supported by the Wellcome Trust, by the Alzheimer's research foundation (UK) and by a grant (agreement from August 27 2013 № 02.B.49.21.0003) between The Ministry of Education and Science of the Russian Federation and Lobachevsky State University of Nizhny Novgorod, by a grant of the Russian Scientific Foundation № 14-15-00633 and by the Ministry of Education of the Russian Federation, unique identity number RFMEFI57814X0079. Govindan Dayanithi belongs to the "Centre National de la Recherche Scientifique-The French Ministry of Research and Higher Education-Paris", France. We are grateful to Kip Allan Bauersfeld, IEM ASCR, for critical reading and helpful comments on the manuscript.

References

[1] G. Dayanithi, N. Sabatier, H. Widmer, Intracellular calcium signalling in magnocellular neurones of the rat supraoptic nucleus: understanding the autoregulatory mechanisms, Exp. Physiol. 85 (2000) 75S–84S (Spec No).
[2] W.E. Armstrong, Morphological and electrophysiological classification of hypothalamic supraoptic neurons, Prog. Neurobiol. 47 (1995) 291–339.
[3] C.H. Brown, J.S. Bains, M. Ludwig, J.E. Stern, Physiological regulation of magnocellular neurosecretory cell activity: integration of intrinsic, local and afferent mechanisms, J. Neuroendocrinol. 25 (2013) 678–710.
[4] M. Ludwig, N. Sabatier, P.M. Bull, R. Landgraf, G. Dayanithi, G. Leng, Intracellular calcium stores regulate activity-dependent neuropeptide release from dendrites, Nature 418 (2002) 85–89.
[5] P. Richard, F. Moos, G. Dayanithi, L. Gouzenes, N. Sabatier, Rhythmic activities of hypothalamic magnocellular neurons: autocontrol mechanisms, Biol. Cell 89 (1997) 555–560.
[6] G. Dayanithi, H. Widmer, P. Richard, Vasopressin-induced intracellular Ca^{2+} increase in isolated rat supraoptic cells, J. Physiol. 490 (Pt 3) (1996) 713–727.
[7] R.C. Lambert, G. Dayanithi, F.C. Moos, P. Richard, A rise in the intracellular Ca^{2+} concentration of isolated rat supraoptic cells in response to oxytocin, J. Physiol. 478 (Pt 2) (1994) 275–287.
[8] N. Sabatier, P. Richard, G. Dayanithi, L-, N- and T- but neither P- nor Q-type Ca^{2+} channels control vasopressin-induced Ca^{2+} influx in magnocellular vasopressin neurones isolated from the rat supraoptic nucleus, J. Physiol. 503 (Pt 2) (1997) 253–268.
[9] N. Sabatier, P. Richard, G. Dayanithi, Activation of multiple intracellular transduction signals by vasopressin in vasopressin-sensitive neurones of the rat supraoptic nucleus, J. Physiol. 513 (Pt 3) (1998) 699–710.
[10] L. Gouzenes, N. Sabatier, P. Richard, F.C. Moos, G. Dayanithi, V1a- and V2-type vasopressin receptors mediate vasopressin-induced Ca^{2+} responses in isolated rat supraoptic neurones, J. Physiol. 517 (Pt 3) (1999) 771–779.
[11] N. Sabatier, I. Shibuya, G. Dayanithi, Intracellular calcium increase and somatodendritic vasopressin release by vasopressin receptor agonists in the rat supraoptic nucleus: involvement of multiple intracellular transduction signals, J. Neuroendocrinol. 16 (2004) 221–236.
[12] Y. Komori, M. Tanaka, M. Kuba, M. Ishii, M. Abe, N. Kitamura, A. Verkhratsky, I. Shibuya, G. Dayanithi, Ca(2+) homeostasis, Ca(2+) signalling and somatodendritic vasopressin release in adult rat supraoptic nucleus neurones, Cell Calcium 48 (2010) 324–332.
[13] M. Ludwig, P.M. Bull, V.A. Tobin, N. Sabatier, R. Landgraf, G. Dayanithi, G. Leng, Regulation of activity-dependent dendritic vasopressin release from rat supraoptic neurones, J. Physiol. 564 (2005) 515–522.
[14] M. Cazalis, G. Dayanithi, J.J. Nordmann, The role of patterned burst and interburst interval on the excitation-coupling mechanism in the isolated rat neural lobe, J. Physiol. 369 (1985) 45–60.
[15] P. Roper, J. Callaway, T. Shevchenko, R. Teruyama, W. Armstrong, AHP's, HAP's and DAP's: how potassium currents regulate the excitability of rat supraoptic neurones, J. Comput. Neurosci. 15 (2003) 367–389.
[16] I. Shibuya, J. Noguchi, K. Tanaka, N. Harayama, U. Inoue, N. Kabashima, Y. Ueta, Y. Hattori, H. Yamashita, PACAP increases the cytosolic Ca^{2+} concentration and stimulates somatodendritic vasopressin release in rat supraoptic neurons, J. Neuroendocrinol. 10 (1998) 31–42.
[17] G. Dayanithi, O. Forostyak, Y. Ueta, A. Verkhratsky, E.C. Toescu, Segregation of calcium signalling mechanisms in magnocellular neurones and terminals, Cell Calcium 51 (2012) 293–299.
[18] J. Sneyd, J. Keizer, M.J. Sanderson, Mechanisms of calcium oscillations and waves: a quantitative analysis, FASEB J. 9 (1995) 1463–1472.
[19] Y. Ueta, H. Fujihara, R. Serino, G. Dayanithi, H. Ozawa, K. Matsuda, M. Kawata, J. Yamada, S. Ueno, A. Fukuda, D. Murphy, Transgenic expression of enhanced green fluorescent protein enables direct visualization for physiological studies of vasopressin neurons and isolated nerve terminals of the rat, Endocrinology 146 (2005) 406–413.
[20] H. Fujihara, K. Sasaki, E. Mishiro-Sato, T. Ohbuchi, G. Dayanithi, M. Yamasaki, Y. Ueta, N. Minamino, Molecular characterization and biological function of neuroendocrine regulatory peptide-3 in the rat, Endocrinology 153 (2012) 1377–1386.
[21] T. Moriya, R. Shibasaki, T. Kayano, N. Takebuchi, M. Ichimura, N. Kitamura, A. Asano, Y.Z. Hosaka, O. Forostyak, A. Verkhratsky, G. Dayanithi, I. Shibuya, Full-length transient receptor potential vanilloid 1 channels mediate calcium signals and possibly contribute to osmoreception in vasopressin neurones in the rat supraoptic nucleus, Cell Calcium 57 (2015) 25–37.
[22] H. Fujihara, Y. Ueta, H. Suzuki, A. Katoh, T. Ohbuchi, H. Otsubo, G. Dayanithi, D. Murphy, Robust up-regulation of nuclear red fluorescent-tagged fos marks neuronal activation in green fluorescent vasopressin neurons after osmotic stimulation in a double transgenic rat, Endocrinology 150 (9) (2009) 5633–5638.
[23] C. Viero, I. Shibuya, N. Kitamura, A. Verkhratsky, H. Fujihara, A. Katoh, Y. Ueta, H.H. Zingg, A. Chvatal, E. Sykova, G. Dayanithi, Oxytocin: crossing the bridge between basic science and pharmacotherapy, CNS Neurosci. Ther. 16 (2010) e138–e156.
[24] G. Grynkiewicz, M. Poenie, R.Y. Tsien, A new generation of Ca^{2+} indicators with greatly improved fluorescence properties, J. Biol. Chem. 260 (1985) 3440–3450.
[25] G. Dayanithi, I. Mechaly, C. Viero, H. Aptel, S. Alphandery, S. Puech, F. Bancel, J. Valmier, Intracellular Ca^{2+} regulation in rat motoneurons during development, Cell Calcium 39 (2006) 237–246.
[26] C. Viero, I. Mechaly, H. Aptel, S. Puech, J. Valmier, F. Bancel, G. Dayanithi, Rapid inhibition of Ca^{2+} influx by neurosteroids in murine embryonic sensory neurones, Cell Calcium 40 (2006) 383–391.
[27] N. Sasaki, G. Dayanithi, I. Shibuya, Ca^{2+} clearance mechanisms in neurohypophysial terminals of the rat, Cell Calcium 37 (2005) 45–56.
[28] F.M. Dreyfus, A. Tscherter, A.C. Errington, J.J. Renger, H.S. Shin, V.N. Uebele, V. Crunelli, R.C. Lambert, N. Leresche, Selective T-type calcium channel block in thalamic neurons reveals channel redundancy and physiological impact of I(T)window, J. Neurosci. 30 (2010) 99–109.
[29] E. Bourinet, S.C. Stotz, R.L. Spaetgens, G. Dayanithi, J. Lemos, J. Nargeot, G.W. Zamponi, Interaction of SNX482 with domains III and IV inhibits activation gating of alpha(1E) (Ca(V)2.3) calcium channels, Biophys. J. 81 (2001) 79–88.

[30] G. Wang, G. Dayanithi, R. Newcomb, J.R. Lemos, An R-type Ca(2+) current in neurohypophysial terminals preferentially regulates oxytocin secretion, J. Neurosci. 19 (1999) 9235–9241.
[31] S. Ortiz-Miranda, G. Dayanithi, E. Custer, S.N. Treistman, J.R. Lemos, Micro-opioid receptor preferentially inhibits oxytocin release from neurohypophysial terminals by blocking R-type Ca^{2+} channels, J. Neuroendocrinol. 17 (2005) 583–590.
[32] S. Kawano, K. Otsu, S. Shoji, K. Yamagata, M. Hiraoka, Ca(2+) oscillations regulated by Na(+)-Ca(2+) exchanger and plasma membrane Ca(2+) pump induce fluctuations of membrane currents and potentials in human mesenchymal stem cells, Cell Calcium 34 (2003) 145–156.
[33] T. Brustovetsky, M.K. Brittain, P.L. Sheets, T.R. Cummins, V. Pinelis, N. Brustovetsky, KB-R7943 an inhibitor of the reverse Na^{+}/Ca^{2+} exchanger, blocks *N*-methyl-D-aspartate receptor and inhibits mitochondrial complex I, Br. J. Pharmacol. 162 (2011) 255–270.
[34] M. Wakui, Y.V. Osipchuk, O.H. Petersen, Receptor-activated cytoplasmic Ca^{2+} spiking mediated by inositol trisphosphate is due to Ca2(+)-induced Ca^{2+} release, Cell 63 (1990) 1025–1032.
[35] I. Bezprozvanny, S. Bezprozvannaya, B.E. Ehrlich, Caffeine-induced inhibition of inositol(1,4,5)-trisphosphate-gated calcium channels from cerebellum, Mol, Biol. Cell 5 (1994) 97–103.
[36] N. Wanaverbecq, S.J. Marsh, M. Al-Qatari, D.A. Brown, The plasma membrane calcium-ATPase as a major mechanism for intracellular calcium regulation in neurones from the rat superior cervical ganglion, J. Physiol. 550 (2003) 83–101.
[37] Y. Hattori, I. Shibuya, K. Tanaka, N. Kabashima, Y. Ueta, H. Yamashita, Ionotropic and metabotropic glutamate receptor agonist-induced $[Ca^{2+}]i$ increase in isolated rat supraoptic neurons, J. Neuroendocrinol. 10 (1998) 383–389.
[38] I. Shibuya, N. Kabashima, N. Ibrahim, S.V. Setiadji, Y. Ueta, H. Yamashita, Pre- and postsynaptic modulation of the electrical activity of rat supraoptic neurones, Exp. Physiol. 85 (2000) 145s–151s (Sec No).
[39] C.H. Brown, G. Leng, In vivo modulation of post-spike excitability in vasopressin cells by kappa-opioid receptor activation, J. Neuroendocrinol. 12 (2000) 711–714.
[40] J. Sneyd, K. Tsaneva-Atanasova, D.I. Yule, J.L. Thompson, T.J. Shuttleworth, Control of calcium oscillations by membrane fluxes, Proc. Natl. Acad. Sci. U.S.A. 101 (2004) 1392–1396.
[41] A. Verkhratsky, Physiology and pathophysiology of the calcium store in the endoplasmic reticulum of neurons, Physiol. Rev. 85 (2005) 201–279.
[42] E.C. Toescu, J.J. Nordmann, Effect of sodium and calcium on basal secretory activity of rat neurohypophysial peptidergic nerve terminals, J. Physiol. 433 (1991) 127–144.

B.II Physiology of spontaneous $[Ca^{2+}]_i$ oscillations in the isolated vasopressin and oxytocin neurones of the rat supraoptic nucleus.

Kortus, S., C. Srinivasan, O. Forostyak, Y. Ueta, E. Sykova, A. Chvatal, M. Zapotocky, A. Verkhratsky and G. Dayanithi (2016). "Physiology of spontaneous $[Ca^{2+}]_i$ oscillations in the isolated vasopressin and oxytocin neurones of the rat supraoptic nucleus." Cell Calcium 59(6): 280-288.

Cell Calcium 59 (2016) 280–288

Contents lists available at ScienceDirect

Cell Calcium

journal homepage: www.elsevier.com/locate/ceca

Physiology of spontaneous $[Ca^{2+}]_i$ oscillations in the isolated vasopressin and oxytocin neurones of the rat supraoptic nucleus

Stepan Kortus[a,b,c], Chinnapaiyan Srinivasan[a], Oksana Forostyak[a,d], Yoichi Ueta[e], Eva Sykova[d,f], Alexandr Chvatal[d,g], Martin Zapotocky[b,c], Alexei Verkhratsky[h,i,j,k,**], Govindan Dayanithi[a,l,m,*]

[a] Department of Molecular Neurophysiology, Institute of Experimental Medicine, Czech Academy of Sciences, Videnska 1083, 14220 Prague, Czech Republic
[b] Institute of Physiology, Czech Academy of Sciences, Videnska 1083, 14220 Prague, Czech Republic
[c] Institute of Biophysics and Informatics, First Faculty of Medicine, Charles University in Prague, Salmovska 1, 12000 Prague, Czech Republic
[d] Department of Neuroscience, Charles University, Second Medical Faculty, V Uvalu 84, 15006 Prague, Czech Republic
[e] Department of Physiology, School of Medicine, University of Occupational and Environmental Health, Kitakyushu 807-8555, Japan
[f] Department of Neuroscience, Institute of Experimental Medicine, Czech Academy of Sciences, Videnska 1083, 14220 Prague, Czech Republic
[g] Department of Cellular Neurophysiology, Institute of Experimental Medicine, Czech Academy of Sciences, Videnska 1083, 14220 Prague, Czech Republic
[h] University of Manchester, School of Biological Sciences, D.4417 Michael Smith Building, Oxford Road, M13 9PT Manchester, United Kingdom
[i] Achucarro Center for Neuroscience, IKERBASQUE, Basque Foundation for Science, 48011 Bilbao, Spain
[j] Department of Neurosciences, University of the Basque Country UPV/EHU and CIBERNED, Leioa, Spain
[k] University of Nizhny Novgorod, Nizhny Novgorod 603022, Russia
[l] Institut National de la Santé et de la Recherche Médicale, Unité de recherche U1198, Université Montpellier 2, 34095 Montpellier, France
[m] Ecole Pratique des Hautes Etudes, Sorbonne, 75014 Paris, France

ARTICLE INFO

Article history:
Received 8 March 2016
Received in revised form 31 March 2016
Accepted 5 April 2016
Available online 6 April 2016

Keywords:
Hypothalamus
Magnocellular neurosecretory cells
Supraoptic nucleus
Vasopressin
Oxytocin
Transgenic rats
Enhanced green fluorescence protein
Monomeric red fluorescence protein

ABSTRACT

The magnocellular vasopressin (AVP) and oxytocin (OT) neurones exhibit specific electrophysiological behaviour, synthesise AVP and OT peptides and secrete them into the neurohypophysial system in response to various physiological stimulations. The activity of these neurones is regulated by the very same peptides released either somato-dendritically or when applied to supraoptic nucleus (SON) preparations *in vitro*. The AVP and OT, secreted somato-dendritically (*i.e.* in the SON proper) act through specific autoreceptors, induce distinct Ca^{2+} signals and regulate cellular events. Here, we demonstrate that about 70% of freshly isolated individual SON neurones from the adult non-transgenic or transgenic rats bearing AVP (AVP-eGFP) or OT (OT-mRFP1) markers, produce distinct spontaneous $[Ca^{2+}]_i$ oscillations. In the neurones identified (through specific fluorescence), about 80% of AVP neurones and about 60% of OT neurones exhibited these oscillations. Exposure to AVP triggered $[Ca^{2+}]_i$ oscillations in silent AVP neurones, or modified the oscillatory pattern in spontaneously active cells. Hyper- and hypo-osmotic stimuli (325 or 275 mOsmol/l) respectively intensified or inhibited spontaneous $[Ca^{2+}]_i$ dynamics. In rats dehydrated for 3 or 5 days almost 90% of neurones displayed spontaneous $[Ca^{2+}]_i$ oscillations. More than 80% of OT-mRFP1 neurones from 3 to 6-day-lactating rats were oscillatory *vs.* about 44% (OT-mRFP1 neurones) in

Abbreviations: AVP, arginine vasopressin; OT, oxytocin; MNCs, magnocellular neurosecretory cells; eGFP, enhanced green fluorescence protein; mRFP1, monomeric red fluorescence protein; SON, supraoptic nucleus; $[Ca^{2+}]_i$, intracellular Ca^{2+} concentration; FFP, Fast Fluorescence Photometer; SD, Standard Deviation.

* Corresponding author at: Department of Molecular Neurophysiology, Institute of Experimental Medicine, Czech Academy of Sciences, Videnska 1083, CZ-142 20 Prague 4, Czech Republic.
** Correspondence author at: University of Manchester, School of Biological Sciences, Oxford Road, Manchester, M13 9PT, United Kingdom.
E-mail addresses: Alexej.Verkhratsky@manchester.ac.uk (A. Verkhratsky), gdaya@univ-montp2.fr, gdaya@biomed.cas.cz (G. Dayanithi).

http://dx.doi.org/10.1016/j.ceca.2016.04.001

Osmoregulation
Hyper-osmolarity
Hypo-osmolarity
Dehydration
Lactation
Electrical activity
Ca^{2+} oscillations
Fura-2
Fluorescence spectrofluorimetry
Spationtemporal dynamics
Skewness

virgins. Together, these results unveil for the first time that both AVP and OT neurones maintain, via Ca^{2+} signals, their remarkable intrinsic *in vivo* physiological properties in an isolated condition.

1. Introduction

The hypothalamic supraoptic nucleus (SON) contains magnocellular neurosecretory neurones that synthesise the neurohormones arginine vasopressin (AVP) and oxytocin (OT). These hormones are released from axonal projections from these neurones to the neurohypophysis into the portal blood circulation in response to various physiological stimuli such as dehydration, osmotic stimulation, parturition and lactation. Both AVP and OT neurones exhibit characteristic electrical activities. Under physiological settings, the AVP neurones exhibit 'phasic' firing activity of action potentials with intervals, whereas OT neurones fire high frequency synchronized bursts of action potentials associated with suckling-induced milk ejection. The characteristic firing patterns, as recorded *in vivo*, are crucial for the efficient release of AVP and OT at the neurohypophysis [1,2] and from the isolated terminals [3]; and are triggered by Ca^{2+}-dependent exocytosis driven by the arrival of action potentials initiated at the cell bodies [4,5].

In the *in vivo* experiments, the somato-dendritic release of AVP modulates the phasic pattern of AVP neurones electrical activity depending on the initial firing pattern [6]. The intranuclear release of OT, which increases during suckling, increases the excitability of OT neurones [7]. At the subcellular level, AVP induces a transient increase in the intracellular Ca^{2+} concentration ($[Ca^{2+}]_i$) in isolated AVP-containing neurones [8]. AVP-induced $[Ca^{2+}]_i$ responses are modulated by specific voltage-gated Ca^{2+} channel subtypes [9] and are mediated by different sub-types of AVP receptors (V_{1a}, V_{1b} and V_2) [6] through activating multiple intracellular transduction signals (PLC and AC) [10]. The autoregulation of AVP and OT neurones is mediated by distinct mechanisms: OT increases $[Ca^{2+}]_i$ in isolated OT-containing neurones through the activation of specific OT receptors and the release of Ca^{2+} from thapsigargin-sensitive intracellular stores [11,12], with subsequent activation of store-operated Ca^{2+} entry [13]. In contrast, $[Ca^{2+}]_i$ responses induced by AVP critically require plasmalemmal Ca^{2+} influx, indicating the primary role for membrane Ca^{2+} channels. Further studies have shown that the existence of a cell specific (AVP and OT) Ca^{2+} homeostasis and Ca^{2+} clearance mechanisms depends upon physiological conditions related to the specific electrical firing patterns of these neurones [14,15].

The changes in AVP release induced in response to plasma osmolarity fluctuations are mediated by regulation of action potential discharge in the cell bodies [16] and the SON neurones are defined as osmosentive [17–19]. Other studies have demonstrated that both AVP and OT neurones are activated during chronic dehydration, but with a marked difference in the pattern of their responses [20]. AVP is also shown to be involved in the promotion of water conservation during periods of dehydration [21]. Several previous studies have periodically observed that some isolated AVP and OT neurones (identified by immunocytochemistry or by their $[Ca^{2+}]_i$ responses to AVP or OT), displayed spontaneous $[Ca^{2+}]_i$ oscillations under normal experimental conditions [6,8,11,12,15,22,23]. Hitherto, however, neither the identity nor characteristics of these oscillatory neurones, nor the physiological properties of these $[Ca^{2+}]_i$ oscillations were clearly established.

In the present study, we studied $[Ca^{2+}]_i$ dynamics in i) AVP-sensitive and OT-sensitive (in terms of their specific $[Ca^{2+}]_i$ responses) neurones from wild type adult male and virgin Wistar rats; and ii) identified AVP and OT neurones from homozygous transgenic male, as well as from virgin and lactating Wistar rats models expressing (1) an arginine vasopressin (AVP)-enhanced green fluorescent protein (AVP-eGFP) [24]; (2) an oxytocin-monomeric red fluorescent protein 1 (OT-mRFP1) [25] and, (3) in homozygous double transgenic rats simultaneously bearing AVP-eGFP and OT-mRFP1 to visualize both AVP and OT neurones in the same animal [15,21,26].

2. Materials and methods

2.1. Animals and experimental procedures

Adult male Wistar rats (wild type) and three different homozygous transgenic rats were used in this study: transgenic rats expressing an arginine vasopressin-enhanced green fluorescent protein (AVP-eGFP) [25], transgenic male or female or lactating rats expressing an oxytocin-monomeric red fluorescent protein 1 (OT-mRFP1) [25] and double transgenic (expressing both markers) to visualize AVP and OT neurones [15]. A homozygous line was identified among the offspring of two heterozygous parents by finding exclusively heterozygous progeny from the mating of transgenic offspring rat with a wild-type Wistar rat. The double transgenic AVP-eGFP/OT-mRFP line was generated by mating homozygous AVP-eGFP with OT-mRFP transgenic rats. All transgenic rats used in the study were screened by polymerase chain reaction analysis of genomic DNA extracted from rat ear or tail biopsies before breeding and use in the experiments. The PCR was performed using the oligonucleotide primers (AVP-eGFP: sense sequence, 5′-CAC CAT CTT CTT CAA GGA CGA C-3′; antisense sequence, 5′-ATG ATA TAG ACG TTG TGG CTG TTG T-3′; and OT-mRFP: sense sequence, 5′-GTG AAG CAC CCC GCC GAC AT-3′; antisense sequence, 5′- TGC ATT ACG GGG CCG TCG GA-3′). The animals (weighting 150–300 g; 4–8 weeks old) were bred and housed at 22–23° C, 12:12 h light/dark cycle (lights on 07:00–19:00 h), with food and drinking water available ad libitum. The animals were sacrificed by decapitation after anaesthesia with 5% isoflurane for 5 min, the brain was rapidly removed and SON was dissected.

All animals (weighting 150–300 g; 3–8 weeks old; lactating rats weighted about 500 g; 12–16 weeks old) were bred and housed at 22–23° C under normal laboratory conditions (12:12 h light/dark cycle, lights on 07:00–19:00 h) with food and drinking water available *ad libitum*. Transgenic rats were screened by polymerase chain reaction analysis of genomic DNA extracted from rat ear or tail biopsies before breeding and use in the experiments. For each experiment, animals were sacrificed by decapitation after deep

anaesthesia with 5% isofluran for 5 min, the brain was rapidly removed and SON was dissected (see below). All experiments were performed in accordance with the European Communities Council Directive of 24 November 1986 (86/609/EEC) regarding the use of animals in research, and were approved by the Ethics Committee of the Institute of Experimental Medicine, Academy of Sciences of the Czech Republic, Prague, Czech Republic (project experiment license #CZ 205/2010 revised in 2013).

2.2. Isolation of supraoptic neurones

SON neurones were acutely dissociated by enzymatic and mechanical treatments as described previously [8,11] with some modifications [14,27]. In brief, SON tissues (1 mm long, 0.5 mm thick, 0.5 mm wide) were dissected and enzymatically dissociated by incubation for 30 min in oxygenated HEPES-buffered normal Locke's solution (NL; in mM: 140 NaCl, 5 KCl, 2$CaCl_2$, 1 $MgCl_2$, 10 glucose, 10HEPES, pH was adjusted to 7.25 with Tris; the osmolarity was 298–300 mOsm/l; temperature 37° C) supplemented with 1 mg/ml deoxyribonuclease I, 0.5 mg/ml proteases X, and 0.5 mg/ml protease XIV. Unless stated otherwise, most of the chemicals were purchased from Sigma-Aldrich (St. Louis, USA). After incubation, tissues were washed with NL and triturated gently using a Gilson-Pipetman (1 ml) with polypropylene white pipette-tip to isolate SON cells. Cells were plated onto glass bottom dishes (22 mm in diameter, 0.17 mm in thick: WillCo Wells-Amsterdam). Unless otherwise stated, all stock solutions of the drugs used in this study were dissolved in this total ion-free distilled H_2O (EMD Millipore Corporation, Germany). The hypotonic solution was prepared by reducing the appropriate Na^+ concentration and in the hypertonic solution the osmolarity was increased by adding mannitol.

2.3. $[Ca^{2+}]_i$ measurements using fluorescence photometer system

The $[Ca^{2+}]_i$ in isolated SON neurones was measured with a fluorescent Ca^{2+} indicator Fura-2 according to the procedure previously described [8] with appropriate revisions [27]. In brief, the SON cells were incubated with 2.5 μM Fura-2 AM (Invitrogen, Carlsbad, CA, USA) with 0.02% Pluronic F-127 (Molecular Probes, Eugene, OR, USA) at 37 °C for 50 min. Two microscope systems were used for $[Ca^{2+}]_i$ measurements: a fluorescence microspectrofluorimetry system (FFP; Fast Fluorescence Photometer, Zeiss, Jena, Germany) for single-detector experiments and an imaging system using a CCD camera as a detector for video imaging and for measurement of $[Ca^{2+}]_i$ from neurones obtained from transgenic animals.

2.4. $[Ca^{2+}]_i$ measurements using the FFP system

This system is based on an epi-fluorescence inverted microscope (Axiovert 10, Zeiss, Jena Germany). The excitation light from a Xenon lamp passed through bandpass filters mounted on a computer-controlled rotating wheel that allows alternate stimulation at 340 ± 10 and 380 ± 10 nm with a frequency of 3.3 Hz. The excitation light was deflected by a dichroic mirror (FT 425, Zeiss, Jena, Germany) through an oil-immersion objective (Plan Neofluar 100 × 1.30, ph. 3, Zeiss, Jena, Germany). Fluorescence emission from individual cells was spatially limited by a diaphragm adjusted to the cell size (10–15 μm).

2.5. $[Ca^{2+}]_i$ measurements using CCD video-imaging system

Video imaging of $[Ca^{2+}]_i$ was performed using an Axio Observer D1 (Zeiss) inverted microscope equipped with filters for monitoring GFP and RFP fluorescence, and epifluorescence oil immersion objectives (Plan Neofluar 100 × 1.30, FLUAR 40X/1.3 oil and FLUOR 20 × 0.75, Zeiss). This allowed us to visualize and identity the SON neurones obtained from AVP-eGFP and OT-mRFP1expressing animals. The excitation light from a Xenon lamp passed through a Lambda D4 ultra-fast wavelength switching system (Sutter Instruments) with a maximum switching frequency of 500 Hz. The fluorescence intensity was detected by using a cooled CCD camera (AxioCam MRm, Zeiss) and the whole system was controlled by Zeiss ZEN Imaging software (2012-SP2/AxioVision SE64 Rel. 4.8.3). The fluorescence intensity was measured with excitations at 340 and 380 nm, and emission at 510 nm.

To estimate $[Ca^{2+}]_i$ in nM a calibration was performed on a few neurones for both systems. An estimation of $[Ca^{2+}]_i$ was determined from the f_{340}/f_{380} ratio using the Grynkiewicz equation [28]. The calibration parameters for the FFP system were R_{min} = 0.24, R_{max} 4.66, β = 3.39. Calibration performed with the imaging system gave R_{min} = 0.2, R_{max} = 7.2, β = 7.7. The dissociation constant for Fura-2 at 37 °C was assumed as K_D = 224 nM.

2.6. Drugs application

Solutions were exchanged using a multiple capillary perfusion system, as described previously [29,30] with appropriate modifications [31]. Briefly, the 200 μm inner diameter capillary tubing was placed close to the tested cell (<500 μm). Solutions were applied through a temperature controlled (set at 37 °C) device, applied through a computer controlled multichannel peristaltic pump (REGLO ICC, Ismatec) using tubing with 0.64 mm inner diameter. Each tubing was fed by a reservoir 30 cm above the bath and connected to a temperature control device (Model: TC-324B; Harvard-Paris, France). The solutions flow rate was set to 500 μl/min for inlet and about 5% slower for outlet. Additional outlet tubing was placed close to the edge of the dish for maintaining 2 mm solution (about 750 μl volume) level in the dish throughout the measurement period. This setup ascertains local perfusion with linear flow without any mechanical disturbance and minimal fluctuation of solution level.

2.7. Data pre-processing

Each $[Ca^{2+}]_i$ trace was first classified as oscillating or non-oscillating. Changes in $[Ca^{2+}]_i$ with an amplitude of at least 30 nM that occurred within 120 s (or faster) were considered to be "Ca^{2+} events", and traces or parts of traces in which such events occurred repeatedly were considered "$[Ca^{2+}]_i$ oscillations". The threshold of 30 nM was used as a value sufficient for excluding the interference of the noise inherent in the signal. Only $[Ca^{2+}]_i$ traces with sustained oscillations lasting for at least 10 min were included in further analysis. Traces with strong trend or obvious artefacts were removed from the data set. To reduce noise, all data were filtered by a 2nd-order Butterworth low-pass filter with a cut-off frequency of 0.5 Hz (with filter coefficients estimated by the MATLAB function *butter* and filtration performed by *filtfilt*). MATLAB 2015a and its Statistics, Machine Learning, and Signal Processing toolboxes were employed in all numerical procedures.

Although ratiometric measurements using Fura-2 reduce the effect of photo bleaching, some trend of it exists, especially in longer-lasting experiments. This is because signals from 340 nm and 380 nm do not bleach equally and the ratio is rising even without a change in $[Ca^{2+}]_i$. We estimated this trend by averaging 55 traces with a duration of more than 15 min and fitting the averaged trace with a linear function of time. This gave a trend expressed as 0.011 nM/s (or; 0.66 nM/min). This increase was then subtracted from all individual traces.

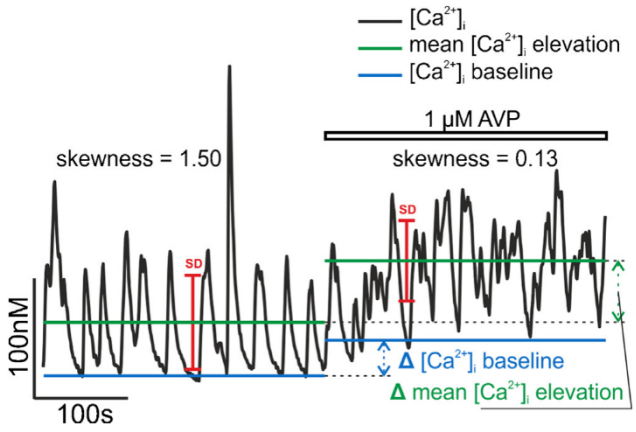

Fig. 1. Example of evaluation of $[Ca^{2+}]_i$ oscillations.
For both segments of the recording (300 s in NL buffer and 300 s with added 1 µm AVP), four basic parameters are evaluated: the $[Ca^{2+}]_i$ baseline, the mean $[Ca^{2+}]_i$ level, the standard deviation of the trace, and the skewness of the $[Ca^{2+}]_i$ distribution (Methods, Section 2.8). The difference in parameter values is shown graphically for the $[Ca^{2+}]_i$ baseline and the mean $[Ca^{2+}]_i$ level.

2.8. Data analysis and statistical evaluation

Four basic parameters were computed for each individual trace or its segment: the $[Ca^{2+}]_i$ baseline, the mean $[Ca^{2+}]_i$ level, the standard deviation of the trace, and the skewness of the $[Ca^{2+}]_i$ values. These parameters were computed separately for each trace segment corresponding to a defined physiological condition (for example, application of AVP). Only trace segments longer than 300 s were considered. An example of such evaluation is shown in Fig. 1.

The $[Ca^{2+}]_i$ baseline c_B was estimated as the mean of the 20 smallest $[Ca^{2+}]_i$ values in each trace or trace segment. The mean $[Ca^{2+}]_i$ level was calculated as the average of all $[Ca^{2+}]_i$ values. *i.e.*, $\bar{c} = (1/N)\left(\sum_{k=1}^{N} c_k\right)$, where N is the number of $[Ca^{2+}]_i$ samples in the trace segment and c_k are the sample values.

The standard deviation SD_{Ca} was computed as the square root of the variance of $[Ca^{2+}]_i$ values within the trace segment. *i.e.*, $SD_{Ca} = \sqrt{Var}$, where $Var = (1/N)(\sum_{k=1}^{N}(c_k - \bar{c})^2)$. The parameter SD_{Ca} quantifies the spread of the $[Ca^{2+}]_i$ values within the trace. The asymmetry of this spread is quantified by the distribution skewness γ, defined as

$$\gamma = \frac{\mu_3}{(SD_{Ca})^3},$$

where $\mu_3 = \frac{1}{N}\sum_{k=1}^{N}(c_k - \bar{c})^3$ is the third central moment of the distribution of $[Ca^{2+}]_i$ values. For a symmetric distribution (such as the normal distribution), $\gamma = 0$, while for an exponential distribution, $\gamma = 2$. Positive or negative values of γ indicate a distribution skewed to the right or to the left, respectively (see Section 3.1).

Differences between the trace segments were evaluated based on the four trace parameters defined above. For each parameter, the difference of its value before and after drug application was calculated for each cell trace (see example in Fig. 1). This difference was then averaged over the cells in the given group, and the paired *t*-test was used to determine if the difference was statistically significant. The *p*-values reported in Results represent the significance level for rejecting the null hypothesis of zero difference. The MATLAB function *t*-test was used.

In figures displaying data fitted by a linear approximation, least-squares fitting were performed using the MATLAB function *polyfit*. As a measure of goodness of the linear fit we use the coefficient of determination R^2 calculated as

$$R^2 = 1 - \frac{\sum_{k=1}^{N}\left(c_k - c_k'\right)^2}{\sum_{k=1}^{N}(c_k - \bar{c})^2},$$

where c_k denotes the measured $[Ca^{2+}]_i$ values and c_k' the values estimated by the linear approximation.

In all $[Ca^{2+}]_i$ trace figures, the bars above the trace denote an application of test substances. Unless otherwise indicated specifically, the data are presented as mean values ± SEM (n = the number of observations).

3. Results

3.1. General features of the calcium oscillations in SON neurones

We observed spontaneous $[Ca^{2+}]_i$ oscillations in 79 out of 112 unidentified neurones (71%). Among identified neurons, 12 out of 15 AVP cells (80%) and 9 out of 15 OT cells (60%) exhibited oscillations. Fig. 2 shows a typical example of $[Ca^{2+}]_i$ oscillation in an identified AVP-eGFP neurone (A) and in OT-mRFP1 neurone (B). To compare the course of spontaneous oscillations *vs.* an evoked transient, we show in Fig. 3A; (video file-1) a typical transient $[Ca^{2+}]_i$ response induced by 50 mM K^+ observed in an AVP-eGFP neurone, while Fig. 3B; (video file-2) shows the spontaneous $[Ca^{2+}]_i$ oscillations observed in an AVP-eGFP neurone. The corresponding spatial changes in the fluorescence are shown in Fig. 3C and D, respectively.

For each spontaneous oscillation trace, we computed the four basic parameters defined in Section 2.8. We then evaluated if these parameter values differed among the three cell groups (unidentified, AVP and OT). No statistically significant difference was found (assessed by unpaired *t*-test). This primarily reflects the large variability among the oscillation traces within each cell group.

The pattern of $[Ca^{2+}]_i$ oscillations was highly heterogeneous, and can be qualitatively classified into the following three types. The type I pattern is characterized by Ca^{2+} events of regular amplitude and frequency (Fig. 4A); type II consists of irregular events that frequently overlap and form bursts (Fig. 4B); type III contains of oscillations of high frequency, during which $[Ca^{2+}]_i$ remains continually elevated above the baseline level (Fig. 4C). We visually examined the $[Ca^{2+}]_i$ traces recorded in 79 unidentified neurones and classified them, based on the qualitative criteria stated above. Type I activity was observed in 29 cells, type II in 34, and type III in 16 cells.

As we observed that the pattern of oscillation often changed when an external stimulus was presented (see following subsections), we sought a simple quantitative classifier that would allow us to systematically express such pattern changes. The frequency or amplitude of the oscillation peaks could not be used for this purpose, as these parameters become ill-defined for irregular oscillations (Fig. 4C). We found, however, that the skewness of the distribution of $[Ca^{2+}]_i$ values permits distinguishing the basic oscillation patterns. As shown in Fig. 4D–F, the distribution of the $[Ca^{2+}]_i$ values within the trace has a highly asymmetrical shape in case of the oscillation pattern of Type I (as in Fig. 4A), moderately asymmetrical for the type II pattern (as in Fig. 4B), and symmetrical for the type III pattern (as in Fig. 4C). The strong asymmetry of the distribution in type I arises from the shape of the stereotypical oscillation peaks: a fast rise in $[Ca^{2+}]_i$ followed by a slower, exponential decay. Correspondingly, the distribution of $[Ca^{2+}]_i$ values is approximately exponential, with skewness value $\gamma = 2.04$ in the example in Fig. 4D. In type II, the irregular parts of the oscillation result in a nonexponential tail in the distribution and a lower skew-

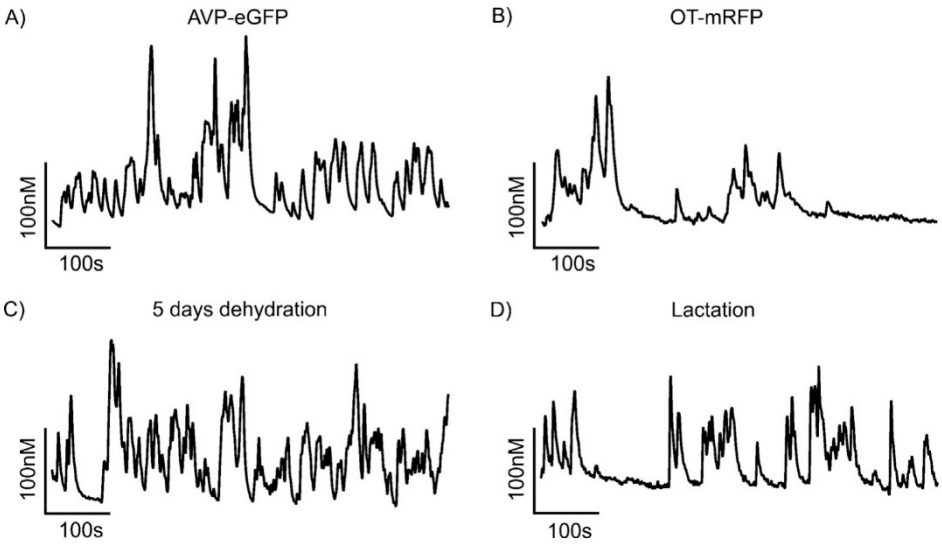

Fig. 2. Representative traces of spontaneous $[Ca^{2+}]_i$ oscillations. Panels A, B: recorded under normal condition in identified OT neurone (A) and AVP neurone (B). Panels C, D: recorded in neurone obtained from 5 days dehydrated rat (C) and from 6-day lactating rat (D).

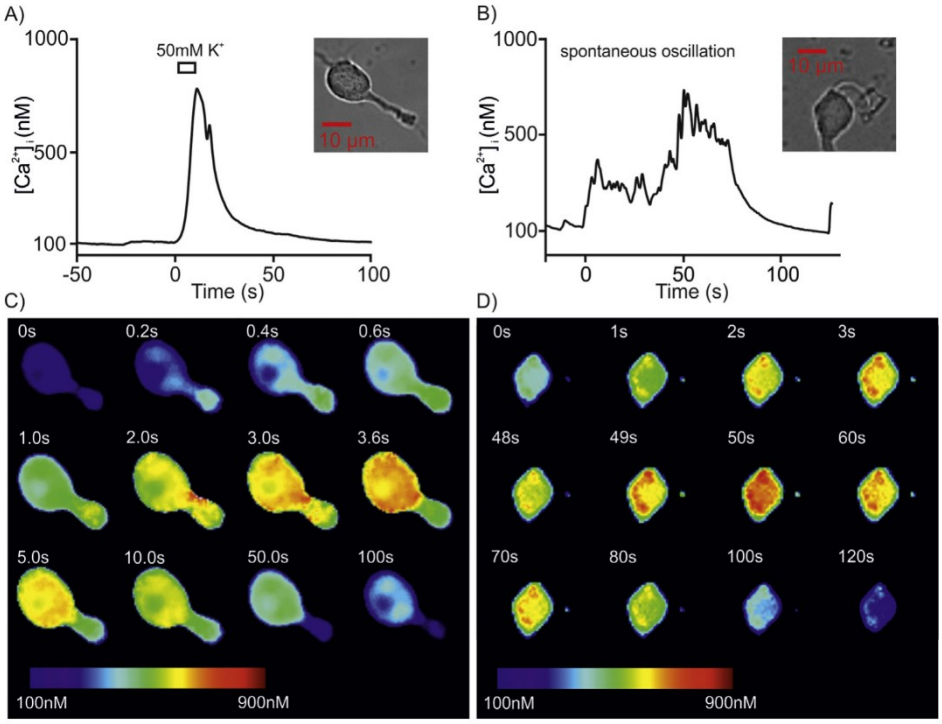

Fig. 3. Trace (A) shows a typical transient $[Ca^{2+}]_i$ response induced by 50 mM K^+ observed in an AVP-eGFP neurone (inset). Trace (B) shows the spontaneous $[Ca^{2+}]_i$ oscillations observed in an AVP-eGFP neurone (inset). The corresponding changes in the spatial pattern of fluorescence are shown in C and D, respectively.

ness ($\gamma = 1.09$, Fig. 4E). Finally in type III, the fast deviations up and down from the mean $[Ca^{2+}]_i$ level result in an approximately symmetrical distribution with nearly zero skewness ($\gamma = 0.5$ in Fig. 4F). Fig. 4G shows the range of skewness values in the neurones of each type, where the type was determined by visual examination of the trace as discussed above. As these ranges have low overlap, the skewness can be used as a quantitative classifier, replacing the qualitative visual inspection. In the following, we consider traces with skewness above 1.52 as type I, between 1.52 and 0.53 as type II, and below 0.53 as type III.

3.2. Effect of osmolarity on spontaneous $[Ca^{2+}]_i$ oscillations

To evaluate the effect of osmolarity, $[Ca^{2+}]_i$ dynamics in oscillating neurones was monitored for 300 s in NL with a standard osmolarity of 295–300 mOsm/l. Then the perfusion solution was switched to either hypo-osmotic (275 mOsm/l) or hyper-osmotic (325 mOsm/l) solution and $[Ca^{2+}]_i$ dynamics was monitored for another 300 s. Representative examples of oscillating neurones subjected to hyper- (A) or to hypo- (B) osmotic stimuli are shown in Fig. 5.

For each neurone, we calculated the four basic trace parameters, and evaluated if the change in these parameters in normal

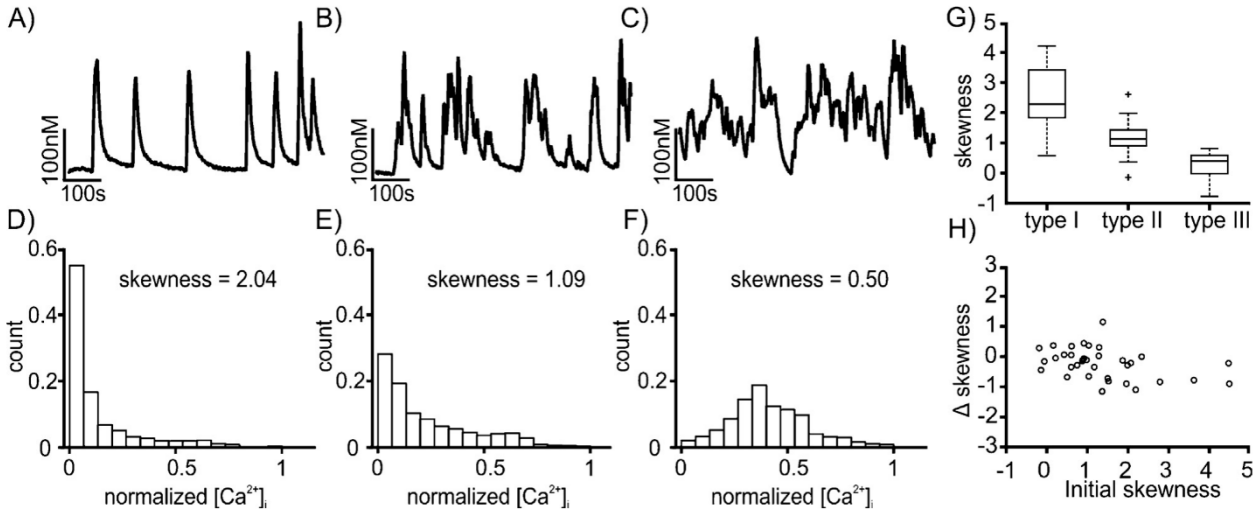

Fig. 4. A-C show representative traces from AVP-eGFP neurones in normal condition, and correspond to oscillations of type I, II, and III, respectively (see main text). D-F show the corresponding histograms of $[Ca^{2+}]_i$ values recorded in the traces located above the histograms. (G) Range of skewness values (showed as standard box plot) in oscillation traces of the indicated type. (H) Control plot showing the difference of skewness in 2nd half and 1st half of $[Ca^{2+}]_i$ trace recorded in normal conditions (compare to Figs. 5 C, D and 7 C).

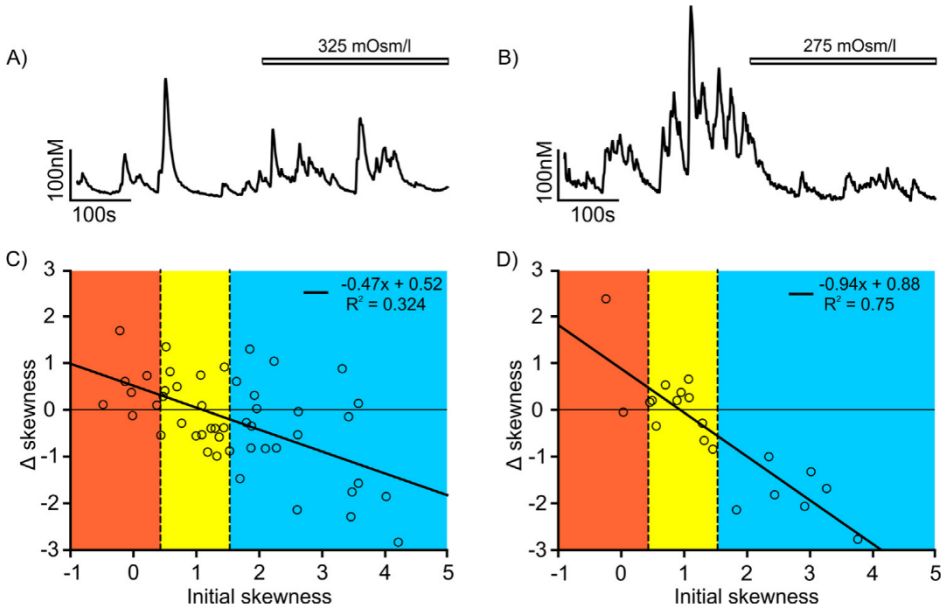

Fig. 5. Effect of osmotic change on $[Ca^{2+}]_i$ oscillations.
(A, B): The $[Ca^{2+}]_i$ trace from neurones subjected to A: hypertonic solution (325 mOsm/l; bar), (B) hypotonic solution (275 mOsm/l; bar). (C, D) Change in skewness resulting from exposure to tonic solution, plotted as function of initial skewness (before exposure). (C) hypertonic, (D) hypotonic solution.

vs. hypo- or hyper osmolarity condition was statistically significant (using the paired *t*-test as described in Section 2.8). The results are summarized in Fig. 6. For neurones exposed to hypo-osmotic solution (n = 20) we recorded a significant decrease in mean $[Ca^{2+}]_i$ level (22.8 ± 5.0 nM, *p*-value 0.01) and in the spread SDCa of $[Ca^{2+}]_i$ within the trace segment (28.3 ± 8.0 nM, *p*-value 0.02). The other two evaluated parameters, the $[Ca^{2+}]_i$ baseline and the skewness of the $[Ca^{2+}]_i$ distribution, did not change significantly (p = 0.82 and 0.08). For neurones exposed to hyper-osmotic solution (n = 48), the increase of mean $[Ca^{2+}]_i$ level was 11.8 ± 5.1 nM and the increase of SDCa was 7.0 ± 3.7 nM. Similarly the hypo-osmotic case, these changes were statistically significant (with *p*-value 0.02), while the changes in baseline and skewness were not (p = 0.1 and 0.9).

Even though the change in skewness was not significant when averaged over all neurones in the group, we did observe significant trends when the initial state of the neurone (*i.e.*, the state in the normal osmotic condition) was taken into account. The skewness of the $[Ca^{2+}]_i$ distribution tends to increase in neurones that had low initial value of skewness, and to decrease in neurones that had high initial skewness (Fig. 5). This observation is valid for both hyper- (Fig. 5C) and hypo- (Fig. 5D) osmotic stimuli. To summarise, exposure to an osmotic stimulus tends to make $[Ca^{2+}]_i$ activity more regular, bringing the oscillation into a type II pattern (intermediate range of skewness values, marked in yellow in Fig. 5C, D).

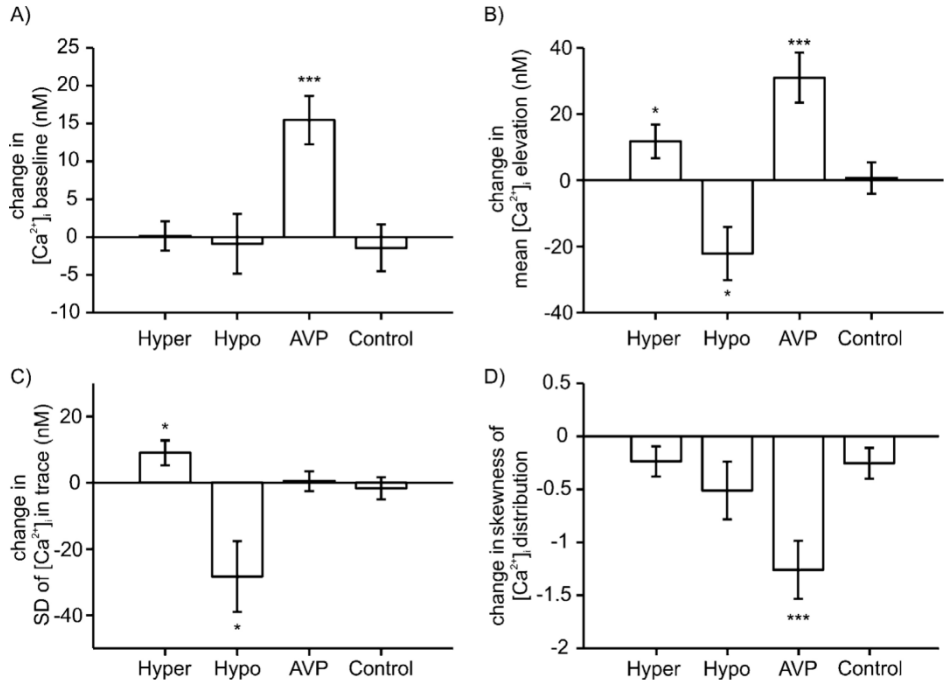

Fig. 6. Modulatory effect of AVP and osmolarity on $[Ca^{2+}]_i$ oscillations. The four panels show, for each evaluated $[Ca^{2+}]_i$ trace parameter, the change in its value following the application of the specified stimulus (hyper-osmolar, hypo-osmolar, AVP). The respective numbers of measured neurones are: hyper-osmolar, n = 48; hypo-osmolar, n = 20; AVP, n = 31. Panel (A) shows the change in $[Ca^{2+}]_i$ baseline, (B) in mean $[Ca^{2+}]_i$ level, (C) in spread (SD) of $[Ca^{2+}]_i$ within the trace, and (D) in skewness of the $[Ca^{2+}]_i$ distribution. The bars show the mean value of the parameter change and the respective standard error of the mean. Statistical significance is indicated as: * for p-value < 0.05; ** for $p < 0.01$, and *** for $p < 0.001$ (paired t-test). In the column marked "Control", the panels show the differences between the first and second half of a $[Ca^{2+}]_i$ trace, with the entire trace recorded in normal condition (no stimulus); n = 38. None of these differences were statistically significant.

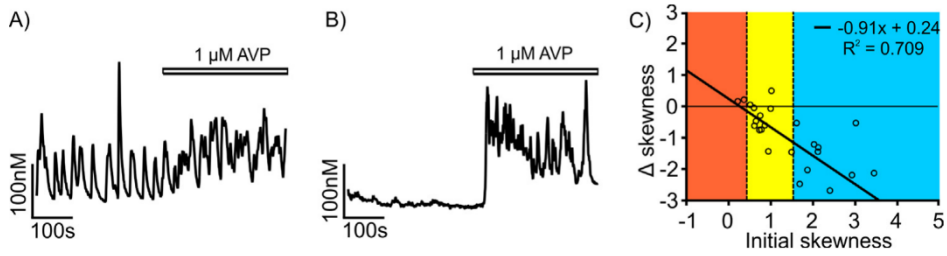

Fig. 7. Trace A represents spontaneous Ca^{2+} oscillations observed from SON neurone. The same neurone was subjected to 1 μM AVP (shown in bar). Trace B is an example of a silent and non-oscillating neurone which 1 mM AVP was applied and triggered oscillation. C: Change of the skewness introduced by application of AVP plotted as a function of initial skewness. Coloured areas correspond to oscillatory types (blue—type I, yellow—type II, red—type III) introduced in Fig. 1. Majority of neurones display decrease in skewness corresponding to higher activity. (For interpretation of the references to colour in this figure legend, the reader is referred to the web version of this article.)

3.3. *Effect of AVP on $[Ca^{2+}]_i$ oscillations*

We tested the response of 28 oscillating neurones to 1 μM AVP. In each neurone, we compared the oscillations before and after application AVP; the results are summarized in Fig. 6. In majority of neurones the AVP had an obvious enhancing effect on the oscillation (for an example, see Fig. 7A). While SD_{Ca} of $[Ca^{2+}]_i$ for the trace did not change (Fig. 6C), AVP caused a highly significant increase ($p = 0.0003$) of the mean $[Ca^{2+}]_i$ level with average change of 31.0 ± 7.5 nM and a highly significant increase ($p = 0.0002$) of $[Ca^{2+}]_i$ baseline with an average change of 13.4 ± 3.2 nM. In addition, AVP elicited very significant ($p = 0.001$) negative change in the skewness of the $[Ca^{2+}]_i$ distribution giving a strong average decrease of 1.26 ± 0.27. When the initial skewness was in the intermediate range (type II oscillation), it was only weakly affected by AVP, while in neurones with high initial skewness (type III), AVP typically prompted a switch to type II oscillatory behaviour (Fig. 7C). Beside the effect on oscillating neurones, in some cases (n = 5) AVP triggered oscillations in silent neurone (example in Fig. 7B) and in one case, the AVP attenuated the oscillations (Fig. not shown).

These results mainly indicate a strong enhancing effect of the AVP on $[Ca^{2+}]_i$ oscillations in magnocellular neurones. These AVP effects on oscillations were mimicked by the specific AVP-V_{1a} receptor agonist [6] and were unaffected by a specific V_{1a} antagonist, SR 49059 [8] (results not shown).

3.4. *$[Ca^{2+}]_i$ oscillations persist in neurones obtained from rats subjected to dehydration*

Three groups of animals were prepared. In the control group, the rats were maintained under normal conditions (see Section 2) with unlimited access to water. In two other groups, the animals were deprived of water for 3-day and 5-day, respectively. In neurones obtained from 3-day dehydrated rats 18 of 20 cells were spontaneously oscillating. In neurones isolated from 5-day dehydrated rats 9 of 10 neurones were continuously oscillating. The percentages of the spontaneously oscillating neurones form both

3-day and 5-day dehydration animals were 90%, as compared to 71% in the control group of unidentified neurones (Section 3.1). The pattern of oscillations obtained from dehydrated rats was not different from oscillations in normal conditions and none of the four trace parameters exhibited statistically significant differences among these groups (unpaired *t*-test).

3.5. Spontaneous $[Ca^{2+}]_i$ oscillations in neurones from lactating rats

We also measured the $[Ca^{2+}]_i$ oscillations in identified OT-mRFP1 neurones from 3 to 6-day- lactating rats. The number of oscillating neurones isolated from lactating animals, 18 of 23 (78%), was significantly increased compared to the OT-mRFP1 neurones from transgenic adult virgin rats: 7 of 16 (44%). However, no significant difference was detectable among the patterns of oscillations in these groups of neurones (normal and lactation; Fig. 2A *vs*. D).

4. Discussion

In the present study, we report, for the first time, a detailed analysis of the spontaneous $[Ca^{2+}]_i$ oscillations of SON AVP and OT neurones in isolated condition, and show how these oscillations are affected by the physiological state of the animal (dehydration, lactation) and by exposure to extracellular stimuli (osmotic change, AVP). The majority of AVP neurones (about 80%) and about 60% of OT neurones were oscillatory. Under lactating conditions, there was a significant increase in the number of oscillatory OT neurones (from 44% to about 80%). Spontaneous $[Ca^{2+}]_i$ oscillations exhibited a wide range of patterns, ranging from regular oscillations with stereotypical $[Ca^{2+}]_i$ peaks to irregular fast oscillations (Section 3.1). To our knowledge, AVP and OT neurones of the SON represent the exceptional case of defined neuronal sub-populations with distinct electrical activities [1] but with highly heterogeneous patterns of spontaneous $[Ca^{2+}]_i$ dynamics (present study). Given the heterogeneous character of the oscillations, their consistent characterization by frequency and amplitude was not feasible. Instead, we relied on a combination of four quantitative parameters: the $[Ca^{2+}]_i$ baseline, the mean $[Ca^{2+}]_i$ level, the spread (standard deviation) of $[Ca^{2+}]_i$ values, and the skewness of the $[Ca^{2+}]_i$ distribution. The skewness parameter, which quantifies the asymmetry of the distribution of $[Ca^{2+}]_i$ values, was used to classify the oscillation patterns (Section 3.1), and permitted a quantitative evaluation of the change in oscillation character following the presentation of a stimulus (Sections 3.2–3.3).

It has been known that SON neurones are osmosensitive and that their behaviour, notably, the electrical activity of AVP neurones acutely isolated from the rat supraoptic nucleus, is increased by hypertonicity and inhibited by hypotonicity in the absence of neighbouring glial cells and without any synaptic connectivity [32,33]. Under these conditions, hypertonic stimuli excited the cells by increasing the activity of non-selective cation channels and thus causing membrane depolarisation, whereas hypo-osmotic solutions inhibit AVP neurones through a hyperpolarisation caused by a reduction in the basal activity of the non-selective cation channels. In terms of Ca^{2+} signalling, we report, for the first time, that a vast majority of SON neurones were sensitive to osmotic changes, suggesting that both AVP and OT neurones employ Ca^{2+} signals for osmoregulation. We found that both hypo- and hyper-osmolarity changed the mean $[Ca^{2+}]_i$, level as well as the amplitude of the variations around this mean (*i.e.*, SD of $[Ca^{2+}]_i$ in the traces).

The effects of dehydration on AVP and OT neuronal activity, as well as on release of AVP and OT at the level of soma and neurohypophysis have been widely discussed [33–36]. Of interest, we found that almost all SON neurones (about 90%) became oscillatory during 3–5 days of dehydration, consistent with the need to have more AVP release both at soma and at nerve terminals; and therefore to increase the plasma AVP level to fulfil the physiological demands.

Another aspect of our study was in dissecting various effects of AVP on the spontaneous $[Ca^{2+}]_i$ oscillations. In previous studies, using *in vivo* electrophysiology and push-pull techniques, the somatodendritic release of AVP was shown to modulate electrical activity of magnocellular neurones [7,37]. Similar results were obtained in the SON slice preparations [13,38]; as well as in the *in vitro* release at the level of neurohypophysis or from isolated SON neurones [39]. In addition, it was also demonstrated using SON slice preparations that the electrical activities of AVP neurones show several patterns: (i) regular bursting at regular intervals, (ii) slow-irregular and (iii) fast-continuous (see review of [12,15]); and are regulated (positive or negative) by the AVP itself [38]. Here we demonstrate that $[Ca^{2+}]_i$ oscillations observed in AVP neurones similarly display several patterns and AVP modulated these oscillations in a likewise manner: in silent neurones, AVP triggered the oscillations; in oscillating neurones, AVP intensified these oscillations, and in a rare case, AVP attenuated a pronounced oscillation.

The autoregulatory mechanism of OT neurones has been clearly established [11,12] in terms of Ca^{2+} signals. OT-induced $[Ca^{2+}]_i$ responses are not only modulated by OT receptors but also OT activates thapsigargin-sensitive intracellular Ca^{2+} stores [13,15]. In *in vivo* experiments, or in slice preparations, OT always showed an excitatory/positive and synchronised effect on their firing behaviour, leading to the release of a bolus amount of OT to meet their end functions. In our experiments, about 60% of OT neurones showed spontaneous oscillations in $[Ca^{2+}]_i$ (44% in identified OR-mRFP1 neurones from virgins), these neurones were osmosensitive and sensitive to dehydration. More strikingly, nearly 80% of OT neurones from lactating rats became oscillatory. This finding suggests the possibility, as of *in vivo* effects, that almost all OT neurones should exhibit spontaneous $[Ca^{2+}]_i$ oscillation, which would facilitate a massive release of OT during lactation *vs*. non-lactating/virgin state or in males. However, further experiments are necessary to identify whether spontaneous $[Ca^{2+}]_i$ oscillations of all OT-mRFP1 neurones are synchronised during lactation, as well.

5. Conclusions

In the present paper we show, for the first time, that fluorescent magnocellular supraoptic AVP-eGFP and OT-mRFP1 neurones exhibit distinct spontaneous $[Ca^{2+}]_i$ oscillations in an isolated condition under various experimental conditions. These properties are shown to mimic their intrinsic electrical behaviour under physiological conditions such as osmotic shock, dehydration and lactation. The understanding of autoregulatory mechanisms of AVP and OT neurones [12], regulated by peptides they synthesize on their own, is reinforced by the present data on their spontaneous $[Ca^{2+}]_i$ activity.

Conflict of interest

The authors state that they have no conflict of interest pertaining to this manuscript.

Authors' contribution

SK, CS, OF, GD: performed experiments.

YU, OF: prepared and maintained the heterozygous and homozygous transgenic rats for both AVP and OT and developed double transgenic rats for AVP and OT; performed genotyping, manuscript writing.

SK, MZ, AV, GD: data and statistical methods and analysis; manuscript writing.

AV, GD: prepared the concept of the project.

AC, ES, GD: project management and logistics, manuscript writing.

Acknowledgements

This work was supported by the grants 14-34077S and GACR P304/12/G069 from the Grant Agency of the Czech Republic, GAUK 22214 from the Grant Agency of Charles University in Prague, and by institutional support RVO#67985823. CS and GD were supported in part by the FP7 Initial Training Network Edu-GLIA program (PITN-GA-2009-237956). This publication is partly a result of the "Advanced Bioimaging of Living Tissues" project, registration number #CZ.2.16/3.1.00/21527, which was financed from the budget of the European Regional Development Fund and public budgets of the Czech Republic through the Operational Programme Prague-Competitiveness. AV was supported by the Wellcome Trust, by the Alzheimer's research foundation (UK) and by the grant (agreement from August 27, 2013 no. 02.B.49.21.0003) between The Ministry of Education and Science of the Russian Federation and Lobachevsky State University of Nizhny Novgorod, by the grant of the Russian Scientific Foundation №14-15-00633 and by the Ministry of Education of the Russian Federation, unique identity number RFMEFI57814X0079. Govindan Dayanithi belongs to the "Centre National de la Recherche Scientifique-The French Ministry of Research and Higher Education-Paris", France. We are grateful to Kip Allan Bauersfeld, IEM ASCR, for critical reading and helpful comments on the manuscript.

Appendix A. Supplementary data

Supplementary data associated with this article can be found, in the online version, at http://dx.doi.org/10.1016/j.ceca.2016.04.001.

References

[1] M. Cazalis, G. Dayanithi, J.J. Nordmann, The role of patterned burst and interburst interval on the excitation-coupling mechanism in the isolated rat neural lobe, J. Physiol. 369 (1985) 45–60.
[2] M. Cazalis, G. Dayanithi, J.J. Nordmann, Requirements for hormone release from permeabilized nerve endings isolated from the rat neurohypophysis, J. Physiol. 390 (1987) 71–91.
[3] M. Cazalis, G. Dayanithi, J.J. Nordmann, Hormone release from isolated nerve endings of the rat neurohypophysis, J. Physiol 390 (1987) 55–70.
[4] D. Brethes, G. Dayanithi, L. Letellier, J.J. Nordmann, Depolarization-induced Ca^{2+} increase in isolated neurosecretory nerve terminals measured with fura-2, Proc. Natl. Acad. Sci. U. S. A. 84 (1987) 1439–1443.
[5] G. Dayanithi, M. Cazalis, J.J. Nordmann, Relaxin affects the release of oxytocin and vasopressin from the neurohypophysis, Nature 325 (1987) 813–816.
[6] L. Gouzenes, N. Sabatier, P. Richard, F.C. Moos, G. Dayanithi, V1a- and V2-type vasopressin receptors mediate vasopressin-induced Ca^{2+} responses in isolated rat supraoptic neurones, J. Physiol. 517 (Pt 3) (1999) 771–779.
[7] F. Moos, L. Gouzenes, D. Brown, G. Dayanithi, N. Sabatier, L. Boissin, A. Rabie, P. Richard, New aspects of firing pattern autocontrol in oxytocin and vasopressin neurones, Adv. Exp. Med. Biol. 449 (1998) 153–162.
[8] G. Dayanithi, H. Widmer, P. Richard, Vasopressin-induced intracellular Ca^{2+} increase in isolated rat supraoptic cells, J. Physiol. 490 (Pt 3) (1996) 713–727.
[9] N. Sabatier, P. Richard, G. Dayanithi, L-, N- and T- but neither P- nor Q-type Ca^{2+} channels control vasopressin-induced Ca^{2+} influx in magnocellular vasopressin neurones isolated from the rat supraoptic nucleus, J. Physiol 503 (Pt 2) (1997) 253–268.
[10] N. Sabatier, P. Richard, G. Dayanithi, Activation of multiple intracellular transduction signals by vasopressin in vasopressin-sensitive neurones of the rat supraoptic nucleus, J. Physiol. 513 (Pt 3) (1998) 699–710.
[11] R.C. Lambert, G. Dayanithi, F.C. Moos, P. Richard, A rise in the intracellular Ca^{2+} concentration of isolated rat supraoptic cells in response to oxytocin, J. Physiol. 478 (Pt 2) (1994) 275–287.
[12] G. Dayanithi, N. Sabatier, H. Widmer, Intracellular calcium signalling in magnocellular neurones of the rat supraoptic nucleus: understanding the autoregulatory mechanisms, Exp. Physiol. 85 (2000) 75s–84s.
[13] M. Ludwig, N. Sabatier, P.M. Bull, R. Landgraf, G. Dayanithi, G. Leng, Intracellular calcium stores regulate activity-dependent neuropeptide release from dendrites, Nature 418 (2002) 85–89.
[14] Y. Komori, M. Tanaka, M. Kuba, M. Ishii, M. Abe, N. Kitamura, A. Verkhratsky, I. Shibuya, G. Dayanithi, Ca^{2+} homeostasis, Ca^{2+} signalling and somatodendritic vasopressin release in adult rat supraoptic nucleus neurones, Cell Calcium 48 (2010) 324–332.
[15] G. Dayanithi, O. Forostyak, Y. Ueta, A. Verkhratsky, E.C. Toescu, Segregation of calcium signalling mechanisms in magnocellular neurones and terminals, Cell Calcium 51 (2012) 293–299.
[16] S.H. Oliet, C.W. Bourque, Mechanosensitive channels transduce osmosensitivity in supraoptic neurons, Nature 364 (1993) 341–343.
[17] C.W. Bourque, L.P. Renaud, Activity patterns and osmosensitivity of rat supraoptic neurones in perfused hypothalamic explants, J. Physiol 349 (1984) 631–642.
[18] M. Prager-Khoutorsky, C.W. Bourque, Osmosensation in vasopressin neurons: changing actin density to optimize function, Trends Neurosci. 33 (2010) 76–83.
[19] W.T. Mason, Supraoptic neurones of rat hypothalamus are osmosensitive, Nature 287 (1980) 154–157.
[20] J.B. Wakerley, D.A. Poulain, D. Brown, Comparison of firing patterns in oxytocin- and vasopressin-releasing neurones during progressive dehydration, Brain Res. 148 (1978) 425–440.
[21] Y. Ueta, G. Dayanithi, H. Fujihara, Hypothalamic vasopressin response to stress and various physiological stimuli: visualization in transgenic animal models, Horm. Behav. 59 (2011) 221–226.
[22] F. Jamen, G. Alonso, I. Shibuya, H. Widmer, C.M. Vacher, A. Calas, J. Bockaert, P. Brabet, G. Dayanithi, Impaired somatodendritic responses to pituitary adenylate cyclase-activating polypeptide (PACAP) of supraoptic neurones in PACAP type I—receptor deficient mice, J. Neuroendocrinol. 15 (2003) 871–881.
[23] N. Sabatier, I. Shibuya, G. Dayanithi, Intracellular calcium increase and somatodendritic vasopressin release by vasopressin receptor agonists in the rat supraoptic nucleus: involvement of multiple intracellular transduction signals, J. Neuroendocrinol. 16 (2004) 221–236.
[24] Y. Ueta, H. Fujihara, R. Serino, G. Dayanithi, H. Ozawa, K. Matsuda, M. Kawata, J. Yamada, S. Ueno, A. Fukuda, D. Murphy, Transgenic expression of enhanced green fluorescent protein enables direct visualization for physiological studies of vasopressin neurons and isolated nerve terminals of the rat, Endocrinology 146 (2005) 406–413.
[25] A. Katoh, H. Fujihara, T. Ohbuchi, T. Onaka, T. Hashimoto, M. Kawata, H. Suzuki, Y. Ueta, Highly visible expression of an oxytocin-monomeric red fluorescent protein 1 fusion gene in the hypothalamus and posterior pituitary of transgenic rats, Endocrinology 152 (2011) 2768–2774.
[26] C. Viero, I. Shibuya, N. Kitamura, A. Verkhratsky, H. Fujihara, A. Katoh, Y. Ueta, H.H. Zingg, A. Chvatal, E. Sykova, G. Dayanithi, Review: Oxytocin: crossing the bridge between basic science and pharmacotherapy, CNS Neurosci. Ther. 16 (2010) e138–156.
[27] T. Moriya, R. Shibasaki, T. Kayano, N. Takebuchi, M. Ichimura, N. Kitamura, A. Asano, Y.Z. Hosaka, O. Forostyak, A. Verkhratsky, G. Dayanithi, I. Shibuya, Full-length transient receptor potential vanilloid 1 channels mediate calcium signals and possibly contribute to osmoreception in vasopressin neurones in the rat supraoptic nucleus, Cell Calcium 57 (2015) 25–37.
[28] G. Grynkiewicz, M. Poenie, R.Y. Tsien, A new generation of Ca^{2+} indicators with greatly improved fluorescence properties, J. Biol. Chem. 260 (1985) 3440–3450.
[29] G. Dayanithi, I. Mechaly, C. Viero, H. Aptel, S. Alphandery, S. Puech, F. Bancel, J. Valmier, Intracellular Ca^{2+} regulation in rat motoneurons during development, Cell Calcium 39 (2006) 237–246.
[30] C. Viero, I. Mechaly, H. Aptel, S. Puech, J. Valmier, F. Bancel, G. Dayanithi, Rapid inhibition of Ca^{2+} influx by neurosteroids in murine embryonic sensory neurones, Cell Calcium 40 (2006) 383–391.
[31] O. Forostyak, N. Romanyuk, A. Verkhratsky, E. Sykova, G. Dayanithi, Plasticity of calcium signaling cascades in human embryonic stem cell-derived neural precursors, Stem Cells Dev. 22 (2013) 1506–1521.
[32] S.H. Oliet, C.W. Bourque, Properties of supraoptic magnocellular neurones isolated from the adult rat, J. Physiol. 455 (1992) 291–306.
[33] E. Trudel, C.W. Bourque, Circadian modulation of osmoregulated firing in rat supraoptic nucleus neurones, J. Neuroendocrinol. 24 (2012) 577–586.
[34] W.D. Knight, L.L. Ji, J.T. Little, J.T. Cunningham, Dehydration followed by sham rehydration contributes to reduced neuronal activation in vasopressinergic supraoptic neurons after water deprivation, Am. J. Physiol. Regul. Integr. Comp. Physiol. 299 (2010) R1232–1240.
[35] J.J. Nordmann, M. Cazalis, G. Dayanithi, E. Castanas, P. Giraud, J.J. Legros, F. Louis, Are opioid peptides co-localized with vasopressin or oxytocin in the neural lobe of the rat? Cell Tissue Res. 246 (1986) 177–182.
[36] W.C. Huang, D.W. Ploth, L.G. Navar, Angiotensin-mediated alterations in nephron function in goldblatt hypertensive rats, Am. J. Physiol. 243 (1982) F553–F560.
[37] F.C. Moos, K. Rossi, P. Richard, Activation of *N*-methyl-D-aspartate receptors regulates basal electrical activity of oxytocin and vasopressin neurons in lactating rats, Neuroscience 77 (1997) 993–1002.
[38] V. Chevaleyre, G. Dayanithi, F.C. Moos, M.G. Desarmenien, Developmental regulation of a local positive autocontrol of supraoptic neurons, J. Neurosci 20 (2000) 5813–5819.
[39] M. Ludwig, P.M. Bull, V.A. Tobin, N. Sabatier, R. Landgraf, G. Dayanithi, G. Leng, Regulation of activity-dependent dendritic vasopressin release from rat supraoptic neurones, J. Physiol. 564 (2005) 515–522.

B.III Physiology of Ca^{2+} signalling in stem cells of different origins and differentiation stages

Forostyak, O., S. Forostyak, S. Kortus, E. Sykova, A. Verkhratsky and G. Dayanithi (2016). "Physiology of Ca2+ signalling in stem cells of different origins and differentiation stages." Cell Calcium 59(2-3): 57-66.

Cell Calcium 59 (2016) 57–66

Contents lists available at ScienceDirect

Cell Calcium

journal homepage: www.elsevier.com/locate/ceca

Review

Physiology of Ca^{2+} signalling in stem cells of different origins and differentiation stages

Oksana Forostyak[a,b,*], Serhiy Forostyak[a,b], Stepan Kortus[a,c,d], Eva Sykova[a,b], Alexei Verkhratsky[e,f,g], Govindan Dayanithi[a,h,i,*]

[a] Institute of Experimental Medicine, Czech Academy of Sciences, Videnska 1083, Prague 14220, Czech Republic
[b] Department of Neuroscience, Charles University, Second Faculty of Medicine, V Uvalu 84, 15006 Prague, Czech Republic
[c] Institute of Physiology, Czech Academy of Sciences, Videnska 1083, 14220 Prague, Czech Republic
[d] Institute of Biophysics and Informatics, First Medical Faculty, Charles University, Salmovska 1, 12000 Prague, Czech Republic
[e] University of Manchester, School of Biological Sciences, D.4417 Michael Smith Building, Oxford Road, Manchester M13 9PT, UK
[f] Achucarro Center for Neuroscience, IKERBASQUE, Basque Foundation for Science, 48011 Bilbao, Spain
[g] Department of Neurosciences, University of the Basque Country UPV/EHU and CIBERNED, Leioa, Spain
[h] Institut National de la Santé et de la Recherche Médicale, Unité de recherche U1198 and University of Montpellier, 34095 Montpellier, France
[i] Ecole Pratique des Hautes Etudes-Sorbonne, Les Patios Saint-Jacques, 4-14 rue Ferrus, 75014 Paris, France

ARTICLE INFO

Article history:
Received 12 January 2016
Received in revised form 28 January 2016
Accepted 2 February 2016
Available online 17 February 2016

Keywords:
Stem cells
Ca^{2+} channels
Ca^{2+} signalling
Spontaneous Ca^{2+} oscillations
Intracellular $[Ca^{2+}]_i$ stores
Inositol trisphosphate
Ryanodine receptors
Glutamate
Purinergic receptors
Vasopressin
Oxytocin
Human embryonic stem cells
Neural precursors
Bone marrow mesenchymal stromal cells
Adipose tissue derived mesenchymal stromal stem cells
Human induced pluripotent stem cells
Cell differentiation
Neurodegeneration
Cell therapy
Transplantation

ABSTRACT

Stem cells (SCs) of different origins have brought hope as potential tools for the treatment of neurodegenerative diseases such as Parkinson's disease, Alzheimer's disease, and Amyotrophic Lateral Sclerosis. Calcium signalling plays a key role in SC differentiation and proliferation, and dysregulation of Ca^{2+} homeostasis may instigate pathological scenarios. Currently, the role of ion channels and receptors in SCs is not fully understood. In the recent years, we found that (i) the pre-differentiation of human embryonic SCs (hESCs) led to the activation of Ca^{2+} signalling cascades and enhanced the functional activities of these cells, (ii) the Ca^{2+} homeostasis and the physiological properties of hESC-derived neural precursors (NPs) changed during long term propagation *in vitro*, (iii) differentiation of NPs derived from human induced pluripotent SCs affects the expression of ion channels and receptors, (iv) these neuronal precursors exhibited spontaneous activity, indicating that their electrophysiological and Ca^{2+} handling properties are similar to those of mature neurones, and (v) in mesenchymal SCs isolated from the adipose tissue and bone marrow of rats the expression profile of ion channels and receptors depends not only on the differentiation conditions but also on the source from which the cells were isolated, indicating that the fate and functional properties of the differentiated cells are driven by intrinsic mechanisms. Together, identification and assignment of a unique ion channel and a Ca^{2+} handling footprint for each cell type would be necessary to qualify them as physiologically suitable for medical research, drug screening, and cell therapy.

Abbreviations: AMSCs, adipose mesenchymal stem/stromal cells; AVP, arginine vasopressin; ATP, adenosine-5′-triphosphate; BM, bone marrow; BMSCs, bone marrow stem/stromal cells; $[Ca^{2+}]_i$, intracellular Ca^{2+} concentration; CNS, central nervous system; CPA, cyclopiazonic acid; EC, embryonal carcinoma; ER, endoplasmic reticulum; ESCs, embryonic stem cells; GABA, *gamma*-aminobutyric acid; HVA, high voltage-activated; hESCs, human embryonic SCs; hESC-NPs, hESC-derived neural precursors; iPSCs, induced pluripotent stem cells; $InsP_3R$, inositol-1,4,5-trisphosphate receptor; LVA, low voltage activated; MSCs, mesenchymal stem/stromal cells; NCX, Na^+/Ca^{2+} exchanger; NGF, nerve growth factor; OT, oxytocin; pAMSCs, pre-differentiated AMSCs; pBMSCs, pre-differentiated BMSCs; PLC, Phospolipase-C; PMCAs, plasmamembrane-Ca^{2+}-ATPase; rMSCs, rat mesenchymal stem/stromal cells; ROCC, receptor-operated Ca^{2+} channels; RyR, ryanodine receptor; SCs, stem cells; SERCA, sarcoendoplasmic reticulum Ca^{2+}-ATPase; SOCs, store-operated Ca^{2+} channels; uAMSCs, undifferentiated AMSCs; uBMSCs, undifferentiated BMSCs; uSCs, undifferentiated SCs; LVA, voltage-activated; VEGF, vascular endothelial growth factor; VGCC, voltage-gated Ca^{2+} channels.

* Corresponding authors at: Institute of Experimental Medicine, Czech Academy of Sciences, Videnska 1083, Prague 14220, Czech Republic. Fax: +420 241 062 732.
E-mail addresses: oxfor@biomed.cas.cz (O. Forostyak), gdaya@univ-montp2.fr, gdaya@biomed.cas.cz (G. Dayanithi).

http://dx.doi.org/10.1016/j.ceca.2016.02.001
0143-4160/

1. Introduction

Public and professional interest in stem cells (SCs) has risen markedly over the last few decades. Two Nobel Prizes in Physiology and Medicine, in 2007 and 2012, were awarded for research in this field. There are many reasons why SCs capture the imagination of so many researches. Firstly, understanding the unique properties of stem cells provides a deeper insight into cell biology and embryology. Secondly, SCs represent the basis for cell replacement therapies in a multitude of degenerative and traumatic diseases. Finally, SCs can serve as an *in vitro* model of various diseases as well as a tool for drug development. SCs of different origin display many differences in molecular phenotype, growth rate, cell marker expression, and the ability to differentiate. The mechanisms underlying these differences remain poorly understood. In particular, the repertoire, major properties and the role of ion channels and receptors in SCs are the subject of intense examination. In this review, we emphasize the notion that the type of SCs used in cell replacement therapies should be carefully chosen based not only on gene expression, morphological features, or cell surface markers, but also on their origin and functional properties correlated with the type of application. Furthermore, identifying the physiological profile of stem cells is essential for assessing the suitability of these cells for their potential use.

2. Historic remarks

"Generatio spontanea"—a theory of spontaneous life generation from nonliving things pronounced by ancient Greeks existed throughout many centuries when in 17th century Francesco Redi and later in 19th century Louis Pasteur by their experiments finally disapproved it and demonstrated that life cannot emerge spontaneously but only from pre-existing life—"*Omne vivum ex vivo*" [1]. This formula was further elaborated by Rudolf Virchow to: "*Omnis cellula e cellula*" [2], which proclaimed that all cells in the organism derive from pre-existing cells. Indeed, all the cells in multicellular organisms (including humans) arise from the fertilized egg, which effectively is the "totipotent" stem cell. The term "stem cell" or "*Stammzelle*" was introduced in 1868 by Ernst Haeckel [3], by which he meant the common cellular ancestor of all living forms. Somewhat later Haekel also applied this term to a fertilized egg [4] (see also Refs. [5,6]). By the beginning of the twentieth century, the notion of SCs had been firmly established, although they were not considered a specific cell population, but rather cells that were transiently formed during development as precursors for differentiated cells. Another meaning of the term 'stem cell' was introduced in 1896 by Arthur Pappenheim to describe the precursor cell of the red and white blood cells lineage [7]. Similar ideas of the common precursor for all blood cells were proposed by Alexandr Maximov, who appointed the lymphocyte to this role [8]. These discoveries not only founded the concept of haematopoietic lineages, but also described the existence of other types of SCs in the organism [5].

The simultaneous capacity of SCs to self-renew and to generate different cell types led to the development of two highly different lines of research. The first resulted as a continuation of work on the characterization and isolation of "true" haematopoietic SCs. The presence of mesenchymal progenitor cells in bone marrow has been documented since the late nineteenth century [9,10]. Goujon was the first to show the osteogenic potential of bone marrow [10]. In 1973, Friedenstein and colleagues showed that the osteogenic potential was a feature of a specific subgroup of cells termed colony-forming unit fibroblastic (CFU-f) cells representing a heterogeneous population of stem and progenitor cells [11,12]. All these experiments provided the theoretical basis for bone marrow transplant studies and started mesenchymal stem/stromal cells (MSCs) research.

The second line of research focused on pluripotent SCs and began in the 1950s from the studies of teratocarcinomas, the latter being malignant germ cells tumours composed of undifferentiated embryonal carcinoma (EC) cells that can include all three germ layers [13]. Subsequently, the EC cells were shown to be capable of both unlimited self-renewal and multilineage differentiation [14], providing a ground for the further generation of embryonic stem cells (ESCs). Isolation and maintenance of mouse ESCs *in vitro* was, for the first time, reported independently by Sir Martin Evans together with Matthew H. Kaufman [15] and by Gail Martin [16]. Somewhat later, in 1998, Thomson and colleagues generated ESCs from human blastocyst [17]. In 2007 Mario J. Capecci, Martin J. Evans and Oliver Smithies shared a Nobel Prize for the "discoveries of principles for introducing specific gene modifications in mice by the use of embryonic stem cells". The establishment of human embryonic stem cells (hESCs) stimulated the rapid rise of stem cell research as well as worldwide debates about the ethical issues of using human embryos, which waned after the discovery of induced pluripotency [18]. The newly generated induced pluripotent stem cells (iPSCs) were produced by reprogramming mature somatic cells to a pluripotent state by gene transfer and possessed properties similar to ESCs. Similar to MSCs, iPSCs can be generated from a patient's cells, allowing "personalized medicine". At the same time, due to their pluripotency, the iPSCs have broader differentiation potential and therapeutic applications compared to MSCs. The importance of this research was recognized by the Nobel Prize committee, who later awarded the 2012 Nobel Prize in Medicine and Physiology to Sir John B. Gurdon and to Shinya Yamanaka "for the discovery that mature cells can be reprogrammed to become pluripotent".

3. Definition and fundamental properties of SCs

Stem cells are defined as undifferentiated, karyotypically normal cells that have the capacity of self-renewal as well as the ability to generate differentiated cells [19]. Self-renewal is the ability to generate at least one identical copy of the mother cell, and is the most important criterion of "stemness". The ability of cells to differentiate into other cell types is known as cell potency. Characteristic SCs are classified as totipotent, pluripotent and multipotent. Totipotent cells can give rise to all cell types, including cells of the trophectoderm lineage. In mammals, only zygote and early blastomeres (up to 8-cell stage) are totipotent. Pluripotent cells can generate the cells of all three germ layers as well as germline, but not the extraembryonic trophoblast. Multipotent cells can give rise to a restricted subset of tissue-specific cell types (within one germ layer). Based on the time of appearance, SCs can be further sub-classified into ESCs, which occur during embryogenesis, and somatic or adult-derived stem cells, that are present in different tissues in postnatal life. Correspondingly, SCs can be isolated from embryonic, foetal or adult tissues.

The SC lines have been characterized by their developmental potential, transcriptional and epigenetic profiles, cell-surface markers and teratomas formation in nude (*i.e.* immunosuppressed) mice. The criteria for these assessments include the expression of surface markers and transcription factors associated with the undifferentiated state. In addition proliferative capacity, pluripotency and euploid karyotype as well as epigenetic status are being assessed [20]. Several approaches have been used to characterize SCs, but the most widespread are analyses of the cell surface-antigen phenotype, often by flow cytofluorimetry, and gene expression studies, commonly assessed by RT-PCR or by microarray analyses. These methods are the first, and very often

the only, applied to characterize SCs in the undifferentiated state and during differentiation. However these techniques fail to characterize the functional properties of SCs.

4. Calcium as a life and death signal

It is generally recognized that Ca^{2+} is one of the most universal carriers of biological signals, controlling numerous cellular functions. It prompts conception, regulates cell proliferation and differentiation into a certain type. In differentiated cells Ca^{2+} signals regulate gene transcription, vesicular secretion, membrane excitability, muscle contraction, synaptic plasticity, *etc.* Finally, excessive elevations of Ca^{2+} initiate cell death either *via* necrotic or programmed death pathways [21–23]. Cellular Ca^{2+} is regulated by a sophisticated molecular network that has developed through evolution. This network is assembled of multiple components, many of which have several isoforms with different properties. More variations are achieved due to the interactions of Ca^{2+} with other signalling pathways. In addition, Ca^{2+} signals are able to act distinctly in the context of time, space and amplitude. Therefore each specific cell type is able to exploit this system to construct versatile Ca^{2+} signalling systems (also known as "Ca^{2+} signalling toolkits") with variable spatial and temporal properties [24].

The underlying mechanism of Ca^{2+} signalling is relatively simple and is based on the increase of cytosolic concentrations of this ion (commonly denoted as $[Ca^{2+}]_i$). The $[Ca^{2+}]_i$ in eukaryotic cells at rest is set around 50–100 nM, and it can rapidly increase (to the range of 1–10 μM or even higher in microdomains) in response to stimulation. These increases in $[Ca^{2+}]_i$, which regulate cellular activity, can operate over a broad time and space range, therefore allowing multiple variations of this relatively simple theme. The molecular components of the Ca^{2+} signalling network can be divided into a few groups according to their function. There are plasmalemmal Ca^{2+} channels that control Ca^{2+} entry from outside the cell. There are Ca^{2+} release channels that control Ca^{2+} release from the intracellular stores. There are Ca^{2+} buffers setting the Ca^{2+} concentration in the cytoplasm. There are Ca^{2+} pumps and exchangers that remove Ca^{2+} from the cytosol to the extracellular space or into intracellular stores. Finally there are numerous Ca^{2+} sensors that translate Ca^{2+} signals into cellular activity. Conceptually, Ca^{2+} might act both as a first and as a second messenger. Acting as a first messenger it, for example, controls axon guidance and neurite outgrowth through activation of plasma membrane calcium-sensing receptors [25]. Acting as a second messenger it regulates numerous processes in neuronal development such as proliferation, migration, differentiation, axon guidance and dendrite outgrowth [26,27]. SCs express multiple Ca^{2+} signalling pathways, which are summarised in Fig. 1 and Table 1.

5. Ca^{2+} signals in undifferentiated SCs (uSCs)

uSCs possess a primitive Ca^{2+} signalling toolkit. They are non-excitable cells, although some voltage-activated ion channels are known to be expressed in uSCs, especially in adult uSCs [28,29]. In recent years we performed an in depth analysis of Ca^{2+} signalling pathways in ESCs and MSCs, focusing in particular on voltage-gated Ca^{2+} channels (VGCCs), on Ca^{2+} signals controlled by receptors to glutamate, GABA, ATP, oxytocin and vasopressin, as well as on Ca^{2+} release from intracellular stores [30]. None of the undifferentiated ESCs or MSCs responded to glutamate, GABA, oxytocin or depolarization, confirming the non-excitable nature of uSCs. The majority of uSCs however, generated $[Ca^{2+}]_i$ transients in response to ATP: these were observed in 88% of uESCs, 90% of undifferentiated adipose-derived mesenchymal SCs (uAMSCs) and 62% of undifferentiated bone marrow-derived mesenchymal SCs (uBMSCs). In all these cells Ca^{2+} signals were triggered by activation of P2X (uAMSCs); or both P2X and P2Y (uBMSCs) types of purinoceptors [31]. In addition uMSCs expressed functional V_1 vasopressin receptors, the activation of which triggered Ca^{2+} release from intracellular stores [31].

uESCs have been shown to express functional purinergic receptors [32], store-operated Ca^{2+} channels [33], $InsP_3$ receptors [33], low voltage-activated (LVA) Ca^{2+} channels [34], but no high-voltage activated (HVA) Ca^{2+} channels. Undifferentiated cells of the CCTL14 hESC line were only partially sensitive to ATP and these responses were mediated mainly through $P2X_2$, $P2X_3$, $P2X_7$ and P2Y purinoceptors [30]. The expression of genes encoding $P2X_{2,5,7}$ and $P2Y_{1,2,6}$ receptors was identified in mouse ESCs [35]. In the same mouse ESCs plasmalemmal Ca^{2+} entry mainly occurs through store-operated Ca^{2+} channels (SOCs), whereas Ca^{2+} release from intracellular stores is mediated by $InsP_3$ receptors, but not by ryanodine receptors [33]. Extrusion of Ca^{2+} in mouse ESCs was mediated by both Na^+/Ca^{2+} exchanger (NCXs) and plasmamembrane-Ca^{2+}-ATPase (PMCAs) [33].

Undifferentiated MSCs are rather heterogeneous, although similar to uESCs the majority of these cells express functional purinoceptors [36]. Functional P2X ($P2X_{4,7}$) and P2Y receptors were identified in uMSCs [31,36,37]. The ATP autocrine/paracrine signalling pathway was involved in $[Ca^{2+}]_i$ oscillations observed in uBMSCs [38]. The uAMSCs also expressed purinergic, vasopressin, adrenergic and histamine linked to $InsP_3$ receptor-mediated $[Ca^{2+}]_i$ dynamics [31,36,39]. Of note, receptors expression in SCs varies among species. All three subtypes (V_{1a}, V_{1b} and V_2) of vasopressin receptors were identified in adipose mesenchymal SCs (AMSCs) isolated from mice [40], whereas human AMSCs expressed only the V_{1a} (AVP V_{1a}) subtype of vasopressin receptor [39].

6. Changes of Ca^{2+} signalling toolkit during differentiation towards neuronal phenotype

The exposure of SCs to certain environmental and differentiation conditions initiates cell maturation and their transformation into a certain cell type. These processes are accompanied by changes in the expression of various genes and proteinatious cell markers as well with functional metamorphosis. Functional properties of NPs derived from ESCs change during maintenance *in vitro* [41], which is manifested by an increased Ca^{2+} signalling during a certain time period [30,42]. This finding demonstrates that ESCs may acquire a specific pattern of Ca^{2+} signalling for a limited period and that evaluation of Ca^{2+} signals in stem cells can be used to predict the fate of the cells during differentiation and can serve as an important criterion for assessing the quality of stem cells before their use in cell replacement therapy.

7. Voltage-gated calcium channels in SCs

Voltage-gated Ca^{2+} channels (VGCCs) represent the major Ca^{2+} entry pathway in excitable cells and thereby control a variety of cellular functions both during development and in mature cells. During embryogenesis Ca^{2+} entry through VGCCs contributes to cell proliferation and cell differentiation. Depending on biophysical and pharmacological properties in many cell types VGCCs have been classified into two major groups: high voltage-activated channels (HVA), which include L-, N-, P/Q- and R-type channels and low voltage-activated channels (LVA) or T-type channels [43–46].

The expression of L- and T-type VGCC (but not P/Q- or R-VGCC) was identified in many types of SCs. In particular they were detected by immunocytochemistry and immunoblotting in ESCs [47], AMSCs [48,49] and in BMSCs [28,29,50]; however functional VGCCs could be identified only in undifferentiated BMSCs and mouse ESCs. Small

Table 1
Expression of Ca^{2+} channels and receptors linked to Ca^{2+} signalling in SCs.

Channel/ Receptor	Type of SCs	Species	Differentiation	Functional expression	Gene/mRNA expression	Protein expression	Reference
Voltage-gated Ca^{2+} channels (VGCC)							
VGCC:LVA	ESCs	mouse	neuronal	LVA	–	–	[52]
VGCC: L P/Q N R	ESCs	mouse	neuronal	Yes (L-, P/Q-, N-, R-VGCC)	–	Yes (P/Q-,N-, R-VGCC)	[47]
VGCC: L, P/Q T	ESCs	mouse	undifferentiated	No	No	–	[33]
VGCC: T	ESCs	mouse	undifferentiated	Yes (T-VGCC)	Yes (T-VGCC)	Yes (T-VGCC)	[34]
VGCC: L	ESCs	mouse	neuronal	Yes (L-VGCC)	–	Yes (L-VGCC)	[113]
VGCC: L	ESCs	mouse	neuronal	Yes (L-VGCC)	–	–	[55]
VGCC: L P/Q N	ESCs	human	undifferentiated neuronal	No Yes (L-, P/Q-VGCC)	– –	No Yes (L-, P/Q-, N-VGCC)	[30]
VGCC	ESCs	human	undifferentiat ed neuronal (dopaminergic)	No Yes (VGCC)	– –	– –	[32]
VGCC: L P/Q T N	ESCs	human	neuronal	–	Yes (L-, N-, T-VGCC) No (P/Q-VGCC)	–	[66]
VGCC: L P/Q T N	Foetal SPC-01	human	motoneurons	Yes (L-, N-, P/Q-, T-VGCC)	–	–	[53]
VGCC: L T	AMSCs	human	undifferentiated	No	Yes (L-, T-VGCC)	Yes (L-VGCC)	[48]
VGCC: L T	AMSCs	human	undifferentiated neuronal	No No	Yes (L-, T-VGCC) Yes (L-, T-VGCC)	– –	[49]
VGCC: L P/Q N	AMSCs	rat	undifferentiated neuronal	No Yes (L-VGCC)	– –	No Yes (L-, P/Q-VGCC)	[31]
VGCC: L T	BMSCs	human	undifferentiated	Yes (L-VGCC)	Yes (L-VGCC)	–	[28]
VGCC: L T	BMSCs	human	undifferentiated	Yes (L-VGCC)	Yes (L-, T-VGCC)	–	[29]
VGCC: L P/Q T N R	BMSCs	human	undifferentiated	Yes (L-VGCC)	Yes (L-, P/Q-, T-VGCC)	–	[50]
VGCC: L P/Q N	BMSCs	murine	neuronal	Yes (L-VGCC)	–	–	[57]
VGCC: L T	BMSCs	rat	undifferentiated	Yes (L-VGCC)	Yes (L-VGCC)	–	[51]
VGCC: L	BMSCs	rat	osteogenic	Yes (L-VGCC)	Yes (L-VGCC)	–	[58]
VGCC: L P/Q N	BMSCs	rat	undifferentiated neuronal	No Yes (L-, P/Q-VGCC)	–	No Yes (L-, P/Q-VGCC)	[31]
Intracellular Ca^{2+} stores							
$InsP_3$ R1-3 RyR R1-3	ESCs	mouse	undifferentiated	Yes ($InsP_3$) No (RyR)	Yes ($InsP_3$ R 1,2,3)	–	[33]
$InsP_3$	ESCs	human	cardiomyocytes	Yes ($InsP_3$)	–	Yes ($InsP_3$)	[97]
RyR2	ESCs		neuronal	Yes (RyR2)	Yes (RyR2)	Yes (RyR2)	[55]
RyR2 $InsP_3$	ESCs	human	cardiomyocytes	Yes (RyR2 $InsP_3$)	Yes (RyR2 $InsP_{3)}$	Yes (RyR2 $InsP_3$)	[98]
RyR	ESCs	human	neuronal	Yes (RyR)	–	Yes (RyR1,3)	[30]
$InsP_3$ R RyR	AMSCs	human	undifferentiated	Yes ($InsP_3$) No (RyR)	–	–	[36]
$InsP_3$	AMSCs	human	adipocyte	Yes ($InsP_3$)	–	–	[39]
$InsP_3$	AMSCs	human	adipocyte	Yes ($InsP_3$)	–	–	[96]
$InsP_3$ R1-3 RyR 1-3	BMSCs	murine	neuronal	Yes (RyR, $InsP_3$)	Yes (RyR2, RyR3, $InsP_3$R1, $InsP_3$R2, $InsP_3$R3)	–	[57]
$InsP_3$ RyR	BMSCs	human	undifferentiated	Yes ($InsP_3$)	Yes ($InsP_3$ R1-3)	–	[50]
$InsP_3$	BMSCs	human	adipocytes	Yes ($InsP_3$)	–	–	[38]
P2 purinergic receptors							
$P2X_{2,3,4,5,7}$	ESCs	human	neuronal precursors (NPs) Differentiated NPs	– –	Yes ($P2X_5$, $P2X_4$) Yes ($P2X_5$)	–	[66]
$P2X_{2,3,4,6,7}$ P2Y	ESCs	human	neuronal	Yes ($P2X_{2,3,7,}$ P2Y)	–	Yes ($P2X_{2,3,7}$)	[30]
$P2X_{1,2,3,45,7}$ $P2Y_{1,2,4,6}$	ESCs	mouse	undifferentiated neuronal GABAergic	– Yes ($P2X_{2,4,}$ $P2Y_1$)	Yes ($P2X_{2,5,7}$ $P2Y_{1,2,6}$ Yes ($P2X_{1,2,3,4,5,6,7}$ $P2Y_{1,2,6}$)	– –	[35]
$P2X_{1\text{-}7}$ $P2Y_{1,2,4,6,11,12,13,14}$	AMSCs	human	adipogenic osteogenic	$P2Y_{1,2,4,12,13}$	Yes ($P2X_{3,4,5,6,7,}$ $P2Y_{1,2,4,6,11,12,13,14}$)	–	[75]
P2X P2Y	AMSCs	rat	undifferentiated neuronal	Yes (P2X) Yes (P2X, P2Y)	– –	–	[31]
$P2Y_2$	BMSCs	rat	undifferentiated	Yes ($P2Y_2$)	Yes ($P2Y_2$)	Yes ($P2Y_2$)	[74]
P2X P2Y	BMSCs	rat	undifferentiated neuronal	Yes (P2X) Yes ($P2X_7$)	–	– Yes ($P2X_7$)	[31]
$P2Y_1$ P2X	BMSCs	human	undifferentiated	Yes ($P2Y_1$, P2X)	–	–	[73]
$P2Y_1$	BMSCs	human	adipogenic	Yes ($P2Y_1$)	–	–	[38]
Oxytocin (OT) and vasopressin (AVP) receptors							
AVP V_{1a} AVP V_{1b} AVP V_2	ESCs	mouse	cardiac	–	Yes (AVP V_{1a}, AVP V_{1b}, AVP V_2)	–	[40]
AVP V_{1a} AVP V_{1b} AVP V_2	AMSCs	human	adipogenic	Yes (V_{1a} R)	Yes (V1a R)	–	[39]
OT R	AMSCs	mouse	neuronal	–	Yes (OT R)	–	[81]
OT R AVP-V_{1a} AVP V_2	BMSCs	rat	undifferentiated	Yes (OT R)	Yes (OT R, AVP-V_{1a} R	Yes (OT R)	[82]
OT R AVP-V_1	BMSCs	rat	undifferentiated neuronal	Yes (AVP V_1) Yes (OT R, AVP V_1)	– –	Yes (AVP) Yes (OT, AVP)	[31]
OT R	AMSCs BMSCs	human	adipogenic osteogenic	Yes (OT R)	–	–	[80]

Abbreviations: AMSCs, adipose tissue derived mesenchymal stromal cells; AVP, vasopressin; BMSCs, bone marrow mesenchymal stromal cells; ESCs, embryonic stem cells; InsP3, Inositol 1,4,5-trisphosphate receptor; LVA, low voltage activated Ca^{2+} channels, OT, oxytocin; OT R – oxytocin receptor; RyR, ryanodine receptor.

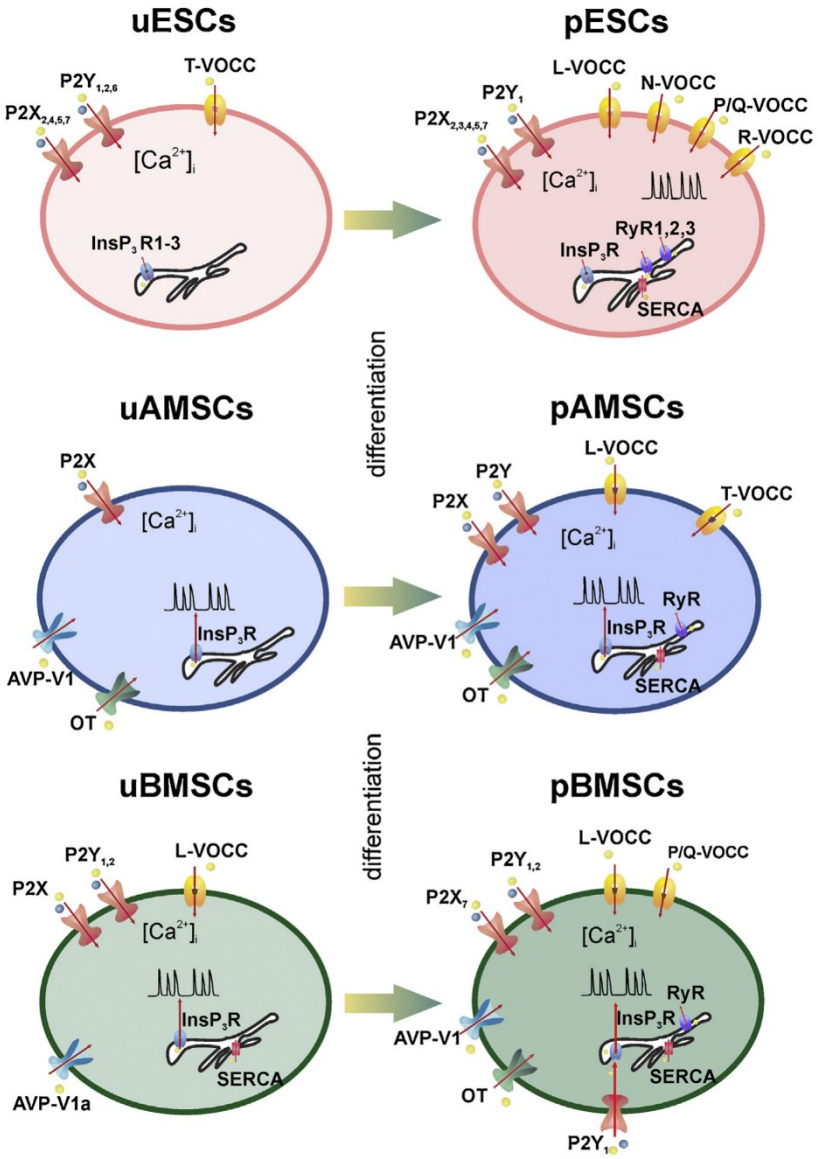

Fig. 1. Schematic drawing showing the functional expression of Ca^{2+}-sensitive channels and receptors in ESCs, AMSCs and BMSCs. Growth, lineage commitment and maturation demands SCs develop more various and sophisticated signalling pathways. The universality of the Ca^{2+} signal makes it an ideal tool for this purpose. The recent reports on the functional expression of Ca^{2+}-sensitive channels and receptors in ESCs, AMSCs and BMSCs are schematically presented in the figure. In particular, voltage-gated Ca^{2+} channels (VGCC), $InsP_3$, inositol trisphosphate receptors ($InsP_3R$), ryanodine receptors (RyR), P2 purinergic, vasopressin and oxytocin receptors, as well as spontaneous Ca^{2+} oscillations and sarcoendoplasmic reticulum Ca^{2+}-ATPase (SERCA pump) are shown.

subpopulations of human undifferentiated BMSCs (~15%) express functional L-type Ca^{2+} channels [28,29,50]; similarly L-type Ca^{2+} currents were recorded from rat BMSCs [51]. Unlike human cells, the undifferentiated AMSCs isolated from rat do not possess operational VGCCs [31]. These findings further confirm the distinct expression of cell markers and specificity of cell signalling pathways in SCs isolated from different species. Only T-type VGCC has been shown to be functional in mouse ESCs [34,52]. It was claimed that the modulation of T-type channels that occurs during cell cycle progression might contribute to maintenance of ESCs self-renewal capacity [34]. Activation of LVA VGCC was shown to trigger $[Ca^{2+}]_i$ oscillations in ESC-derived neural progenitors and therefore was speculated to induce cell proliferation [52]. To the best of our knowledge there is no evidence of functional VGCCs in undifferentiated human ESCs. None of the undifferentiated human ESCs from the CCTL-14 line responded with $[Ca^{2+}]_i$ elevation to depolarisation, although during differentiation towards the neuronal phenotype almost half of the cells expressed functional L- and P/Q-type VGCCs [30]. Similarly, the uESCs lines H9 and HS181 were not responsive to depolarisation [52]. Human foetal stem cells differentiated to motor neurones have been shown to express functional L-, N-, P/Q- and T-type VGCCs [53]. The influx of Ca^{2+} through L-VGCC induces gene activation, enhances neurogenesis and differentiation. For example, it was shown that L-type VGCCs contribute to neuronal and odontogenic differentiation of dental pulp stem cells [54]. The L-type VGCCs enhanced the neuronal differentiation of ESCs as well as in adult MSCs. In particular, it has been shown that neuronal differentiation of ESCs depends on the cooperation between L-type VGCC and RyR2 intracellular Ca^{2+} release channels [55]. The L-type VGCCs play a key role in promoting neuronal differentiation of neural stem cells [56]; whereas in BMSCs L-type VGCCs regulate both neuronal and osteogenic differentiation [57,58].

The P/Q-type VGCCs in adult neurons trigger the release of neurotransmitters at synaptic terminals [22] and the Q-type VGCCs are involved in vasopressin secretion from neurohypophysial terminals [59]. They performed the same function during development of hippocampal neurons [60]. The role of P/Q-VGCCs in SCs remains somewhat obscure, however, there are several reports showing activation of P/Q-VGCCs during differentiation towards neurons. In our experiments, we were not able to detect P/Q-VGCCs in any type of undifferentiated SCs (hESCs, rBMSCs, rAMSCs). However, after differentiation of these cells into neuronal phenotype the P/Q-VGCC could be identified both functionally and immunocytochemically in hESCs [30] and rat BMSCs [31]. Similarly, activation of P/Q-VGCC was detected in bi- and multipolar neurons derived from mESCs and a shift in channel pattern from N- and L-types in apolar cells to P/Q- and R-type channels in bi- and multipolar cells was reported [47].

The functional N-type VGCCs are present in central [61,62] and peripheral embryonic motoneurons [63], and in the neurons of the dorsal horn of the spinal cord and of the dorsal root ganglia [64]. These channels regulate neurotransmitter release in presynaptic nerve terminals and they also contribute to pain pathways [65]. Expression of N-type channels have been analysed only in ESCs. Specific mRNA has been detected in human in neural progenitors derived from hESCs [66]; whereas in mouse ESCs N-type channels were detected at the protein and functional level [47]. Functional and mRNA expression analysis on BMSCs failed to detect N-type VGCCs [50].

8. Neurotransmitter receptors linked to Ca^{2+} signalling

8.1. P2 purinergic receptors

Evolutionary purinergic signalling systems are among the most ancient, are present virtually in every cell and control a wide variety of cell functions [67]. Purinergic receptors have been implicated in a wide variety of physiological and pathological conditions including neurotransmission, myocardium rhythm regulation, brain development, apoptosis, inflammation, pain, central nervous system injury and neurodegenerative disorders, *etc*. [68–71]; they also contribute to regulating cell proliferation at the early stages of brain development [72]. The P2 subfamily of purinergic receptors comprises the ionotropic P2X and metabotropic G protein coupled P2Y receptors. There are seven subtypes of P2X ($P2X_{1-7}$) and eight subtypes of P2Y ($P2Y_{1,2,4,6,11-14}$) receptors, all of which have been identified solely or in different combinations in various SCs.

The first indications for functional P2 receptors were obtained in human BMSCs where ATP, secreted through connexin hemichannels, stimulated Ca^{2+} release from ER and $[Ca^{2+}]_i$ oscillations through activating the $P2Y_1$ receptor and the PLC-β/$InsP_3$ signalling pathway [38]. Subsequently it was argued that ATP released at the early life stages of human BMSCs modulates their proliferation rate and likely acts as one of the early factors determining their cell fate [73]. Undifferentiated AMSCs and BMSCs isolated from rat express only P2X receptors, while neuronal induction of AMSCs leads to the emergence of P2Y receptors [31]. Functional expression of $P2Y_2$ receptors in rat BMSCs depends on cell density and may correlate with cell cycle progression [74]. In humans AMSCs $P2Y_4$ and $P2Y_{14}$ receptors regulate the onset of mesenchymal differentiation, whereas $P2X_5$ and $P2X_6$ receptors are responsible for lineage commitment [75]. Down-regulation of $P2Y_1$ and $P2Y_2$ can serve as markers for early osteogenic differentiation [75]. The release of ATP by MSCs is also able to promote osteogenic differentiation by activating $P2X_7$ receptors [76]. Expression of $P2X_4$ and $P2X_5$ mRNA was demonstrated in human uESCs [66], while in mouse uESCs expression of $P2X_{2,5,7}$ and $P2Y_{1,2,6}$ has been detected [35]. All seven P2X receptors as well as $P2Y_{1,2,6}$ receptors were expressed in GABAergic neurons differentiated from mouse ESCs, although Ca^{2+} signals were mainly associated with activation of $P2X_2$, $P2X_4$ and $P2Y_1$ receptors [35]. Functional $P2X_{2,3,7}$ and P2Y receptors were also found in neural precursors derived from human ESCs [30].

8.2. Vasopressin and oxytocin receptors

Vasopressin (AVP) and oxytocin (OT) are closely related neuropeptides synthesized in the neurons of supraoptic and paraventricular nuclei in the hypothalamus; these neurohormones control a wide range of functions [77–79]. Both AVP and OT regulate various aspects of SCs life. The AVP, for example, promotes cardiomyocyte differentiation of mouse ESCs through *Gata-4* and NO signalling [40]. In addition AVP acting through AVP V_{1a} receptors and PLC/$InsP_3$/Ca^{2+} pathways may inhibit differentiation of hAMSCs to adipocytes [39]. In our studies all BMSCs were sensitive to AVP, independent of differentiation stage. A vast majority of uAMSCs (75%) and pre-differentiated AMSCs (94%), responded to the application of AVP by an increase in $[Ca^{2+}]_i$. The effects of AVP were dose-dependent and were mediated through the AVP V_1 receptor [31,39]. The MSCs express OT receptors activation, have trophic and protective effects; control differentiation [80] and proliferation [81]. Treatment of BMSCs with OT reduced apoptosis increased cellular proliferation and angiogenesis, and augmented glucose uptake [82]. There is evidence that OT negatively modulates adipogenesis, while promoting osteogenesis in human AMSCs and BMSCs [80].

9. Spontaneous $[Ca^{2+}]_i$ activity

Spontaneous $[Ca^{2+}]_i$ oscillations have been observed in both excitable and non-excitable cells and are essential for embryonic development. Due to their heterogeneous spatio-temporal parameters they contribute to regulating fertilization, cell proliferation, secretion, neuronal differentiation, axonal outgrowth, radial glia proliferation and neuronal migration, *etc*. [83–87]. Spontaneous $[Ca^{2+}]_i$ transients occur predominantly during the early stages of neural precursor differentiation and regulate neurite outgrowth and the onset of the GABAergic phenotype [88]. Spontaneous $[Ca^{2+}]_i$ activity has been observed in 31% of neural precursors derived from hESCs; this spontaneous $[Ca^{2+}]_i$ dynamic was mediated by Ca^{2+} influx through HVA VGCC [30]. The L-VGCC and TRPC1-dependent spontaneous $[Ca^{2+}]_i$ transients were detected in postmitotic neurones derived from hESCs. Inhibition of these spontaneous $[Ca^{2+}]_i$ dynamics lead to a significant reduction in cell proliferation [89]. Spontaneous $[Ca^{2+}]_i$ activity in human foetal neural stem cells (NSC)-derived neural progenitors was critically dependent on connexin 43-formed gap junctions [90] and VGCC. In addition gap junctions mediated electrical connectivity between these progenitors. Inhibition of the functional networks by blocking the gap junctions terminated both the spontaneous Ca^{2+} activity and the proliferation rate [52].

Undifferentiated BMSCs and neural precursors from BMSCs also exhibit spontaneous $[Ca^{2+}]_i$ transients and oscillations [31,57,91]. In human undifferentiated BMSCs as well as in BMSCs-derived adipocytes, spontaneous $[Ca^{2+}]_i$ transients result from $InsP_3$-mediated Ca^{2+} release from the endoplasmic reticulum (ER) stores [38,91]. In 29% of rat BMSCs spontaneous $[Ca^{2+}]_i$ activity was detected. This was dependent not only on Ca^{2+} release from ER, but also on plasmalemmal Ca^{2+} influx [31]. In rat AMSCs $[Ca^{2+}]_i$ oscillations were solely dependent on ER Ca^{2+} stores and were detected in 12–13% of cells [31]. Similarly, spontaneous $[Ca^{2+}]_i$ oscillations were also observed in a subpopulation of human AMSCs [36,92]. In

summary, spontaneous $[Ca^{2+}]_i$ oscillations occur in many types of SCs; in embryonic SCs they are dependent on Ca^{2+} influx through plasma membrane, whereas in adult SCs they are triggered mainly by Ca^{2+} release from ER. Without a doubt these oscillations play an important role in cell development [93]. While further research is needed, understanding the mechanisms and control of these oscillations may offer a tool to regulate cell proliferation.

10. Intracellular Ca^{2+} stores

The endoplasmic reticulum (ER) is the major Ca^{2+} storage organelle that contributes to multiple Ca^{2+} signalling pathways. There are two major Ca^{2+} release channels localized in the ER, the ryanodine receptors (RyR) and inositol 1,4,5-triphosphate ($InsP_3$) receptors; Ca^{2+} accumulation into the ER is mediated by the sarco/endoplasmic reticulum Ca^{2+}-ATPase, also known as SERCA (for details of ER handling see [94,95]) serving to replenish the depleted stores. The metabotropic PLC/$InsP_3$ signalling cascade has been shown to be the major pathway for Ca^{2+} release from the ER in various types of SCs. The effect of ATP, histamine, vasopressin, noradrenalin and endothelin I and II on SCs is mediated *via* the PLC/$InsP_3$ signalling pathway [36,38,39,96,97]. Only $InsP_3$ receptors, not RyRs, are functional in undifferentiated embryonic mESC [33]; in adult hAMSCs [36,96] and in undifferentiated hMSCs [50]. The PLC/$InsP_3$/Ca^{2+} release pathway seems to be conserved in all SCs, since it remains functional throughout the whole period independent of SC origin and differentiation stage. For example, ESCs and MSCs differentiated to cardiomyocytes, adipocytes or neurons, all possess functional $InsP_3$ receptors [38,39,57,97,98]. Ryanodine receptors have not been identified in undifferentiated SCs, although they do emerge during differentiation. For example, neural and cardiac cells derived from ESCs, or MSCs express functional RyRs [30,31,57,98]. Moreover, the functional coupling between RyR type 2 and L-VGCC is important in neuronal differentiation as demonstrated in ESCs [55] and BMSCs [57].

11. Plasticity of Ca^{2+} signalling cascades

Experiments *in vitro* and *in vivo* have shown that despite their origin all types of SCs have a broad range of regenerative capabilities acting either as neuroprotective or cell replacement agents. Early-stage oligodendrocyte progenitor cells derived from human ESCs after being grafted into the rodent model of spinal cord injury were able to secrete factors enhancing neurites extension and resulted in decreased cavitation, remyelination and enhanced functional recovery. Eventually, these changes lead to the significant restoration of motor functions in the transplantation group compared with the control group [99]. In addition, a mixed lymphocyte reaction assay indicated that embryonic stem cell-derived neural stem/progenitor cells (ESC-NS/PCs) modulated the allogeneic immune rejection. These results demonstrated a significant cell replacement effect after implantation of ESCs and resulted in an FDA approved first phase I clinical trial involving human embryonic stem cells [100,101]. Another study involving transplantation of nonhuman primates allogeneic ESCs demonstrated that the grafted ESC-NS/PC-derived oligodendrocytes contributed to the remyelination of demyelinated axons; moreover some transplanted neurones were myelinated by host cells whereas some grafted neurons formed synaptic connections with host tissues [102]. Thus allogeneic transplantation of ESC-NS/PCs from a nonhuman primate promoted functional recovery after spinal cord trauma without tumorigenicity.

Although the characteristics of ion channels and membrane receptors and intracellular signalling mechanisms of these cells have yet to be identified, a few attempts were made in our laboratory to demonstrate the functional differences between undifferentiated hESCs and predifferentiated cells. Undifferentiated hESCs cells were partially responsive only to ATP, whereas pre-differentiated cells expressed more sophisticated Ca^{2+} signalling mechanisms, reminiscent of a neural phenotype (functional Ca^{2+} channels, purinergic, glutamate and ryanodine receptors) and exhibited spontaneous $[Ca^{2+}]_i$ oscillations [30]. A similar approach was used to test the stem cell model—an immortalized neural stem cell line from human foetal spinal cord which preserves specific physiological and differentiation features of ventral spinal cord progenitors even after extensive *in vitro* propagation and engraftment onto a lesioned rodent spinal cord [53]. From the cell lines generated, individual SPC-01-derived neurones exhibited similar Ca^{2+} signalling patterns to what was described previously in the case of CCTL14-derived NPs; particularly the presence of functional L- and P/Q-type Ca^{2+} channels and the occurrence of spontaneous $[Ca^{2+}]_i$ oscillations.

Other studies have shown that mouse embryonic stem cell-derived neurons in the early stages of differentiation possess a complex pattern of VGCC, with a shift in channel contribution from N- and L-types in apolar cells to P/Q- and R-type channels in bi- and multipolar cells [47].

Other cell types that resemble ESCs are induced pluripotent stem cells derived from somatic cells *via* transduction of their properties by a cocktail of factors Oct3/4, Sox2, c-Myc, and Klf4 [103]. These cells have the potential to differentiate towards mature cell types of all three germ layers. Neural progenitor cells derived from iPSCs cells have shown changes in protein and gene expression levels during differentiation and expression of neural growth factors (BDNF and NT3) and neuronal/glial markers [104]. Transplantation of the aforementioned cells led to stimulation of axonal ingrowth and renewal of neural tissue accompanied by a significant improvement in motor functions. The same cell-type has been shown to decrease astroglial scar formation and stimulate intrinsic growth factors (vascular endothelial growth factor, VEGF; nerve growth factor, NGF; and glia cell-line derived neurotrophic factor, GDNF [105]).

It is generally accepted that the regenerative efficacy of MSCs is based on the secretion of a wide range of substances that play a crucial role in nourishing and protecting neurons, either by host cells (stimulation of internal neurogenesis and modification of gene expression levels) or by the MSCs themselves (paracrine function) [106]. Delivery of bone marrow MSCs into rodents modulated the immune response by over-expression of some chemokines (IL-α and MCP-1) and reconstitution of T cells following transplantation [107,108]. After transplantation of MSCs grafted cells are safely integrated into the host nervous tissue, they are capable of long-term survival and migration along cranio-caudal orientation where they form scaffolds for neurites outgrowth [109,110]. Grafting of MSCs has also been shown to modulate adult CNS plasticity through normalization/stabilization of extracellular matrix dense structure (perineuronal nets) and by antiapoptotic effects [108]. Some studies have demonstrated that transplantation of MSCs enables the transfer of functional mitochondria from the graft into the host cells [111,112].

12. Conclusions

Ca^{2+} signalling contributes to SCs function, proliferation and differentiation from the very early stages of development. A wide variety of functions, including the fate and overall survival of SCs, are regulated by Ca^{2+} signals. In addition, studying the functional properties of stem cells *in vitro* may help to predict their behaviour and the fate of their physiopathological status *in vivo* and may serve as criteria to evaluate the quality of such cells. Understanding the physiology of stem cells may allow us to better control

their regenerative potential, which in turn may help to improve strategies for their use in transplantation and the treatment of neurodegenerative diseases. Therefore we suggest including Ca^{2+} signalling profiles in routine laboratory practice in order to use cells of the same type and same conditional state in experiments. Detailed research of Ca^{2+} signalling pathways in stem cells would help to develop new strategies in cell therapies.

Conflict of interest

The authors state that they have no conflict of interest pertaining to this manuscript.

Acknowledgements

This work was supported by the grants GACR P304/11/2373, GACR 14-34077S, GACR P304/12/G069 and GACR 10504P from the Grant Agency of the Czech Republic. This publication is partly a result of the "Advanced Bioimaging of Living Tissues" project, registration number #CZ.2.16/3.1.00/21527, which was financed from the budget of the European Regional Development Fund and public budgets of the Czech Republic through the Operational Programme Prague–Competitiveness. Govindan Dayanithi belongs to the "Centre National de la Recherche Scientifique-The Ministry of Research and Higher Education-Paris", France. We are grateful to Kip Allan Bauersfeld IEM ASCR, for critical reading of the manuscript.

References

[1] L. Pasteur, Vallery Radot Œuvres de Pasteur. Volume 2: Fermentations et générations dites spontanées, Masson and Cie, Paris, 1939.
[2] R. Virchow, Die Cellularpathologie in ihrer Begründung auf physiologische and pathologische Gewebelehre. Zwanzig Vorlesungen gehalten während der Monate Februar, März und April 1858 im pathologischen Institut zu Berlin. August Hirschwald, Berlin, 1858.
[3] E. Haeckel, Natürliche Schöpfungsgeschichte, Georg Reimer, Berlin, 1868.
[4] E. Haeckel, Anthropogenie, 3rd edition, Wilhelm Engelmann, Leipzig, 1877.
[5] F. Calegari, C. Waskow, Stem cells: from basic research to therapy, in: Basic Stem Cell Biology, Tissue Formation during Development, and Model Organisms, Taylor & Francis, 2014.
[6] M. Ramalho-Santos, H. Willenbring, On the origin of the term stem cell, Cell Stem Cell 1 (2007) 35–38.
[7] A. Pappenheim, Ueber entwickelung und ausbildung der erythroblasten, Virchows Arch. Pathol. Anat. 145 (1896) 587–643.
[8] A.A. Maximow, Über Zellformen des lockeren bindegewebes, Arch. Mikr. Anat. 67 (1905) 680–757.
[9] J. Cohnheim, Über entzündung und eiterung, Path. Anat. Physiol. Klin. Med. 40 (1867) 1–79.
[10] E. Goujon, Recherches experimentales sur les proprietes physiologiques de la moelle des os, J. Anat. Physiol. 6 (1869) 399–412.
[11] A.J. Friedenstein, R.K. Chailakhyan, N.V. Latsinik, A.F. Panasyuk, I.V. Keiliss-Borok, Stromal cells responsible for transferring the microenvironment of the hemopoietic tissues. Cloning *in vitro* and retransplantation *in vivo*, Transplantation 17 (1974) 331–340.
[12] M. Owen, A.J. Friedenstein, Stromal stem cells: marrow-derived osteogenic precursors, Ciba Found. Symp. 136 (1988) 42–60.
[13] J. Yu, J.A. Thomson, Pluripotent stem cell lines, Genes Dev. 22 (2008) 1987–1997.
[14] L.J. Kleinsmith, G.B. Pierce Jr., Multipotentiality of single embryonal carcinoma cells, Cancer Res. 24 (1964) 1544–1551.
[15] M.J. Evans, M.H. Kaufman, Establishment in culture of pluripotential cells from mouse embryos, Nature 292 (1981) 154–156.
[16] G.R. Martin, Isolation of a pluripotent cell line from early mouse embryos cultured in medium conditioned by teratocarcinoma stem cells, Proceedings of the National Academy of Sciences of the United States of America 8 (1981) 7634–7638.
[17] J.A. Thomson, J. Itskovitz-Eldor, S.S. Shapiro, M.A. Waknitz, J.J. Swiergiel, V.S. Marshall, J.M. Jones, Embryonic stem cell lines derived from human blastocysts, Science 282 (1998) 1145–1147.
[18] K. Takahashi, K. Tanabe, M. Ohnuki, M. Narita, T. Ichisaka, K. Tomoda, S. Yamanaka, Induction of pluripotent stem cells from adult human fibroblasts by defined factors, Cell 131 (2007) 861–872.
[19] H.R. Schöler, The potential of stem cells: an inventory, in: Nikolaus Knoepffler, Dagmar Schipanski, Stefan Lorenz Sorgner (Eds.), Human Biotechnology as Social Challenge, Ashgate Publishing, Ltd., 2007, p. p.28, ISBN 978-0-7546-5755-2.
[20] L.M. Hoffman, M.K. Carpenter, Characterization and culture of human embryonic stem cells, Nat. Biotechnol. 23 (2005) 699–708.
[21] M.J. Berridge, M.D. Bootman, P. Lipp, Calcium—a life and death signal, Nature 395 (1998) 645–648.
[22] M.J. Berridge, P. Lipp, M.D. Bootman, The versatility and universality of calcium signalling, Nat. Rev. Mol. Cell Biol. 1 (2000) 11–21.
[23] S. Orrenius, B. Zhivotovsky, P. Nicotera, Regulation of cell death: the calcium-apoptosis link, Nat. Rev. Mol. Cell Biol. 4 (2003) 552–565.
[24] M.J. Berridge, M.D. Bootman, H.L. Roderick, Calcium signalling: dynamics, homeostasis and remodelling, Nat. Rev. Mol. Cell Biol. 4 (2003) 517–529.
[25] T.N. Vizard, G.W. O'Keeffe, H. Gutierrez, C.H. Kos, D. Riccardi, A.M. Davies, Regulation of axonal and dendritic growth by the extracellular calcium-sensing receptor, Nat. Neurosci. 11 (2008) 285–291.
[26] L. Munaron, S. Antoniotti, D. Lovisolo, Intracellular calcium signals and control of cell proliferation: how many mechanisms? J. Cell. Mol. Med. 8 (2004) 161–168.
[27] S.S. Rosenberg, N.C. Spitzer, Calcium signaling in neuronal development, Cold Spring Harbor Perspect. Biol. 3 (2011) a004259.
[28] J.F. Heubach, E.M. Graf, J. Leutheuser, M. Bock, B. Balana, I. Zahanich, T. Christ, S. Boxberger, E. Wettwer, U. Ravens, Electrophysiological properties of human mesenchymal stem cells, J. Physiol. 554 (2004) 659–672.
[29] I. Zahanich, E.M. Graf, J.F. Heubach, U. Hempel, S. Boxberger, U. Ravens, Molecular and functional expression of voltage-operated calcium channels during osteogenic differentiation of human mesenchymal stem cells, J. Bone Miner. Res. 20 (2005) 1637–1646.
[30] O. Forostyak, N. Romanyuk, A. Verkhratsky, E. Sykova, G. Dayanithi, Plasticity of calcium signaling cascades in human embryonic stem cell-derived neural precursors, Stem Cells Dev. 22 (2013) 1506–1521.
[31] O. Forostyak, L. Baranovicova, D. Arboleda, S. Forostyak, O. Butenko, M. Anderova, S. Kubinova, E. Sykova, G. Dayanithi, Physiological properties of neural precursors derived from adipose and bone marrow mesenchymal stem cells 8th Federation of European Neuroscience Societies. Forum of European Neuroscience FENS Abstract. 7, 2012. 026.16.
[32] S. Malmersjo, I. Liste, O. Dyachok, A. Tengholm, E. Arenas, P. Uhlen, Ca^{2+} and cAMP signaling in human embryonic stem cell-derived dopamine neurons, Stem Cells Dev. 19 (2010) 1355–1364.
[33] E. Yanagida, S. Shoji, Y. Hirayama, F. Yoshikawa, K. Otsu, H. Uematsu, M. Hiraoka, T. Furuichi, S. Kawano, Functional expression of Ca^{2+} signaling pathways in mouse embryonic stem cells, Cell Calcium 36 (2004) 135–146.
[34] J.A. Rodriguez-Gomez, K.L. Levitsky, J. Lopez-Barneo, T-type Ca^{2+} channels in mouse embryonic stem cells: modulation during cell cycle and contribution to self-renewal: American journal of physiology, Cell Physiol. 302 (2012) C494–504.
[35] S.K. Khaira, C.W. Pouton, J.M. Haynes, $P2X_2$, $P2X_4$ and $P2Y_1$ receptors elevate intracellular Ca^{2+} in mouse embryonic stem cell-derived GABAergic neurons, Br. J. Pharmacol. 158 (2009) 1922–1931.
[36] P.D. Kotova, V.Y. Sysoeva, O.A. Rogachevskaja, M.F. Bystrova, A.S. Kolesnikova, P.A. Tyurin-Kuzmin, J.I. Fadeeva, V.A. Tkachuk, S.S. Kolesnikov, Functional expression of adrenoreceptors in mesenchymal stromal cells derived from the human adipose tissue, Biochim. Biophys. Acta 1843 (2014) 1899–1908.
[37] A. Faroni, S.W. Rothwell, A.A. Grolla, G. Terenghi, V. Magnaghi, A. Verkhratsky, Differentiation of adipose-derived stem cells into Schwann cell phenotype induces expression of P2X receptors that control cell death, Cell Death Dis. 4 (2013) e743.
[38] S. Kawano, K. Otsu, A. Kuruma, S. Shoji, E. Yanagida, Y. Muto, F. Yoshikawa, Y. Hirayama, K. Mikoshiba, T. Furuichi, ATP autocrine/paracrine signaling induces calcium oscillations and NFAT activation in human mesenchymal stem cells, Cell Calcium 39 (2006) 313–324.
[39] T.D. Tran, S. Yao, W.H. Hsu, J.M. Gimble, B.A. Bunnell, H. Cheng, Arginine vasopressin inhibits adipogenesis in human adipose-derived stem cells, Mol. Cell. Endocrinol. 406 (2015) 1–9.
[40] N. Gassanov, M. Jankowski, B. Danalache, D. Wang, R. Grygorczyk, U.C. Hoppe, J. Gutkowska, Arginine vasopressin-mediated cardiac differentiation: insights into the role of its receptors and nitric oxide signaling, J. Biol. Chem. 282 (2007) 11255–11265.
[41] N. Kozubenko, K. Turnovcova, M. Kapcalova, O. Butenko, M. Anderova, V. Rusnakova, M. Kubista, A. Hampl, P. Jendelova, E. Sykova, Analysis of *in vitro* and *in vivo* characteristics of human embryonic stem cell-derived neural precursors, Cell Transplant. 19 (2010) 471–486.
[42] C. Viero, O. Forostyak, E. Sykova, G. Dayanithi, Getting it right before transplantation: example of a stem cell model with regenerative potential for the CNS, Front. Cell Dev. Biol. 2 (2014) 36.
[43] G. Wang, G. Dayanithi, R. Newcomb, J.R. Lemos, An R-type Ca^{2+} current in neurohypophysial terminals preferentially regulates oxytocin secretion, J. Neurosci. 19 (1999) 9235–9241.
[44] V. Leuranguer, A. Monteil, E. Bourinet, G. Dayanithi, J. Nargeot, T-type calcium currents in rat cardiomyocytes during postnatal development: contribution to hormone secretion, Am. J. Physiol. Heart Circ. Physiol. 279 (2000) H2540–2548.
[45] J.R. Lemos, S.I. Ortiz-Miranda, A.E. Cuadra, C. Velazquez-Marrero, E.E. Custer, T. Dad, G. Dayanithi, Modulation/physiology of calcium channel sub-types in neurosecretory terminals, Cell Calcium (2012).

[46] W.A. Catterall, T.M. Swanson, Structural basis for pharmacology of voltage-gated sodium and calcium channels, Mol. Pharmacol. 88 (2015) 141–150.
[47] S. Arnhold, C. Andressen, D.N. Angelov, R. Vajna, S.G. Volsen, J. Hescheler, K. Addicks, Embryonic stem-cell derived neurones express a maturation dependent pattern of voltage-gated calcium channels and calcium-binding proteins, Int. J Dev. Neurosci. 18 (2000) 201–212.
[48] X. Bai, J. Ma, Z. Pan, Y.H. Song, S. Freyberg, Y. Yan, D. Vykoukal, E. Alt, Electrophysiological properties of human adipose tissue-derived stem cells, Am. J. Physiol. Cell Physiol. 293 (2007) C1539–1550.
[49] S. Jang, H.H. Cho, Y.B. Cho, J.S. Park, H.S. Jeong, Functional neural differentiation of human adipose tissue-derived stem cells using bFGF and forskolin, BMC Cell Biol. 11 (2010) 25.
[50] S. Kawano, S. Shoji, S. Ichinose, K. Yamagata, M. Tagami, M. Hiraoka, Characterization of Ca(2+) signaling pathways in human mesenchymal stem cells, Cell Calcium 32 (2002) 165–174.
[51] G.R. Li, X.L. Deng, H. Sun, S.S. Chung, H.F. Tse, C.P. Lau, Ion channels in mesenchymal stem cells from rat bone marrow, Stem Cells 24 (2006) 1519–1528.
[52] S. Malmersjo, P. Rebellato, E. Smedler, H. Planert, S. Kanatani, I. Liste, E. Nanou, H. Sunner, S. Abdelhady, S. Zhang, M. Andang, A. El Manira, G. Silberberg, E. Arenas, P. Uhlen, Neural progenitors organize in small-world networks to promote cell proliferation, Proceedings of the National Academy of Sciences of the United States of America 10 (2013) E1524–E1532.
[53] G. Cocks, N. Romanyuk, T. Amemori, P. Jendelova, O. Forostyak, A.R. Jeffries, L. Perfect, S. Thuret, G. Dayanithi, E. Sykova, J. Price, Conditionally immortalized stem cell lines from human spinal cord retain regional identity and generate functional V_{2a} interneurons and motorneurons, Stem Cell Res. Ther. 4 (2013) 69.
[54] Y. Ju, J. Ge, X. Ren, X. Zhu, Z. Xue, Y. Feng, S. Zhao, Cav1.2 of L-type calcium channel is a key factor for the differentiation of dental pulp stem cells, J. Endod. 41 (2015) 1048–1055.
[55] H.M. Yu, J. Wen, R. Wang, W.H. Shen, S. Duan, H.T. Yang, Critical role of type 2 ryanodine receptor in mediating activity-dependent neurogenesis from embryonic stem cells, Cell Calcium 43 (2008) 417–431.
[56] M. D'Ascenzo, R. Piacentini, P. Casalbore, M. Budoni, R. Pallini, G.B. Azzena, C. Grassi, Role of L-type Ca^{2+} channels in neural stem/progenitor cell differentiation, Eur. J. Neuroscie. 23 (2006) 935–944.
[57] R.R. Resende, J.L. da Costa, A.H. Kihara, A. Adhikari, E. Lorencon, Intracellular Ca^{2+} regulation during neuronal differentiation of murine embryonal carcinoma and mesenchymal stem cells, Stem Cells Dev. 19 (2010) 379–394.
[58] L. Wen, Y. Wang, H. Wang, L. Kong, L. Zhang, X. Chen, Y. Ding, L-type calcium channels play a crucial role in the proliferation and osteogenic differentiation of bone marrow mesenchymal stem cells, Biochem. Biophys. Res. Commun. 424 (2012) 439–445.
[59] G. Wang, G. Dayanithi, S. Kim, D. Hom, L. Nadasdi, R. Kristipati, J. Ramachandran, E.L. Stuenkel, J.J. Nordmann, R. Newcomb, J.R. Lemos, Role of Q-type Ca^{2+} channels in vasopressin secretion from neurohypophysial terminals of the rat, J. Physiol. 502 (Pt 2) (1997) 351–363.
[60] C. Verderio, S. Coco, G. Fumagalli, M. Matteoli, Calcium-dependent glutamate release during neuronal development and synaptogenesis: different involvement of omega-agatoxin IVA- and omega-conotoxin GVIA-sensitive channels, Proceedings of the National Academy of Sciences of the United States of America 2 (1995) 6449–6453.
[61] G. Dayanithi, N. Martin-Moutot, S. Barlier, D.A. Colin, M. Kretz-Zaepfel, F. Couraud, J.J. Nordmann, The calcium channel antagonist omega-conotoxin inhibits secretion from peptidergic nerve terminals, Biochem. Biophys. Res. Commun. 156 (1988) 255–262.
[62] N. Sabatier, P. Richard, G. Dayanithi, L-, N- and T- but neither P- nor Q-type Ca^{2+} channels control vasopressin-induced Ca2+ influx in magnocellular vasopressin neurones isolated from the rat supraoptic nucleu, J. Physiol. 503(Pt. 2 (1997) 253–268.
[63] F. Scamps, S. Valentin, G. Dayanithi, J. Valmier, Calcium channel subtypes responsible for voltage-gated intracellular calcium elevations in embryonic rat motoneurons, Neuroscience 87 (1998) 719–730.
[64] D.J. Adams, G. Berecki, Mechanisms of conotoxin inhibition of N-type ($Ca_v2.2$) calcium channels, Biochim. Biophys. Acta 1828 (2013) 1619–1628.
[65] J. Krebs, M. Michalak, Calcium: A Matter of Life or Death Preface, Calcium: A Matter of Life or Death, 41 (2007) Elsevier, Pages 584.
[66] A. Young, D.W. Machacek, S.K. Dhara, P.R. Macleish, M. Benveniste, M.C. Dodla, C.D. Sturkie, S.L. Stice, Ion channels and ionotropic receptors in human embryonic stem cell derived neural progenitors, Neuroscience 192 (2011) 793–805.
[67] A. Verkhratsky, G. Burnstock, Purinergic and glutamatergic receptors on astroglia, Adv. Neurobiol. 11 (2014) 55–79.
[68] G. Burnstock, Physiology and pathophysiology of purinergic neurotransmission, Physiol. Rev. 87 (2007) 659–797.
[69] G. Burnstock, Purinergic signalling and disorders of the central nervous system, Nat. Rev. Drug Discov. 7 (2008) 575–590.
[70] G. Burnstock, H. Ulrich, Purinergic signaling in embryonic and stem cell development, Cell. Mol. Life Sci. 68 (2011) 1369–1394.
[71] G. Vassort, Adenosine 5′-triphosphate: a P2-purinergic agonist in the myocardium, Physiol. Rev. 81 (2001) 767–806.
[72] G. Burnstock, Historical review: ATP as a neurotransmitter, Trends Pharmacol. Sci. 27 (2006) 166–176.
[73] E. Coppi, A.M. Pugliese, S. Urbani, A. Melani, E. Cerbai, B. Mazzanti, A. Bosi, R. Saccardi, F. Pedata, ATP modulates cell proliferation and elicits two different electrophysiological responses in human mesenchymal stem cells, Stem Cells 25 (2007) 1840–1849.
[74] J. Ichikawa, H. Gemba, Cell density-dependent changes in intracellular Ca^{2+} mobilization via the $P2Y_2$ receptor in rat bone marrow stromal cells, J. Cell Physiol. 219 (2009) 372–381.
[75] N. Zippel, C.A. Limbach, N. Ratajski, C. Urban, C. Luparello, A. Pansky, M.U. Kassack, E. Tobiasch, Purinergic receptors influence the differentiation of human mesenchymal stem cells, Stem Cells Dev. 21 (2012) 884–900.
[76] D. Sun, W.G. Junger, C. Yuan, W. Zhang, Y. Bao, D. Qin, C. Wang, L. Tan, B. Qi, D. Zhu, X. Zhang, T. Yu, Shockwaves induce osteogenic differentiation of human mesenchymal stem cells through ATP release and activation of $P2X_7$ receptors, Stem Cells 31 (2013) 1170–1180.
[77] C. Viero, I. Shibuya, N. Kitamura, A. Verkhratsky, H. Fujihara, A. Katoh, Y. Ueta, H.H. Zingg, A. Chvatal, E. Sykova, G. Dayanithi, REVIEW: Oxytocin Crossing the bridge between basic science and pharmacotherapy, CNS Neurosci. Ther. 16 (2010) e138–156.
[78] G. Dayanithi, N. Sabatier, H. Widmer, Intracellular calcium signalling in magnocellular neurones of the rat supraoptic nucleus: understanding the autoregulatory mechanism, Exp. Physiol. 85 (s1) (2000) 75S–84S.
[79] G. Dayanithi, O. Forostyak, Y. Ueta, A. Verkhratsky, E.C. Toescu, Segregation of calcium signalling mechanisms in magnocellular neurones and terminals, Cell calcium 51 (2012) 293–299.
[80] C. Elabd, A. Basillais, H. Beaupied, V. Breuil, N. Wagner, M. Scheideler, L.E. Zaragosi, F. Massiera, E. Lemichez, Z. Trajanoski, G. Carle, L. Euller-Ziegler, G. Ailhaud, C.L. Benhamou, C. Dani, E.Z. Amri, Oxytocin controls differentiation of human mesenchymal stem cells and reverses osteoporosis, Stem Cells 26 (2008) 2399–2407.
[81] N. Jafarzadeh, A. Javeri, M. Khaleghi, M.F. Taha, Oxytocin improves proliferation and neural differentiation of adipose tissue-derived stem cells, Neurosci. Lett. 564 (2014) 105–110.
[82] N. Noiseux, M. Borie, A. Desnoyers, A. Menaouar, L.M. Stevens, S. Mansour, B.A. Danalache, D.C. Roy, M. Jankowski, J. Gutkowska, Preconditioning of stem cells by oxytocin to improve their therapeutic potential, Endocrinology 153 (2012) 5361–5372.
[83] D.E. Clapham, Calcium signaling, Cell 131 (2007) 1047–1058.
[84] M.J. Berridge, Neuronal calcium signaling, Neuron 21 (1998) 13–26.
[85] N.C. Spitzer, N.J. Lautermilch, R.D. Smith, T.M. Gomez, Coding of neuronal differentiation by calcium transients, BioEssays 22 (2000) 811–817.
[86] H. Komuro, P. Rakic, Intracellular Ca^{2+} fluctuations modulate the rate of neuronal migration, Neuron 17 (1996) 275–285.
[87] R.J. Montoro, R. Yuste, Gap junctions in developing neocortex: a review Brain research, Brain Res. Rev. 47 (2004) 216–226.
[88] F. Ciccolini, T.J. Collins, J. Sudhoelter, P. Lipp, M.J. Berridge, M.D. Bootman, Local and global spontaneous calcium events regulate neurite outgrowth and onset of GABAergic phenotype during neural precursor differentiation, J. Neurosci. 23 (2003) 103–111.
[89] J.P. Weick, M. Austin Johnson, S.C. Zhang, Developmental regulation of human embryonic stem cell-derived neurons by calcium entry via transient receptor potential channels, Stem Cells 27 (2009) 2906–2916.
[90] J. Jaderstad, L.M. Jaderstad, J. Li, S. Chintawar, C. Salto, M. Pandolfo, V. Ourednik, Y.D. Teng, R.L. Sidman, E. Arenas, E.Y. Snyder, E. Herlenius, Communication via gap junctions underlies early functional and beneficial interactions between grafted neural stem cells and the host, Proceedings of the National Academy of Sciences of the United States of America 07 (2010) 5184–5189.
[91] S. Kawano, K. Otsu, S. Shoji, K. Yamagata, M. Hiraoka, Ca^{2+} oscillations regulated by Na^+-Ca^{2+} exchanger and plasma membrane Ca(2+) pump induce fluctuations of membrane currents and potentials in human mesenchymal stem cells, Cell Calcium 34 (2003) 145–156.
[92] H. Sauer, F. Sharifpanah, M. Hatry, P. Steffen, C. Bartsch, R. Heller, M. Padmasekar, H.P. Howaldt, G. Bein, M. Wartenberg, NOS inhibition synchronizes calcium oscillations in human adipose tissue-derived mesenchymal stem cells by increasing gap-junctional coupling, J. Cell. Physiol. 226 (2011) 1642–1650.
[93] X.H. Zhang, M. Morad, Calcium signaling in human stem cell-derived cardiomyocytes: Evidence from normal subjects and CPVT afflicted patients, Cell Calcium (2015).
[94] D. Burdakov, O.H. Petersen, A. Verkhratsky, Intraluminal calcium as a primary regulator of endoplasmic reticulum function, Cell Calcium 38 (2005) 303–310.
[95] A. Verkhratsky, Physiology and pathophysiology of the calcium store in the endoplasmic reticulum of neurons, Physiol. Rev. 85 (2005) 201–279.
[96] T.D. Tran, O. Zolochevska, M.L. Figueiredo, H. Wang, L.J. Yang, J.M. Gimble, S. Yao, H. Cheng, Histamine-induced Ca^{2+} signalling is mediated by TRPM4 channels in human adipose-derived stem cells, Biochem. J. 463 (2014) 123–134.
[97] K. Sedan, N. Zeevi-Levin, N. Leibovich, M. Amit, J. Itskovitz-Eldor, O. Binah, 1,4,5-Inositol trisphosphate-operated intracellular Ca^{2+} stores and angiotensin-II/endothelin-1 signaling pathway are functional in human embryonic stem cell-derived cardiomyocytes, Stem Cells 26 (2008) 3130–3138.

[98] J. Satin, I. Itzhaki, S. Rapoport, E.A. Schroder, L. Izu, G. Arbel, R. Beyar, C.W. Balke, J. Schiller, L. Gepstein, Calcium handling in human embryonic stem cell-derived cardiomyocytes, Stem Cells 26 (2008) 1961–1972.
[99] M. Nakamura, H. Okano, Y. Toyama, H.N. Dai, T.P. Finn, B.S. Bregman, Transplantation of embryonic spinal cord-derived neurospheres support growth of supraspinal projections and functional recovery after spinal cord injury in the neonatal rat, J. Neurosci. Res. 81 (2005) 457–468.
[100] H.S. Keirstead, G. Nistor, G. Bernal, M. Totoiu, F. Cloutier, K. Sharp, O. Steward, Human embryonic stem cell-derived oligodendrocyte progenitor cell transplants remyelinate and restore locomotion after spinal cord injury, J. Neurosci. 25 (2005) 4694–4705.
[101] C.A. Priest, N.C. Manley, J. Denham, E.D. Wirth 3rd, J.S. Lebkowski, Preclinical safety of human embryonic stem cell-derived oligodendrocyte progenitors supporting clinical trials in spinal cord injury, Regen. Med. 10 (2015) 939–958.
[102] H. Iwai, H. Shimada, S. Nishimura, Y. Kobayashi, G. Itakura, K. Hori, K. Hikishima, H. Ebise, N. Negishi, S. Shibata, S. Habu, Y. Toyama, M. Nakamura, H. Okano, Allogeneic neural stem/progenitor cells derived from embryonic stem cells promote functional recovery after transplantation into injured spinal cord of nonhuman primates, Stem Cells Transl. Med. 4 (2015) 708–719.
[103] K. Takahashi, S. Yamanaka, Induction of pluripotent stem cells from mouse embryonic and adult fibroblast cultures by defined factors, Cell 126 (2006) 663–676.
[104] N. Romanyuk, T. Amemori, K. Turnovcova, P. Prochazka, B. Onteniente, E. Sykova, P. Jendelova, Beneficial Effect of Human Induced Pluripotent Stem Cell-Derived Neural Precursors in Spinal Cord Injury Repair, Cell transplant. 24 (2015) 1781–1797.
[105] T. Amemori, J. Ruzicka, N. Romanyuk, M. Jhanwar-Uniyal, E. Sykova, P. Jendelova, Comparison of intraspinal and intrathecal implantation of induced pluripotent stem cell-derived neural precursors for the treatment of spinal cord injury in rats, Stem Cell Res. Ther. 6 (2015) 257.
[106] S. Forostyak, P. Jendelova, E. Sykova, The role of mesenchymal stromal cells in spinal cord injury, regenerative medicine and possible clinical applications, Biochimie 95 (2013) 2257–2270.
[107] D.R. Beers, J.S. Henkel, W. Zhao, J. Wang, S.H. Appel, CD4+ T cells support glial neuroprotection, slow disease progression, and modify glial morphology in an animal model of inherited ALS, Proceedings of the National Academy of Sciences of the United States of America 05 (2008) 15558–15563.
[108] S. Forostyak, A. Homola, K. Turnovcova, P. Svitil, P. Jendelova, E. Sykova, Intrathecal delivery of mesenchymal stromal cells protects the structure of altered perineuronal nets in SOD1 rats and amends the course of ALS, Stem cells 32 (2014) 3163–3172.
[109] S. Forostyak, P. Jendelova, M. Kapcalova, D. Arboleda, E. Sykova, Mesenchymal stromal cells prolong the lifespan in a rat model of amyotrophic lateral sclerosis, Cytotherapy 13 (2011) 1036–1046.
[110] A.J. Hyatt, D. Wang, C. van Oterendorp, J.W. Fawcett, K.R. Martin, Mesenchymal stromal cells integrate and form longitudinally-aligned layers when delivered to injured spinal cord via a novel fibrin scaffold, Neurosci. Lett. 569 (2014) 12–17.
[111] Y.M. Cho, J.H. Kim, M. Kim, S.J. Park, S.H. Koh, H.S. Ahn, G.H. Kang, J.B. Lee, K.S. Park, H.K. Lee, Mesenchymal stem cells transfer mitochondria to the cells with virtually no mitochondrial function but not with pathogenic mtDNA mutations, PloS One 7 (2012) e32778.
[112] J.L. Spees, S.D. Olson, M.J. Whitney, D.J. Prockop, Mitochondrial transfer between cells can rescue aerobic respiration, Proceedings of the National Academy of Sciences of the United States of America 03 (2006) 1283–1288.
[113] L. Zhang, B.E. Blackman, M.D. Schonemann, T. Zogovic-Kapsalis, X. Pan, M. Tagliaferri, H.A. Harris, I. Cohen, R.A. Pera, S.H. Mellon, R.I. Weiner, D.C. Leitman, Estrogen receptor beta-selective agonists stimulate calcium oscillations in human and mouse embryonic stem cell-derived neurons, PloS One 5 (2010) e11791.